



HAL
open science

Adsorption study of sugars in zeolites : understanding the mechanisms of separation

Wassim Ammar

► **To cite this version:**

Wassim Ammar. Adsorption study of sugars in zeolites : understanding the mechanisms of separation. Chemical engineering. Ecole normale supérieure de lyon - ENS LYON, 2022. English. NNT : 2022ENSL0039 . tel-04008318

HAL Id: tel-04008318

<https://theses.hal.science/tel-04008318>

Submitted on 28 Feb 2023

HAL is a multi-disciplinary open access archive for the deposit and dissemination of scientific research documents, whether they are published or not. The documents may come from teaching and research institutions in France or abroad, or from public or private research centers.

L'archive ouverte pluridisciplinaire **HAL**, est destinée au dépôt et à la diffusion de documents scientifiques de niveau recherche, publiés ou non, émanant des établissements d'enseignement et de recherche français ou étrangers, des laboratoires publics ou privés.



Numéro National de Thèse : 2022ENSL0039

THESE

en vue de l'obtention du grade de Docteur, délivré par
l'ÉCOLE NORMALE SUPERIEURE DE LYON

École Doctorale N° 206
École Doctorale de Chimie (Chimie, Procédés, Environnement)

Discipline : Chimie

Soutenue publiquement le 28/11/2022, par :

Wassim AMMAR

Adsorption study of sugars in zeolites: understanding the mechanisms of separation

Étude de l'adsorption des sucres dans les zéolithes: compréhension des
mécanismes de séparation

Devant le jury composé de :

BELLAT, Jean-Pierre	Professeur PR	Université de Bourgogne	Rapporteur
DENAYER, Joeri	Professeur	Université de Bruxelles	Rapporteur
LUTZ, Cécile	Ingénieure de recherche	Arkema	Examinatrice
TAYAKOUT FAYOLLE, Mélaz	Professeur PR	Université Lyon1	Examinatrice
MANKO, Maria	Ingénieure de recherche	IFPEN	Examinatrice
METHIVIER, Alain	Directeur de recherche	IFPEN	Directeur de thèse

Acknowledgements

First of all, I would like to thank the supervising team Kim Larmier, Maria Manko and the PhD director Alain Méthivier for the availability, the help and for sharing their knowledge.

This Phd thesis explored the adsorption mechanisms thanks to theoretical calculations at different levels of theory (DFT and GCMC) and for that I would like to thank Javier Perez Pellitero for the involvement, the assistance in developing and performing force field simulations.

In order to perform breakthrough experiments, a breakthrough unit was built for this project and online Raman spectroscopy was used, I would like to thank Marion Lacoue-Negre for all the interesting meetings and pieces of advice to develop univariate and chemometric models.

Solid state NMR experiments were performed to explore the tautomeric distribution of sugars in adsorbed phase. This gave interesting insights thanks to the fruitful collaboration with the NMR team at IFPEN: Laurent Lemaitre, Frédéric Filali and Florent Moreau so I would like to thank them for the availability and kindness.

The experimental campaigns could not be smooth without the technical assistance of the separation department technicians in particular Quentin Lelong, Morgane Josserand, Danielle Richard and Emily Rey. I also want to thank all the persons involved in the characterization analysis in R05 department.

I want to thank all the friends, colleagues and the tennis section of Alsip for making the journey more pleasant.

Last but not least, I want to thank my family especially my parents for the endless support and the constant encouragements.

Abstract:

Second generation biomass is mainly composed of saccharides building units that are a valuable renewable feedstock to produce high added-value chemicals. In order to obtain separate streams of each sugar (xylose, glucose, ...), the incorporation of a separation step is necessary in a biorefinery after lignocellulose fractionation. This work aims at studying and rationalizing the separation of lignocellulosic monosaccharides molecules (glucose and xylose) by adsorption. Thus, the well-known supercage of Faujasite-type zeolites is selected as a template to promote sugar separation. On the basis of this platform, an adsorbent library is constructed by means of cationic exchange of two structures presenting differentiated electrostatic strengths: NaX (Si/Al = 1.2) and NaY (Si/Al = 2.6). The library of adsorbents is characterized and “screened” for xylose/glucose separation. Thanks to the combination of experimental and theoretical approaches, several parameters are identified at the origin of the separation ability: 1) the extraframework cationic distribution and particularly the nature of the counterion have a large influence on the selectivity. BaX and BaY are good candidates for the separation where BaX is selective to xylose and BaY to glucose. 2) The solvation of sugars has an impact on the adsorption. As an example, the addition of ethanol to the feed (0 to 50 % wt) increases the adsorbed amounts of sugars in both BaX and BaY. The presence of ethanol in the feed mixture impacts as well the selectivities obtained from aqueous solutions. 3) Besides the solvation, the experimental results show a selectivity inversion for BaY when increasing the supercage filling. In the same trend, the microscopic study (force field calculations) reveals that the mentioned parameter has as well an impact on the selectivity. In an attempt to go beyond these microscopic findings, ^{13}C MAS NMR reveals that pyranose forms are adsorbed with the same proportions as the liquid phase. In parallel, Density Functional Theory (DFT) calculations allow to identify the main adsorption modes of glucose and xylose. Thanks to these findings, different improvement axes are identified as candidates to optimize the separation performance by inducing sugar accommodations closer to the ideal key-lock mechanism.

Résumé:

La biomasse de seconde génération est essentiellement composée de sucres qui constituent une matière première pour produire des molécules à haute valeur ajoutée. Pour obtenir des flux séparés de chaque sucre (xylose, glucose, ...), l'incorporation d'une étape de séparation après le fractionnement de la lignocellulose est nécessaire dans une bioraffinerie. Ce travail a pour objectif d'étudier et de rationaliser la séparation de monosaccharides d'origine lignocellulosiques (glucose et xylose) par adsorption. Pour cela, la supercage d'une zéolithe de type faujasite est sélectionnée comme modèle pour promouvoir la séparation de sucres. Une bibliothèque d'adsorbants est construite en utilisant l'échange ionique de deux structures présentant des forces électrostatiques différentes: NaX (Si/Al = 1.2) et NaY (Si/Al = 2.6). La bibliothèque des adsorbants est caractérisée et testée pour la séparation de xylose/glucose. Grâce à la combinaison d'approches expérimentales et théoriques, plusieurs paramètres sont identifiés à l'origine du pouvoir de séparation: 1) la distribution cationique et en particulier la nature du cation compensateur ont une large influence sur la sélectivité. BaX et BaY sont de bons candidats pour la séparation où BaX est sélective vers le xylose et BaY sélective vers le glucose. 2) La solvation des sucres a un impact sur l'adsorption. Par exemple, l'addition de l'éthanol à la charge (entre 0 et 50 % poids) augmente les quantités adsorbées des deux sucres dans BaX et BaY. La présence de l'éthanol dans le mélange impacte également les sélectivités obtenues à partir des solutions aqueuses. 3) Outre la solvation, les résultats expérimentaux montrent une inversion de sélectivité pour BaY en augmentant le remplissage de la supercage. L'étude de modélisation à l'échelle microscopique (calculs champs de forces) confirme que le taux de remplissage a un impact sur la sélectivité. Afin d'obtenir davantage de détails structurels sur les modes d'adsorption, des expériences de ^{13}C MAS NMR ont été menées et révèlent que seules les formes pyranoses sont adsorbées, avec des proportions similaires à celles de la phase liquide. En parallèle, les calculs de la Théorie de la Fonctionnelle de Densité (DFT) permettent d'identifier les principaux modes d'adsorption du glucose et xylose. Grâce à ces résultats, différents axes d'amélioration sont identifiés comme candidats pour optimiser les performances de séparation en induisant un placement proche du mécanisme clé-serrure.

TABLE OF CONTENT

INTRODUCTION.....	5
CHAPTER I: LITERATURE REVIEW	9
I-1 Second generation biomass	9
I-1-1 Lignocellulose composition	9
I-1-2 Pretreatment and hydrolysis of second generation biomass	11
I-1-3 Conversion of sugars to chemicals	14
I-2 Monosaccharides.....	17
I-2-1 Tautomeric equilibrium	20
I-2-2 Conformation of monosaccharides	24
I-3 Adsorption.....	26
I-3-1 Generalities about adsorption	26
I-3-2 Thermodynamics of adsorption	27
I-3-2-1 Henry’s law	27
I-3-2-2 Langmuir isotherm models	27
I-3-3 Adsorbents	29
I-3-3-1 Faujasite-type zeolites.....	29
I-4 Separation of sugars	31
I-4-1 Selectivity in resins	31
I-4-2 Selectivity in faujasite-type zeolites.....	34
I-5 DFT for sugar adsorption.....	38
I-6 Literature review conclusions and thesis strategy	40
CHAPTER II: ONLINE RAMAN SPECTROSCOPY FOR BREAKTHROUGH EXPERIMENTS OF SUGARS.....	43
II-1 Introduction.....	43
II-2 Materials and methods	45
II-2-1 Breakthrough experiments	45
II-2-2 Raman spectroscopy.....	46
II-2-3 HPLC.....	46
II-2-4 Modeling	46
II-2-4-1 Databases.....	46
II-2-4-2 Univariate modeling	47
II-2-4-3 Multivariate modeling	48
II-3 Results and discussion	48
II-3-1 Spectral interpretation	48
II-3-2 Univariate and multivariate calibration modeling.....	51
III-3-3 Models validation.....	53

II-4 Conclusion	54
CHAPTER III: SEPARATION OF GLUCOSE AND XYLOSE WITH ZEOLITES	55
III-1 Introduction	55
III-2 Experimental section.....	57
III-2-1 Chemicals.....	57
III-2-2 Adsorbents ion-exchange.....	57
III-2-3 Characterization of the adsorbents.....	58
III-2-4 Determination of the chemical formula	59
III-2-5 Determination of the number of supercages per gram of zeolite.....	59
III-2-6 Breakthrough experiments	60
III-3 Results and discussion.....	62
CHAPTER IV: ADSORPTION STUDY OF GLUCOSE AND XYLOSE IN EXCHANGED ZEOLITES X AND Y	69
IV-1 Experimental section.....	69
IV-1-1 Adsorbents and Chemicals	69
IV-1-2 Breakthrough experiments.....	69
IV-2 Results and discussion.....	72
IV-2-1 Single component isotherms.....	72
IV-2-2 Sanderson's intermediate electronegativity	75
IV-2-3 Adsorption isotherms from water-ethanol mixtures	76
IV-2-4 Ethanol effect on selectivities	79
IV-2-5 Temperature effect.....	81
IV-3-Conclusion.....	83
CHAPTER V: SOLID STATE NMR OBSERVATION OF GLUCOSE AND XYLOSE ADSORPTION IN BAX AND BAY	85
V-1 NMR analysis and samples preparation	85
V-2 ¹³C NMR of the free sugars in solution	86
V-3 ¹³C MAS NMR of sugars adsorbed in the zeolites	88
V-3-1 Glucose.....	88
V-3-2 Xylose	92
V-4 Conclusion.....	96

CHAPTER VI: DFT INVESTIGATION OF GLUCOSE AND XYLOSE ADSORPTION IN FAUJASITE-TYPE ZEOLITES.....	97
VI-1 Introduction	97
VI-2 Computational methods.....	99
VI-2-1 DFT calculations.....	99
VI-2-2 Structure models	99
VI-2-3 Free energies of adsorption calculation	100
VI-3 Results and discussions	102
VI-3-1 Optimization of sugars.....	102
VI-3-2 Optimization of zeolites.....	103
VI-3-3 Adsorption study.....	106
VI-3-3-1 Adsorption in a siliceous structure	106
VI-3-3-2 Adsorption in single cation exchanged zeolites.....	107
VI-3-3-3 Adsorption on zeolites LSX.....	112
VI-3-3-4 Adsorption of water	120
VI-3-3-5 Closing the thermodynamic cycle	121
VI-4 Conclusion.....	123
 CHAPTER VII: ADSORPTION STUDY OF SUGARS BY GRAND CANONICAL MONTE CARLO (GCMC) SIMULATIONS.....	 125
VII-1 Introduction.....	125
VII-2 Computational methods	126
VII-2-1 BaLSX force field	127
VII-2-2 Sugars force field.....	127
VII-2-3 Water force field.....	129
VII-2-4 Adsorption Equilibrium Theoretical Framework	129
VII-3 Adsorption of pure sugars in BaLSX.....	130
VII-4 Adsorption of aqueous solutions of pure sugars in BaLSX.....	132
VII-5 Adsorption of solutions of monosaccharides mixtures in a BaLSX system.....	135
VII-6 Conclusion	137
 GENERAL CONCLUSION.....	 139
 APPENDIX.....	 145
 REFERENCES.....	 177

Introduction

The increasing concern over the shortage of petroleum oil reserves coupled with the worldwide issues of climate change and rising CO₂ emissions are encouraging to utilize renewable feedstocks as sustainable sources of chemicals and fuels. The quest for such sustainable resources as an alternative and eventually a substitute to petroleum-based products is one of the big modern challenges. Biomass is considered to be an excellent non-petroleum candidate to produce fuels, fine and high value chemicals.¹⁻⁴

In this context, the biorefinery concept was created. In analogy with the conventional petroleum refineries, biomass is valorized and transformed into chemicals and energy.⁵ The first applications started with sugar-based feedstocks originated from sugarcane, sweet sorghum and sugar beet. The sugar obtained from these feedstocks is primarily sucrose (a disaccharide of glucose and fructose), which is directly fermented to ethanol by the yeast *Sacharomyces cerevisiae*.⁶ The origin of the biomass then extended to cover corn, potato and cassava. These feedstocks are composed of starch, a polymer of glucose. Unlike sugar-based feedstocks, starch-based feedstocks need to be hydrolyzed to produce a stream of glucose that will feed the fermentation process for ethanol production.

Sugar-based and starch feedstocks are called first generation biomass and their valorization is not only limited to the production of biofuels. In fact, they yield monomeric sugars that can be converted into high value platform chemicals such as lactic acid, succinic acid and 1,3-propanediol.⁶ However, an important drawback of the first generation biomass is that they are edible raw materials, which may lead to a net, direct diversion of crops to the detriment of human food, or an indirect diversion, when it concerns animal feed. Thus, in order to be truly sustainable, it is preferable that biomass sources do not compete with food production.⁷ For this reason the attention turned towards lignocellulosic feedstocks derived from agricultural wastes and forest residues, also known as second generation biomass. However, the conversion processes of lignocellulosic biomass are much more complex than for 1st generation biomass, and most of the times yield streams consisting of mixtures of sugars at various stages of the treatment. While this is not necessarily an issue to make biofuels through fermentation, it is not desirable for the preparation of high added-value chemicals. The chemical reactions must indeed preferably be carried out on a stream containing a single sugar. Therefore, the

development of efficient processes to separate the main sugars obtained from the lignocellulosic biomass transformation turns essential.

The separation of sugars in general has had the most attention from 1980.^{8,9} Fructose and glucose separation gained the largest part of attention in order to produce the High-Corn Fructose Syrup (HCFS) for the food industry. Chromatographic techniques based on adsorption were the preferred processes for the separation. In this regard, the development of an efficient adsorbent became necessary to obtain good recovery yields and sugars with high purity. Exchanged organic resins and inorganic faujasite-type zeolites were the adsorbents of choice for this application. Numerous ions were tested, calcium-exchanged resins and zeolite Y gave the best separation performances and zeolite CaY showed better selectivity to fructose than calcium-exchanged resins.¹⁰

Both materials have the feature of exchangeable sites with different ions. In addition, zeolites provide a regular microporous network and more customizable properties like the silicon and aluminum content of the framework. The literature proposes that the mechanism behind the separation of fructose and glucose is a complex formation of sugars with calcium present in the resin or the zeolite. Fructose gives a more stable complex than glucose which drive the separation. Nevertheless, the confinement effect of the zeolite, which is more selective than the resin, is still not well understood.

In this context, zeolites seem a promising candidate for the separation of lignocellulosic sugars for potential incorporation in a biorefinery and a better upgrading of lignocellulosic biomass. Nevertheless, this separation is not equally treated compared to fructose and glucose separation, fewer publications and patents treat the subject. Most of the studies are limited to screening tests and adsorption isotherms measurements using resins.¹¹⁻¹⁴

The goal of this PhD thesis is to study the separation of lignocellulosic sugars using adsorption and understand the mechanisms in the process. Several questions could be raised: What are the mechanisms of interactions and separation? What are the key structural factors of the adsorbent and the operating conditions to improve the efficiency of the separation (working capacity and selectivity)? What are the parameters that could be tailored to optimize the separation?

The chemical composition effect of the chosen adsorbents, mainly zeolites, for the separation will be investigated. Both experimental and theoretical approaches will be used, thanks to ab initio molecular modeling and force field simulations.

Regarding the general structure of this work, the manuscript was built based on different independent foreseen publication projects. The excerpts associated with the mentioned projects fit well the general plan of the global manuscript.

The first section of this report will present a literature review, focused on the composition and transformation of second generation biomass, leading to the chemical properties of sugars. The processes of separation mainly by adsorption are discussed and a brief section of this chapter is dedicated to the existing adsorption studies employing of theoretical approaches. To answer the main questions raised in the literature review, both experimental and theoretical approaches were employed. Prior to the experimental tests, Chapter II explores the efficiency of online Raman spectroscopy for breakthrough tests using different sugar solutions. In order to evaluate the chemical composition effect of the adsorbents on the separation, Chapter III describes the physical and chemical properties of the used materials, and the main screening results obtained for the separation tests. To explore the thermodynamics of the adsorption and the effect of operating conditions, Chapter IV discusses adsorption isotherms of the different adsorbents, temperature, and cosolvent influence on the adsorption. To have a better understanding at the microscopic level, Chapter V investigates the adsorbed phase thanks to solid state NMR experiments. In order to have deeper insights at the molecular level of the adsorption, Chapter VI treats the theoretical adsorption study with Density Functional Theory (DFT). The final chapter gives preliminary results of Monte Carlo force field simulations. Molecular simulations not only aim to understand the implicated mechanisms but to predict and design experimental tests. Finally, the general conclusions reached so far are reported.

Chapter I: Literature review

The literature review is divided into five sections. The first part describes the composition and main treatments of lignocellulosic biomass, followed by some possible chemical transformations of sugars. The second part describes the chemistry of sugar molecules. The third section presents some adsorption fundamentals and introduces the chemical composition of faujasite-type zeolite. In the fourth part, the separation of second generation sugars via adsorption is discussed to have a better understanding of the nature effect of adsorbents on the separation. The last part is dedicated to the molecular modeling of sugar adsorption in zeolites.

I-1 Second generation biomass

I-1-1 Lignocellulose composition

The main lignocellulosic feedstocks are forest residues and agricultural wastes (*Table I- 1*).¹⁵ They are composed of three biopolymers : cellulose, hemicellulose and lignin.¹⁶ However, the quantity of these constituents vary depending on the plant species. Nonetheless, cellulose is generally the major component (25-53 %), followed by hemicellulose (11-35 %) and lignin (10-30 %). Hard and softwood are richer in cellulose than agricultural wastes and grasses.

Table I- 1:Types of lignocellulosic biomass and their chemical composition ⁷

Lignocellulosic biomass		Cellulose (%)	Hemicellulose (%)	Lignin (%)
Hardwood	Poplar	50.8–53.3	26.2–28.7	15.5–16.3
	Oak	40.4	35.9	24.1
	Eucalyptus	54.1	18.4	21.5
Softwood	Pine	42.0–50.0	24.0–27.0	20.0
	Douglas fir	44.0	11.0	27.0
	Spruce	45.5	22.9	27.9
Agricultural waste	Wheat Straw	35.0–39.0	23.0–30.0	12.0–16.0
	Barley Hull	34.0	36.0	13.8–19.0
	Barley Straw	36.0–43.0	24.0–33.0	6.3–9.8
	Rice Straw	29.2–34.7	23.0–25.9	17.0–19.0
	Rice Husks	28.7–35.6	12.0–29.3	15.4–20.0
	Oat Straw	31.0–35.0	20.0–26.0	10.0–15.0
	Ray Straw	36.2–47.0	19.0–24.5	9.9–24.0
	Corn Cobs	33.7–41.2	31.9–36.0	6.1–15.9
	Corn Stalks	35.0–39.6	16.8–35.0	7.0–18.4
	Sugarcane Bagasse	25.0–45.0	28.0–32.0	15.0–25.0
	Sorghum Straw	32.0–35.0	24.0–27.0	15.0–21.0
Grasses	Grasses	25.0–40.0	25.0–50.0	10.0–30.0
	Switchgrass	35.0–40.0	25.0–30.0	15.0–20.0

Figure I- 1 illustrates more in detail the composition of each biopolymer:

- Cellulose is the result of the polymerization of glucose monomers through $\beta(1-4)$ glucosidic bonds and has $(C_6H_{10}O_5)_n$ as a chemical formula. The polysaccharide chains are then linked together thanks to the hydrogen bonds formed between the many hydroxyl groups present in the sugars. These bonds form cellulose microfibrils and give crystallinity to the structure.
- Hemicellulose is an amorphous, highly branched, heteropolysaccharide composed of several heteropolymers like xylan, arabinan, arabinoxylan, glucomannan, xyloglucan and many others. These polymers are formed from hexoses, *i.e.* sugars with six carbon atoms (glucose, mannose and galactose), and pentoses, which are sugars with five carbon atoms, such as xylose and arabinose. As mentioned before, the sugar composition depends on the plant species, however, xylose is the most abundant sugar in hemicellulose. Hemicellulose interacts with cellulose and lignin to reinforce the cell wall.
- Lignin is composed of phenyl-propane units: coniferyl, sinapyl, and *p*-coumaryl alcohols, cross-linked thanks to ether and carbon-carbon bonds. It provides tensile strength and water impermeability to the cell walls.

From what it is stated above, it is possible to say that lignocellulosic biomass is composed essentially from sugars, glucose the most abundant one. Thereby, monosaccharides are very interesting molecules with a high potential to be transformed into biofuels or high added-value chemicals. However, we have seen that they are present in polymeric forms and within complex frameworks. Thus, special treatments are needed in order to recover and valorize them. Several pretreatment methods and separation steps will be discussed below.

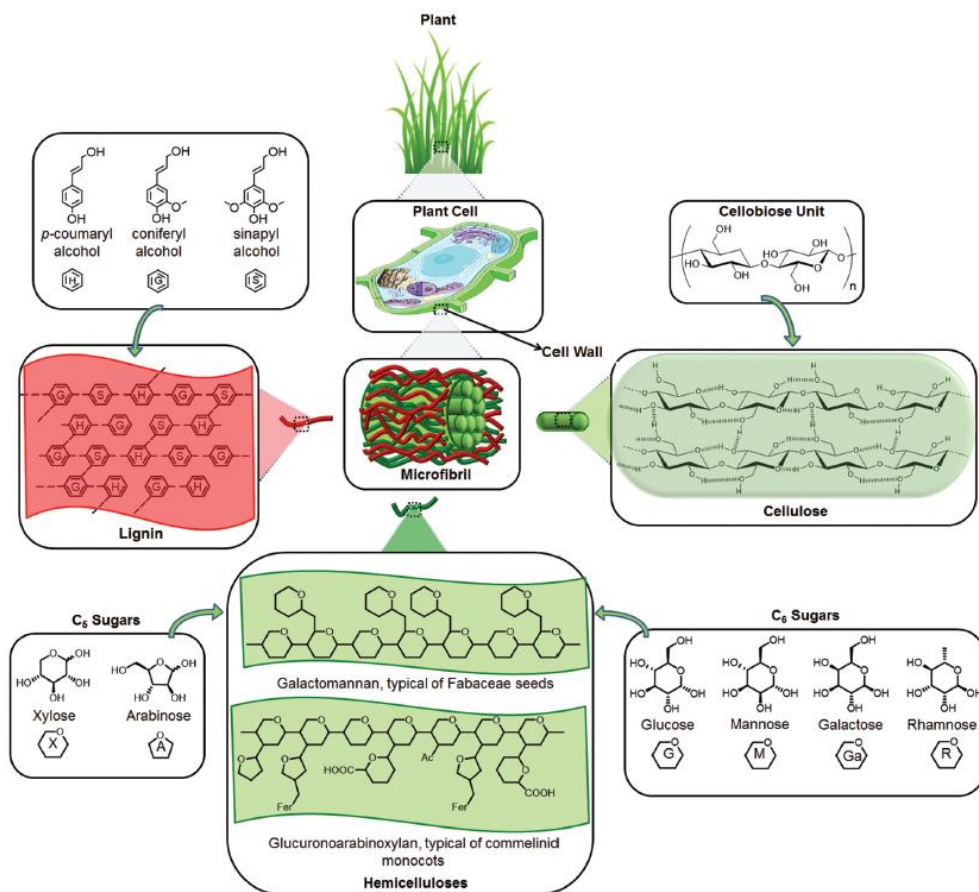


Figure I- 1: Composition and structure of lignocellulose ⁷

I-1-2 Pretreatment and hydrolysis of second generation biomass

Pretreatment of lignocellulosic feedstocks is a crucial step in a biorefinery. Since lignin is considered to be a natural inhibitor of biodegradation of cell wall constituents, the objective of pretreatments is to separate cellulose, hemicellulose and lignin. This will improve the exposure of cellulose to enzymes that will conduct its depolymerization,¹⁷ consequently increasing the efficiency of monosaccharides production. Several biomass pretreatment methods exist, such as steam explosion, alkaline hydrolysis with NaOH, KOH, Ca(OH)₂ or organosolv hydrolysis using methanol, ethanol or acetone, acid hydrolysis with phosphoric, sulfuric, or hydrochloric acid and many others. Among these pretreatments, acid hydrolysis and steam explosion are considered to be the most efficient and cost-effective methods. A possible process scheme of a lignocellulosic hydrolysis is presented in *Figure I- 2*. We study here the example of a steam explosion pretreatment method coupled with acid hydrolysis, followed by an enzymatic hydrolysis.

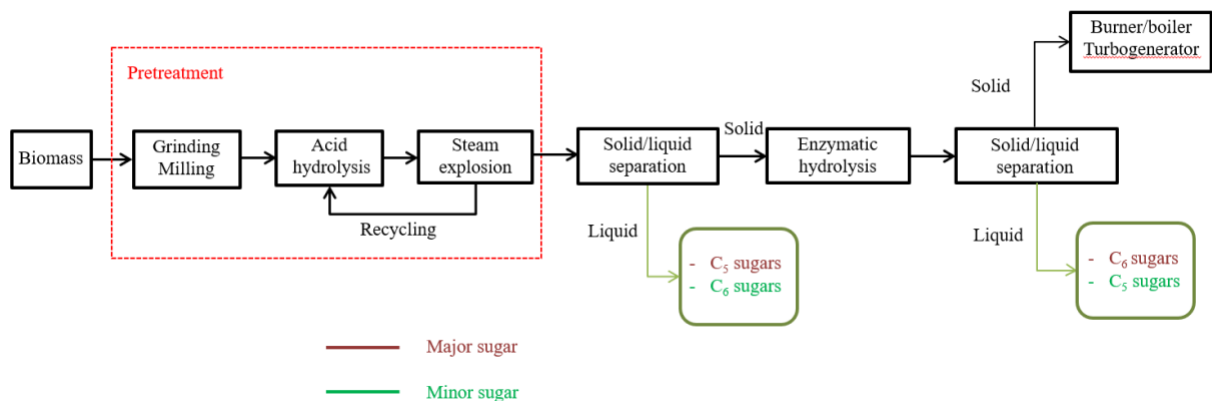


Figure I- 2: Steam explosion-based process diagram of lignocellulose hydrolysis

The biomass (wooden pieces, corn straw) is grinded or milled at first to reduce the particles size. Then it is soaked in an acidic aqueous solution. Here, sulfuric acid is used as the common agent for this application. The obtained pulp (impregnated biomass) is then pressed through a plug screw¹⁸ to feed a pressurized reactor where saturated steam is injected. An acid hydrolysis takes place thanks to the high temperature and pressure, decomposing lignocellulose into cellulose, hemicellulose and lignin and simultaneously hydrolyzing up to 90 % of hemicellulose to its corresponding monomeric sugars.⁷ Steam condenses under high pressure wetting the material which exits the reactor (atmospheric pressure at the reactor outlet) through a small nozzle. The decompression causes the sudden evaporation of condensed moisture inside the material, breaking down more inter and intra-molecular bonds¹⁹ and therefore leaving cellulose more exposed to the next enzymatic hydrolysis step.²⁰

At the downstream of the pretreatment, a solid fraction rich with cellulose, lignin and some residual hemicellulose is obtained along with a liquid fraction which is the hemicellulose hydrolysate. This hydrolysate is a mixture of mainly pentoses (xylose and arabinose) and hexoses (glucose, mannose, and galactose). Zrimbardi et al. reported that after an impregnation of corn stover with sulfuric acid (3 %wt.) followed by steam explosion at 200 °C, the liquid fraction obtained is composed of 0.9 g glucose, 0.6 g galactose, 7.5 g xylose and 1.3 g arabinose out of 100 g of dry feedstock.²¹

After biomass pretreatment, a solid/liquid separation is performed and the solid fraction feeds an enzymatic hydrolysis reactor while the liquid fraction is potentially available for further purification treatments, sugar isolation, enzyme growth facilities or chemical conversion

(detailed below). Cellulose withstands the physicochemical treatments because of its high crystallinity, and for that reason it is preferably hydrolyzed by enzymes called cellulases. In reality several enzymes are often used in combination and can be classified according to their action into three groups: endoglucanases, exoglucanases and β -glucosidases. Endoglucanases target the amorphous regions of cellulose and cut the chains into smaller oligosaccharides, exoglucanases produce cellobiose (disaccharide of two glucose molecules) and β -glucosidases cleave the glucosidic bond of cellobiose to obtain glucose.²² The products of the reaction are glucose and/or cellobiose molecules, depending on the amounts and efficiency of the various enzymes. Enzymatic hydrolysis is an alternative to acid hydrolysis that allows operating under mild conditions (temperature 45 – 50 °C).²⁰ The enzymes can be produced from the sugars recovered after the pretreatment.

At the enzymatic hydrolysis downstream and after a solid/liquid separation, a sugar juice is obtained composed of a mixture of pentoses and hexoses, but primarily hexoses in particular glucose. Zimbari et al. found that after 48 h of enzymatic hydrolysis of the water insoluble fraction resulting from the pretreatment of corn stover, the released glucose out of 100 g of dry feedstock is 32.3 g and the released xylose is 1.3 g.²¹

The remaining solid fraction rich in lignin serves as fuel in the boiler thanks to its high caloric input. The chemical valorization of lignin remains a challenge at the moment because it is composed of complex aromatic molecules that are hard to extract,²³ although a number of research have been devoted to its conversion.²⁴

The two main streams of sugars obtained from the liquid fraction are ready to be either fermented to bio-ethanol in the case of a classic biorefinery application or possibly converted into added-value chemicals by the chemical transformations, detailed in the next paragraph. Nevertheless, at this stage several purification steps are necessary, as the mixture contains a considerable number of impurities produced during the various treatments. These impurities can either be phenolic compounds resulting from the degradation of lignin, furan aldehydes generated from the dehydration of sugars in acid conditions and carboxylic acids produced from the further decomposition of furans.²⁵ Several purification technics have been tested including chemical additives,²⁶ precipitation with lime or others bases, adsorption on activated carbons, resins and liquid-liquid extractions.

I-1-3 Conversion of sugars to chemicals

High added-value platform chemicals produced from sugars can be obtained via fermentation or catalytic conversion. Several reviews counted hundreds of compounds derived from lignocellulose. Isikgora and Becer⁷ summarized the majority of the possible products with a special focus on their potential to be transformed into polymers, Rosales-Calderon and Arantes²⁷ shortened the list and target on derivatives with commercial potential and high readiness to integrate a traditional bioethanol refinery. As mentioned, many different conversion products can be obtained starting from sugars, however, two different classes are nowadays considered particularly promising: furanic compounds and glycols.

The two most interesting furanic compounds are furfural and 5-Hydroxymethylfurfural (5-HMF) which are the result of a triple dehydration of xylose to obtain furfural and glucose or fructose to form 5-HMF. The reactions are performed in acidic conditions where homogeneous or heterogeneous catalysts can be employed.^{28,29} Furfural is used for the recovery of lubricants for cracked crude, in the production of adhesives and as a flavor chemical.²⁷ Moreover, furfural can be transformed as shown in *Figure I- 3* into 2-methylfuran, 2-methyltetrahydrofuran, levulinic acid and furfuryl alcohol, which is at the same time a monomer for the production of poly(furfuryl alcohol), a chemical resistant polymer.

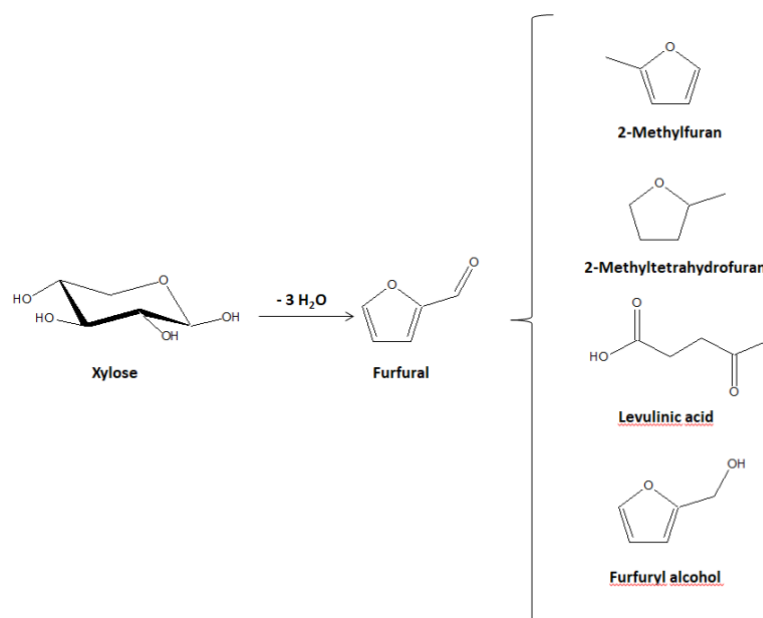


Figure I- 3: Conversion of xylose to furfural and furfural derivatives

Figure I- 4 presents the conversion of hexose (glucose or fructose) to 5-HMF and gives the most important 5-HMF derivatives. Furan-2,5-dicarboxylic acid (FDCA) is a very promising chemical capable of replacing terephthalic acid used in the production of polyethyleneterephthalate (PET) and polybutyleneterephthalate (PBT). The reduction of 5-HMF can lead to products such as 2,5-bis(hydroxymethyl)furan (2,5-BHF) and 2,5-dimethylfuran (2,5-DMF). 2,5-BHF alcohol can react with FDCA to form polyesters,⁵ 2,5-DMF is considered to be an alternative fuel for the future.²⁹

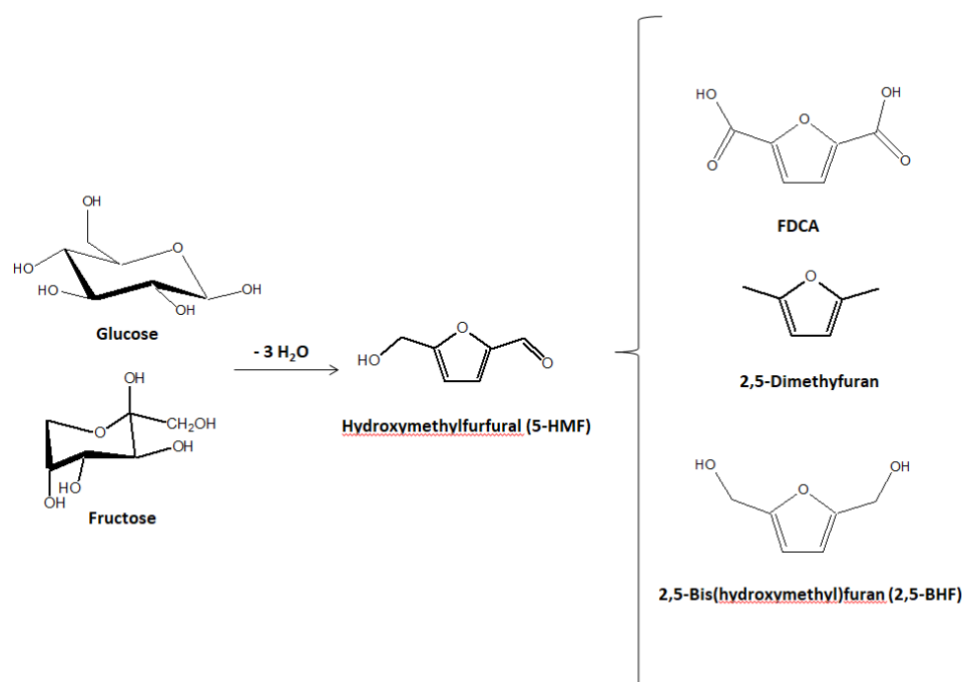


Figure I- 4: conversion of glucose/fructose to 5-HMF and 5-HMF derivatives

Glycols are another set of interesting chemicals obtained from sugars, in particular Ethylene glycol (EG) and 1,2-propylene glycol (1,2-PG) that have a large market demand, especially for EG. They are widely used for the synthesis of polyesters, antifreeze, and fine chemicals.³⁰ EG and 1,2-PG are usually produced together with different selectivities depending on the initial sugar or sugar alcohol (sorbitol or xylitol for example), the catalyst choice and the operating conditions. The main reaction routes to obtain glycols from glucose and xylose are given in Figure I- 5. It has been reported that using tungsten-based catalysts, and after a retro-aldol step followed by a hydrogenation reaction of glucose, high selectivity to EG around 70 % could be obtained.³¹ However, the hydrogenolysis of xylose or xylitol have a maximum selectivity around 30 % to EG.^{32,33}

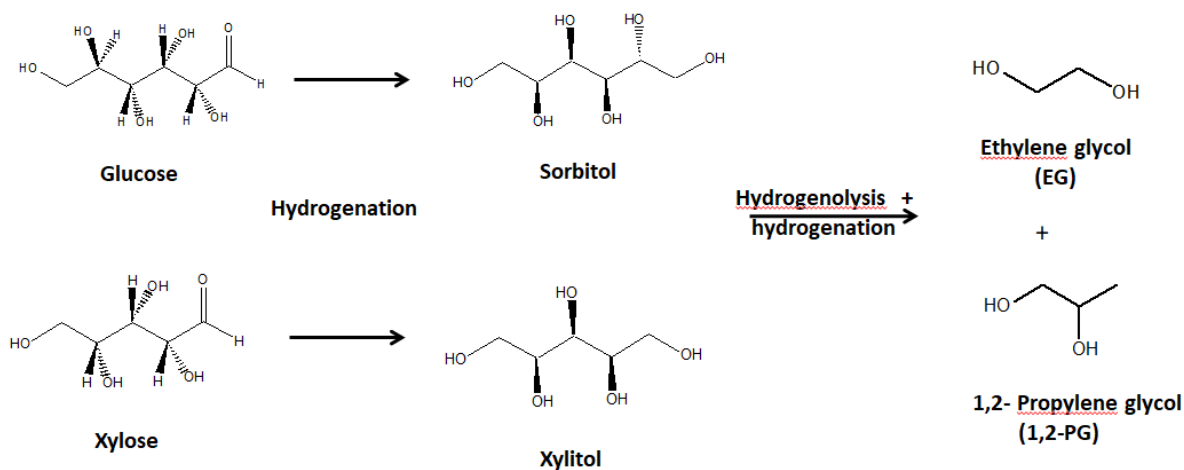


Figure I- 5: Conversion of sugars to glycols

As mentioned, higher selectivities towards EG are obtained from glucose as the initial substrate thus the importance of working with single-sugar feed to produce EG with higher yields. Separating the sugar mixtures and reacting one type of monosaccharide not only improves the yields, but also widens the range of the possible chemicals that can be obtained from fermentation or catalytic conversion.

Conclusion

Lignocellulose is the most abundant source of sugars in nature. Cellulose is a biopolymer of glucose and hemicellulose which are composed of C₅ (xylose and arabinose) and C₆ (glucose, mannose, and galactose) sugars. The recovery of these sugars might be done thanks to the biorefinery concept where lignocellulose undergoes a series of treatments in order to fractionate into cellulose, hemicellulose and lignin. After that, the cellulose is depolymerized into glucose by the mean of enzymatic hydrolysis. Overall, the lignocellulose pretreatment and hydrolysis procedure yield to mainly two streams of solubilized carbohydrates in water:

1. mixture containing mostly C₅ sugars, primarily xylose, with minor amounts of C₆ sugars obtained after the pretreatment,
2. mixture containing mostly C₆ sugars, primarily glucose, with minor amounts of C₅ obtained after the enzymatic hydrolysis.

Although some microorganisms can be genetically modified to be able to digest a mixture of sugars and produce biofuels like bioethanol, chemical valorization, as illustrated in a few examples above, will in most cases benefit from being carried out on a separate substrate of

each type of sugar. This brings about the necessity of the separation of sugars within an aqueous mixture to obtain independent streams of each sugar. The separation can occur after the pretreatment, where pentoses are predominant in the hydrolysate, or after the enzymatic hydrolysis where the obtained hydrolysate is rich with glucose, and thus might require differentiated treatments adapted to the main sugar present in the mixture.

The following chapter will detail the different structures and the biochemistry of carbohydrates before focusing on their separation.

I-2 Monosaccharides

Monosaccharides or simple sugars are molecules composed of carbon, oxygen, and hydrogen atoms. According to the number of carbon atoms in the molecule (from 3 to 7), they can be classified into trioses, tetroses, pentoses, hexoses, and heptoses as shown in *Figure I- 6* and *Figure I- 7*. Additionally, monosaccharides can be classified into aldoses if an aldehyde group (CHO) is present in the acyclic form or ketoses if there is a ketone (carbonyl) group (CO) in the linear form. Each sugar is characterized by its number of carbon atoms, the type of its functional group, and the orientation of the hydroxyl groups concerning to the carbon backbone, *ie* the configuration of each stereogenic center. A two-dimensional representation of linear monosaccharides called the Fischer projection is used which follows two specific rules: the carbon chain is drawn vertically with the carbonyl group at the top, from which the numbering of carbon atoms starts, and the vertical lines represent bonds below an imaginary plane and the horizontal ones represent bonds below the plane.

Pentoses and hexoses will be described in detail in this paragraph since they are the main constituents of lignocellulosic biomass and the sugars of interest for this PhD project. Their Fischer representations are put in rectangles in *Figure I- 6* and *Figure I- 7* respectively. Xylose and arabinose are both aldopentoses (C5-CHO), glucose, galactose and mannose are aldohexoses (C6-CHO) and fructose is a ketohexose (C6-CO). Each existing sugar has two enantiomers (non-overlapped mirror images), if the OH group on the bottom of chiral carbon points to the right in Fisher representation, it is referred to as D- (from Latin *Dextro*), if it points to the left, it is referred to as L- (*Levo*). Most monosaccharides have the D- configuration in nature, some exceptions are arabinose.

However, monosaccharides do not remain in the linear form, intra-molecular hemiacetal group for aldoses and hemiketal group for ketoses are created to close the chain and form cyclic structures from the reaction of the carbonyl group with one of the hydroxyl group side chain. *Figure I- 8* shows the ring formation for glucose, by addition of a hydroxyl group on the carbon of the carbonyl group to give a C-O bond and the double bond of the aldehyde function becomes a C-OH group. This results into the transformation of the achiral aldehyde carbon atom into a chiral hemiacetal carbon atom and therefore the formation of two new isomers called anomers. If the hydroxyl of the anomeric carbon points to the right, the anomer is called α , if it points to the left it's called β .

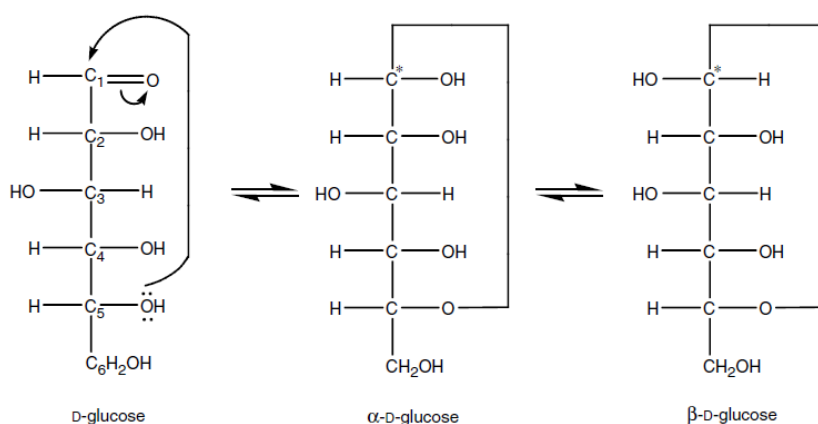


Figure I- 8: Formation of pyranose ring for D-glucose³⁵

If the hydroxyl bound to the fifth carbon of the open chain reacts with the carbon of the carbonyl group, a six-membered ring is formed called pyranose ring. In case of cyclization between the hydroxyl bound to the fourth carbon and the carbon of the aldehyde function, a five-membered ring is formed known as furanose ring and both forms (α and β) are obtained. All the forms of glucose also called tautomers are illustrated in *Figure I- 9*.

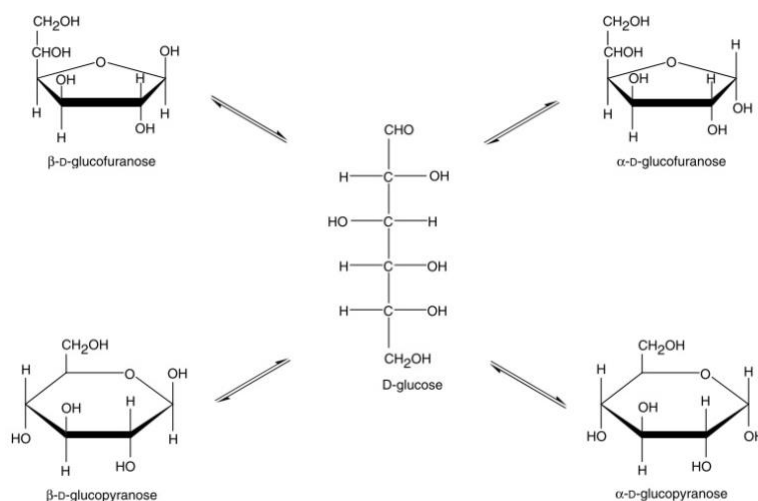


Figure I- 9: Tautomeric forms of D-glucose ³⁵

The same mechanism of ring formation applies to the rest of the aldohexoses and aldopentoses for ketohexoses like fructose. For example, the anomeric carbon in the linear form is where the ketone group is present. The hydroxyl oxygen atom bound to the fifth or the sixth carbon will react with the anomeric carbon to form the furanose and pyranose cycles respectively. Similar to glucose, the cyclization gives two anomers, α and β for each of the pyranose, and furanose rings.

I-2-1 Tautomeric equilibrium

When sugars are dissolved in a liquid solvent, the α and β forms interconvert until equilibrium is established and all the forms (cyclic and linear) are relatively present in the solution with different concentrations. The conversion of one form into another until the equilibrium is reached is called mutarotation and it is characterized by a change in the optical rotation.³⁶ The determination of the concentration of tautomeric components has been conducted using different analytical techniques such as polarimetry,³⁷ FTIR spectroscopy,³⁸ ¹³C NMR and ¹H NMR.^{39–42} Nuclear magnetic resonance techniques are the most convenient and performed methods to study the tautomeric composition of sugars. In fact, performing a proton or carbon NMR on a sugar solution give chemical shifts assigned to specific protons or carbon atoms which makes it possible to identify the present species and quantify them. An example of ¹³C NMR and ¹H NMR spectra of glucose is shown in *Figure I- 10*. The protons belonging to the hydroxyl groups of the anomeric carbons resonate between 4.5 and 6 ppm (4.7 ppm for β -pyranose and 5.5 for α -pyranose), all the other ring protons resonate between 3 and 4.5 ppm. The intensity of the peaks corresponding to the protons of the anomeric carbons is proportional

to concentration of the α -pyranose and β -pyranose forms in the solution, an integration of these peaks gives the composition. The ^{13}C NMR spectra present a chemical shift assigned for each carbon atom, the composition of the solution is determined from the shifts of the anomeric carbons at 91 ppm for α -glucopyranose and 96 ppm for β -glucopyranose in water.

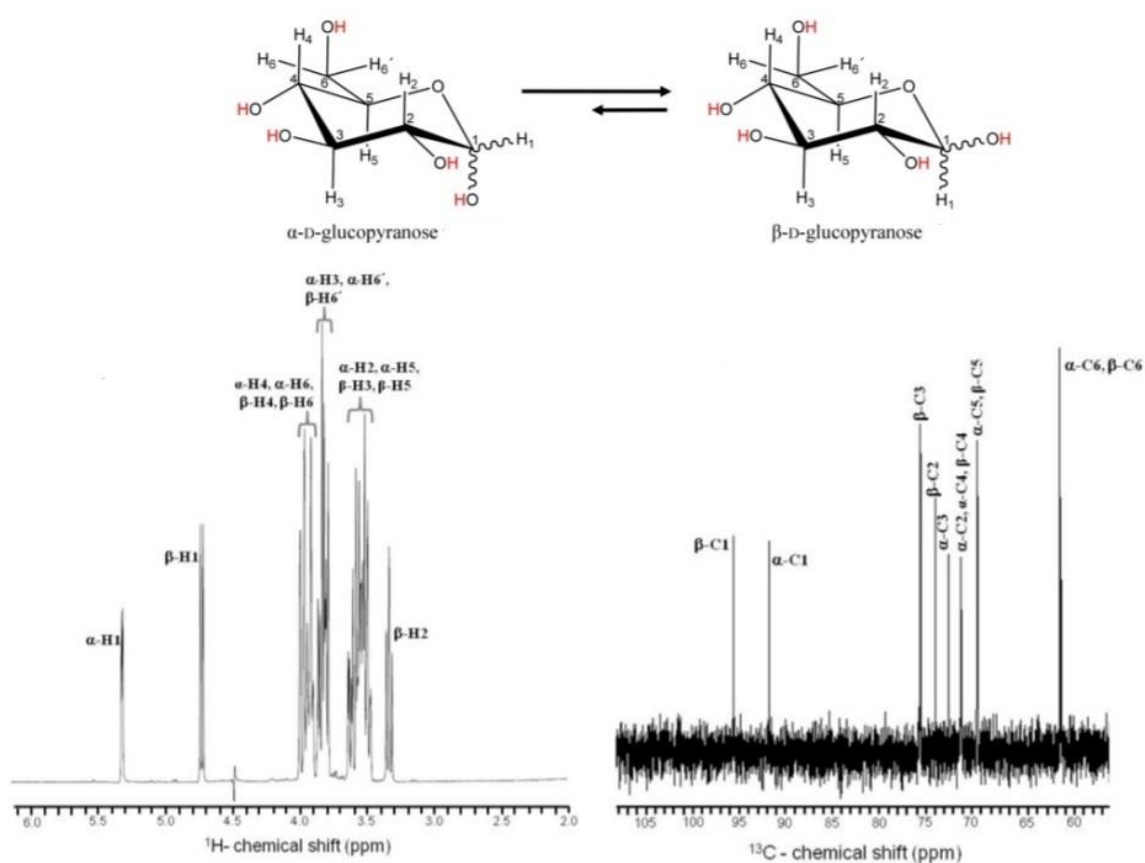


Figure I- 10: ^1H and ^{13}C NMR spectra for glucose in aqueous solution ⁴³

The variation effects of some operating conditions like temperature, concentration and pH on the tautomeric equilibrium have also been studied for certain simple sugars.^{39,44} The tautomeric distribution of a selection of monosaccharides in aqueous solution is given in *Table I- 2*. Regardless the temperature, the pyranose forms (α and β) are the most abundant for most sugars in aqueous solutions, while the open-chain forms are present in very small quantities (< 0.8 %). The β -pyranose form is usually the major tautomer in the solution except for mannose for which the α -pyranose is the main component. Fructose's solution contains primarily β -pyranose forms followed by β -furanose ones. The temperature increases from 20 °C to 31 °C has almost no effect on the composition of glucose and galactose solutions with only a slight change in the distribution (an increase or a decrease of about 2 %). It is not the case for xylose where the concentration of β -pyranose is reduced from 65.2 % to 58.5 % and the concentration of α -

pyranose, β -furanose and α -furanose is increased. Fructose shows the same equilibrium evolution as xylose with the temperature increase, characterized by the decrease of the β -pyranose concentration associated with an increase of the other cyclic and linear forms.

Table I- 2: Tautomeric distribution in aqueous solution ³⁶

Carbohydrate	Temp °C	α -Pyranose %	β -Pyranose %	α -Furanose %	β -Furanose %	Open-chain %
D-Glucose	20	36.4	63.6	—	—	—
	31	38	62	0.5	0.5	0.002
D-Galactose	20	32	63.9	1	3.1	
	31	30	64	2.5	3.5	0.02
D-Xylose	20	34.8	65.2	—	—	
	31	36.5	58.5	6.4	13.5	0.05
D-Fructose	27	—	75	4	21	
	31	2.5	65	6.5	25	0.8
D-Altrose	40	27	40	20	13	
D-Gulose	40	10	88	2		
D-Mannose	20	67.4	32.6	—	—	

The rate of mutarotation increases with an increase in the temperature whether the final tautomeric distribution of the solution will change or not. The mutarotation is spontaneous and slow, it takes several hours to reach equilibrium if sugar is dissolved in water at 20 °C, however, its rate increases from up to 3 times with each 10 °C increase in temperature.³⁵

Le Barc et al.⁴⁵ studied the effect of the sugar concentration on the mutarotation of glucose in an aqueous solution. They found that the concentration has no significant effect on the tautomeric equilibrium composition and a constant rate of mutarotation even at temperature range varying from 30 °C to 45 °C. The authors observed as well, an increase in the mutarotation rate with the temperature but no change in the composition of the solution, which further confirms the studies mentioned above. Barclay et al⁴⁴ found the same conclusions after studying the tautomeric equilibrium of fructose by ¹H NMR.

The pH effect on tautomeric distribution has been also investigated and the variation of pH from 4.8 to 6 was found to have no effect in glucose aqueous solution at 37 °C.³⁹ No significant differences were also found for fructose aqueous solutions even at 50 °C.⁴⁴ Although the pH does not affect the tautomeric composition at equilibrium, addition of acids or bases to the solution increases the rate of mutarotation.³⁵

An important factor that influences the tautomeric composition at equilibrium is the type of solvent used for sugar dissolution. The obtained distribution of pyranose and furanose forms of several sugars dissolved in D₂O, pyridine and DMSO solutions is presented in *Table I- 3*.

Table I- 3: Tautomeric distribution in percentages of sugars in different solutions *D* = D₂O, *P* = Pyridine, *DMSO* = Dimethylsulphoxide (adapted from ref⁴⁶)

Sugar	Temperature (°C)	Solvent	α -pyranose	β -pyranose	α -furanose	β -furanose
Ribose	30	D	24	52	9	15
	30	DMSO	16	55	6	23
Xylose	31	D	36.5	63		<1
	25	P	45	53	1	1
Galactose	31	D	30	64	2.5	3.5
	25	P	33	48	7	12
Glucose	30	D	34	66		
	30	DMSO	44	56		
Mannose	44	D	65.5	34.5	0.6	0.3
	116	P	78	22		
	116	DMSO	86	14		
Fructose	30	D	2	70	5	23
	80	D	2	53	10	32
	33	P	5	43	15	35
	33	DMSO	5	26	21	48

A D₂O solution of xylose contains 63 % β -pyranose and 36.5 % α -pyranose forms but the composition shifts to 53 % β -pyranose and 45 % α -pyranose when pyridine is used as a solvent. The same trend is observed for galactose, when switching from D₂O to pyridine solution but with a considerable increase in the furanoses forms. The DMSO glucose solution is richer in α -pyranose forms than the D₂O solution, but the β -pyranose is the most abundant in both solutions. At around 30 °C in fructose solutions, the percentages of β -pyranose are 70 %, 43 % and 26 % and β -furanose are 23 %, 35 % and 48 % in D₂O, pyridine and DMSO respectively. We can see here a change in the tautomeric equilibrium where β -furanose becomes the predominant tautomer in the DMSO solution.

I-2-2 Conformation of monosaccharides

When the pyranose and furanose rings are drawn in three-dimensional space using the correct bond lengths and angles of the tetrahedral carbons, the obtained structures are not flat in contrast to the Fischer projection. The free rotation of the sigma bonds between two carbons and a carbon and an oxygen atom in the ring are responsible for the formation of numerous shapes in space. The ring's shape, the position of the hydroxyl groups and the hydrogen atoms in the ring are called conformations. *Figure I- 11* illustrates the conformations of the pyranose and furanose rings. These conformers (isomers with different conformation) can be identified as the chair (C), boat (B), half chair (H), skew (S), envelope (E) and twist (T) forms. Each letter is preceded by the number of carbon atom situated above a reference plane of the ring and followed by the number of the atom below that plane.

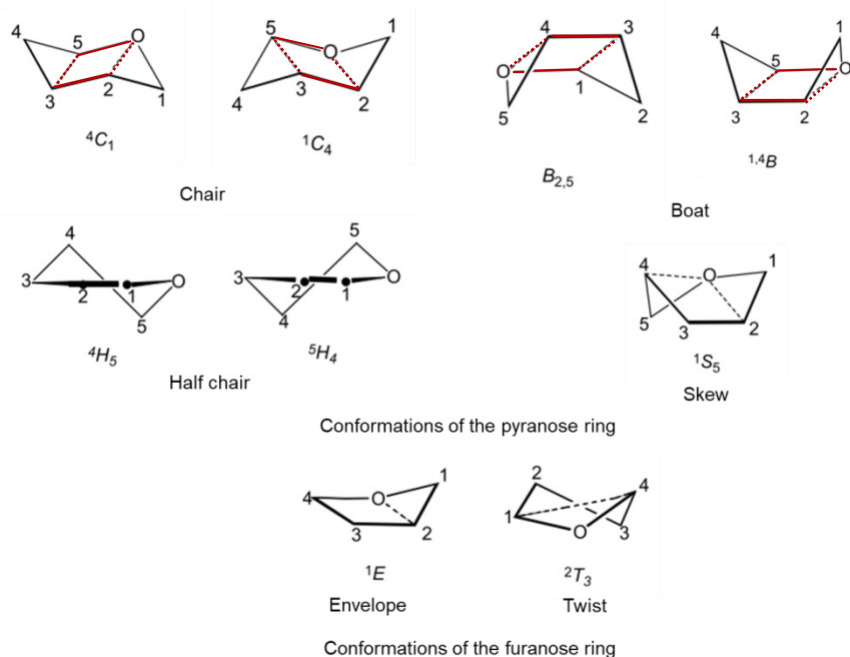


Figure I- 11: Conformations of the pyranose and furanose rings, reference plans for chair and boat conformations are indicated in red (adapted from ref³⁶)

Out the ensemble, the most stable or favored conformer is the one with the minimum free energy. Free energy is determined according to the attractions and repulsions between atoms resulting from van der Waals forces, polar and apolar interactions, steric interactions, hydrogen bonds and solvation effects. One of the methods used to determine the ring conformation of monosaccharides is ¹H NMR. It has been found that the protons at the equatorial positions appear at lower fields compared to axially oriented ones which allows to differentiate between different conformers.⁴⁷

When glucose is dissolved in water and after the tautomeric equilibrium is established, the preferred conformer obtained is chair, precisely 4C_1 for the alpha and beta pyranose rings.³⁶ The reference plan for this conformation is O-C₂-C₃-C₅ where C₁ is placed below the plan and C₄ above as illustrated in *Figure I- 12*. The 4C_1 form for β -glucopyranose is characterized by the positioning of the hydroxyl groups within the plane of the ring (equatorial positions), whereas all hydrogen atoms are perpendicular to the plane (axial positions). The α -glucopyranose has the same conformation as β -glucopyranose with the exception of the anomeric hydroxyl (hydroxyl on the first carbon) which is placed at the axial position. The preferred conformation of xylose is 4C_1 as well, the reference plane is the same as glucose and all the hydroxyl groups are in the equatorial position except for the α -xylopyranose which have an axial -OH on the anomeric carbon.⁴⁷

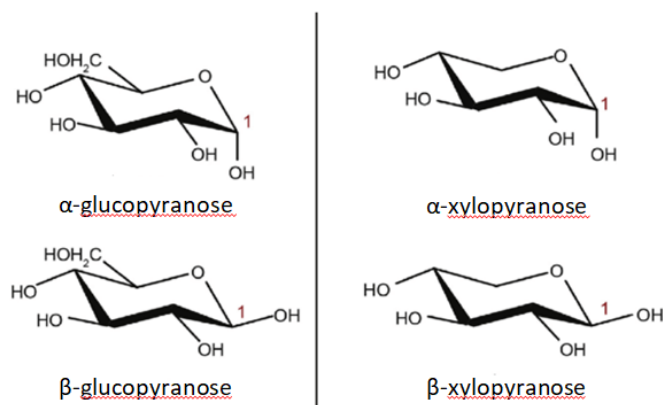


Figure I- 12: 4C_1 conformations of the pyranose forms for glucose and xylose

Conclusions

Monosaccharides can be classified according to their number of carbon atoms and their functional group whether it is an aldehyde or ketone function. In nature, sugars exist in the cyclic form and when dissolved in a solution, an equilibrium is established between five forms called tautomers which are β -pyranose, α -pyranose, β -furanose, α -furanose and the linear form. The distribution of the tautomers depends primarily on the type of sugar and the solvent used, but the temperature is found to have an effect on the equilibrium composition of some sugars like xylose and fructose. The concentration and the pH do not have an effect on the final distribution.

Each sugar has a special conformation in space characterized by the form of the ring, the orientation of the hydroxyl groups, and the position of the hydrogen atoms. The orientation

sequence of the hydroxyl groups in particular (equatorial-equatorial, axial-equatorial, or axial-axial) is an important factor in the molecule stability and its reactivity thanks to the formation of complexes with ions which will be discussed in the next chapter.

I-3 Adsorption

I-3-1 Generalities about adsorption

Adsorption is a process where molecules from a fluid phase called adsorbate are fixed on the external and interior surfaces of a porous solid called adsorbent. An adsorption system is composed of the adsorbent, a fluid, and an interfacial layer between them. The IUPAC (International Union of Pure and Applied Chemistry) defines adsorption as the phenomena in which the fluid is brought into contact with the surface of the adsorbent, resulting in the enrichment of one or more adsorbates in the interfacial layer.⁴⁸ Two types of adsorption exist: physisorption when there is weak intermolecular forces between the solute and the adsorbent, and chemisorption when the formation of a chemical bond is involved. Physisorption involves the formation of a monolayer or multilayer, and the adsorption is weak. Chemisorption generally has a more negative enthalpy of adsorption.⁴⁹

Porous materials are used in particular as adsorbents thanks to their wide surface area. *Figure I- 13* shows the different types of pores in a particle.

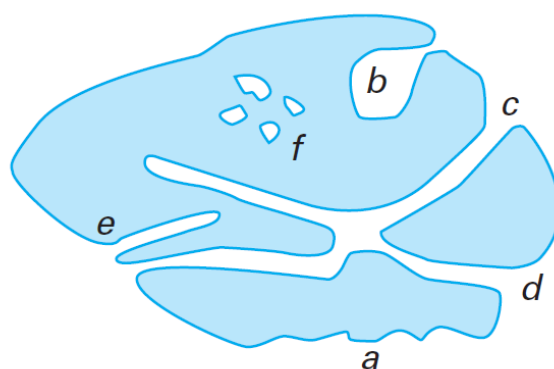


Figure I- 13: Types of pores in a porous material. (f) closed pores, (b, e) blind pores, (c) through pores, (d) interconnectivities between pores and (a) surface roughness.⁵⁰

Roughness (a) can be observed at the external surface, some pores are in connection with the exterior (e, b, c, and d) and others are closed (f). The access to the exterior is possible through

one entry as the case of blind pores (b and e), or through multiple entries (c and d). In general, pores are classified according to their size, micropores have pore diameters smaller than 2 nm, mesopores have pore diameters between 2 and 50 nm and macropores have diameters greater than 50 nm.

I-3-2 Thermodynamics of adsorption

Adsorption is an exothermic process therefore, if we consider working at standard conditions, the enthalpy ($\Delta_r H^\circ$) is negative. It results in the limitation of the degree of freedom of molecules in the fluid phase which means that the entropy ($\Delta_r S^\circ$) is also negative. According to the Gibbs free energy expression (Eq I-1), the free energy ($\Delta_r G^\circ$) can be positive or negative.

$$\Delta_r G^\circ = \Delta_r H^\circ - T \Delta_r S^\circ \quad (\text{Eq I-1})$$

I-3-2-1 Henry's law

Regardless of the adsorption model considered, at low enough concentrations, there is a linear relationship between the concentration of the adsorbate in the fluid phase (we will consider the liquid phase as it is the case of the following study) c (mole per liter) and the specific amount of adsorbed molecules (milligrams per g of adsorbant) q . This linearity is referred to as Henry's law which can be expressed according to (Eq I-2), where K ($\text{mg L g}^{-1} \text{ mol}^{-1}$) is a thermodynamic constant called the Henry constant.

$$q = Kc \quad (\text{Eq I-2})$$

The Henry constant K is a function of temperature and obeys the van't Hoff equation (Eq I-3), where T is the temperature, R the universal constant of ideal gases and $\Delta_r H^\circ$ the molar enthalpy of adsorption. The application of this relationship on several isotherms obtained at different temperatures allows the determination of the enthalpy of adsorption.

$$\frac{d \ln K}{d \left(\frac{1}{T} \right)} = - \frac{\Delta_r H^\circ}{R} \quad (\text{Eq I-3})$$

I-3-2-2 Langmuir isotherm models

Adsorption can be described as a chemical reaction as follows:



A is a sorbate molecule in the fluid phase, S is a vacant site and AS is an adsorbed molecule on an adsorption site.

Langmuir model assumes that molecules are adsorbed at a fixed number of sites, each site can hold only one molecule, all sites are energetically equivalent and there is no interaction between adsorbed neighboring molecules.

Considering $q_s = [AS] + [S]$ is the total number of sites and $\theta = [AS] = q/q_s$ the fractional coverage, the rate of adsorption can be defined as $k_a P(1 - \theta)$ and the rate of desorption as $k_d \theta$, where k_a , k_d are respectively the adsorption and desorption rate constants, $(1 - \theta)$ is the fraction of unoccupied sites and P the pressure. At equilibrium, the rate of adsorption and desorption are equal and gives the following relation.⁴⁹

$$k_a P(1 - \theta) = k_d \theta \quad (\text{Eq I-4})$$

The commonly known Langmuir isotherm (Eq I-5) is obtained by rearranging (Eq I-4)

$$\frac{q}{q_s} = \frac{bP}{1+bP} \quad (\text{Eq I-5})$$

with $b = k_a/k_d$. (Eq I-5) is the isotherm for gases, for liquids the pressure P is replaced by the concentration C (mole per liter) (Eq I-6)

$$\frac{q}{q_s} = \frac{bC}{1+bC} \quad (\text{Eq I-6})$$

To fit the Langmuir model to experimental data, (Eq I-5) or (Eq I-6) is linearized and $1/q$ is plotted against $1/C$ (for liquids), b (liters per mole) and q_s (milligrams per gram) may be determined from the slope and intercept. It is also important to note that at low coverage (low concentrations or pressures), Langmuir model approximates the Henry's Law.

(Eq I-5) and (Eq I-6) represent isotherm equations for a single component, a modified model can be used in case of a multicomponent system containing N adsorbates A_j (Eq I-7).⁵¹

$$q_i = \frac{q_{si} b_i C_i}{1 + \sum_{j=1}^N b_j C_j} \quad (\text{Eq I-7})$$

where i and j are indexes for each component in the system.

I-3-3 Adsorbents

I-3-3-1 Faujasite-type zeolites

Zeolites are crystalline aluminosilicates porous materials whose structures are formed by tetrahedra TO_4 where T is a silicon or an aluminium atom. Each tetrahedra is linked with another one having an oxygen atom in common which creates a T-O-T succession responsible for the formation of a structured microporous network. This network is composed of internal voids such as pores, channels and cavities giving the material with a large surface area. The silicon tetrahedra composing the zeolite are electrically neutral but when Si^{4+} atoms are replaced by aluminum atoms Al^{3+} , the structure becomes negatively charged. The Lowenstein's rule states that two or more aluminum tetrahedra cannot be directly connected.⁵² The aluminum tetrahedron generate a negative charge that must be compensated by cations to achieve the electroneutrality of the material. These cations can be replaced by other ones (Na^+ , K^+ , Ba^{2+} , Cu^{2+} , Ni^{2+} , Li^+ , Cs^+ , Sr^{2+} , etc.) giving to the zeolites their ion exchange property. Ion exchange may change the selectivity, adsorption or catalytic activity of zeolites, therefore it is possible to adjust the application using this feature.⁵³

The combination of the building blocks TO_4 creates secondary complex blocks which will be linked to form cages and channels. A variety of existing (experimental and/or theoretical) structures, assigned with a three-letter code by the Structure Commission of the International Zeolite Association is available online at the Database of Zeolite Structure.⁵⁴ The updated number of zeolite framework types reached a total of 226 and it evolves every year.

In faujasite zeolites, the assembly of six 4-membered-rings and eight 6-membered rings secondary blocks leads to formation of the sodalite cage (or β -cage). This polyhedron is composed by fourteen faces which delimit an inner space of 0.64 nm and the aperture of the 6-membered ring is 0.22 nm. Another complex building block in the faujasite structure is the hexagonal prism (D6R for Double 6 Rings) which is formed by two parallel 6-membered rings linked with six oxygen bonds. The linkage of the sodalite cages through the double six-rings creates the faujasite framework. This also creates a large cavity called supercage with an internal diameter of 1.3 nm which is accessible through a 12-membered window with a diameter of 0.74 nm.⁵⁵ The formation of a supercage from the primary building blocks is illustrated in *Figure I- 14*.

Faujasites can be classified according to their Si/Al ratio. when the ratio is between 1 and 1.5, the zeolite is called X. Faujasites with a ratio higher than 1.5 are denoted by Y type. As mentioned above, to achieve the electroneutrality of the zeolite, countercations must be placed. *Figure I- 14* shows the sites that the cations occupy in a faujasite. Sites I and I' are located in the hexagonal prism, sites II and II' are at the 6-membered ring between a sodalite and a supercage and sites III and III' are at the surface of the supercage. More details about the location of each site are given in *Table I- 4*.

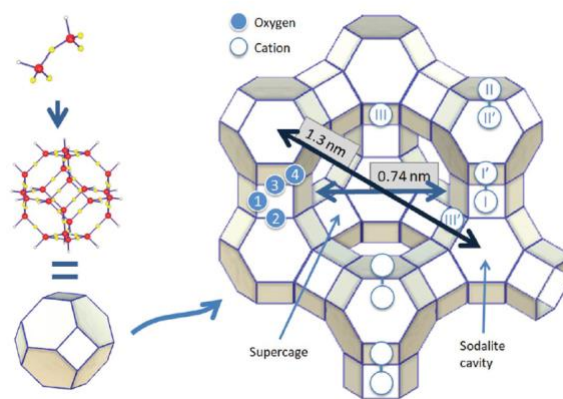


Figure I- 14: Formation of a faujasite structure from the building blocks TO_4 and positions of the counterions ⁵⁶

Table I- 4: Nature, number and location of countercations possible sites in the faujasite structure⁵⁷

Cationic site	Sites/ unit cell	Cavity	Definition
Site I	16	Hexagonal prism	In the hexagonal prism. When in the center of the prism, octahedral coordination with neighbouring oxygen
Site I'	32	Sodalite cage	In the sodalite cage, close to the hexagonal window to the hexagonal prism
Site II'	32	Sodalite cage	In the sodalite cage, close to the hexagonal window to the supercage
Site II	32	Supercage	At the centre of the hexagonal window between the sodalite cage and the supercage.
Site III	48	Supercage	In the supercage, close to a square window between two other square windows.
Site III'	96 or 192	Supercage	In the supercage, close to a square window between two other square windows on the inside wall of the supercage

I-4 Separation of sugars

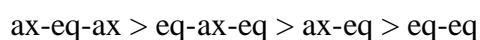
I-4-1 Selectivity in resins

Resins have had a lot of attention for the separation of sugars, since the separation of glucose and fructose, which is currently performed at the industrial scale, uses calcium-exchanged resins.⁵⁸ Calcium gives the highest fructose/glucose selectivity of 1.6 as shown in *Table I- 5* compared to sodium and potassium ones (1.1). Even higher selectivities values up to 2.5 are found in the literature depending on the type of the resin and the degree of cross-linkage.⁵⁹ The choice of cation is crucial in this application where calcium gives the best performance to separate fructose. Although glucose and fructose have the same chemical formula (C₆H₁₂O₆), their stereochemistry is different. Fructose has one ax-eq sequence in α -pyranose and two ax-eq sequences in the β -pyranose ring, these hydroxyl orientations are responsible for the formation of complexes with calcium and thus stronger retention of fructose compared to glucose.⁶⁰

Table I- 5: Selectivities with resins exchanged with sodium, potassium and calcium ⁶¹

Sugars	Na ⁺	K ⁺	Ca ²⁺
Fructose/glucose	1.1	1.1	1.6
Glucose/lactose	1.3	1.3	1.3
Fructose/sucrose	1.7	1.7	2.4

The mechanism responsible for the separation is known to be the formation of a complex between the hydroxyl groups and the metal cations. It has been shown by NMR that the sequence of axial (ax) – equatorial (eq) – axial (ax) of three adjacent hydroxyl groups in pyranose rings give a strong tridentate complex with metal cations.⁶² Goulding et al. confirmed thanks to chromatographic experiments of polyols in exchanged resins that the complexes strength are according to the following order:



The sequence eq-eq is less favored because of the larger distance between the oxygen atoms.⁶⁰ The authors predicted the elution order according to the potential formation of complexes as stated above and compared it to experimental results.

Caruel et al. studied earlier the separation of lignocellulosic sugars and their sugar alcohols using exchanged resins.⁶³ They investigated the cation type effect on the separation with pulse tests, where a selectivity can be calculated from the ratio of capacity factors as defined by the authors. Xylose/glucose selectivities of 1.17, 1.27 and 1.16 are found for Ca²⁺, Sr²⁺ and Ba²⁺ exchanged resins respectively. Strontium shows the highest selectivity but the selectivities are overall low regardless the cation type. *Table I- 6* presents similar observations of low xylose/glucose selectivities using Na⁺, Ca²⁺ and Ba²⁺ exchanged resins (1.13, 1.08 and 1.15 respectively). The type and the size of the cation seems to have no large effect of the separation.

Table I- 6: Selectivities of glucose, xylose and mannose on exchanged strong acid cation (SAC) and strong base anions (SBA) resins⁶⁴

SAC Ca ²⁺				SAC Ba ²⁺			
α	glu	xyl	mann	α	glu	xyl	mann
glu	1	1.08	1.16	glu	1	1.15	1.35
xyl	–	1	1.08	xyl	–	1	1.17
mann	–	–	1	mann	–	–	1

SBA SO ₄ ²⁻				SAC Na ⁺			
α	mann	glu	xyl	α	glu	xyl	mann
mann	1	1.14	1.26	glu	1	1.13	1.12
glu	–	1	1.10	xyl	–	1	1.01
xyl	–	–	1	mann	–	–	1

Lei et al. studied the adsorption behavior of glucose and xylose on exchanged resins with Ca²⁺, K⁺ and Fe³⁺ with different degrees of cross-linking (4 %, 6 % and 8 %) by measuring adsorption isotherms. The authors found that the calcium form is the most suitable adsorbent for this separation and that the 8% cross-linked resin showed the best performance.¹¹ To get closer to industrial conditions, the separation of glucose and xylose was tested with the Simulated Moving Bed (SMB) process and calcium-exchanged resins were used. From a multicomponent feed solution (a hydrolysate composed of glucose, xylose, sulfuric acid, and acetic acid), a recovery of 88 % glucose with 100 % purity was reported.¹³ Further improvements to the stationary phase can be proposed to enhance the recovery.

The cosolvent effect on the stability strength of cation-sugar complexes was also examined. Tiihonen et al. studied the complex formation between Na⁺, Ca²⁺ and La³⁺ and carbohydrates (including glucose, xylose, rhamnose and arabinose) in solvent mixtures by chromatographic measurements.⁶⁵ The authors report that the increasing cosolvent content, ethanol in this case, increases the retention times which reflects a stronger complex stability between the sugars and ions. It is unclear however why the introduction of ethanol has such an effect on the adsorption, sugar-solvent, sugar-cosolvent, cation-solvent, cation-cosolvent and cation-sugar interactions should be investigated more thoroughly to explain these results.

I-4-2 Selectivity in faujasite-type zeolites

Several research projects using faujasites have been conducted to separate monosaccharides and to have a better understanding of the mechanisms implicated in the separation. The most abundant part of the literature concerns the glucose and fructose separation due to its industrial use to produce the High-fructose corn syrup (HFCS), a sweetener from starch.⁶⁶ More recent works have started to investigate the separation of lignocellulosic sugars (glucose, mannose, galactose, xylose, and arabinose) from second generation biomass hydrolyzate.⁶⁷ Two adsorption methods are employed to study the separation, the batch method and the chromatographic one.

When working with zeolites, the effect of two parameters of the chemical structure is usually studied, the Si/Al ratio and the type of the counterion in the zeolite framework. Schollner et al. studied the adsorption of D-glucose, D-fructose, and D-arabinose on K^+ , Sr^{2+} , Ca^{2+} , Ba^{2+} , and La^{3+} ion exchanged X and Y zeolites.⁶⁸ The authors determined and fitted the adsorption isotherms from which they defined a parameter K called the separation factor, the higher the K value, the stronger was the interaction between the monosaccharide and the zeolite. The results are presented in *Table I- 7* and show the effects of Si/Al ratio, the cation type, and the degree of exchange. The number before each zeolite represents the degree of exchange. Glucose has a weak interaction with almost all the zeolite list except for partially and completely potassium-exchanged X zeolites with Si/Al ratio of 1.4. Fructose shows low interactions with exchanged zeolites X but comparing separation factors obtained on zeolite Y (Si/Al = 2.55) exchanged with different cations, the following sequence of increasing interactions is observed:



Despite the similarity of the degree of exchange (63 %), the higher interaction is found between fructose and calcium cations. The authors investigated more this interaction by changing the degree of exchange of Ca^{2+} in a Y zeolite (Si/Al = 2.60) from 26 % to 83 %, the separation factor increased from 0.24 to 3.60 with increasing calcium.

Table I- 7: Separation factors of glucose and fructose in exchanged zeolites X and Y ⁶⁸

zeolite	Si/Al	K	
		D-fructose	D-glucose
NaX	1.2	0.15	0.02
NaX	1.4	0.17	0.02
NaY	2.08	0.08	0.02
NaY	2.55	0.07	0.02
NaY	2.6	0.06	0.02
NaY	2.8	0.03	0.02
55KNaY	2.8	0.67	0.02
KY	1.4	1.62	0.24
20KNaX	1.4	0.35	0.25
44KNaX	1.4	0.43	0.5
59KNaX	1.4	0.52	1.55
KX	1.4	0.84	2.04
82BaNaX	1.4	1.39	0.02
77BaNaY	2.55	1.43	0.02
64LaNaY	2.55	0.4	0.02
64SrNaY	2.55	1.83	0.13
64CaNaY	2.55	2.15	0.02
63CaNaY	2.6	1.54	0.02
63CaNaY	2.42	1.32	0.02
59CaNaX	1.4	0.34	0.02
CaX	1.4	0.3	0.02
26CaNaY	2.6	0.24	0.02
47CaNaY	2.6	0.78	0.02
77CaNaY	2.6	1.95	0.02
83CaNaY	2.6	3.7	0.02

Neuzil et al. studied further the Si/Al ratio and the type of the counterion effects on the separation of fructose and glucose.⁶⁹ Zeolites X and Y exchanged with Na⁺, K⁺, Cs⁺, Mg²⁺, Ca²⁺, Sr²⁺, Ba²⁺ and NH₄⁺ were used to perform chromatographic pulse tests. The authors found that zeolites X and Y exchanged with cesium and magnesium were not selective to either one of the two sugars, the highest selectivity towards fructose in zeolites type X was found with SrX (6.15) and in zeolites type Y with CaY (10) which is coherent with the previous study described above. Surprisingly with CaX, both glucose and fructose eluted at the same time. Although both zeolites X and Y are exchanged with calcium, the highest selectivity was found with CaY and no selectivity was observed with CaX which highlights the importance of Si/Al ratio on the separation.

The separation of lignocellulosic sugars including glucose and xylose in an array of exchanged zeolites X and Y was studied as shown in *Table I- 8*.⁷⁰ Pulse tests of a multicomponent sugar solution were performed as previously described and a high retention volume reflects a strong

affinity. KX, NaX, and NaY have close retention volumes which make them inefficient for the separation of glucose and xylose, CaY shows weak interaction with xylose compared to mannose, arabinose, galactose and glucose. The strongest interactions are found with BaY where a high affinity to mannose is observed. BaX shows a strong affinity to arabinose. Considering only glucose and xylose, the major carbohydrates in the lignocellulosic biomass, BaX and BaY seem to be good candidates for a separation process. Interestingly, the affinity completely changed from BaX to BaY where BaX is selective to xylose and BaY has an affinity to glucose.

Table I- 8: Retention volumes (in mL) of lignocellulosic sugars in zeolites X and Y (Adapted from ⁷⁰)

Zeolite	Inulin	Mannose	Arabinose	Galactose	Glucose	Xylose
KX	0	6.3	7.4	5.8	6	6.6
NaX	0	1.5	2	1	1.5	1
NaY	0	2.7	2.7	2.6	1.7	1.7
CaY	0	2.9	2.9	1.6	1.2	0.7
SrY	0	4	4.1	3.9	2.2	2.2
BaX	0	8.2	16.8	4	3	5.4
BaY	0	37.3	23.6	27.6	14.4	8.9

The effect of the solvent on selectivity has been also investigated. Competitive adsorption of glucose and fructose on CaX was studied with batch experiments by changing the solvent (water, pyridine, methanol, and dimethyl sulfoxide). ⁷¹ The amount of adsorbed carbohydrate is found to be strongly dependent from the solvent used, the fructose/glucose selectivity increased from 1.6 in water to 3.4 in DMSO to 9.3 and 9.1 in pyridine and aqueous methanol respectively. Figure 15 shows the increasing evolution of the selectivity as a function of methanol content in water, it can be seen that CaX became highly selective to fructose just by adding more methanol to the aqueous solution. Similar observations were found when studying the adsorption of sucrose, a disaccharide of glucose and fructose, on zeolites Y. The sugar uptake at saturation increased from 20 mg/g from an aqueous solution to 200 mg/g from 90 % ethanol aqueous solution (v/v) in zeolite Y with an Si/Al ratio of 2.8. ⁷²

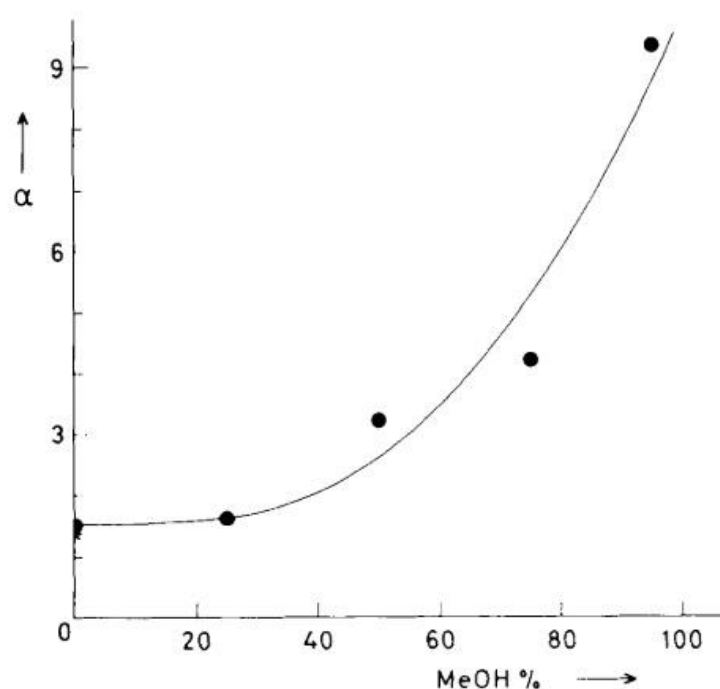


Figure I- 15: Fructose/glucose selectivity from aqueous methanol on CaX (adapted from ⁷¹)

Conclusions:

The separation of glucose and fructose has been extensively researched thanks to the application of fructose in the food industry. Zeolite CaY and calcium-exchanged resin are the most suitable adsorbents for this application. However, the separation of lignocellulosic sugars mainly glucose and xylose is not being equally treated and less research projects address the subject.

It is established that the mechanism behind glucose and fructose separation in resins is a complex formation between hydroxyl groups of sugars and calcium. The orientation of neighboring OH groups seems to define the stability strength of sugar-cation complex. Resins are amorphous materials where the distribution of cations is random. The majority of literature assimilate one cation to one adsorption site and explains the interactions of one sugar molecule with one metal ion.

Zeolite CaY showed greater fructose/glucose selectivities which marks the beneficial effect of confinement. Faujasite-type zeolites provide structured microporous network with well-defined distances between the exchangeable counterions in the supercage. The regular positions of cations in the framework could be the host of multiple specific interactions in analogy to resins.

The latter explanation however is not plausible, CaY showed greater affinity to fructose than CaX where there are more calcium ions in the zeolite and therefore more potential complexation sites. This brings the question of whether there are non-specific interactions that contribute to the obtained affinities/selectivities and are these contributions comparable to specific interactions.

The affinity to each sugar changes as a function of the type of the counterion and its number (*i.e.* the Si/Al ratio). To this day, the effect of the chemical properties of zeolites and the mechanisms responsible for sugar separation, especially glucose and xylose, are still not well known. *Ab initio* Molecular modeling calculations are useful tools to unravel the specific interactions between sugars and zeolites, and this method will be discussed in the next paragraph.

I-5 DFT for sugar adsorption

Few publications are available in the literature that discusses the interactions between sugars and zeolites, the majority of existing works treat the isomerization of glucose to fructose in Sn-BEA zeolite.⁷³⁻⁷⁷ The authors usually work with one sugar taking into account one or two conformers. Cheng et al. studied the adsorption of fructose in zeolite HZSM-5 using clusters and a periodic model. The study showed that Clusters present a major drawback where they fail to represent the electronic environment of zeolite pores.⁷⁸

Yang et al. studied the adsorption of α -D-glucopyranose and linear glucose on BEA (beta-zeolite), FER (Ferrierite), and CHA (Chabazite) zeolites incorporated with Sn, Zr, and Ge. They investigated different modes of interaction of the hydroxyl groups with the adsorption site. Monodentate structures were the most energetically stable structures within all investigated zeolites except for Sn-CHA. Pore topology had a great effect on the adsorption, the authors found high dispersion effects in the order of -218 kJ mol^{-1} for Sn-FER.⁷⁹ The competitive adsorption of glucose and water over Sn centers in Sn-BEA was also studied to understand experimental reactivities.⁸⁰ The solvent effect is a key parameter of the adsorption as mentioned in the previous paragraph, Siepmann et al. explored the adsorption of glucose into zeolite Beta from an aqueous solution using Monte Carlo force field simulation.⁸¹ The authors quantified the enthalpy, entropy, and free energy of transfer of glucose from the aqueous phase to the zeolite and found a positive entropic contribution closely compensating for enthalpy of transfer.

These results were explained by the unstructuring of the hydration shell around the molecules as it leaves the solution. Since sugars are usually dissolved in water, many DFT research projects investigated the hydrogen bonds between carbohydrates and water molecules.^{82,83} Song et al. studied the first hydration shell of glucose, the shell was found composed of fifteen water molecules and three hydration sites around glucose were identified. After adding 15 water molecules, a hydration energy of around -80 kJ mol^{-1} was quantified.⁸³

From these investigations, we can see that three contributions are responsible for sugar adsorption, the first one is the interaction with the zeolite framework manifested by Van der Waals energies. The second one is the complex formation between a specific cation and the hydroxyl groups of the sugar, monodentate and bidentate modes were stated. The third contribution is in relation with the solvent and it seems that it is an entropic one, adding to that the solvent-sugar competition to the adsorption sites.

Although some articles mention the competition between the solvent and sugar, no work is yet to be found treating the competition between two different sugars. Most of the previous studies focus on the catalysis of glucose to fructose in Sn-BEA zeolite, and no study is found addressing the adsorption of sugars in faujasite-type zeolites.

I-6 Literature review conclusions and thesis strategy

Conclusions

Second generation biomass is considered as a valuable renewable feedstock to produce high added-value chemicals. It is composed essentially from sugars, mainly glucose and xylose. Many research projects have been conducted to transform these sugars into platform molecules and design green processes to even compete with oil-based ones. It has been shown that the best selectivities and yields are obtained starting from a pure sugar for the conversion reactions which highlights the necessity of sugars separation at different levels in a biorefinery.

From reviewing the existing literature, very few publications address the separation of lignocellulosic sugars, primarily glucose and xylose, by adsorption methods. The existing works focus on the adsorption with resins by means of either static (“batch”) or dynamic approaches. Faujasite-type zeolites seem to be a promising adsorbent for this application. Their synthesis is mature, and they are used in several industrial separative processes like the production of paraxylene among others. Both glucose and xylose (molar diameters of 0.72 nm and 0.68 nm respectively)⁸⁴ can access the adsorption sites in the supercage by passing through the 12-membered ring (window opening of 0.74 nm). In addition, Faujasites present the possibility of tuning their adsorptive properties thanks to the modulation of their cationic distributions. Thus, a large number of adsorbents can be obtained either by means of ionic exchange operations or the choice of different synthetic procedures leading to different silicon to aluminum ratios. In this way, the type and number of compensating cations is modified. As a consequence, important modifications are induced in terms of size and electrostatic potential leading to specific confined environments. A better understanding of the interaction between the different sugars and the zeolite in the mentioned spaces seems necessary to optimize the separation either in terms of adsorbent features or operating conditions.

Regarding the existing bibliographic information for the glucose/xylose system object of this study, only static and pulse chromatographic tests can be found treating the separation of both compounds. To the best of our knowledge, up to date no dynamic tests with zeolites (frontal or SMB) are available. Nevertheless, based on the more widely studied separation of glucose and fructose, the main guidelines governing sugar separation can be drawn. Thus, as expected, the chemical composition of zeolites affects the selectivity and therefore on the separation efficiency. When looking at the nature of the adsorptive interactions at the origin of the selective behavior, complex formation plays a major role in defining the affinity towards one type of

sugar. Nevertheless, the link between the adsorbent features (mainly in terms of composition) and the selective behavior seems not be fully understood. Thus, significant progress seems necessary to rationalize the global effect of confinement or determining the relative weights of specific and nonspecific interactions. In the same direction, the very limited amount (to the best of our knowledge) of dedicated molecular studies (particularly DFT or GCMC simulations) confirms the room for improvement in the optimization of the separation conditions between glucose and xylose.

The study of interactions with DFT between sugars and zeolites, precisely between glucose/xylose and faujasite-type zeolites, does not exist to the best of our knowledge. Most articles deal with the catalysis of glucose or fructose in Sn-beta zeolite and only one or two conformers are considered (α -pyranose and β -pyranose). The understanding of the modes and strengths of interactions could help to understand the experimental affinities/selectivities and design a more performant adsorbent.

Strategy

The followed strategy for this thesis consists in studying the adsorption of glucose and xylose in different faujasite-type zeolites by combining experimental and theoretical approaches.

- Experimental section:

Serval adsorbents will be prepared by an ionic exchange procedure and will be then characterized. In order to understand the chemical composition effect on the adsorption and the separation, breakthrough tests (experiments close to an industrial separation) will be performed. To record quick breakthrough curves, online Raman spectroscopy efficiency will be evaluated.

Single component adsorption isotherms will be measured to study the thermodynamics of the systems and to understand the nature of the sugars-zeolites interactions and their strengths. The influence of the operating conditions is evaluated, temperature and cosolvent addition effects are investigated.

In the objective of determining the tautomeric distribution of glucose and xylose in adsorbed phase and compare them to the distribution in the liquid phase, liquid and solid-state NMR experiments will be performed.

- Theoretical section:

The adsorption study with molecular modeling (DFT) will describe the interactions between every conformer of glucose and xylose in different exchanged zeolites models. These calculations will allow to determine dispersion contributions and compare adsorption free energies.

To get closer to the experimental system, Grand Canonical Monte Carlo (GCMC) simulations will be performed. These calculations will take into account the solvent effect on the adsorption of sugars. In addition, the competitive adsorption between glucose and xylose in presence of water will be explored.

Chapter II: Online Raman spectroscopy for breakthrough experiments of sugars

In this PhD project, a breakthrough unit for the adsorption study of liquids was used. A quick and reliable solution was preferable to obtain breakthrough curves. For this purpose, an online Raman spectrometer was installed to record the concentrations at the column's outlet. In the following chapter, the efficiency of Raman spectroscopy to monitor breakthrough curves will be investigated. Univariate and chemometric models quality and robustness will be discussed compared to the reference off-line technique, which is High-performance liquid chromatography (HPLC).

II-1 Introduction

Lignocellulosic biomass is considered as valuable renewable feedstock to produce fuels and chemicals.^{27,85} It is composed of three main constituents, (i) cellulose a polymer of glucose molecules, hexoses ($C_6H_{12}O_6$), (ii) hemicellulose a polymer chain of several pentoses ($C_5H_{10}O_5$), and hexoses such as mannose, arabinose, and xylose, (iii) lignin a polyphenolic compound.⁷ The composition differs from one vegetal specie to another, but overall glucose and xylose are the major monosaccharides in lignocellulosic biomass.⁷ It is valuable to extract pure single monosaccharides to convert them into high added-value chemicals. Reactions starting from a pure sugar yield better conversion rates and higher selectivities towards the desired products, such as ethylene glycol from glucose transformation or furfural obtained from xylose.^{29,30} A separation step is therefore necessary. Nanofiltration on piperazine-based membranes is reported in the literature as an efficient method to separate glucose and xylose.^{86,87} However, chromatographic adsorption (with a Simulated Moving Bed) is employed at an industrial scale to separate glucose and fructose to produce high-fructose corn syrup (HFCS) for the food industry.^{58,66} Compared to nanofiltration, the SMB process is more efficient and can achieve 99.9 % of purity while the first does not exceed 99.4 %⁸⁸ Separation based on adsorption has been investigated in literature for many monosaccharides and disaccharides.^{61,89,90} Two methods are mainly used for adsorption experiments. The first is batch tests, which is a simple way to study the adsorption capacity of different adsorbents by mixing a solid with a sugar solution over a fixed time and constant temperature. The concentration variation is

measured before and after adsorption occurred.^{53,91} The second way is known as breakthrough experiment, which consists in pumping the feed solution through a fixed bed (column filled with an adsorbent) and recording the concentration profile at the column outlet. Plotting the concentration as a function of time results in breakthrough curves, from which valuable information about the adsorption process can be explored like thermodynamic parameters (selectivity and capacity) and mass transfer coefficients.⁸ Determination of the first statistical moment in particular allows to calculate the adsorbed amount in an adsorbent and gives also an assessment to the height of a theoretical plate (HETP) in a fixed bed.⁴⁹ In general, offline analytical methods are especially used to measure the concentration of the adsorbed species. However, High-performance liquid chromatography (HPLC) is still considered as the reference technique for frontal adsorption tests in the liquid phase thanks to its robustness and reliable results. Nevertheless, it is costly in consumables and time analysis. Online techniques are often an alternative for this kind of application, they provide quick breakthrough curves ready to be analyzed. For single component sugar aqueous solution, online refractive index (RI) detectors were used to study the adsorption of sugars (glucose or fructose) for breakthrough experiments.^{8,92} This method is limited for monitoring sugar mixtures since glucose and fructose have the same refractive indexes regardless of the concentration, off-line HPLC is then used to obtain the sugar concentration.⁹³

Online spectroscopy is adventitious compared to offline analysis in breakthrough tests application, it provides quick reliable data ready to be treated and especially it is cost-effective due to the reduction of consumables usage. Optical spectroscopy in particular is a powerful tool for online monitoring, identification and quantification of chemicals in complex systems.⁹⁴ Fourier-transform infrared spectroscopy (FTIR), Mid-infrared spectroscopy (MIR) and Near-infrared (NIR) spectroscopy for instance have found large applications in bioprocess, medical or pharmaceutical fields thanks to their advantages such as nondestructively, rapidity, robustness and simple sample preparation.⁹⁵

Raman spectroscopy in particular showed promising results in analyzing lignocellulosic components. The calibration is not frequent and most importantly, the analyte spectra are not hindered by the presence of water. Biomass treatment has been successfully followed with different Raman techniques in real time to monitor cellulose and lignin, especially with the objective of proposing better pretreatments to maximize yields.^{96,97} Shih et al. reported good quantification of glucose and xylose in hydrolysates obtained with acidic and basic treatments using univariate and partial least squares regression methods (PLS).⁹⁸ The most common

application employing on-line Raman spectroscopy is the fermentation of sugars into ethanol, simple systems with a single carbon source, usually glucose, showed good agreement with off-line monitoring.^{99–101} Gray et al. studied corn mash fermentation under industrial conditions, starch, dextrans, maltotriose, maltose, glucose and ethanol were monitored using chemometric modeling and the authors reported accurate predictions for this complex system.¹⁰²

In this work, Raman spectroscopy was used for the first time to our knowledge to monitor breakthrough curves of sugars aqueous mixtures, mainly glucose and xylose, with ethanol as cosolvent. The aim of this investigation is to compare the efficiency of models performed by multivariate calibration, based on the PLS algorithm, with univariate linear regression model for the quantification of sugars during breakthrough experiments. Predictions of breakthrough curves were compared to HPLC ones.

II-2 Materials and methods

II-2-1 Breakthrough experiments

Zeolite NaY provided by Arkema was exchanged into barium form (BaY) and packed into a 25 cm length column with an internal diameter of 0.77 cm. The column was then placed inside an oven in the breakthrough tests unit presented in *Figure II- 1*. The setup is composed of two pumps, (SHIMADZU LC-40D) the first to deliver the feed solution and the second to pump the eluent for the regeneration step (ultrapure water in this case). Feed solutions are aqueous mixtures of glucose or xylose dissolved in water in with or without ethanol as cosolvent. D-glucose and D-xylose were purchased from Sigma-Aldrich with a purity > 99% and absolute ethanol from VWR. At the column outlet, a Raman probe was placed, and a fractions collector (GILSON 206) was installed at the end of the line to collect samples and determine the concentrations also with HPLC.

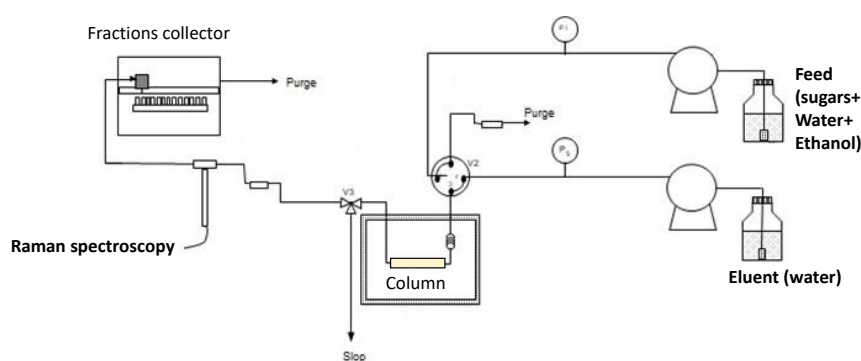


Figure II- 1: Adsorption breakthrough tests unit

The adsorbent was initially hydrated by filling the column with water at room temperature. Then the feed solution was injected. When the adsorption equilibrium was established, (*i.e.* when the breakthrough curve reaches a plateau and the recorded concentration is the same as the feed) a four way valve was turned and water was pumped to desorb the sugar molecules from the solid. Plotting the column outlet concentration as a function of time gives a breakthrough curve from which the retention time, also known as the first statistical moment, is determined. The first moment μ_1 (min) is calculated thanks the trapezoidal iterative integration method with the following equation:

$$\mu_1 = \int_0^{\infty} \left(1 - \frac{c(t)}{c_0}\right) dt \quad (\text{Equation II-1})$$

II-2-2 Raman spectroscopy

The Raman measurements were carried out using a dispersive spectrometer RXN2 from Kaiser Optical Systems equipped with a 785 nm diode laser and a Peltier cooled charge coupled device (CCD) array detector. The fiber optic was connected to a Process Elite Flowcell Ballprobe® from Marqmetrix placed at the outlet of the column. Data acquisition was performed using IC Raman 4.4. Spectra were collected in a spectral range from 100 to 3400 cm^{-1} . The exposure time was 14 seconds, and 2 accumulations were performed for each spectrum. Cosmic ray filter was applied.

II-2-3 HPLC

Samples were injected (20 μl) into a Rezex™ RCM-Monosaccharide Ca^{2+} (8 %) column. The mobile phase (ultrapure water) was pumped thanks to Waters 1515 isocratic pump with a flow rate of 0.6 mLmin^{-1} . Waters 2414 refractive index detector was used and the temperature of the column was 50 °C.

II-2-4 Modeling

II-2-4-1 Databases

Two systems were an interest in the study. The first was the adsorption from a mixture of glucose and xylose in BaY when the sugars are only dissolved in water. Thirty-six aqueous standard sugars solutions with concentrations between 15 g kg^{-1} and 250 g kg^{-1} were used to build the calibration model

The second system was the sugars adsorption in presence of ethanol as a cosolvent. Thirty-two standard solutions were considered with sugars concentrations between 5 g kg⁻¹ and 150 g kg⁻¹. Ethanol content was between 1 % and 60 % (% wt) corresponding to concentrations between 10 g kg⁻¹ and 480 g kg⁻¹.

Single component solutions and mixtures (binary and ternary in presence of ethanol) were used in both systems for the calibration sets. All reference concentrations for the two systems were measured with a Mettler Toledo semi-microbalance MS with a precision of 0.01 mg.

Two breakthrough experiments were used as validation. The predicted concentrations determined from the application of univariate and multivariate models on the spectra recorded during these tests were compared with HPLC measurements. The first moments μ_1 (min) calculated with each model were compared to the HPLC ones considered as validation references.

II-2-4-2 Univariate modeling

Univariate modeling for glucose and xylose in the first system was done by taking the height of the peaks between 974 and 1000 cm⁻¹ for xylose and between 1128 and 1217 cm⁻¹ for glucose. Peaks between 603-635 cm⁻¹, 878-895 cm⁻¹ and 1124-1192 cm⁻¹ were considered for xylose, ethanol, and glucose respectively in the second system. The first derivative was used as pretreatment for all univariate models in association with spectral subtraction, the spectrum of 100 g kg⁻¹ of glucose was subtracted from all the calibration spectra of the first system for example to quantify xylose and vice versa. These pretreatments resolved peaks overlaps since the two sugars have close chemical structures. Overall, five individual univariate models were developed for the two systems using IC Raman 4.4. The Root Mean Square Errors of calibration (RMSEC) were also calculated for all univariate models according to Equation II-2, as well as correlation coefficients (R²)

$$RMSEC = \sqrt{\frac{\sum_{i=1}^N (Y_i - \widehat{Y}_i)^2}{N}} \quad (\text{Equation II-2})$$

were Y_i is the reference concentration, \widehat{Y}_i the predicted concentration and N the number of standard solutions.

II-2-4-3 Multivariate modeling

Raman spectra were exported from IC Raman to PLS Toolbox version 9.0 for MATLAB (R2021b version) to develop the multivariate models. The partial least squares (PLS) regression was used.¹⁰³ Spectral regions between 250-1600 cm^{-1} were used to model glucose and xylose in both systems, and between 800-1600 cm^{-1} for ethanol. A Savitzky-Golay first derivative (window points: 15 and order: 2) was used as pretreatment for all models and the optimal number of latent variables (LV) was selected considering the values of Root Mean Square Error of Cross Validation (RMSECV) obtained by cross validation of calibration data. Venetian blinds cross validation was applied using 2 splits for glucose and xylose in the first system and 2, 10 and 4 splits for glucose, xylose, and ethanol respectively for the second. The Root Mean Square Errors of calibration (RMSEC) were also calculated for all univariate and multivariate models.

II-3 Results and discussion

II-3-1 Spectral interpretation

Figure II- 2 shows Raman spectra of 150 g kg^{-1} aqueous solution of glucose, 150 g kg^{-1} aqueous solution of xylose and an aqueous mixture of 150 g kg^{-1} of each sugar. These spectra are different from each other, and unique peaks can be distinguished for each constituent allowing for quantitative analysis. In the low wavenumber region, a band at 535 cm^{-1} can be seen for xylose which corresponds to C-C-C bending and ring deformation. The band at 445 cm^{-1} arises from the same latter reasons for glucose, the bending of C-C-O at the CH_2OH group gives the peak at 350 cm^{-1} . At the anomeric region (where the anomeric carbon is involved), the bending of O-C-O for xylose is identified at 600 cm^{-1} and the stretching of C-O at 845 cm^{-1} for glucose. In the fingerprint region, the peak at 980 cm^{-1} for xylose arises from bending of C-O-H bonds.¹⁰⁴ Although specific peaks can be isolated, the most intense regions in the mixture spectrum cannot be exploited due to the hindrance of sugars between each other, and thus the importance of spectral pretreatments.

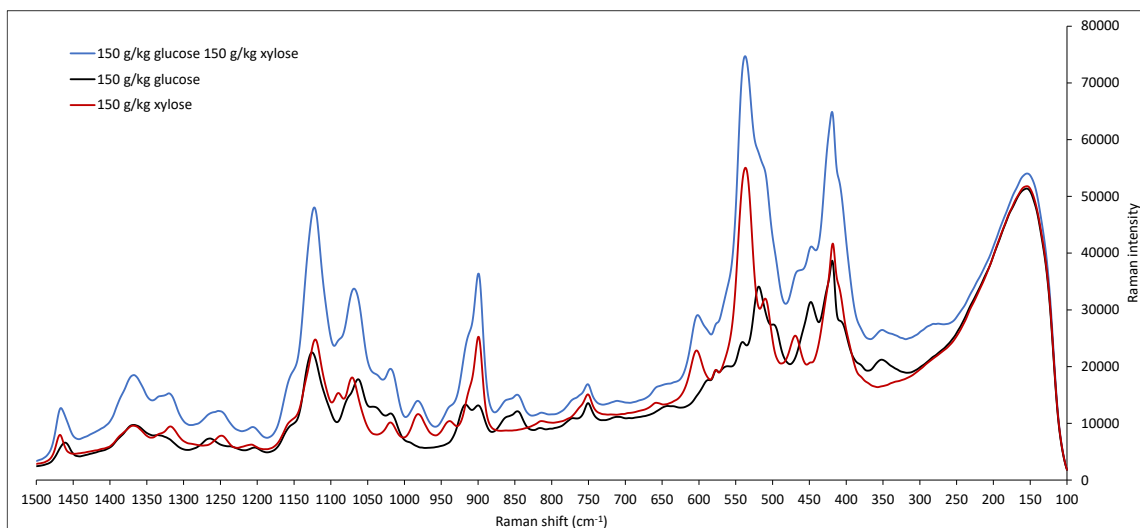


Figure II- 2: Raw Raman spectra of individual glucose (black line) and xylose (red line) aqueous sugar solutions and their equivalent mixture (blue line)

Figure II- 3 presents the selected peaks for univariate models development after pretreatments. After applying a first derivative, the spectrum of 100 g kg⁻¹ xylose is subtracted from the three spectra showed in Figure II- 3A and Figure II- 3B. This reduces xylose contributions in the mixture spectra and makes glucose unique peaks more apparent and therefore improve univariate modeling. (see Figure A 1 in appendix) Identical methodology is used to build the rest of univariate models to identify a unique peak for each constituent. The same spectral range 1115-1215 cm⁻¹ is used to quantify glucose in presence or absence of ethanol (Figure II- 3A and Figure II- 3C), the region includes two peaks at 1135 cm⁻¹ and 1165 cm⁻¹ which arise from C-C stretching and C-O bending respectively.¹⁰⁵ The peak around 990 cm⁻¹ arises from the stretching of C-O-H when xylose is dissolved in water (Figure II- 3B), this peak did not give good correlation coefficient of calibration (R^2) when ethanol is present in the solution because of overlapping, the band around 610 cm⁻¹, characteristic for O-C-O stretching, is used instead (Figure II- 3D).¹⁰⁴ Ethanol concentration is monitored by using the intense 888 cm⁻¹ peak resulting from stretching of C-C bond as shown in Figure II- 3E.

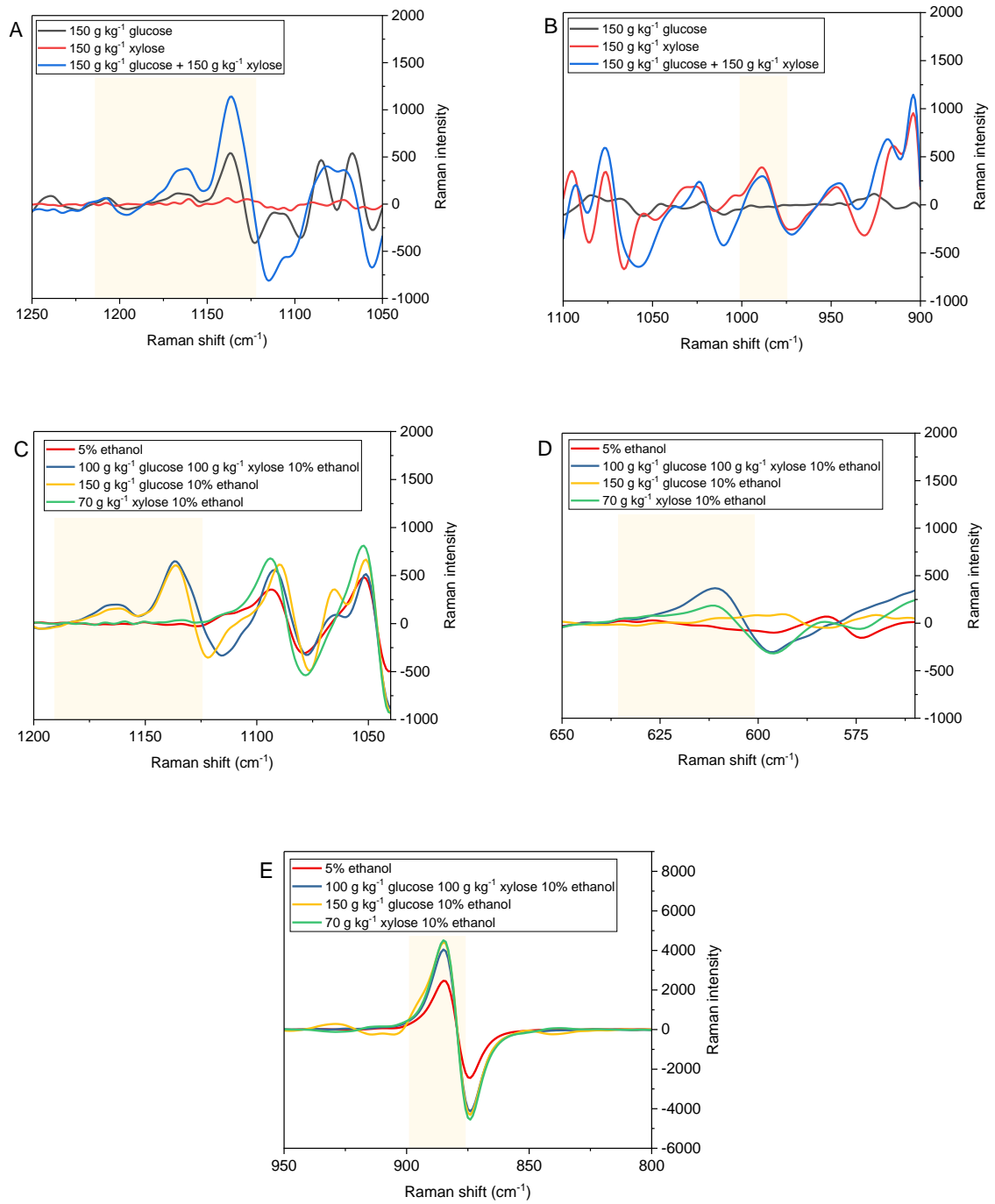


Figure II- 3: Pretreated Raman spectra to identify characteristic peaks for (A) glucose, (B) xylose dissolved in water and (C) glucose, (D) xylose, (E) ethanol in the ternary system

II-3-2 Univariate and multivariate calibration modeling

Although it is possible to isolate specific peaks in every system for each component, it is harder to identify fingerprint peaks for sugars especially in the presence of ethanol. Multivariate modeling using PLS regression allows accurate quantification to overcome overlapping in complex systems. *Table II- 1* shows the calibration results for univariate and PLS multivariate modeling of glucose and xylose with and without ethanol in the mixture. Correlation coefficients (R^2) and RMSEC, indicate the fit quality of calibration models. Cross validation evaluates the statistical quality of PLS models, a value close to RMSEC is recommended. 3 LV are used for single sugars models without ethanol and 5 LV with ethanol, 8 LV are required for ethanol. High values of R^2 (over 0.989) are found for all models, similar calibration errors around 2.6 g kg^{-1} are obtained for glucose in the first system for univariate and multivariate models, RMSEC is lowered from 3.5 g kg^{-1} to 2.9 g kg^{-1} for xylose using chemometric model. PLS modeling lowers RMSEC to around 1.3 g kg^{-1} in the second system containing ethanol which suggest better predictions compared to univariate models.

Table II- 1: Univariate and multivariate calibration results

	Univariate		PLS		
	RMSEC	R^2	RMSEC	RMSECV	R^2 calibration
Glucose/xylose					
Glucose	2.7000	0.996	2.5614	2.6622	0.997
Xylose	3.4764	0.997	2.8912	3.4278	0.998
Glucose/xylose/ethanol					
Glucose	2.4774	0.989	1.2330	2.4384	0.999
Xylose	2.2750	0.994	1.4068	2.2392	0.999
Ethanol	3.7435	0.996	1.3200	3.6855	0.999

The comparison of calibration results obtained with univariate and multivariate modeling with the reference is presented in *Figure II- 4*. Overall, both methods yield similar results with slight improvements using PLS modeling. This improvement can be seen when the calibration data contains fixed single constituent concentration but with varying fractions of the other mixture components. The calibration data of the system with ethanol for instance, contains mixtures with fixed concentrations of 100 g kg^{-1} glucose and 100 g kg^{-1} xylose with ethanol content ranging from 10 % to 60 % (% wt). *Figure II- 4C* shows that univariate model at 100 g kg^{-1} glucose tends to over and underestimate the concentration, the addition of ethanol dampens glucose signature peaks which results in the decrease of the measured concentration.

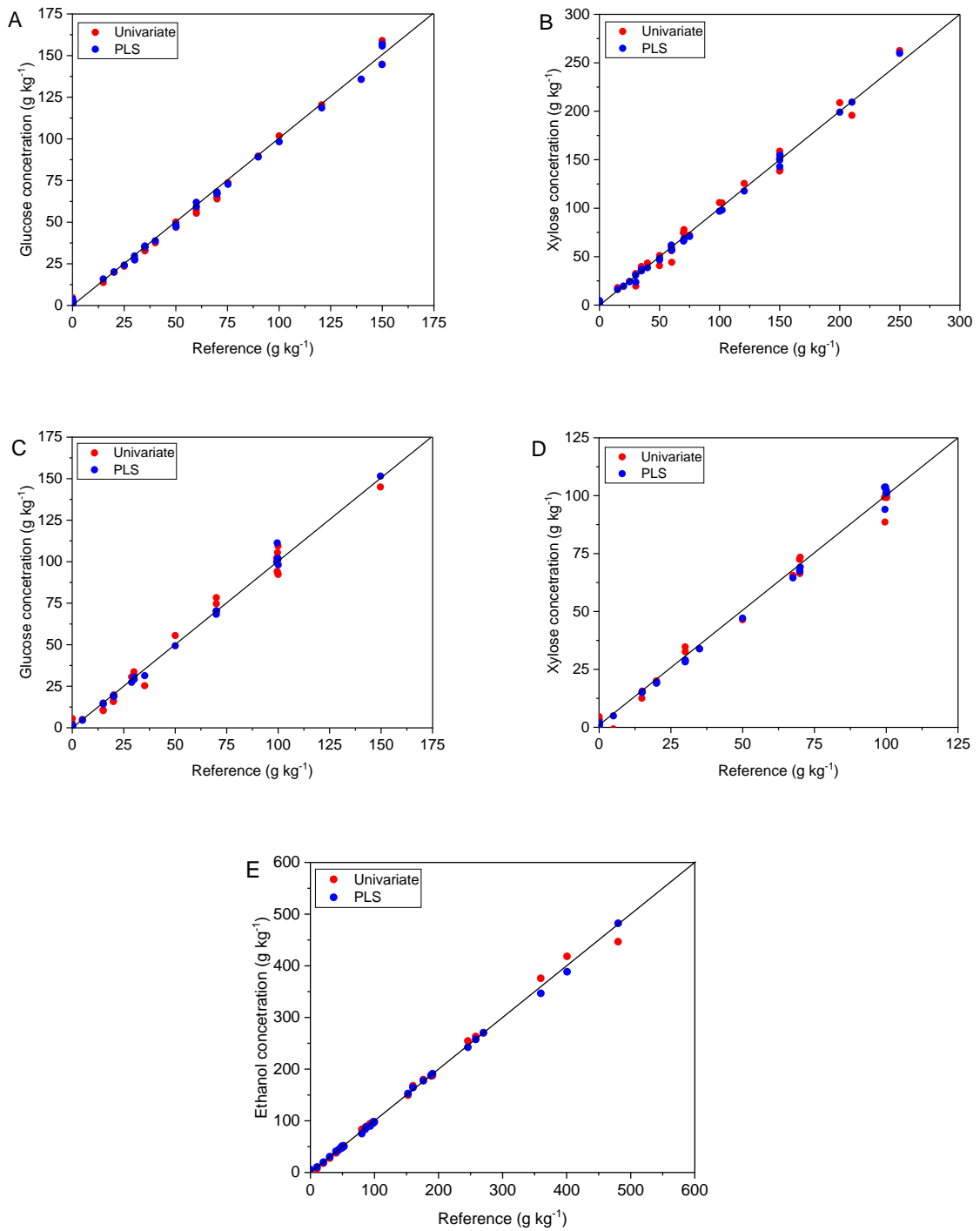


Figure II- 4: Calibration results with univariate and multivariate methods for (A) glucose, (B) xylose dissolved in water and (C) glucose, (D) xylose, (E) ethanol in the ternary system

III-3-3 Models validation

Two breakthrough experiments are performed to validate all developed models, the first is a test with an aqueous mixture of 100 g kg⁻¹ glucose and 100 g kg⁻¹ xylose (*Figure II- 5A* and *Figure II- 5B*), the second with 100 g kg⁻¹ glucose, 100 g kg⁻¹ xylose and 5 % ethanol (% wt) showed in *Figure II- 5C* and *Figure II- 5D*. In both cases xylose curve precedes glucose one indicating that the adsorbent has an affinity to glucose which delays its exit from the column. A good agreement is found with univariate and PLS models, PLS curves are smoother than univariate ones. First moments of 19.8 min and 22.4 min are calculated for xylose and glucose respectively in case of the first system, 18.1 min, 20.3 min and 23.3 min are found for ethanol, xylose, and glucose respectively for the second. The beginnings of the curves at the start of the breakthrough, when solutes start to exit the column, are well predicted, Raman spectroscopy is known to be limited at low concentrations because of low signal noise ratios and signal decrease with water and ethanol. ¹⁰⁶ PLS model for ethanol do not fit perfectly at the end of the curve, *ie.* when adsorption equilibrium is reached nevertheless, this do not affect the calculated first moment (18.1 min). Less than 1 % error is obtained for all models compared to HPLC curves, simple univariate models are robust and accurate for this application. We further tested the adsorption of a binary system containing glucose and fructose dissolved in water in a calcium-exchanged zeolite Y (CaY). Predicted breakthrough curves obtained with univariate and PLS models developed following the same methodology for glucose/xylose systems are reported in the supplementary information (*Figure A5*). All predictions are accurate compared to HPLC and no preprocessing was applied to develop univariate model. Well isolated peaks between 620-640 cm⁻¹ and 1120-1135 cm⁻¹ are selected to quantify fructose and glucose respectively. On-line Raman spectroscopy is a powerful tool for breakthrough experiments and testing different adsorbents for the separation of monosaccharides. Univariate modeling gives satisfactory predictions in case of binary sugar solutions very close to chemometrics methods, the latter can rather be used in more complex systems containing more than two sugars.

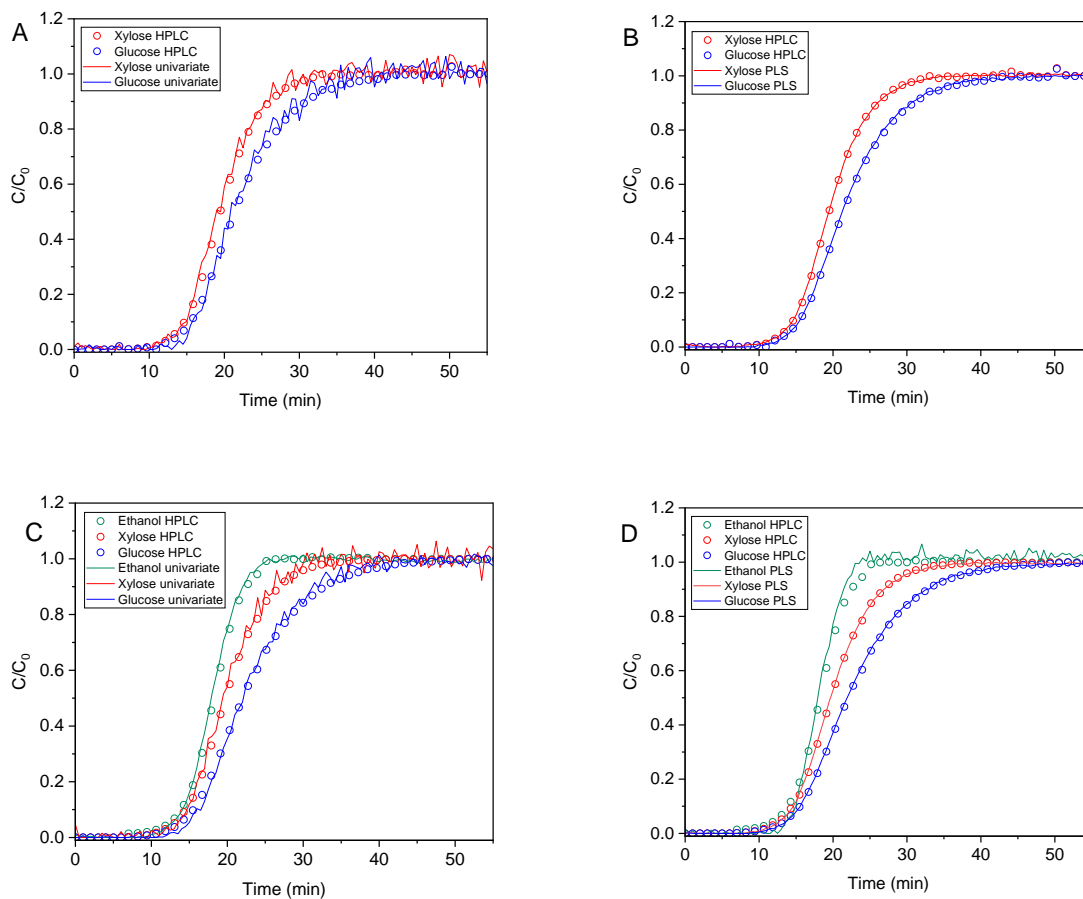


Figure II- 5: Breakthrough curves predictions with univariate and PLS models compared to HPLC curves

II-4 Conclusion

This work demonstrates the utilization of Raman spectroscopy for breakthrough adsorption experiments to monitor breakthrough curves. Adsorption of lignocellulosic sugars, glucose, and xylose in a BaY zeolite with and without ethanol in the feed mixture was studied. Univariate and multivariate models proved accurate compared to reference HPLC analysis. Univariate models, which are simple to implement, provide robust results in the concentration range used in this study (from 0 to 100 g kg⁻¹ for sugars). Preprocessing is essential to enhance accuracy and avoid overlapping interference in the measurements, first derivative coupled with spectral subtraction of the components not desired to be quantified proved to be efficient to develop univariate models.

Chapter III: Separation of glucose and xylose with zeolites

From the presented literature review, faujasite-type zeolites looked like promising adsorbents for the separation of glucose and xylose. We showed previously that univariate models are robust to monitor sugar breakthrough curves. In the following chapter, we screened a series of faujasite adsorbents to identify the most performant. The impact of the zeolite chemical composition on the separation is explored. First, exchanged zeolites X and Y are characterized. Then, breakthrough experiments are performed with a mixture feed solution, and xylose/glucose selectivity is determined for each adsorbent.

III-1 Introduction

In the frame of lignocellulosic biomass valorization into chemicals or fuels, developing separation methods for streams of carbohydrates by chromatographic separation is necessary. In this work, we prepared and characterized X and Y zeolites exchanged by K^+ , Ca^{2+} , Sr^{2+} and Ba^{2+} as adsorbents for xylose/glucose separation. We tested their separation performance with breakthrough experiments. We find that BaX and BaY are the most selective with a selectivity inversion (xylose/glucose selectivity of 1.52 and 0.67 respectively)

Lignocellulosic biomass derived from agricultural wastes and forest residues is an attractive raw material thanks to its non-competitiveness with food production.⁷ It is composed of three major biopolymers: cellulose, formed from the polymerization of glucose (sugar with six carbon atoms, called hexose); hemicellulose, which is composed from hexoses isomers like glucose, mannose and galactose, and pentoses (sugars with five carbon atoms) mainly xylose and arabinose⁷ and lignin, a polymer composed of polyphenol units. The quantity of these components varies depending on the plant species. Nonetheless, cellulose is generally the major component, followed by hemicellulose and lignin.^{15,16} Hence sugars are the main constituents of lignocellulosic biomass they can be used for various applications, including the production of fuels and chemicals for pharmaceuticals and personal care products. However, to obtain the sugars from lignocellulosic biomass suitable for such applications, a fractionation step is required. In the most common transformation methods^{19,20}, the biomass yields two main streams of sugars (in form of hydrolysates). The first is a hemicellulose hydrolysate rich with pentoses mainly xylose and the second is a cellulose hydrolysate composed primarily of glucose.^{17,18,21} The hydrolysates are either fermented to bioethanol in the case of a classic

application or converted into high added-value platform chemicals.²⁷ Furanic compounds, like furfural and 5-hydroxymethylfurfural (5-HMF)^{28,29} or glycols such as ethylene glycol (EG) and 1,2-propylene glycol (1,2-PG)³⁰ are considered as promising conversion products from sugars derived from lignocellulosic biomass. However, such transformations are better carried out on a stream of a single sugar rather than on a mixture in order to achieve high selectivity and efficiency. Thus, a separation method suitable for aqueous streams of mixed sugars is of high importance in the development of biorefineries.

The most common separation method of sugars at the industrial scale is the chromatographic separation of glucose and fructose to produce the high-fructose corn syrup (HFCS), a sweetener for the food industry. This separation, originally developed by UOP in 1977, known as SAREX process, is performed with calcium-exchanged resins as adsorbent using a simulated moving bed technology (SMB) based on adsorption.^{69,107,108} The separation of glucose and xylose is however not extensively treated in literature. Lei et al. studied the adsorption behavior of glucose and xylose, the major sugars in lignocellulosic hydrolysate, on exchanged resins with Ca^{2+} , K^+ and Fe^{3+} with different degrees of cross-linking by measuring adsorption isotherms.¹¹ The authors found that the calcium form could be the most suitable adsorbent for this separation and that the 8% cross-linked resin showed the best performance, based on the single component isotherms results. Hence there is a lack of development of suitable methods dedicated to glucose/xylose separation.

Zeolites are considered to be interesting materials for sugars separation. These crystalline aluminosilicates microporous materials are formed by the association of tetrahedral building blocks (SiO_4 and $(\text{AlO}_4)^-$). Faujasite-type structure is formed from a specific assembly of sodalite cages and hexagonal prisms creating a large cavity called supercage with an internal diameter of 1.3 nm which is accessible through a 12-membered ring with a diameter of 0.74 nm.⁵⁵

In this work we have explored the effect of faujasite-type zeolites composition on the separation of glucose and xylose. Zeolite X and Y in sodium form were exchanged with potassium, calcium, strontium, and barium. The adsorbents were characterized, and their separation performances were evaluated thanks to breakthrough experiments.

III-2 Experimental section

III-2-1 Chemicals

Zeolites X (Si/Al =1.2) and Y (Si/Al=2.6) were provided by Arkema in the sodium form. D-glucose and D-xylose were purchased from Sigma-Aldrich with a purity > 99%. KCl, CaCl₂, SrCl₂ and BaCl₂ salts were purchased from VWR with a purity > 99% Ultrapure water was produced with the Milli-Q® IQ Water Purification System from Merck.

III-2-2 Adsorbents ion-exchange

The preparation of the adsorbents is done by exchanging the initial cation Na⁺ to other monovalent or bivalent ions. The exchange is performed thanks to an automated unit that allows the preparation of six different zeolites in parallel. The unit is composed of a quaternary pump which delivers water and salt solutions and an oven where the columns are placed. The complete exchange operation is controlled with a software and a complete exchange cycle is described by the following steps:

- 1) Hydration: zeolites (around 8 g of NaX) were packed in a column (25 cm of length and an internal diameter of 0.77 cm) and hydrated by percolation at a flowrate of 3 mL min⁻¹ at room temperature.
- 2) Exchange: aqueous solutions of chloride salts of the metallic cations with a concentration of 0.25 N are flown (1.5 mL min⁻¹) through the columns at 80 °C and Na⁺ are replaced with K⁺, Ca²⁺, Sr²⁺ and Ba²⁺, at 80 °C.
- 3) Water washing: during this step chlorides are rinsed (3 mL min⁻¹) from the solids after the exchange at 80 °C.
- 4) Pre-drying: the objective of this step is to evacuate the interstitial water under a nitrogen flow at 100 NL/min for 30 minutes.
- 5) Drying: under N₂ flow (240 NL/h) for 5 hours at 110 °C. During this step, a part of water contained in the pores is eliminated to avoid a hydrothermal degradation during the activation step
- 6) Activation: this final step is done at 225 °C for 6 hours to control the amount of water inside the zeolite.

The hydration, exchange, washing and pre-drying steps are done column per column. The final drying and activation are done for all the columns at the same time. For each cation two columns were exchanged, the first will be used in the breakthrough experiments and the second for the

characterization of the new solid with the assumption that the two zeolites in both columns have the same exchange degree.

III-2-3 Characterization of the adsorbents

Powder X-ray diffraction patterns were obtained with a PANalytical X'pert Pro (35 mA, 35 kV) diffractometer equipped with a copper anticathode ($\lambda K_{\alpha 1} = 1.5406 \text{ \AA}$). The data acquisition was done for a 2θ angle between 5° and 72° with a step size of 0.02° and a step time of 5 s. In order to determine the degree of crystallinity of the binder shaped beads of NaX and NaY, reference binderless samples of the same adsorbents considered as 100 % crystalline were measured at the same conditions. The crystallinity was determined by comparing the ratio between the areas of the peaks without the background and the areas of the peaks with the background for $9^\circ < 2\theta < 38^\circ$ of the considered sample with the ratio of its reference.

For the cell parameter determination, an internal standard (certified silicium “Gem Dugot”) was introduced to the sample and the data was treated with TOPAS software. The number of aluminum atoms in the cell is determined from the formula given by Cherif et al. ¹⁰⁹

$$N_{Al} = 115 * (a - 24.191) \quad (\text{Eq III-1})$$

where (a) is the lattice parameter. From N_{Al} , we can estimate the Si/Al ratio thanks to the following equation:

$$\frac{Si}{Al} = \left(\frac{192}{N_{Al}}\right) - 1 \quad (\text{Eq III-2})$$

Prior to the XRD measurements the samples were grinded and prehydrated in a desiccator at room temperature filled with a $Mg(NO_3)_2$ saturated solution (around 56% relative humidity).

The chemical composition of the samples was analyzed by Inductively Coupled Plasma coupled with Optical Emission Spectroscopy (ICP-OES) using an Arcos Spectro-Ametek ICP-OES. Before the measurement the samples were dissolved in hydrofluoric acid for two days and then aluminum, sodium, potassium, calcium, strontium, and barium were quantified. The exchange rate for each cation is determined as follows:

$$\text{Exchange rate (\%)} = \frac{n_{cation}}{n_{cation} + n_{Na}} \times 100 \quad (\text{Eq III-3})$$

where n_{cation} and n_{Na} are respectively the number of moles of the cation and the number of moles of residual sodium after the ionic exchange.

Nitrogen adsorption-desorption isotherms were measured with a Micrometrics ASAP 2420. The microporous volume was evaluated from the Dubinin Radushkevich equation, and the specific surface area was estimated according to Brunauer-Emmett-Teller theory taking P/P_0 between 0.05 and 0.30. All samples were pretreated at 400 °C under vacuum for 6h prior the measurement.

In addition, the adsorbents bulk density, the mesopores and macropores volumes were determined by mercury intrusion using an IV Autopore from Micrometrics. The pore diameter was calculated by applying the Washburn-Laplace equation. The pre-treatment was carried out at 250 °C for 2h in a ventilated oven.

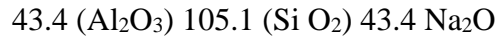
III-2-4 Determination of the chemical formula

Considering the general formula $x(\text{Al}_2\text{O}_3) y(\text{SiO}_2) x\text{M}_n\text{O}$ of a faujasite, where M is the counterion and knowing that in a unit cell there is 192 atoms of silicon and aluminum, the formula of NaX can be determined with the resolution of the following system of equations:

$$2x + y = 192$$

$$y/2x = 1.2$$

The formula of the zeolite is therefore:



III-2-5 Determination of the number of supercages per gram of zeolite

From the chemical formula of NaX and knowing the exchange rates, the formula of the exchanged zeolites can be deduced. The number of supercages per gram of zeolite (SP) is estimated as follows:

$$SP = \frac{m_z \times \chi}{M} \times 8N \quad (\text{Eq III-4})$$

where δ is the number of supercages per unit cell, M the molecular weight, χ the cristallinity (79 % for zeolites X and 82% for zeolites Y) and m_z the mass of the zeolite after exchange determined as follows:

$$m_z = \chi \times \frac{M_{\text{exchanged zeolite}}}{M_{\text{NaX or NaY}}} + (1 - \chi) \quad (\text{Eq III-5})$$

III-2-6 Breakthrough experiments

The homemade experimental setup is equipped with two SHIMADZU LC-40D pumps, the first one is used to inject the sugar feed solution to the column and the second one to pump the eluent, water in our case. In a typical experiment, the column filled with the adsorbent was placed inside an oven to control the temperature of the process and the concentration of sugars at the outlet was recorded thanks to a Kaiser Raman RXN2 in-line Raman spectrometer with an excitation wavelength of 785 nm. An optical probe was placed in the outlet stream with a special flow cell and the spectra were recorded thanks to the IC Raman 4.4 software. The acquisition parameters were 2 scans and 14 seconds of exposure time. The quantification of glucose and xylose was done by building a univariate model, the chosen peaks were in the range of 1217-1128 cm^{-1} for glucose and in the range of 974-1000 cm^{-1} for xylose with first derivative and spectral subtraction as pretreatments. We verified that the quantification obtained with this method matches the one obtained by sampling of the outlet and quantification by HPLC. Samples are injected (20 μl) into a RezexTM RCM-Monosaccharide Ca^{2+} (8 %) column. The mobile phase, water in this case, is pumped thanks to Waters 1515 isocratic pump with a flow rate of 0.6 mL min^{-1} . Waters 2414 refractive index detector is used and the temperature of the column is 50 $^{\circ}\text{C}$ (see Chapter II).

Initially, the column is filled with ultrapure water with the flowrate of 0.5 mL min^{-1} at room temperature in order to get rid of air and fill the porosity with water molecules. Then, the temperature of the oven is raised to 30 $^{\circ}\text{C}$ and the system is ready to receive the feed solution injected at the same flowrate (0.5 mL min^{-1}). When the adsorption equilibrium is established, *i.e.* when the breakthrough curve reaches a plateau and the recorded concentration at the outlet is the same as the feed, a four way valve is turned and water is pumped through the column to desorb the sugar molecules from the solid.

The amount of adsorbed sugars was calculated using the following equations:

$$q_{ads} = (\mu_1 \times Q \times C_{plateau}) - (C_{plateau} \times V_{ns}) \quad (\text{Eq III-6})$$

$$\mu_1 = \int_0^{\infty} \left(1 - \frac{c(t)}{c_0}\right) dt \quad (\text{Eq III-7})$$

where q_{ads} is the quantity of adsorbed sugar (mol), μ_1 the first moment (min) defined by (Eq III-7) and calculated thanks to the trapezoidal iterative integration method, Q the flow rate

(mL min^{-1}), $C_{plateau}$ the concentration of the feed solution (mol mL^{-1}) and V_{ns} the non-selective volume where we suppose the adsorption does not take place (mL) expressed as :

$$V_{ns} = V_{dead} + V_p + V_{interparticle} \quad (\text{Eq III-8})$$

where V_{dead} is the volume of the lines of the experimental setting / apparatus without the column (approximately 1.77 mL with the volume of the column being of 11.44 mL), V_p the volume of mesopores and macropores estimated from mercury intrusion analysis and $V_{interparticle}$ the volume between the beads determined as follows:

$$V_{interparticle} = V_{column} - \frac{m_{zeolite}}{\rho_{zeolite}} \quad (\text{Eq III-9})$$

with $m_{zeolite}$ the mass of adsorbent inside the column and $\rho_{zeolite}$ the bulk density of the zeolite bead determined by mercury intrusion.

In the case of the mixture adsorption of two sugars, the selectivity can be defined from the adsorbed quantities of each sugar at equilibrium by the following equation:

$$\alpha_{mixture_{xyl/glu}} = \frac{q_{ads\ xyl} \times C_{glucose}}{q_{ads\ glu} \times C_{xylose}} \quad (\text{Eq III-10})$$

Defined in such a way, a selectivity greater than unity indicates an affinity of the adsorbent towards xylose. $C_{glucose}$ and C_{xylose} are the concentrations at equilibrium which are the concentrations of the feed solution in the case of a breakthrough test. After calculating the number of supercages per gram of each zeolite (SP), the adsorption of sugars per supercage is determined as follows:

$$N_{sugar/\alpha\ cage} = \frac{q_{ads\ sugar} \times N}{SP \times m_{dry\ zeolite}} \quad (\text{Eq III-11})$$

where $q_{ads\ sugar}$ the adsorbed quantity (mol), N the Avogadro number, SP the number of supercages per gram of zeolite and $m_{dry\ zeolite}$ the mass of dry zeolite introduced in each column.

III-3 Results and discussion

Exchanged zeolites were prepared by ionic exchange of a NaX or NaY zeolite (provided from Arkema) with an aqueous solution of the desired cation chloride (either KCl, CaCl₂, SrCl₂ or BaCl₂). The experiment was performed in flow before rinsing with deionized water. The measure of the X-ray diffractograms was performed to estimate the zeolite content in starting zeolites (78 % for NaX and 82 % for NaY) and to determine the cell parameters of all obtained adsorbents once the ion-exchange was made. Cell parameters of 24.949 Å and 24.628 Å are obtained for NaX and NaY respectively, from which Si/Al ratios of 1.2 and 2.6 are calculated (Eq III-1 and Eq III-2). Similar Si/Al ratios were found using X-ray fluorescence and we assume that the crystallinity and the Si/Al ratios are unaltered by the ionic exchange procedure.

The exchange rates (Eq III-3) from elemental analysis by ICP-OES after the ion-exchange procedure are given in Table 1. The exchange rate is high for the X zeolite (around 90 %), while for the Y zeolite only the potassium gives nearly a complete exchange (96 %) whereas the divalent cations only reach 60-75 % of exchange rate. This indicates that residual sodium exists in these adsorbents and it is in good agreement with several results reported in the literature.¹¹⁰⁻

112

Cell parameters increase with ionic radii for both zeolites X and Y compared to the initial NaX and NaY (Table III- 1). The value remains almost identical when sodium is exchanged with calcium because both of them have close ionic radii (116 pm for Na and 114 pm for Ca). One can expect that the parameters of the barium-exchanged zeolites are greater than the strontium ones since the ionic radius of barium is higher than strontium (132 pm for Sr and 149 pm for Ba) nevertheless, we find opposite trend.

Table III- 1: Chemical and structural properties of exchanged zeolites

Zeolite	Exchange rate (%)	Cell parameter (Å)	Chemical formula	Molar mass (g mol ⁻¹)	Number of supercages (10 ²⁰ g ⁻¹)
NaX	-	24.949	43.4 (Al ₂ O ₃) 105.1 (SiO ₂) 43.4 Na ₂ O	13429	2.80
KX	94	25.088	43.4 (Al ₂ O ₃) 105.1 (SiO ₂) 40.8 K ₂ O 2.6 Na ₂ O	14744	2.74
CaX	89	24.872	43.4 (Al ₂ O ₃) 105.1 (SiO ₂) 38.6 CaO 4.8 Na ₂ O	13202	2.81
SrX	92	25.045	43.4 (Al ₂ O ₃) 105.1 (SiO ₂) 39.9 SrO 3.5 Na ₂ O	15091	2.73
BaX	91	25.017	43.4 (Al ₂ O ₃) 105.1 (SiO ₂) 39.5 BaO 3.9 Na ₂ O	17038	2.67
NaY	-	24.628	26.7 (Al ₂ O ₃) 138.7 (SiO ₂) 26.7 Na ₂ O	12710	3.11
KY	96	24.710	26.7 (Al ₂ O ₃) 138.7 (SiO ₂) 25.6 K ₂ O 1.1 Na ₂ O	13533	3.07
CaY	72	24.650	26.7 (Al ₂ O ₃) 138.7 (SiO ₂) 19.2 CaO 7.5 Na ₂ O	12597	3.11
SrY	74	24.727	26.7 (Al ₂ O ₃) 138.7 (SiO ₂) 19.8 SrO 6.9 Na ₂ O	13535	3.07
BaY	58	24.685	26.7 (Al ₂ O ₃) 138.7 (SiO ₂) 15.5 BaO 11.2 Na ₂ O	14126	3.05

The textural properties of all zeolites are presented in Table A1 (Appendix). The specific surface area of NaX ($688 \text{ m}^2 \text{ g}^{-1}$) is greater than that those of KX, SrX and BaX, and is almost similar to the surface value obtained for CaX within the uncertainty of the analysis ($\pm 34 \text{ m}^2 \text{ g}^{-1}$) and the lowest value is obtained for BaX ($541 \text{ m}^2 \text{ g}^{-1}$). The same observations can be made when comparing the microporous volumes values which decrease from $0.26 \text{ cm}^3 \text{ g}^{-1}$ for NaX to $0.20 \text{ cm}^3 \text{ g}^{-1}$ for BaX. The exact trend can be seen with the exchanged zeolites type Y. The mesoporous and macroporous volumes remain almost unchanged considering an error of $\pm 0.03 \text{ cm}^3 \text{ g}^{-1}$ for the determination of the macroporous volume. Hence, the ionic exchange from sodium to K^+ , Sr^{2+} and Ba^{2+} forms tend to decrease the specific surface area and the microporous volume except for Ca^{2+} where the textural properties remain almost identical to the initial NaX and NaY. These results are consistent with the fact that the exchange is done inside the crystals which will impact the final microporous volume and will not change the size of the crystals and therefore the mesoporous and macroporous volumes.

Considering the general formula of a faujasite: $x(\text{Al}_2\text{O}_3) y(\text{SiO}_2) x\text{M}_n \text{O}$ where M is the counterion and by combining the DRX and the ICP-OES data (exchange rates), the chemical formulas of all exchanged zeolites are obtained (*Table III- 1*). With these experimental data, the number of supercages per gram of exchanged zeolite was calculated.

The separation of an aqueous mixture of glucose and xylose was tested with all the adsorbents thanks to breakthrough experiments detailed before. The breakthrough curves obtained for zeolites X for a binary aqueous solution of 150 g kg^{-1} of glucose and 150 g kg^{-1} of xylose at 30°C with a flowrate of 0.5 mL min^{-1} are presented in *Figure III- 1* in the case of zeolites X. We find that NaX is slightly selective for glucose, while BaX and KX have a higher affinity for xylose. CaX and SrX show overlapped breakthrough for both sugars, indicating that no selectivity is observed on these materials.

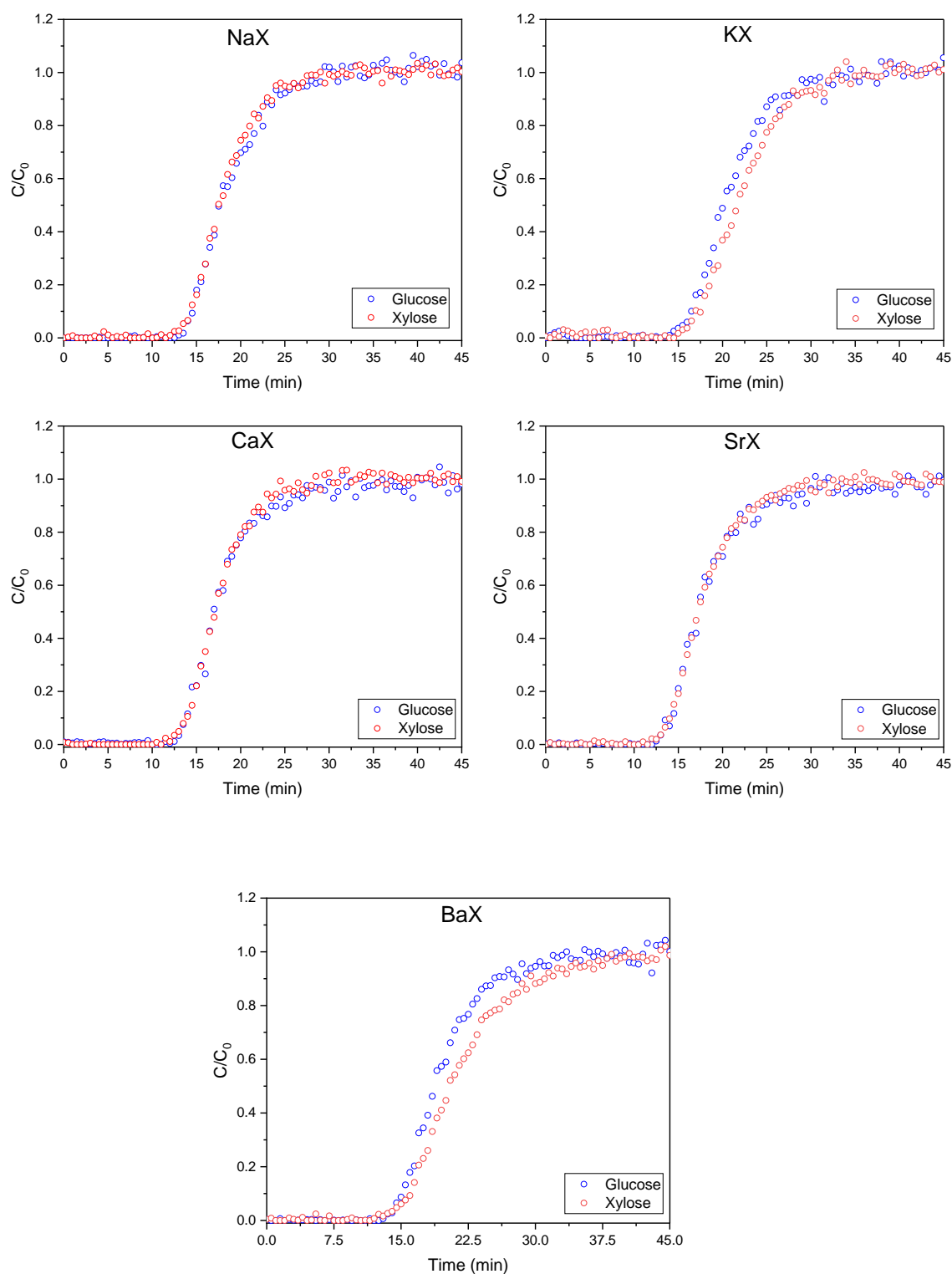


Figure III- 1: Breakthrough curves of zeolites X with a feed mixture of 150 g kg^{-1} glucose and 150 g kg^{-1} xylose in a BaY at $30 \text{ }^\circ\text{C}$ with a flowrate of 0.5 mL min^{-1}

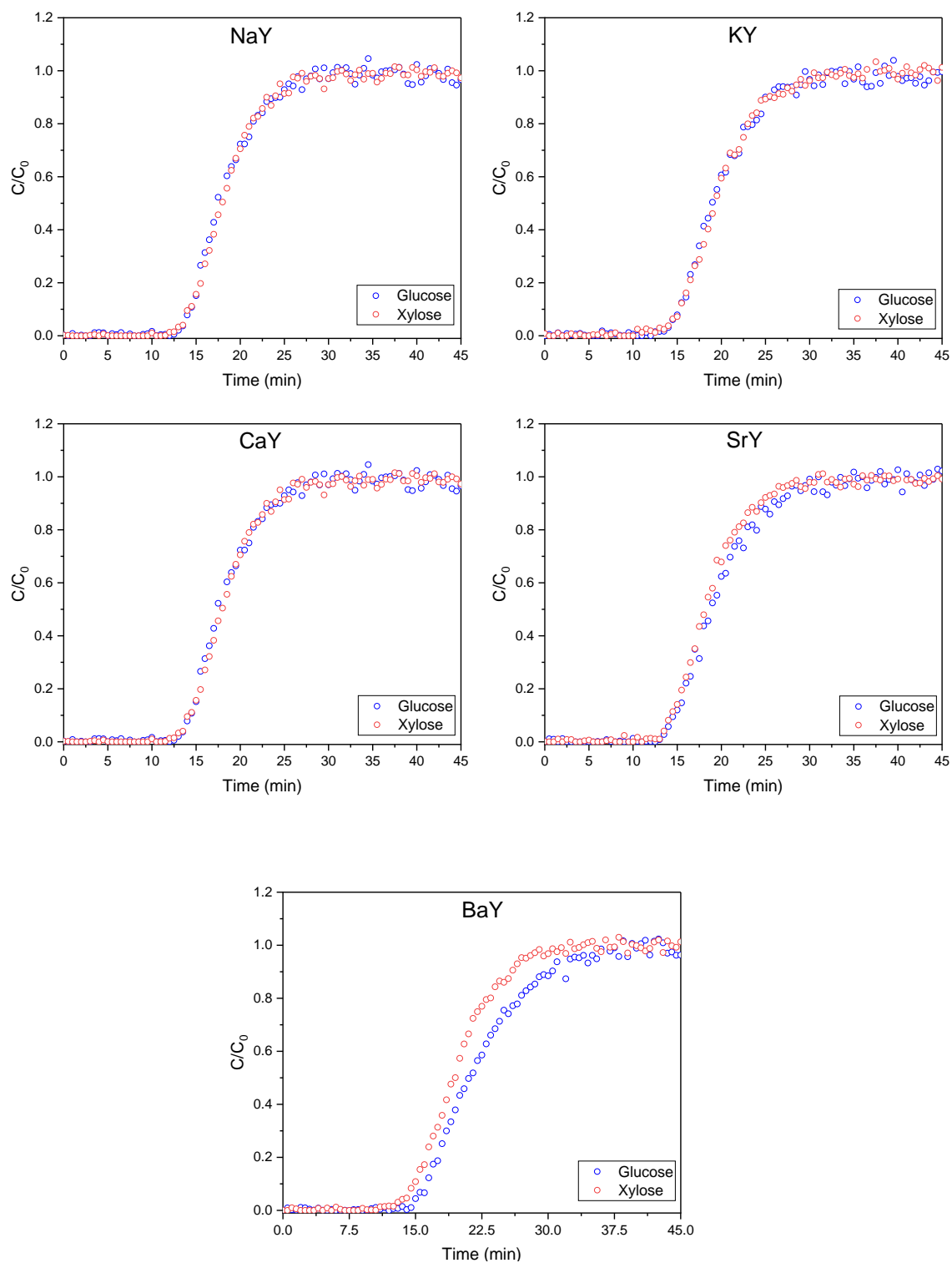


Figure III- 2: Breakthrough curves of zeolites Y with a feed mixture of 150 g kg^{-1} glucose and 150 g kg^{-1} xylose in a BaY at $30 \text{ }^\circ\text{C}$ with a flowrate of 0.5 mL min^{-1}

The curves obtained with zeolites X show that the selectivity increases with the ionic radii for monovalent cations from sodium to potassium and for bivalent cations from calcium to barium.

In the case of exchanged Y zeolites (*Figure III- 2*) in the same experimental conditions as zeolites X, NaY, KY, and CaY do not separate the sugars, and the selectivity increases with the ionic radii only for bivalent ions for zeolites Y with the BaY the most selective towards glucose.

The adsorbed quantities of each sugar on each zeolite expressed in mg g^{-1} and in adsorbed molecule per supercage are summarized in *Table III- 2*. The increase of Si/Al ratio reduces the total sugars uptakes for monovalent cations, changing from 99 mg g^{-1} in NaX to 22 mg g^{-1} in NaY and from 150 mg g^{-1} in KX to 68 mg g^{-1} in KY. The total adsorbed amount increases for calcium and strontium from 32 mg g^{-1} in CaX to 74 mg g^{-1} in CaY and from 44 mg g^{-1} in SrX to 64 mg g^{-1} in SrY. However, it remains the same (around 106 mg g^{-1}) for the barium-exchanged zeolites with BaX adsorbing more xylose (64 mg g^{-1}) and BaY more glucose (62 mg g^{-1}).

Table III- 2: Adsorbed amounts and selectivities

zeolite	q_{ads} (mg g^{-1})		Molecules per supercage		xylose/glucose Selectivity
	xylose	glucose	xylose	glucose	
NaX	46	53	0.7	0.6	0.87 (± 0.04)
KX	81	69	1.2	0.8	1.18 (± 0.02)
CaX	13	19	0.2	0.2	0.73 (± 0.23)
SrX	21	23	0.3	0.3	0.92 (± 0.10)
BaX	64	42	1.0	0.5	1.52 (± 0.01)
NaY	11	11	0.1	0.1	1.02 (± 0.06)
KY	35	33	0.5	0.4	1.09 (± 0.14)
CaY	37	37	0.5	0.4	0.99 (± 0.08)
SrY	30	34	0.4	0.4	0.89 (± 0.07)
BaY	41	62	0.5	0.7	0.67 (± 0.08)

Zeolite KX presents the highest filling with around 1 molecule of each sugar per supercage. One molecule of xylose and 0.5 molecule of glucose per supercage are calculated for BaX. In the case of BaY, 0.5 molecule of xylose and 0.7 molecule of glucose per supercage are determined.

Among all the adsorbents, BaX presents the highest xylose/glucose selectivity of 1.5 followed by KX with a selectivity of 1.2 and BaY have an affinity to glucose with a selectivity of 0.67

(glucose/xylose selectivity of 1.5). Interestingly, the selectivity in BaX and BaY is inverted, the reasons behind these results are still unknown and require further investigations.

In conclusion, we show herein that cation-exchange faujasite zeolites can be a good candidate for the separation of sugar streams obtained from lignocellulosic biomass fractionation. We show that a suitable combination of cation and Si/Al ratio is important to obtain a selectivity suitable for industrial application. Only a restricted number of the materials tested showed a significant selectivity towards xylose or glucose. In particular, the case of Ba-exchanged zeolites is very interesting, since BaX was found selective to xylose and BaY selective to glucose, showing the versatility of such materials depending on the target application. We show that, at equilibrium in our experimental conditions, around 1.5 molecules of sugar per supercage is adsorbed, indicating a rather high density in the zeolite framework.

Chapter IV: Adsorption study of glucose and xylose in exchanged zeolites X and Y

We showed in a previous study the performance of exchanged zeolites X and Y in separating a mixture of glucose and xylose. BaX and BaY were the most suitable adsorbents for this application with BaX being selective to xylose and BaY to glucose. Adsorption isotherms provide useful information about the interaction's strength, thermodynamics of adsorption, and supply parameters to design a chromatographic process for the separation. The following chapter focuses on the determination of single adsorption isotherms of glucose and xylose in exchanged zeolites X and Y by means of dynamic tests. The influence of temperature and ethanol addition as cosolvent were also investigated.

IV-1 Experimental section

IV-1-1 Adsorbents and Chemicals

Zeolites X and Y beads were provided by Arkema in sodium form. An ionic exchange to K^+ , Ca^{2+} , Sr^{2+} and Ba^{2+} forms was performed, and all the adsorbents were characterized (the exchange procedure and the characterization results are detailed in a previous chapter). D-glucose and D-xylose were purchased from Sigma-Aldrich with a purity > 99 %. Absolute ethanol was purchased from VWR, Milli-Q water was used to prepare all sugar solutions.

IV-1-2 Breakthrough experiments

The experimental setup is equipped with two SHIMADZU LC-40D pumps, the first one is used to inject the sugar feed solution to the column and the second one to pump the eluent, water in our case. In a typical experiment, the column filled with the adsorbent was placed inside an oven to control the temperature of the process and the concentration of sugars at the outlet was recorded thanks to a Kaiser Raman RXN2 online Raman spectrometer with an excitation wavelength of 785 nm. An optical probe was placed in the outlet stream with a special flow cell and the spectra were recorded thanks to the IC Raman software. The acquisition parameters were 2 scans and 14 seconds of exposure time. The quantification to build single component isotherms with or without ethanol in the feed solution was recorded with two separate univariate models for each sugar. The first one measures the concentration of glucose and ethanol with the fingerprint bands $539-504\text{ cm}^{-1}$ for glucose and $920-840\text{ cm}^{-1}$ for ethanol. The second quantifies xylose and ethanol taking as reference the bands $561-531\text{ cm}^{-1}$ for xylose and $920-$

859 cm⁻¹ for ethanol. For sugar mixtures dissolved in water, another univariate model was built with bands in the range of 1217-1128 cm⁻¹ for glucose and in the range of 1000-974 cm⁻¹ for xylose. When the two sugars are dissolved in water and ethanol, a model was developed with the specific bands 1192-1124 cm⁻¹ for glucose, 635-603 cm⁻¹ for xylose and 895-878 cm⁻¹ for ethanol. For the four Raman models, the first derivative was chosen as spectral pretreatment and spectrum subtraction was employed in addition for glucose/xylose and glucose / xylose / ethanol models (see Chapter II).

We verified that the quantification obtained with the Raman methods match the ones obtained by sampling in the column outlet and quantification by HPLC (Waters chromatographic system equipped with a column REZEX RCM-Monosaccharide Ca²⁺ (8 %), oven temperature 90 °C, isocratic mode with ultrapure water as mobile phase 0.6 mL min⁻¹, refractive index detector). The results are given in Figure A6 and Figure A7

Initially, the column is filled with Milli-Q water with a flow rate of 0.5 mL min⁻¹ at room temperature to get rid of air. Then the temperature is raised to 30 °C and the system is ready to receive the feed solution which is injected at the same flow rate (0.5 mL min⁻¹). When the adsorption equilibrium is established, *i.e.* when the breakthrough curve reaches a plateau and the recorded concentration at the outlet is the same as those of the feed, a four-way valve is turned and water is pumped through the column to desorb the sugar molecules from the solid.

The amount of adsorbed sugars was calculated using the following equations:

$$q_{ads} = (\mu_1 \times Q \times C_{plateau}) - (C_{plateau} \times V_{ns}) \quad (\text{Eq IV-1})$$

$$\mu_1 = \int_0^{\infty} \left(1 - \frac{c(t)}{c_0}\right) dt \quad (\text{Eq IV-2})$$

where q_{ads} is the quantity of adsorbed sugar (mol), μ_1 the first moment (min) defined by (Eq IV-2) and calculated thanks to the trapezoidal iterative integration method, Q the flow rate (mL min⁻¹), $C_{plateau}$ the concentration of the feed solution (mol mL⁻¹) and V_{ns} the non-selective volume where we suppose the adsorption does not take place (mL) expressed as:

$$V_{ns} = V_{dead} + V_p + V_{interparticle} \quad (\text{Eq IV-3})$$

where V_{dead} is the volume of the lines of the experimental apparatus without the column (approximately 1.77 mL with the volume of the column being 11.44 mL), V_p the volume of

mesopores and macropores estimated from mercury intrusion analysis and $V_{interparticle}$ the volume between the beads determined as follows:

$$V_{interparticle} = V_{column} - \frac{m_{zeolite}}{\rho_{zeolite}} \quad (\text{Eq IV-4})$$

with $m_{zeolite}$ the mass of adsorbent inside the column and $\rho_{zeolite}$ the density of the zeolite determined by mercury intrusion.

In the case of the mixture adsorption of two sugars dissolved in water or water and ethanol, the selectivity can be defined from the adsorbed quantities of each sugar at equilibrium by the following equation:

$$\alpha_{xyl/glu} = \frac{q_{ads\ xyl} \times C_{glucose}}{q_{ads\ glu} \times C_{xylose}} \quad (\text{Eq IV-5})$$

Defined in such a way, a selectivity greater than unity indicates an affinity of the adsorbent towards xylose. $C_{glucose}$ and C_{xylose} are the concentrations at equilibrium which are the concentrations of the feed solution in the case of a breakthrough test. After calculating the number of supercages per gram of each zeolite (SP) (see Chapter III), all the adsorbed amounts calculated with (Eq IV-1) are converted to adsorbed sugar per supercage as follows:

$$N_{sugar/\alpha\ cage} = \frac{q_{ads\ sugar} \times N}{SP \times m_{dry\ zeolite}} \quad (\text{Eq IV-6})$$

where $q_{ads\ sugar}$ the adsorbed quantity (mol), N the Avogadro number, SP the number of supercages per gram of zeolite and $m_{dry\ zeolite}$ the mass of dry zeolite introduced in each column.

Isotherms are fitted according to Langmuir model:

$$\frac{q}{q_s} = \frac{kC}{1+kC} \quad (\text{Eq IV-7})$$

where q is the adsorbed quantity, q_s is the maximum uptake, k is the equilibrium constant and C is the concentration at equilibrium. At low coverage, the Langmuir model approximates to a linear Henry Model:

$$q = q_s k C = KC \quad (\text{Eq IV-8})$$

with $K=q_s k$ being the slope of the linear isotherm or Henry coefficient. A theoretical selectivity can be defined from the ratio of Henry's constants defining a selectivity in an ideal case where the sugars do not interact between them:

$$\alpha'_{xyl/glu} = \frac{K_{xylose}}{K_{glucose}} \quad (\text{Eq IV-9})$$

IV-2 Results and discussion

IV-2-1 Single component isotherms

Breakthrough curves of glucose and xylose were recorded using their aqueous solutions as a feed with concentrations ranging between 0.34 mol.L^{-1} and 1.53 mol.L^{-1} (corresponding to concentrations between 60 g/kg and 250 g/kg) at $30 \text{ }^\circ\text{C}$. From each breakthrough curve (*Figure A 8*), an adsorbed amount of sugar was calculated and used for isotherm construction. The adsorbed amount was converted from moles to molecules per supercage thanks to (Eq IV-6).

The adsorption isotherms in exchanged zeolites X are shown in *Figure IV- 1*. All the isotherms are linear in the explored concentration range which defines the Henry region. Of note, we could not further increase the concentration because of the feed pump viscosity limitation. For the adsorbents with the counterions of the same valence, the order of affinities for both sugars is: $\text{Na} < \text{K}$ for monovalent ions and $\text{Ca} < \text{Sr} < \text{Ba}$ for bivalent ions. The strongest affinity toward monosaccharides is found with KX with uptakes of 1.5 molecules of glucose and 2 molecules of xylose per supercage at the highest concentration of 250 g/kg (1.53 mol.L^{-1}). An inversion of affinities can be seen between the two sugars with NaX and BaX where xylose is preferably adsorbed in BaX and glucose in NaX. We can observe that the affinity increases with the ionic radii for monovalent ions (102 pm for Na and 138 pm for K) and also for bivalent ions (100 pm for Ca, 118 pm for Sr, and 135 pm for Ba).

Similar linear isotherms are obtained for zeolites Y, and the strongest affinity for both sugars is found with barium rather than potassium in comparison to zeolites X. The affinity order of glucose did not change with respect to the ions' valence, but it changed for bivalent ions in the case of xylose ($\text{Sr} < \text{Ca} < \text{Ba}$) although the two isotherms of CaY and SrY are very close.

Overall, after fitting the isotherms with a linear model, the increase in Si/Al ratio from 1.2 to 2.6 results in a decrease of the Henry constants of glucose and xylose for the monovalent counterions and an increase for calcium and strontium zeolites. However, in case of barium, Henry constant decreases for xylose and increases for glucose (*Table A 3*). It was suggested in

the literature that the formation of sugar-cation complexes is responsible for the adsorption⁶⁸. The reduction of the number of ions results in less coordination sites which can explain the weakening of the interactions between the two sugars and the monovalent ions (if we suppose that all the adsorbents have the same q_{max} since the slope that we show is equal to kq_{max}). This results in the lowering of the uptakes in NaY and KY compared to NaX and KX. Nevertheless, the latter explanation does not apply for calcium and strontium-exchanged zeolites, where the increase of Si/Al favors high affinities considering the latter hypothesis. The reduction of the compensating ions when increasing the Si/Al ratio in the zeolite framework comes with a decrease of the electrostatic contributions in the confined space. The electrostatic environment and Van der Waals components created according to the composition of each zeolite could define and drive the sugars-zeolites interactions and the way they are going to be placed in the supercage.

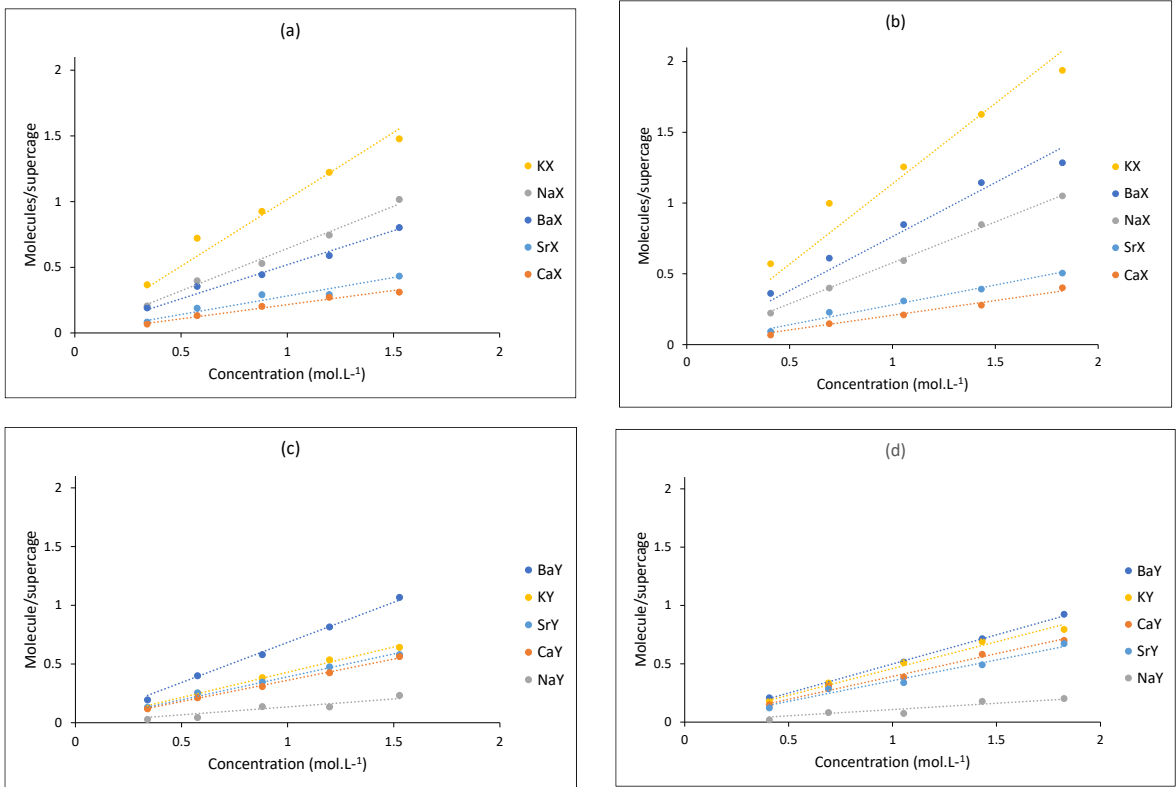


Figure IV- 1: Single adsorption isotherms of a) glucose and b) xylose in exchanged zeolites X and c) glucose and d) xylose in exchanged zeolites Y at 30 °C

From the single-component isotherms, we determined ideal selectivities using (Eq IV-9) which assumes the absence of any interactions between the adsorbates. The comparison of the selectivities obtained from the breakthrough curves with sugars mixtures (see Chapter III) and the ideal ones are given in *Figure IV- 2*. Overall, both obtained selectivities are close which indicates that the mixture behavior can be predicted by the single-component isotherms.

These results show that the sugar-sugar interactions do not interfere with the separation and that is rather the zeolite-sugar interactions that are responsible of the process. The xylose/glucose selectivity in BaX and BaY is inverted. The contribution of complexation in that case is difficult to evaluate due to the presence of 42 % sodium in BaY.

Caruel et al. studied the separation of lignocellulosic sugars and their sugar alcohols using exchanged resins.⁶³ They investigated the cation type effect on the separation with pulse tests, where a selectivity can be calculated from the ratio of capacity factors as defined by the authors. Xylose/glucose selectivities of 1.17, 1.27 and 1.16 are found for Ca²⁺, Sr²⁺ and Ba²⁺ exchanged resins respectively. Considering the same ions in the zeolites prepared in this work, we can see that the selectivity order is different, with higher selectivity of 1.52 found for BaX. Complex formation is the mechanism responsible for adsorption using resins, this allows to highlight the confinement effect of zeolites and show that the separation mechanism is much more complex and does not only depend on complex formation.

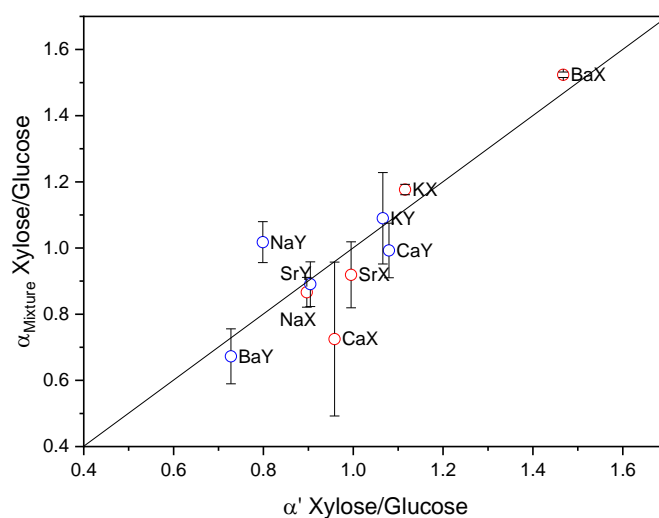


Figure IV- 2: Comparison between the mixture and ideal xylose/glucose selectivities

IV-2-2 Sanderson's intermediate electronegativity

Adsorption equilibrium constants k (can be obtained from Henry's constants if we suppose that all zeolites have the same saturation q_s) correspond to the exchange reaction between water and a sugar molecule according to the following simplified reaction:



These constants represent the interactions between a zeolite and a sugar. Two types of interactions can be distinguished: the first, described as specific, representing the electrostatic interactions generated by cations. The second, nonspecific, representing Van der Waals interactions created by the confinement in the presence of cations. Sanderson's intermediate electronegativity (S_{int}) gives a first approximation to evaluate the specific interactions effect.

The values of S_{int} are calculated for all zeolites and given in *Table A 2*. Sanderson's intermediate electronegativity increase as: (a) Si/Al increases from 1.2 to 2.6, (b) the valence of cations on the same Si/Al increases such as from Na to Ca and (c) the ionic radii decreases for ions with the same valence.¹¹³ In *Figure IV- 3* we plotted Henry's coefficients as a function of Sanderson's intermediate electronegativity. We can see that the affinity decreases for glucose and xylose when S_{int} increases for monovalent cations (from K to Na) and bivalent cations (from Ba to Ca) in zeolites X and Y. Both sugars have an intermediate electronegativity of 2.865 which is higher than S_{int} of all the zeolites. The high value of S_{int} reflects a high electro-accepting ability, and the strongest adsorbent-adsorbate interaction is the one with the highest difference between the two electronegativities. Potassium and barium-exchanged zeolites X and Y have the lowest S_{int} (2.331 for KX, 2.627 BaX and 2.549 for KY 2.710 BaY) resulting in the strongest interactions and therefore the highest affinities. Henry's constants are linearly correlated to Sanderson's intermediate electronegativities with respect to the cation valence. Nevertheless, the latter parameter does not explain by itself the experimental affinities and selectivities. Henry's constants depend on the size and number of cations, a high number, and a big cation size result into more impacting confinement and therefore a high Henry's constant (the case KX as an example).

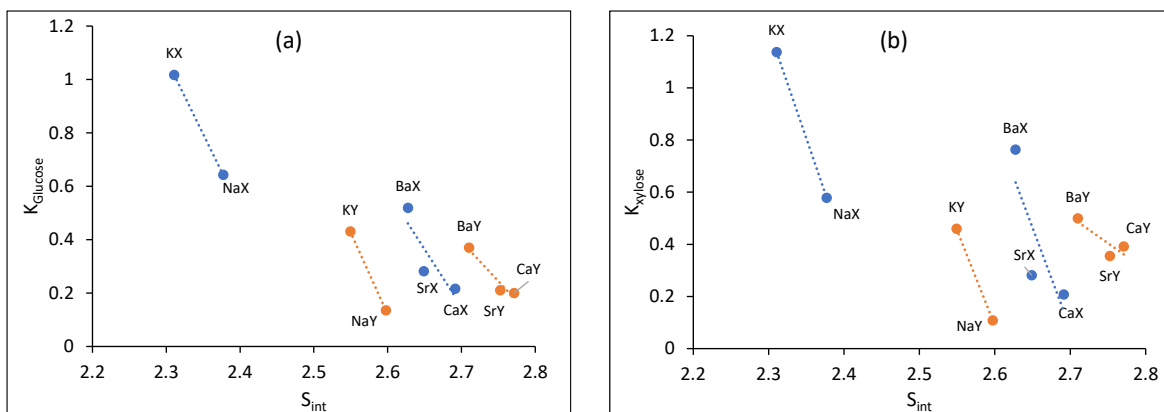


Figure IV- 3: Correlation between Henry's constants and Sanderson's intermediate electronegativity for a) glucose and b) xylose

IV-2-3 Adsorption isotherms from water-ethanol mixtures

In order to understand the effect of the chemical composition of zeolites on adsorption constant k and the saturation q_s (since the slope $K=kq_s$), it is important to get access to the information about the maximum uptake of glucose and xylose. While increasing the feed concentration was technically not a viable solution, the second option was to add a cosolvent. Zeolites have higher affinities towards water than sugars, so the addition of a cosolvent should reduce the amount of water in the feed and adjust of the solvent-zeolite, sugar-zeolite competition in a way that favors sugars uptake. Similar experiments are reported in the literature, it was found that the adsorbed amount of fructose in CaX from 1 part water and 3 parts methanol in volume increases compared to adsorption from an aqueous solution. The adsorption isotherm adding methanol in the mixture showed a fructose saturation value of 130 mg g^{-1} that was unknown from the isotherm when the sugar is dissolved only in water.⁷¹ Fornefett et al. investigated the adsorption of sucrose, a disaccharide of glucose and fructose, in dealuminated zeolites Y. They observed that the adsorption in zeolite Y with Si/Al ratio of 2.8 is enhanced when sucrose is dissolved in a 90 vol % ethanol.⁷² We tested the adsorption of glucose in BaY from water-ethanol mixtures containing 10 %, 30 %, and 50 % (% wt.) ethanol. *Figure IV- 4* shows the ethanol effect on the glucose breakthrough curves. The first moment increases with the increase of ethanol content in the feed, it passes from 21.6 min to 25.5, 29.9 and 38.6 min for the water : ethanol ratios of 90:10, 70:30 and 50:50 %wt. respectively which will therefore increase the adsorbed amount according to (Eq IV-1).

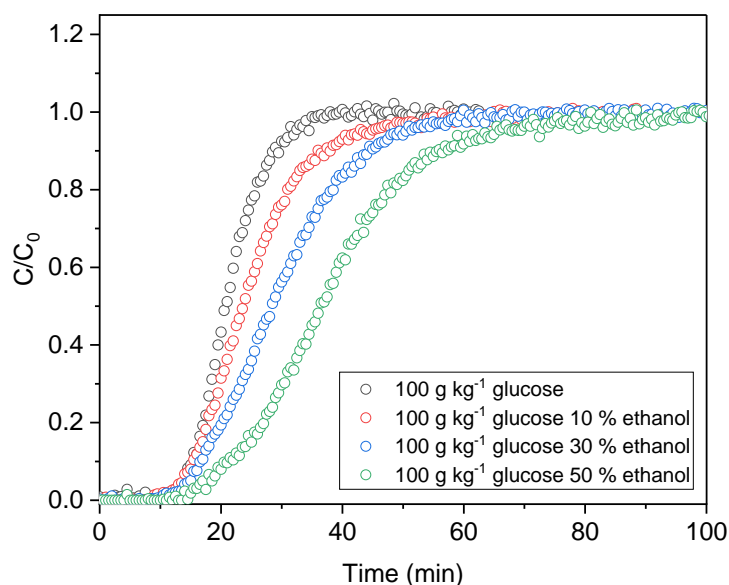


Figure IV- 4: Ethanol effect on the breakthrough curve of 100 g kg^{-1} glucose solution in BaY at $30 \text{ }^\circ\text{C}$

Single component isotherms for glucose and xylose dissolved in 50:50 %wt. water ethanol mixtures in BaX, BaY, KX and KY are presented in *Figure IV- 5* and *Figure IV- 6*. Solubilities in aqueous ethanol for both sugars must be taken into consideration, the solubility of glucose¹¹⁴ in 50 % ethanol at 30°C is 230 g kg^{-1} and for xylose, it is 320 g kg^{-1} at $25 \text{ }^\circ\text{C}$.¹¹⁵ The adsorbed amount is significantly enhanced in all tested zeolites and isotherms are fitted using Langmuir model using OriginPro 2021b software. The extrapolated maximum loadings of glucose and xylose in BaX are 1.5 and 2 molecules per supercage, the same loading is found for glucose in BaY but an estimated 3 xylose molecules per supercage is calculated in BaY. Similar saturation values are obtained for KX and KY, which are around 2.6 glucose molecules per supercage and 3 xylose molecules. Knowing the saturation amounts, we can say that the variation in Henry's constants for the adsorption isotherms from aqueous solutions is due to a change in the equilibrium constant k ($K = kq_s$) in KX and KY and therefore different interaction modes in the two zeolites. Glucose has the same maximum loading in BaX and BaY meaning that also k is responsible for the change in K . The dealumination in this case increases Henry's constant from 0.52 to 0.68 and the presence of sodium in BaY (42 %) seems to strengthen glucose-zeolite interactions. Although BaY has a higher xylose maximum loading (3 molecules per supercage) than BaX (2 molecules per supercage), this does not increase K but instead

Henry's constant decreases from BaX to BaY (from 0.76 to 0.50). These observations suggest that xylose forms more stable complexes in the presence of high barium content.

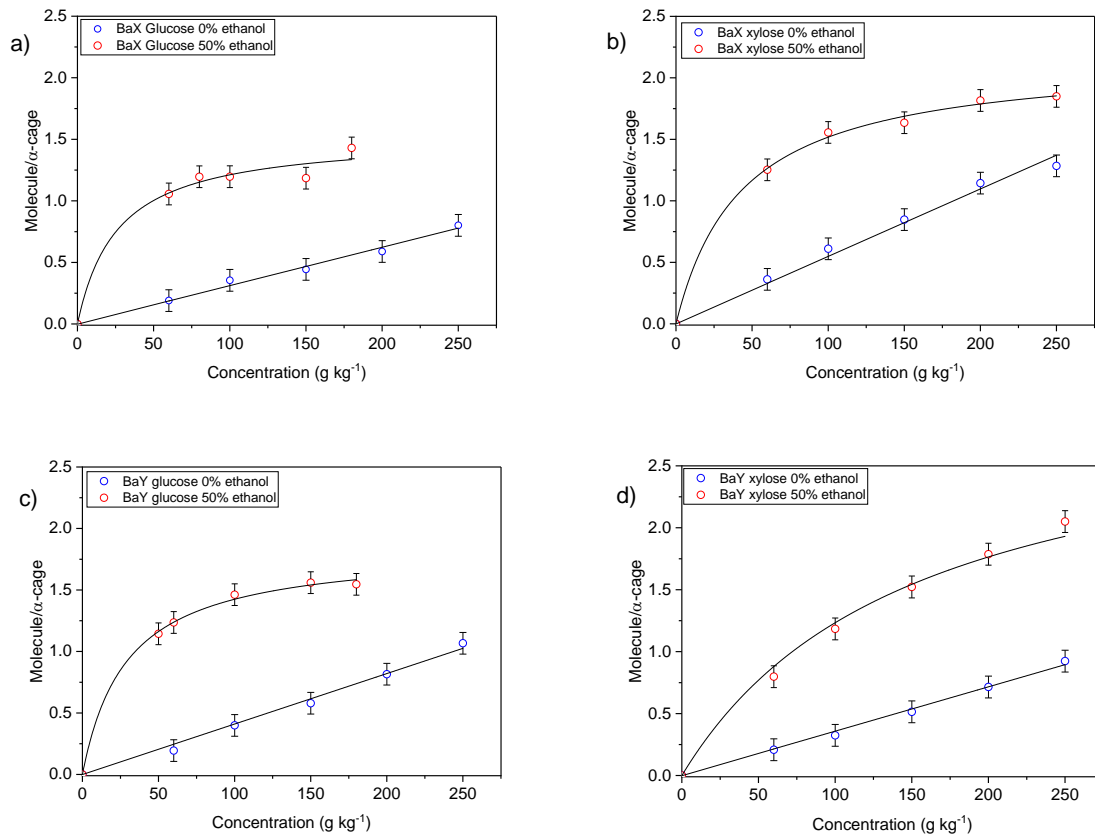
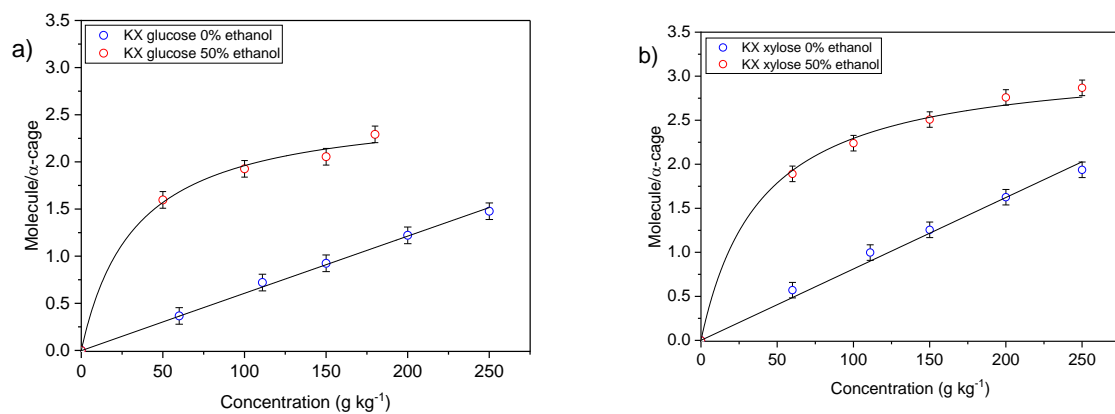


Figure IV- 5: Single adsorption isotherms with 50 % ethanol in BaX (a and b) and BaY (c and d) at 30 °C



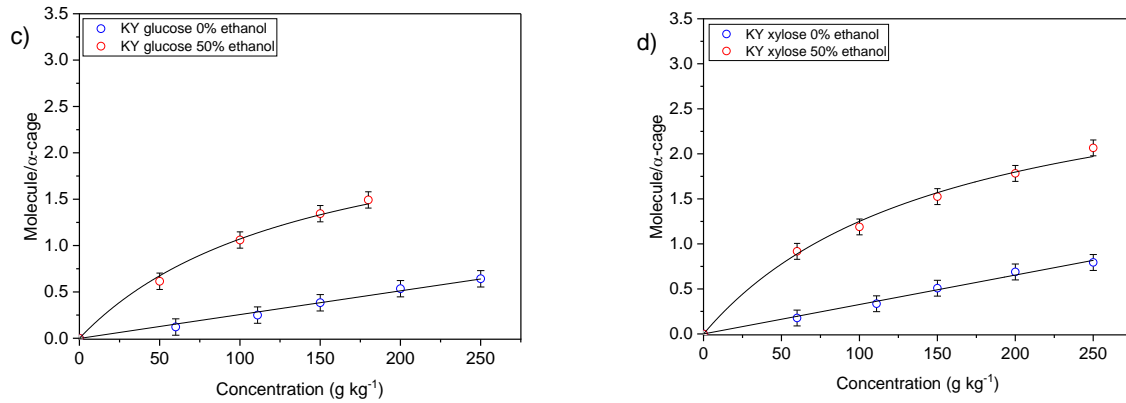


Figure IV- 6: Single adsorption isotherms with 50% ethanol in KX (a and b) and KY (c and d) at 30 °C

IV-2-4 Ethanol effect on selectivities

Previous experiments were done with a single sugar dissolved in water and ethanol, thus we wanted to study the effect of ethanol when it is added to a mixture of glucose and xylose. *Figure IV- 7* shows the evolution of the mixture selectivity as a function of feed ethanol content in BaX and BaY. Xylose/glucose selectivity decreases from 1.6 to around 1.3 and stays constant adding 10 % to 60 % (% wt.) ethanol in BaX which stays selective to xylose regardless of the feed composition. However, in the case of BaY, the selectivity increases from 0.6 to almost 1 where the zeolite becomes nonselective. Xylose uptake becomes more important by adding ethanol and equals glucose uptake when 60 % ethanol is introduced. These results suggest that the selectivity in the Henry zone and at saturation are different. By plotting the single component isotherms of glucose and xylose dissolved in 50:50 wt% water ethanol mixtures for BaX and BaY in the same graph ,(Figure A 9) we can see that for BaX, the zeolite is selective towards xylose in the Henry regime and at saturation. However, BaY is selective to glucose until the concentration of 150 g kg⁻¹ (in 50:50 wt% water ethanol) where it becomes non selective, and beyond this concentration close to saturation, the selectivity is inverted and BaY becomes selective to xylose. These observations can be applied in case of aqueous solutions without ethanol as well.

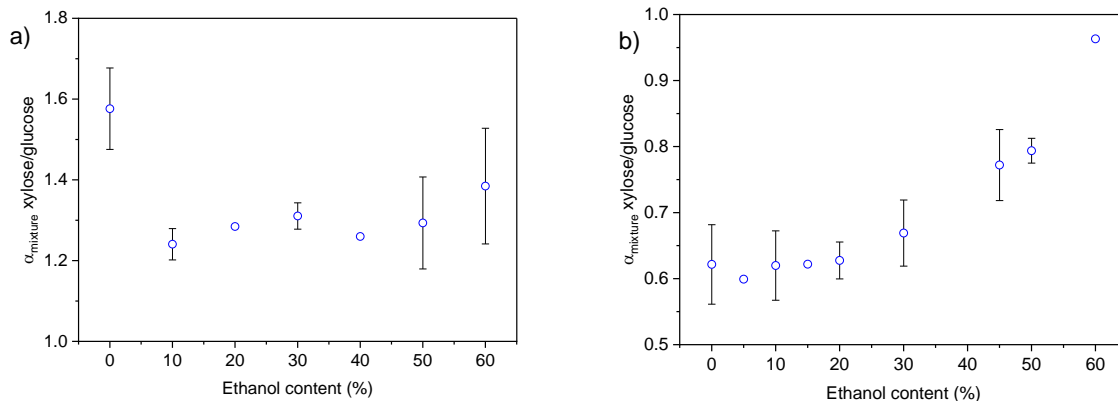


Figure IV- 7: Ethanol effect on the mixture selectivity in a) BaX and b) BaY. Mixture concentration of 100 g kg⁻¹ glucose and 100 g kg⁻¹ xylose is used

Figure IV- 8 presents a comparison between selectivities obtained from the aqueous mixture (150 g kg⁻¹ glucose and 150 g kg⁻¹ xylose) and a mixture dissolved in 50 wt% ethanol (100 g kg⁻¹ glucose and 100 g kg⁻¹ xylose) in all exchanged zeolites X and Y. By adding ethanol, the selectivity in NaX, KX, BaX, NaY, KY and SrY decreases. Interestingly, NaY which is non-selective with an aqueous mixture, becomes selective towards glucose with ethanol in the feed. CaX and SrX became selective to xylose (selectivities of 1.3 and 1.23 respectively) after being non-selective.

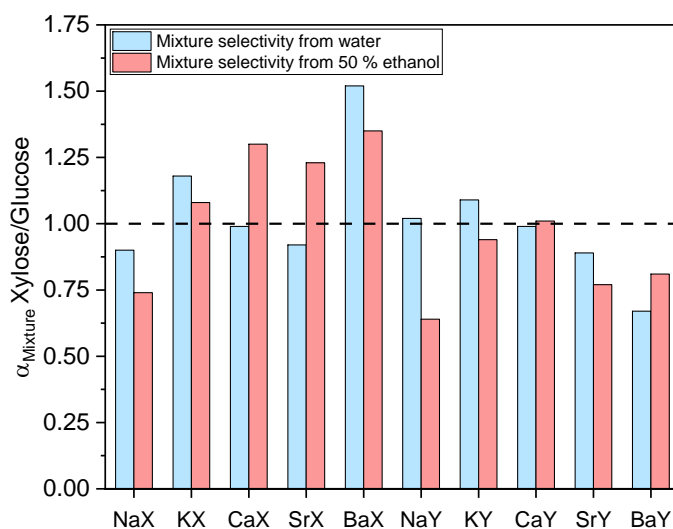
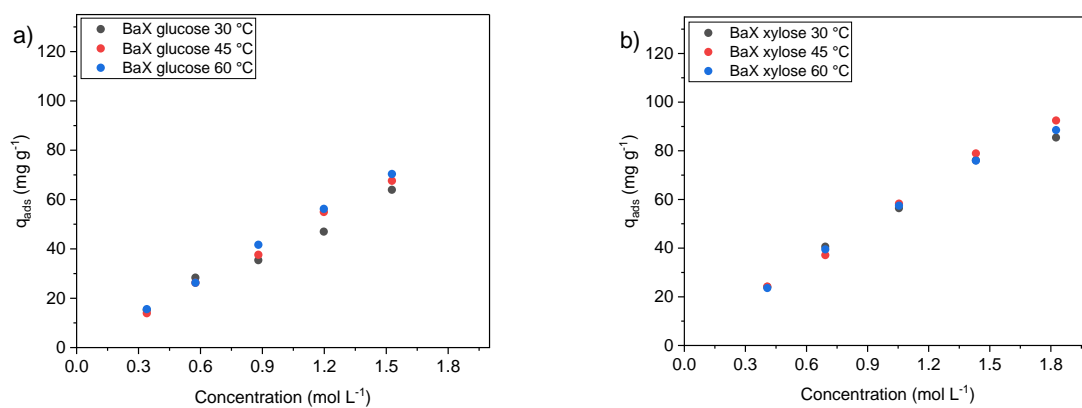


Figure IV- 8: Ethanol effect on the mixture selectivity

IV-2-5 Temperature effect

Single adsorption isotherms measured at 30, 45, and 60 °C for BaX, BaY, KX and KY and are presented in *Figure IV- 9*. The isotherms obtained for potassium and barium exchanged zeolites are close and overlapped in the case of BaX. In a typical adsorption experiment, the increase of temperature decreases the adsorbed amount since it is an exothermic process, but it is not the case in this study. Zeolites are hydrated with water prior the breakthrough tests or following a desorption step, when the sugars are introduced into the supercages, a displacement of previously adsorbed water molecules by the monosaccharides will take place in the adsorption sites. This displacement seems to be not affected by the temperature reflecting that the adsorption enthalpy of sugars and water are close. Van't Hoff relation can be applied to determine the enthalpy and entropy of displacement¹¹⁶, the slopes of the isotherms represent Henry's constants ($K = kq_s$) which are divided by the maximum adsorbed amount assessed in the previous paragraph by adding ethanol as a cosolvent, to access the equilibrium adsorption (which is expressed without units considering a reference standard solution with a concentration of 1 mol L⁻¹ as detailed in the latter mentioned reference) constants and evaluate the enthalpic and entropic contributions.



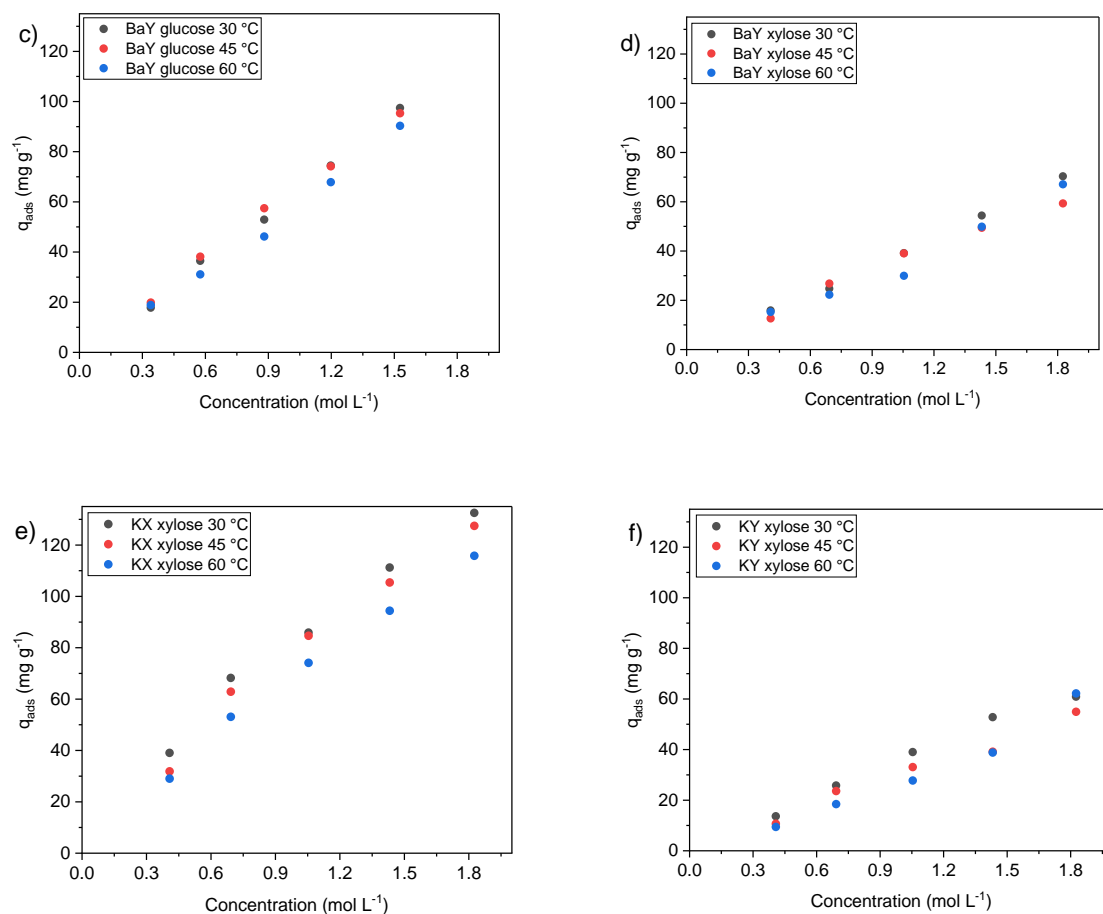


Figure IV- 9: Adsorption isotherms at 30 °C, 45 °C, and 60 °C in BaX, BaY, KX, and KY zeolites

The obtained thermodynamic parameters are collected in *Table IV- 1*. All values of free energies are positive reflecting that water displacement is not a spontaneous process. The entropic effect is stronger than the enthalpic contribution as expected, the displacement entropy of zeolites X (BaX and KX) is more important than zeolites Y (BaY and KY) for glucose and xylose. A high entropy reflects the increase of randomness at the adsorbent-solution interface during the displacement of water molecules. Glucose is a bigger molecule than xylose having a molar diameter of 0.72 nm while xylose has a diameter of 0.68 nm⁸⁴ and thus it gives higher entropies of 2 and -16 J mol⁻¹ K⁻¹ in BaX and BaY respectively compared to xylose (-7 and -24 J mol⁻¹ K⁻¹ in BaX and BaY respectively). Nevertheless, the differences between the two displacement entropies of the two sugars are not important. It was shown thanks to Monte Carlo calculations that the transfer of glucose from an aqueous solution to an all silica zeolite beta goes with an unstructuring of the hydration sphere resulting in a high entropy of transfer compensating the enthalpy of transfer as it is the case in our experimental study.¹¹⁷

Table IV- 1: Enthalpies, entropies and free energies of displacement

	$\Delta_r S^\circ$ (J mol ⁻¹ K ⁻¹)	$\Delta_r H^\circ$ (kJ mol ⁻¹)	$\Delta_r G^\circ$ (kJ mol ⁻¹) at 30 °C
Xylose			
BaX	-7	0	3
BaY	-24	-3	5
KX	-23	-4	3
KY	-31	-4	5
Glucose			
BaX	2	3	3
BaY	-16	-3	2

IV-3-Conclusion

In conclusion, we show that the modification of the counterion type and the Si/Al ratio has a large impact on the affinities towards glucose and xylose. The highest affinities for both sugars are with potassium and barium in zeolites X and Y with respect to the ions valence. We show that the affinities are correlated to Sanderson's intermediate electronegativities, the smaller value of the electronegativity the greater the affinity for monovalent and bivalent cations. Glucose and xylose uptakes are enhanced from water ethanol solutions as shown for the first time, which allowed to determine the saturation and the maximum loading per supercage. The addition of ethanol in the feed mixtures showed interesting results as it changes in some cases the mixture selectivities Zeolite NaY which does not show any selectivity from pure aqueous solutions became selective to glucose. The same effect has been observed for zeolites CaX and SrX which became selective to xylose.

Overall, the displacement of water by sugars is "athermic", entropy drives the displacement of water by sugars but enthalpic and entropic contributions do not explain the affinities and the selectivities observed. Complex formation, electrostatic contributions and hydration of sugars are most likely the elements that define the zeolite-sugar interactions. Further studies at a molecular scale are required to identify the effect of these elements.

Chapter V: Solid state NMR observation of glucose and xylose adsorption in BaX and BaY

In this chapter, the adsorption of glucose and xylose in selective zeolites BaX and BaY was investigated thanks to magic angle spinning nuclear magnetic resonance (MAS NMR) of ^{13}C . NMR spectra of labelled sugars in their anomeric carbon were recorded, then the α -pyranose and β -pyranose content was determined in mobile and adsorbed phases. In this section, we decided to work in water-ethanol mixtures (50:50 in weight) since in these conditions the quantity of sugars adsorbed is increased compared to using pure water as a solvent, according to the results reported in Chapter IV.

V-1 NMR analysis and samples preparation

D-Glucose-1- ^{13}C labelled in the anomeric carbon was purchased from Sigma-Aldrich with a purity > 99 %. D-Xylose-1- ^{13}C was supplied from Eurisotop (99 % purity).

Liquid NMR spectra were recorded on a Bruker Avance III spectrometer (7 T magnet) equipped with a Broadband probe (BBFO) at 300 K. The applied frequency was 75.47 MHz for ^{13}C nuclei. Proton decoupled ^{13}C spectra were recorded with the following parameters: acquisition time of 1.66 s, pulse duration of 9 μs with 38.8 W power pulse force, relaxation delay of 2 s and a sweeping range of 19736.8 Hz. The number of scans was adjusted according to the sample.

Solid-state ^{13}C MAS NMR spectroscopy experiments were performed on an Avance NEO 400 spectrometer equipped with a 9.4 T magnet, using a 4 mm CPMAS probe. The applied frequency was 100.61 MHz for ^{13}C nuclei. ^{13}C spectra were recorded with ^1H SPINAL-64 decoupling ($\nu\text{RF} = 100$ kHz), the rotor spun at 14 kHz and acquisition time was 13 min (160 scans).

The sugars (glucose or xylose) were dissolved in a water ethanol mixture (50:50) %weight to obtain a concentration of 150 g kg^{-1} . Then BaX or BaY (about 300 mg) were mixed with 1.5 ml of the prepared solution at room temperature for 16 hours. According to the results shown in the previous chapter, these conditions should correspond to an adsorbed quantity at equilibrium

of around 1.5 molecule of glucose or xylose per superpage of BaX or BaY. The rotors were packed with the slurry recovered by centrifugation at 6400 rpm for 30 min.

Spectra decompositions were performed using Dmfit software. First, sharp peaks were fixed to every signal (position and full width at half maximum (FWHM)) taking a Gaussian-Lorentzian ratio of 0.5. Then, broad peaks were added and adjusted (positions and FWHM as well) to obtain the best global fit.

V-2 ^{13}C NMR of the free sugars in solution

Prior to the adsorption study, a pinch of labelled glucose and xylose are dissolved each in 50:50 wt% D_2O and ethanol and analyzed with liquid NMR. *Figure A 10* and *Figure A 11* present the spectra in the range of 0-250 ppm. *Figure V- 1* shows the obtained spectrum of glucose with two C1 signals representing α -glucopyranose (AGP) at 92.2 ppm and β -glucopyranose (BGP) at 96.2 ppm. A weak signal at 102.7 ppm is also identified, which represents the β -glucofuranose tautomer (BGF).¹¹⁸ The integration of the signals yields a BGP:AGP tautomeric ratio of 59:41, while the BGF form accounts for around 0.3 %.

Figure V- 2 presents the obtained spectra of xylose solution, the two intense bands at 92.4 ppm and 96.9 ppm correspond to α -xylopyranose (AXP) and β -xylopyranose (BXP) respectively. The small chemical shift at 102 ppm arises from the β -furanose form of xylose (BXF). We notice also the presence of a signal at 95.8 ppm which is assigned to the β -pyranose form of lyxose, which is the epimer of xylose.¹¹⁹ The determined BXP:AXP ratio is 59:41 (%). Estimated amount of lyxose and BXF at around 0.8 % each are found, based on the integration of their respective signals.

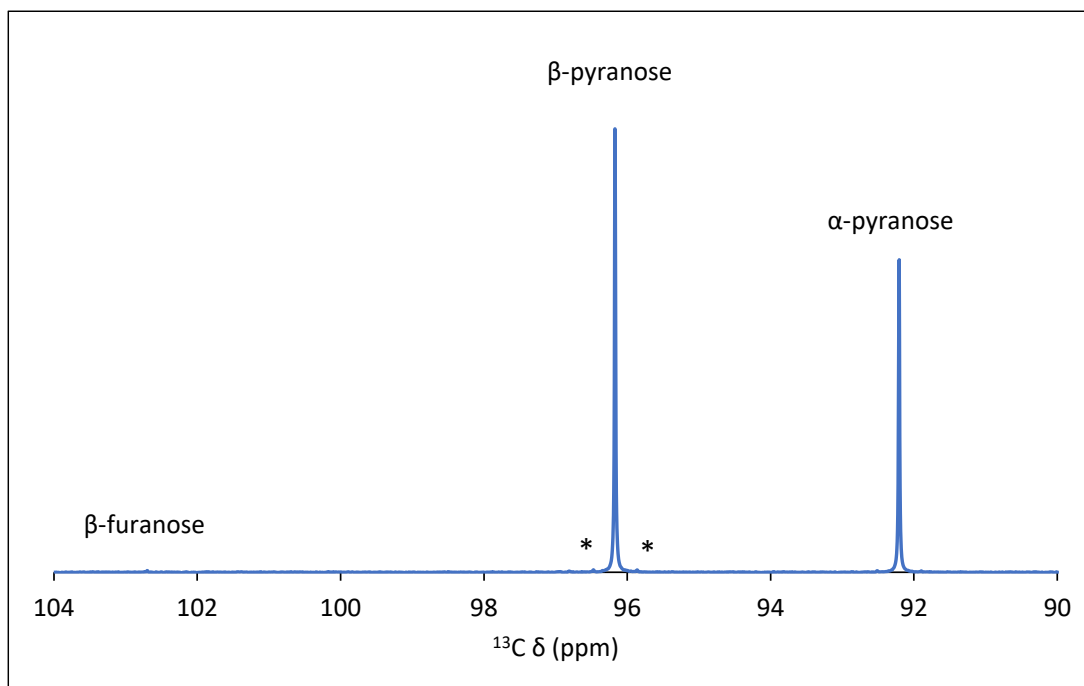


Figure V- 1: Liquid Carbon NMR spectra of labelled C1-glucose dissolved in 50:50 %wt D₂O and ethanol at 25 °C. * refers to carbon satellites occurring from the coupling of labelled carbon with neighboring unlabeled carbons

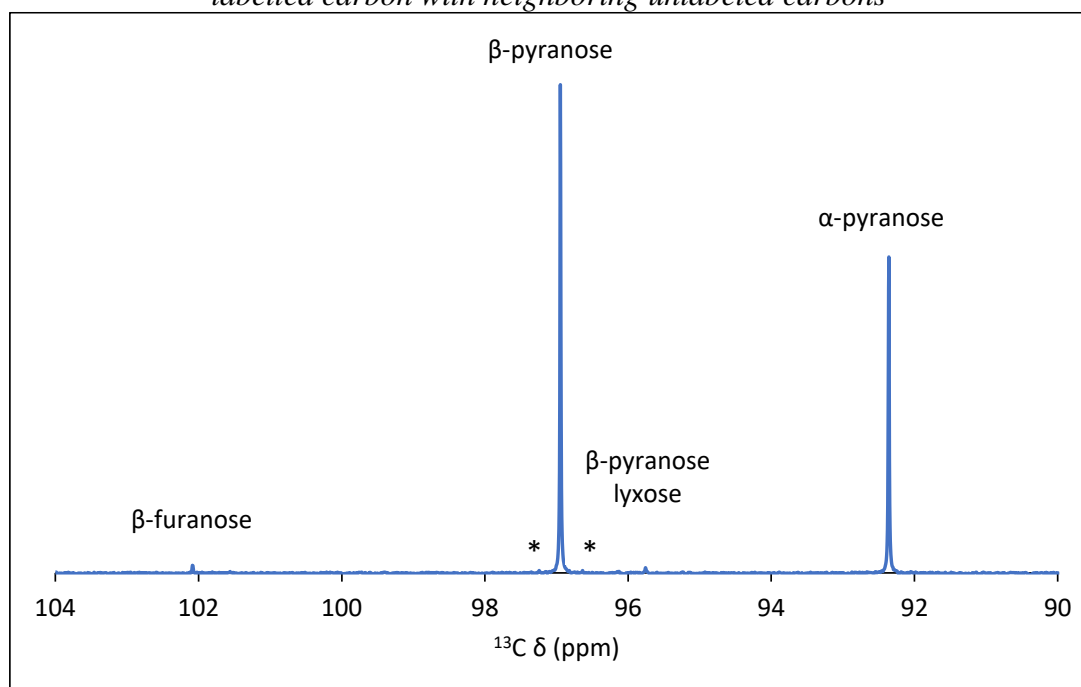


Figure V- 2: Liquid Carbon NMR spectra of labelled C1-xylose dissolved in 50:50 %wt D₂O and ethanol at 25 °C. * refers to carbon satellites occurring from the coupling of labelled carbon with neighboring unlabeled carbons

V-3 ¹³C MAS NMR of sugars adsorbed in the zeolites

V-3-1 Glucose

Glucose spectra are recorded at 25 °C and 75 °C in BaX and BaY and signals assignments are presented in *Table V- 1*. According to interpretations reported in similar previous work in the literature, sharp peaks represent highly mobile analyte in the bulk solution, while broad peaks arise from restricted mobility and the loss of degrees of freedom when molecules are adsorbed on an adsorption site or confined in pores.¹²⁰ We consider herein that when a recorded peak has a FWHM of less than 0.7 ppm, the corresponding species is in the mobile phase, and when the FWHM is higher than 0.7 ppm it is in the adsorbed phase. The two anomeric signals, as shown in *Figure V- 3*, are composed of sharp peaks assigned to the pyranose tautomers in the mobile phase (AGP, 91.9 ppm; BGP, 95.7 ppm for BaX, AGP, 91.8 ppm; BGP, 95.7 ppm for BaY) and broad signals arising from the same tautomers when they are adsorbed in the pores (AGP, 91.7 ppm; BGP, 95.4 ppm for BaX, AGP, 92.0 ppm; BGP, 95.6 ppm for BaY). The chemical shifts of the adsorbed forms vary by less than 1 ppm compared to the chemical shifts of their mobile counterparts (usually upfield), these observations are also valid at 75 °C and consistent with previous work on NaX.¹²⁰ Decomposition of the spectra and analysis of the areas of the different contributions allows for analyzing the populations and tautomeric ratios in both mobile and adsorbed phase and evaluate the influence of the zeolite and the temperature. The tautomeric distributions determined are presented in *Figure V- 4*.

- In BaX, the (BGP:AGP) tautomeric ratios are almost the same in the mobile (62:38) and adsorbed (64:36) phases at 25 °C. These ratios are very close to the ratios in the solution obtained previously with the liquid NMR measurements (59:41) at room temperature. At 75 °C, the ratio BGP:AGP in the liquid phase varies slightly (56:44) compared to 25 °C, but does not differ much from the ratio in adsorbed phases (60:40) considering the uncertainty of these measurements (estimated to ± 3.6 % for adsorbed phase and 4.4 % for mobile phase). The BGP is thus the favored form in all phases.
- With BaY, at 25 °C, we surprisingly found a BGP:AGP ratio of 52:48 in the mobile phase, which is significantly different from the ratio observed in BaX or in solution, although it should not. We note however that on BaY, the peaks observed are generally broader than on the spectra with BaX, which might yield a higher uncertainty in the deconvolution procedure. The ratios in adsorbed phase are slightly in favor of the AGP tautomer (BGP:AGP of 45:55). At 75 °C, however, the liquid phase ratio is found of

56:44 (similar to the value obtained at this temperature on BaX) and the ratio in the adsorbed phase reflects that in the liquid phase (57:43).

- In total and considering both AGP or BGP forms, 47 % of glucose is confined in BaX at 25 °C (53 % in the mobile phase) while 67 % is adsorbed in BaY (33 % in the mobile phase). At 75 °C, a total of 47 % is found as well in BaX while a decrease to 58 % is obtained in BaY. This is consistent with our previous results showing that for this concentration, the quantity adsorbed at equilibrium is higher for BaY than for BaX (see Chapter IV).
- Additionally, a signal at a chemical shift of 93.9 ppm appears in BaX spectra at 25 °C and 75 °C which is not present in the liquid spectrum. The latter result can be the product of glucose epimerization by BaX into mannose since the signal corresponds to the β -pyranose ring of mannose.¹¹⁹ Nevertheless, in our breakthrough experiments followed by HPLC, it was not possible to assess the occurrence of this reaction and only 2 peaks (for glucose and ethanol) were found in the chromatogram. The signal around 102.3 ppm characteristic of the β -furanose ring already detected in the liquid NMR experiments, is identified at 75 °C for both zeolites. This is due to the displacement of the tautomeric equilibrium. We find that BGF it should be in the adsorbed phase according to the obtained FWHM (1.2 ppm) and represents around 1% of the total tautomeric composition of this phase.

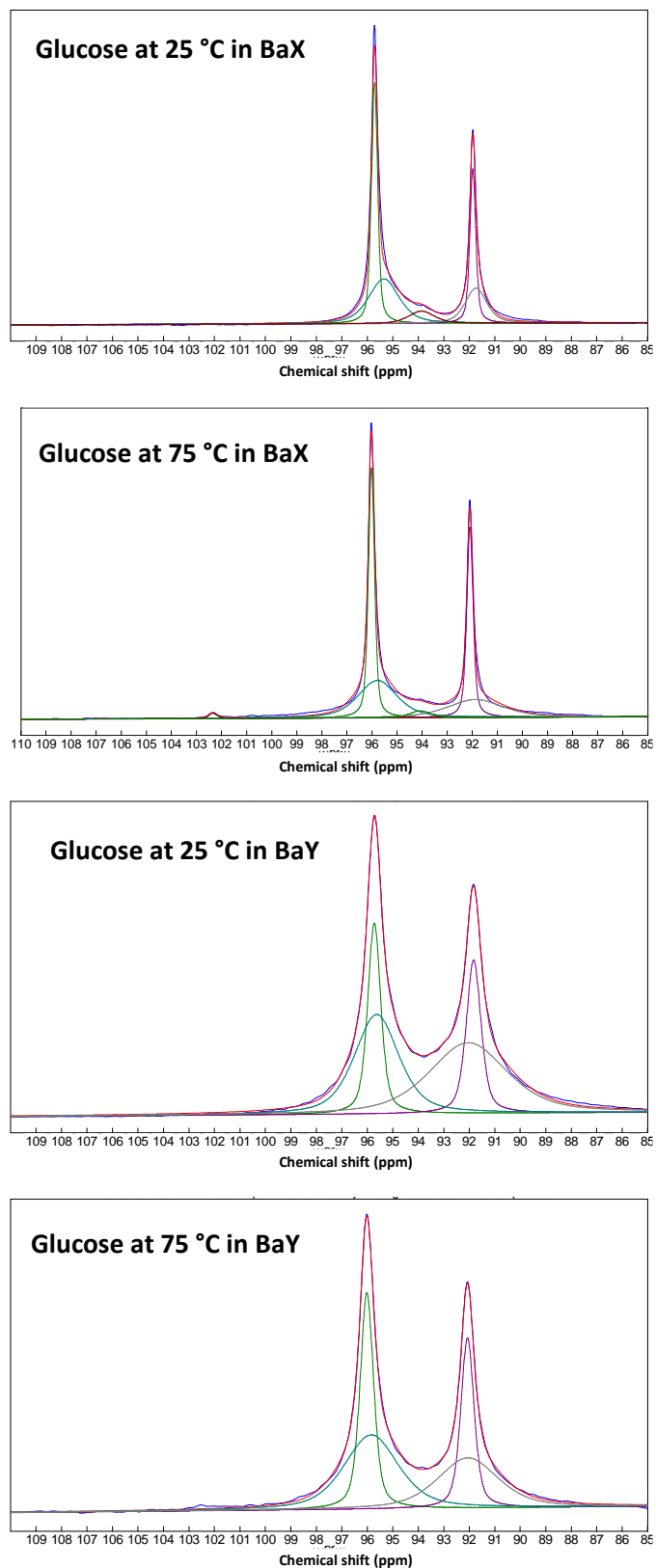


Figure V- 3: Glucose MAS solid-state ^{13}C NMR spectra recorded at 25 °C and 75 °C for BaX and BaY (blue line), fitted spectra (red line)

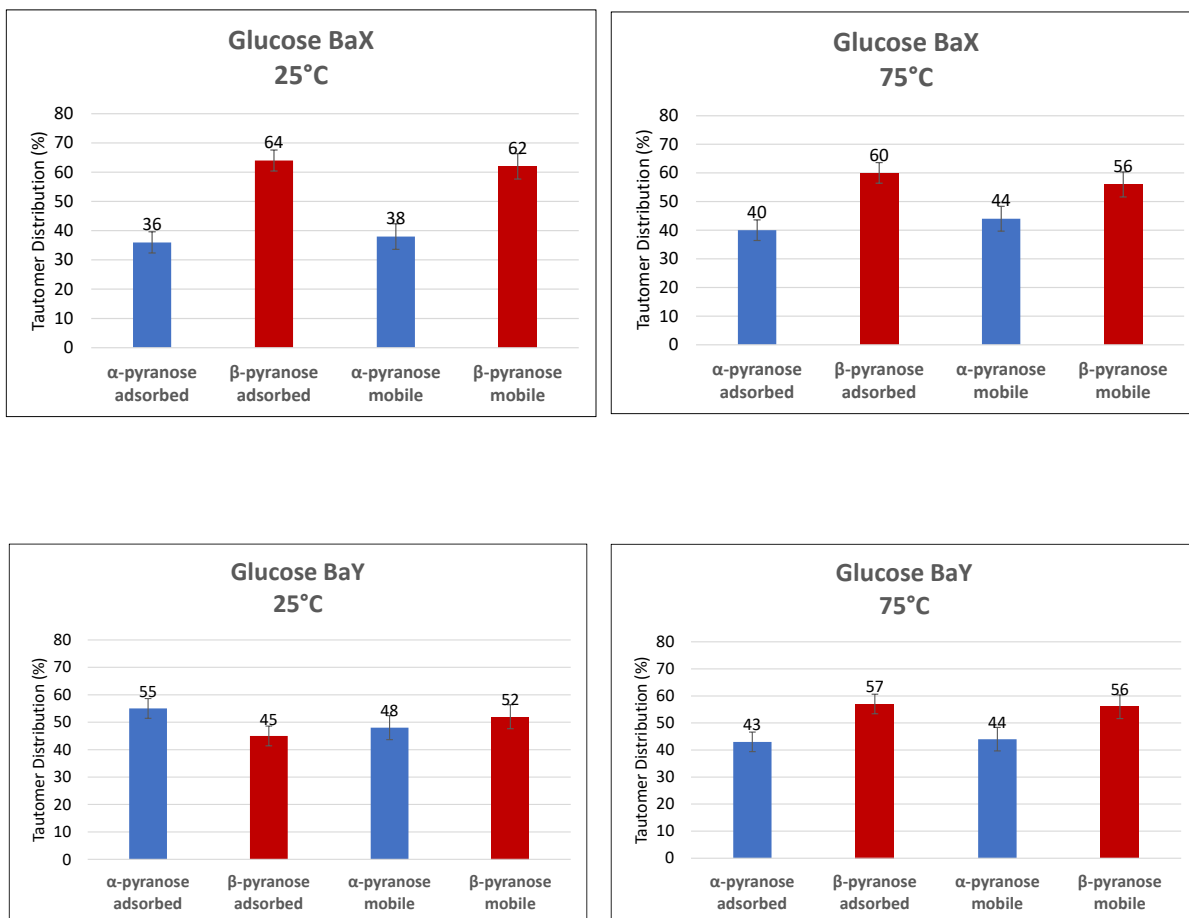


Figure V- 4: Relative amounts of AGP and BGP tautomers in the adsorbed or solution phases, as determined by solid-state NMR at 25 °C and 75 °C (error bars represent the standard deviations of three independent measurements).

V-3-2 Xylose

The same analysis of recorded spectra has been made for xylose. The decomposed signals of xylose in BaX and BaY are shown in *Figure V- 5* and *Table V- 1* details the obtained fitting parameters. We can identify the sharp peaks of mobile pyranose forms in the bulk solution (AXP, 92.0 ppm; BXP, 96.5 ppm for BaX, AXP, 92.0 ppm; BXP, 96.5 ppm for BaY) and adsorbed tautomers signals (AXP, 93.0 ppm; BXP, 96.2 ppm for BaX, AXP, 92.0 ppm; BXP, 96.3 ppm for BaY). A total of 50 % and 66 % of xylose is confined in BaX and BaY pores respectively at 25 °C, indicating that more xylose is present in the pores of the Y zeolite which is again consistent with the adsorption isotherms of xylose compared for BaX and BaY reported previously. At 75 °C, 56 % and 58 % of xylose is adsorbed in BaX and BaY respectively. The increase of temperature results in a decrease of the total adsorbed quantity of glucose and xylose in BaY. *Figure V- 6* shows the ratios of α -xylopyranose (AXP) and β -xylopyranose (BXP). A BXP:AXP ratio of (56:44) is obtained in BaX at 25 °C for the mobile phase which is consistent with the ratio found for the solution using liquid NMR experiments (59:41). The distribution changes in the adsorbed phase to (66:34) in favor of BXP. Increasing the temperature to 75 °C did not significantly affect the mobile phase composition relative to 25 °C. Nevertheless, in the adsorbed phase the ratio shifts in favor of BXP (72:28).

In case of BaY, the BXP:AXP ratio is of 52:48 and 58:42 at 25 and 75 °C, respectively, in the mobile phase, while it is of 56:44 and 63:37 in the adsorbed phase at 25 °C and 75 °C, respectively. Thus, no significant perturbation of the tautomeric equilibrium by the adsorption process is observed here.

The commercial xylose initially contains traces of lyxose (xylose epimer) as we showed with liquid NMR experiments prior the adsorption tests. The chemical shift characteristic of lyxose at 95.4 ppm is found in the spectra when BaX is tested. Lyxose represent around 1 % of the mobile phase at 25 °C and 75 °C (FWMH of 0.22 and 0.25 ppm at 25 °C and 75 °C respectively). The β -furanose tautomer is present in the mixture as well, it represents around 2 % of the mobile phase at 25 °C (FWHM of 0.3) and 6 % at 75 °C (FWHM of 0.51) in BaX. Similar proportions are obtained in BaY.

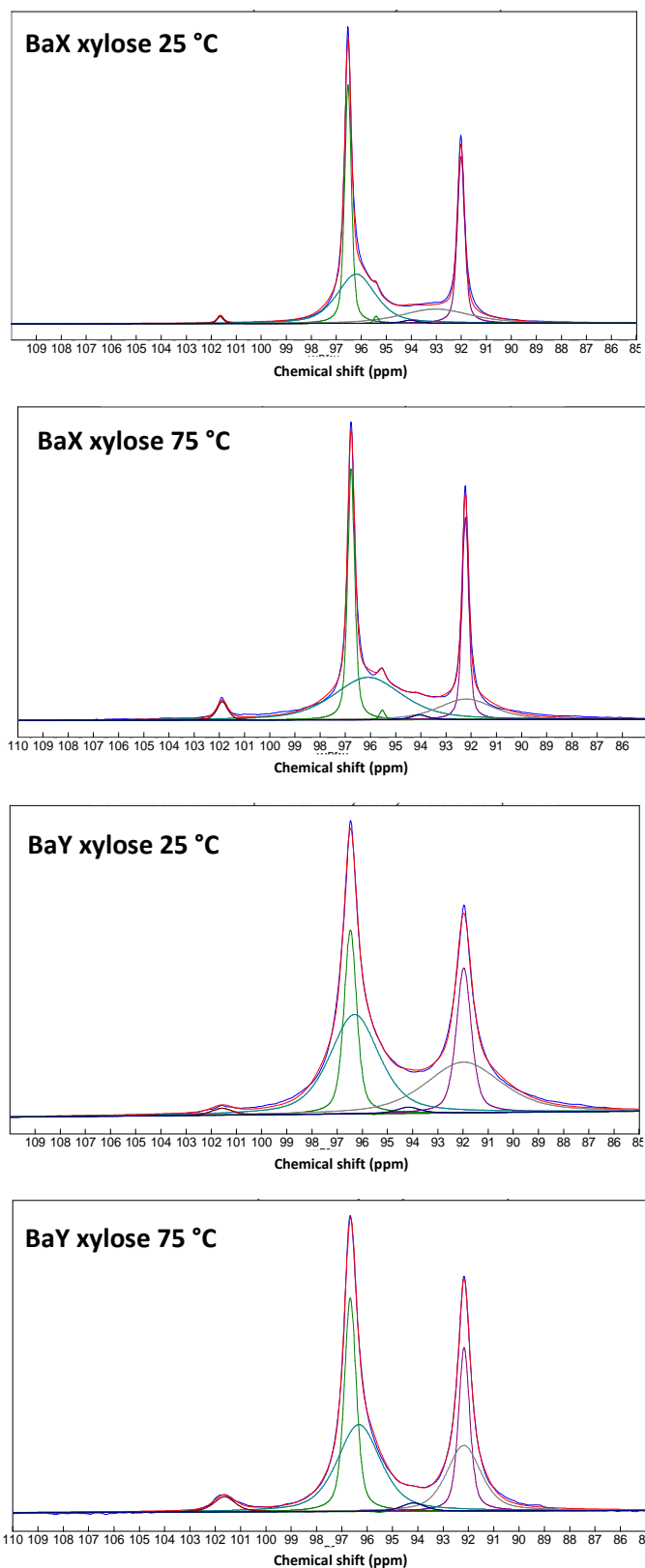


Figure V- 5: Xylose MAS solid-state ^{13}C NMR spectra recorded at 25 °C and 75 °C for BaX and BaY (blue line), fitted spectra (red line)

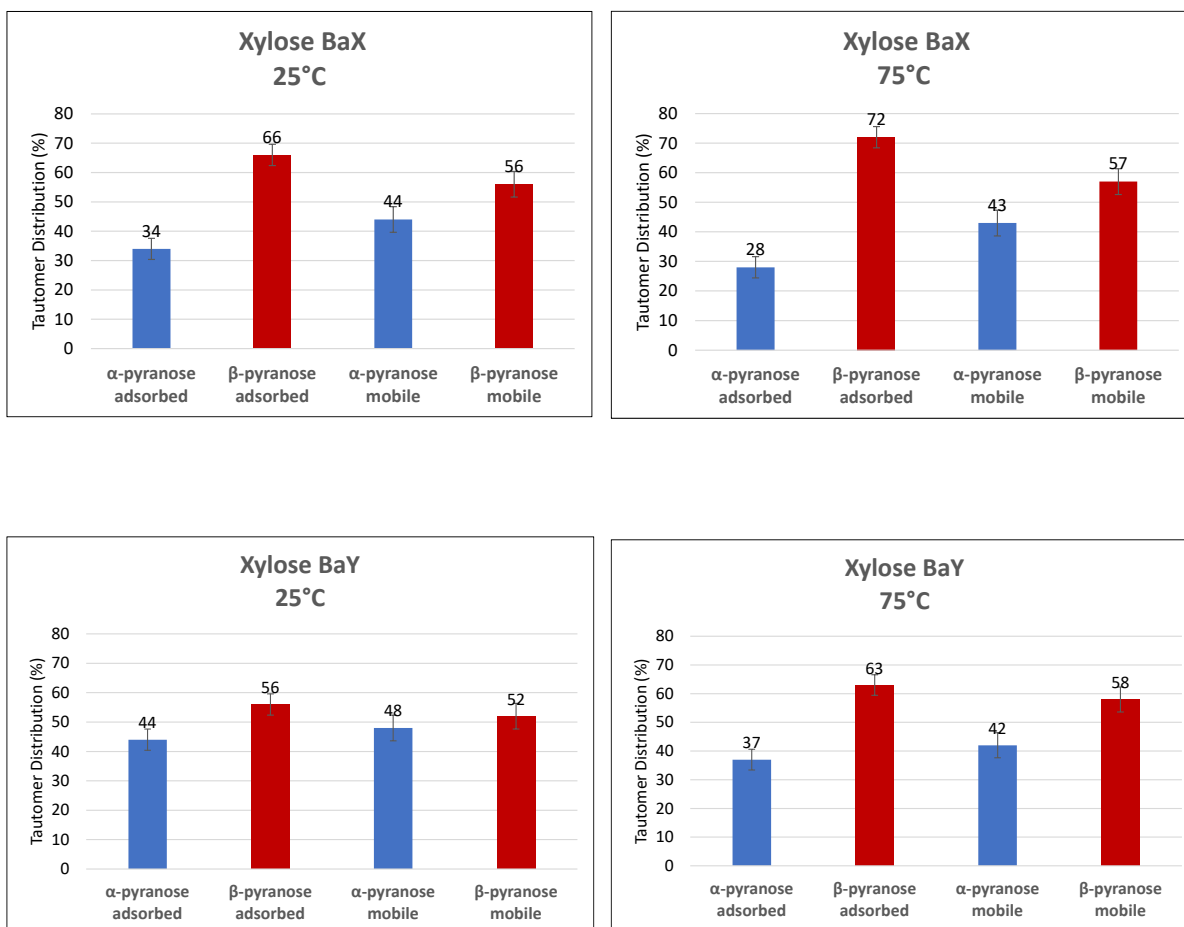


Figure V- 6: Relative amounts of AXP and BXP tautomers in the adsorbed or solution phases, as determined by solid-state NMR at 25 and 75 °C (error bars represent the standard deviations of three independent measurements).

Table V- 1: Chemical shifts and full width at half maximum of glucose and xylose signals

	Position (ppm)	FWHM (ppm)	Assignment	Phase
BaX at 25 °C glucose				
	95.7	0.29	β -pyranose	mobile
	91.9	0.27	α -pyranose	mobile
	95.4	1.41	β -pyranose	adsorbed
	91.7	0.99	α -pyranose	adsorbed
	93.9	1.19	β -pyranose mannose	adsorbed
BaX at 75 °C glucose				
	96.0	0.29	β -pyranose	mobile
	92.0	0.30	α -pyranose	mobile
	95.8	1.82	β -pyranose	adsorbed
	91.9	2.58	α -pyranose	adsorbed
	102.3	0.38	β -furanose	mobile
	94.0	0.97	β -pyranose mannose	adsorbed
BaY at 25 °C glucose				
	95.7	0.60	β -pyranose	mobile
	91.8	0.68	α -pyranose	mobile
	95.6	2.04	β -pyranose	adsorbed
	92.1	3.59	α -pyranose	adsorbed
BaY at 75 °C glucose				
	96.0	0.62	β -pyranose	mobile
	92.0	0.61	α -pyranose	mobile
	95.9	2.51	β -pyranose	adsorbed
	92.1	2.80	α -pyranose	adsorbed
BaX 25 °C xylose				
	96.5	0.31	β -pyranose	mobile
	92.0	0.35	α -pyranose	mobile
	96.2	1.81	β -pyranose	adsorbed
	93.0	3.24	α -pyranose	adsorbed
	101.6	0.30	β -furanose xylose	mobile
	95.4	0.22	β -pyranose lyxose	mobile
BaX 75 °C xylose				
	96.8	0.33	β -pyranose	mobile
	92.2	0.31	α -pyranose	mobile
	96.1	3.18	β -pyranose	adsorbed
	92.2	2.56	α -pyranose	adsorbed
	101.9	0.51	β -furanose xylose	mobile
	95.5	0.25	β -pyranose lyxose	mobile
BaY 25 °C xylose				
	96.5	0.59	β -pyranose	mobile
	92.0	0.70	α -pyranose	mobile
	96.3	2.31	β -pyranose	adsorbed
	92.0	3.54	α -pyranose	adsorbed
	101.6	0.97	β -furanose xylose	adsorbed
BaY 75 °C xylose				

96.7	0.56	β -pyranose	mobile
92.2	0.52	α -pyranose	mobile
96.3	2.00	β -pyranose	adsorbed
92.2	1.59	α -pyranose	adsorbed
101.6	1.00	β -furanose xylose	adsorbed

V-4 Conclusion

This ^{13}C MAS NMR study allows to identify and rationalize glucose and xylose tautomers in solution and adsorbed phase. The adsorbed species in BaX and BaY are very similar to the tautomeric forms in solutions corresponding to pyranose rings, and we generally observe ratios of tautomeric forms in the adsorbed phase that reflect the ratios in the liquid phase, with little to no perturbation. This means that (i) either these forms are also the most stable forms in the adsorbed phase, as they are in solution, or (ii) that the tautomeric equilibrium is very slow at these temperatures and it is not catalyzed efficiently by the zeolites, and thus a potential favored adsorption mode in another form (furanose or linear) cannot be observed. Nonetheless, we observed modifications of the liquid phase composition by change in temperature from 25 to 75 °C, which would indicate that the modification of the tautomeric forms should be allowed kinetically. This would be an argument in favor of the first hypothesis (i). Besides, we show by this series of experiments that the assessed proportions between the two main tautomers are close enough to 50:50 and do not vary much. This suggests that their Gibbs free energy of adsorption $\Delta_r G_{ads}$ should be close for both pyranose forms.

Chapter VI: DFT investigation of glucose and xylose adsorption in faujasite-type zeolites

In the previous sections, we examined the adsorption behavior of glucose and/or xylose in aqueous or water/ethanol solutions on cation exchanged zeolites as potential adsorbent for separation. We found that the selectivity depends on several key factors, such as the nature of the cation and Si/Al ratio, with BaX or BaY being found as the most selective adsorbents (towards xylose and glucose, respectively). Nonetheless, despite several additional experimental studies, including breakthrough experiments and ^{13}C MAS NMR spectroscopy, and literature study, the mechanisms underlying the processes of sugar separation in such systems remain unknown.

In this section, we aim at providing insights at the molecular level into the adsorption process by means of molecular modeling. We studied in a first section the specific interactions between sugar and the zeolite, more specifically the cations, with quantum mechanics calculations (DFT). In the next chapter (Chapter VII), we expose preliminary results aiming at examining more in detail the collective behaviors between the possible adsorbates (glucose, xylose, and the solvent water).

VI-1 Introduction

As mentioned in the previous sections and in past literature, the adsorption phenomenon of a given sugar from aqueous solution in the zeolite previously occupied by a solvent involves several elementary processes, including desorption of a number of solvent molecules from the zeolite and adsorption of the sugar itself, and thus may be referred to as an “exchange”. Hence, the thermodynamics of the adsorption (considering the standard conditions) of one given sugar in the zeolite may be described as a Born-Haber thermodynamical cycle such as the one given in *Figure VI- 1*. This cycle features a few steps corresponding to several contributions to the overall Gibbs free energy of exchange $\Delta_r G_{exc}^\circ$: n water molecules are initially desorbed ($-n\Delta_r G_{ads}^\circ(\text{H}_2\text{O})$) and added to the liquid bulk solution ($+n\Delta_r G_{solv}^\circ(\text{H}_2\text{O})$), sugars are introduced dissolved in water ($-\Delta_r G_{solv}^\circ(S)$) and will occupy the free adsorption sites ($+\Delta_r G_{ads}^\circ(S)$). We suppose in this scheme that adsorption of sugars and desorption of water are done from gas phase, and sugars are adsorbed without considering their hydration shell. Gibbs free energy of exchange can therefore be determined as follows:

$$\Delta_r G_{exc}^\circ = -n\Delta_r G_{ads}^\circ(H_2O) + n\Delta_r G_{solv}^\circ(H_2O) - \Delta_r G_{solv}^\circ(S) + \Delta_r G_{ads}^\circ(S)$$

$\Delta_r G_{ads}^\circ(H_2O)$ and $\Delta_r G_{ads}^\circ(S)$ can be determined thanks to density functional theory calculations presented below, that describe adsorption from gas phase. $n\Delta_r G_{solv}^\circ(H_2O)$ and $\Delta_r G_{solv}^\circ(S)$ can be found in the literature through molecular modeling or experimental measurements.

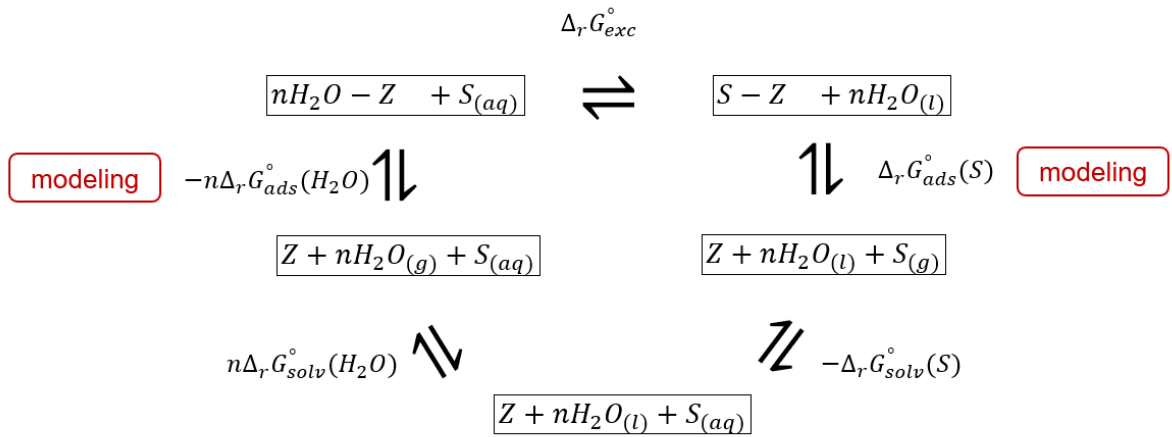


Figure VI- 1: Thermodynamic cycle of sugar (S) adsorption in a zeolite (Z) in presence of water

Below we investigate thanks to DFT calculations the possible adsorption modes of glucose and xylose tautomers in different zeolite structures. The effect of the number and type of cations in the framework on the adsorption free energy $\Delta_r G_{ads}^\circ(S)$ is studied. Finally, the adsorption of water is treated in the objective of determining a free energy of exchange $\Delta_r G_{exc}^\circ$ and compare it to the experimental values.

VI-2 Computational methods

VI-2-1 DFT calculations

DFT calculations have been performed using the Vienna Ab initio Simulation Package (VASP).^{121,122} The PBE functional was used which is a GGA functional and the Projected Augmented Wave method (PAW) method was employed.^{123–125} In order to take into account the Van der Waals interactions, the dispersion correction (DFT + D2) reported by Grimme was considered.¹²⁶ Geometry optimization calculations were done with a plane-wave cutoff energy of 400 eV and were considered converged when the inter-cycles energy difference became lower than 10^{-7} eV. The structural relaxations have been carried out without freezing any atom in the systems until all forces were smaller than 0.02 eV/Å. Frequency calculations were carried out using the finite difference methods as implemented in VASP, by displacing each atom in all 6 directions of space by 0.02 Å.

VI-2-2 Structure models

Faujasite framework was imported from the software Material Studio 7.0 database. The conventional lattice cell is cubic with a total of 576 atoms (Si₉₆ Al₉₆ O₃₈₄). To reduce the computational cost, the cell is reduced to the primitive rhombohedral one with, $\alpha=\beta=\gamma=60^\circ$ and a total of 144 atoms (Si₂₄ Al₂₄ O₉₆). This cell is composed of two supercages and eight hexagonal plans connecting the sodalites to the supercages.

The faujasites were considered in our study with different Si/Al ratios:

- A purely siliceous structure with only silicon and oxygen atoms, all T-sites atoms being Si.
- A high Si/Al faujasite with only one cation in the framework that is Si/Al = 47 for NaFAU and KFAU and Si/Al = 23 for CaFAU, SrFAU and BaFAU. Only one or two T-site atoms are aluminum and were chosen among the T-sites exposed in the supercage. When two aluminum atoms are present, they are in the vicinity of each other, following nonetheless the Lowenstein rule (*i.e.* they are separated by one T-site occupied by a Si atom).⁵²
- A zeolite LSX with Si/Al = 1, where one out of two T-sites are aluminum atoms, again following the Lowenstein rule.

In order to reach electroneutrality in the structures, different cations were placed. Crystallographic investigations show that bivalent ions (Ca²⁺, Sr²⁺ and Ba²⁺ in our case) are

located in site I (center of a hexagonal prism) and site II (center of a hexagonal plan between a sodalite and a supercage) and monovalent ions are located in sites I, II and III (In the supercage, close to a square window between two other square windows).⁵⁷ Before to the geometric optimization, bivalent ions were added in their locations manually and monovalent ones were placed using the Universal Force Field (UFF) implemented in Materials Studio.

VI-2-3 Free energies of adsorption calculation

Adsorption energies were calculated as follows:

$$E_{\text{ads}} = E_{\text{zeolite + sugar}} - (E_{\text{zeolite}} + E_{\text{sugar}}) \quad (\text{Eq VI-1})$$

where $E_{\text{zeolite + sugar}}$ is the electronic energy of the zeolite and the sugar placed inside, E_{zeolite} the energy of the zeolite and E_{sugar} the energy of the most stable form of sugar out of the five tautomers. Dispersion contributions were similarly estimated thanks the following equation:

$$E_{\text{disp}} = E_{\text{disp zeolite + sugar}} - (E_{\text{disp zeolite}} + E_{\text{disp sugar}}) \quad (\text{Eq VI-2})$$

Electronic calculations are performed at 0 K. To consider the temperature effect, thermodynamic parameters were calculated. Molar enthalpy is expressed as follows:

$$H_m = H_{\text{elec}} + H_{\text{vib}} + H_{\text{trans}} + H_{\text{rot}} + PV_m \quad (\text{Eq VI-3})$$

where H_{elec} , H_{vib} , H_{trans} , H_{rot} and V_m are respectively the electronic, vibrational, translational, rotational energies and the molar volume. The latter is considered equal to zero in adsorbed phase (*i.e.* for the zeolite model with and without adsorbates). H_{elec} is assimilated to the result of DFT geometry optimization calculation E and the other terms can be determined thanks to statistical thermodynamics.

The vibrational component is calculated according to the following equation:

$$H_{\text{vib}} = N_A \left[\sum_i \frac{1}{2} h\nu_i + \sum_i \frac{h\nu_i \times \exp\left(-\frac{h\nu_i}{k_B T}\right)}{1 - \exp\left(-\frac{h\nu_i}{k_B T}\right)} \right] \quad (\text{Eq VI-4})$$

where N_A is the Avogadro number, h is Plank constant, k_B is Boltzmann constant, T the temperature and ν_i the vibrational eigen wave numbers of the system accessible through vibrational frequencies calculations. The first term at 0 K called the Zero Point Energy (ZPE).

The rotational and translational components are determined as follows:

$$H_{rot} = H_{trans} = \frac{3}{2} N_A k_B T \quad (\text{Eq VI-5})$$

When the molecule is adsorbed, we consider that the translational and rotational components are converted into vibrational modes due to the limited mobility at adsorbed phase. This consideration also applies to the zeolites structures since they are considered rigid. These assumptions are also considered for the calculation of the molar entropy. We consider that PV_m is negligible compared to the energetic component and therefore H_m reduces to:

$$H_m = H_{elec} + H_{vib} \quad (\text{Eq VI-6})$$

for zeolite models with and without adsorbates. Molar entropy is determined as follows:

$$S_m = S_{vib} + S_{trans} + S_{rot} \quad (\text{Eq VI-7})$$

where S_{vib} , S_{trans} and S_{rot} are respectively the vibrational, translational, rotational entropies. The three components are determined thanks to the following equations:

$$S_{vib} = N_A k_B \left[\sum_i \frac{h c \nu_i \times \exp\left(-\frac{h \nu_i}{k_B T}\right)}{1 - \exp\left(-\frac{h \nu_i}{k_B T}\right)} - \sum_i \ln \left(1 - \exp\left(-\frac{h \nu_i}{k_B T}\right)\right) \right] \quad (\text{Eq VI-8})$$

$$S_{trans} = N_A k_B \left(\frac{5}{2} \ln(T) - \ln(P) + \frac{5}{2} \ln(M) - 1.165 \right) \quad (\text{Eq VI-9})$$

where P is the partial pressure and M the molar mass.

$$S_{trans} = N_A k_B \left[\frac{\sqrt{\pi}}{\sigma} \left(\frac{8\pi^2 k_B}{h^2} \right)^{\frac{3}{2}} \sqrt{A_e \times B_e \times C_e} \right] \quad (\text{Eq VI-10})$$

,where A_e , B_e and C_e are the rotational constants of the molecule (determined using the tool provided on the website: <https://www.colby.edu/chemistry/PChem/scripts/ABC.html>) and σ the number of symmetry. Here again, for a zeolite model, with or without adsorbate, we

consider that the translational and rotational degrees of freedom are converted to vibrational modes and thus $S_{\text{trans}} = S_{\text{rot}} = 0$.

After determining the enthalpy of each system separately, (zeolite, sugar, zeolite+sugar), the adsorption enthalpy is calculated as follows:

$$\Delta_r H_{ads} = H_{zeolite+sugar} - (H_{zeolite} + H_{sugar}) \quad (\text{Eq VI-11})$$

Similarly, for the entropy:

$$\Delta_r S_{ads} = S_{zeolite+sugar} - (S_{zeolite} + S_{sugar}) \quad (\text{Eq VI-12})$$

The adsorption free energy can therefore be determined:

$$\Delta_r G_{ads} = \Delta_r H_{ads} - T \Delta_r S_{ads} \quad (\text{Eq VI-13})$$

Solid state NMR experiments, detailed in the previous chapter, showed that only the pyranose rings are adsorbed in the zeolite cavity to a significant amount, and in proportions similar as the ones in the solution (β - pyranose: α - pyranose ratio around 60:40). Thus, to simplify some reasoning from these results, we consider the hypothesis that the mutarotation is kinetically hindered and thus we estimate a mean adsorption free energy ($\Delta_r G_{\text{mean}}$) that describes a global adsorption energy of one sugar in each structure:

$$\Delta_r G_{\text{mean}} = 0.6 \Delta_r G_{\beta\text{-pyranose}} + 0.4 \Delta_r G_{\alpha\text{-pyranose}} \quad (\text{Eq VI-14})$$

We nevertheless examine the adsorption of all possible tautomers of the sugars.

VI-3 Results and discussions

VI-3-1 Optimization of sugars

The optimization of sugars was done using periodic calculations at the same level of theory. Each glucose and xylose conformers were placed in a 40 Å large box to avoid any interactions between neighboring molecules (which was verified by performing several calculations with increasing box sizes). The results are reported in *Table VI- 1*. The linear form is the least stable for both sugars and the pyranose rings have the lowest energies and thus are the most stable. This result is consistent with experimental observations since aqueous solutions of glucose and

xylose are predominantly composed of pyranose conformers (approximately 64 % β -pyranose and 36 % α -pyranose for glucose and e 65 % β -pyranose and 35 % α -pyranose for xylose at 20 °C ¹²⁷). Our calculations predict that in the case of xylose, the β -pyranose conformer is the most stable, which is again consistent with experimental observations. However, we can see that the α -pyranose is found slightly more stable energetically than the β -pyranose form in the case of glucose, with a difference of 4 kJ mol⁻¹, whereas the latter is predominant in solution. Note that the energy difference between the two forms is rather small compared to expected DFT accuracy (about 10 kJ mol⁻¹). Besides, this apparent inconsistency can also be explained by the fact that these calculations are done in gas phase without considering a solvent model, and thus do not take into account several factors that may affect the relative stability of the conformers in aqueous solution, such as the solvation effect. Nevertheless, in order to keep the calculation consistent, and in order to determine the adsorption energies during the adsorption study, we will take as a reference the most stable form calculated by DFT for each sugar, *i.e.* α -pyranose for glucose and β -pyranose for xylose.

Table VI- 1: Relative electronic energy of glucose and xylose tautomers reported to the most stable form

	Glucose (kJ mol⁻¹)	Xylose (kJ mol⁻¹)
Linear	90	70
α -furanose	51	9
β -furanose	69	21
α -pyranose	0	9
β -pyranose	4	0

VI-3-2 Optimization of zeolites

After placing the ions using the procedure described above, the next objective is to determine the most stable structure for each zeolite. For each cation and each Si/Al ratio, structure optimizations were performed for several lattice cell parameters and an energetic minimum can be identified for each model, which corresponds to the most stable structure that was considered in the following. An example for the optimization of CaLSX is shown in *Figure VI- 2* where the optimal cell parameter is 17.922 Å (25.345 Å for the conventional cell).

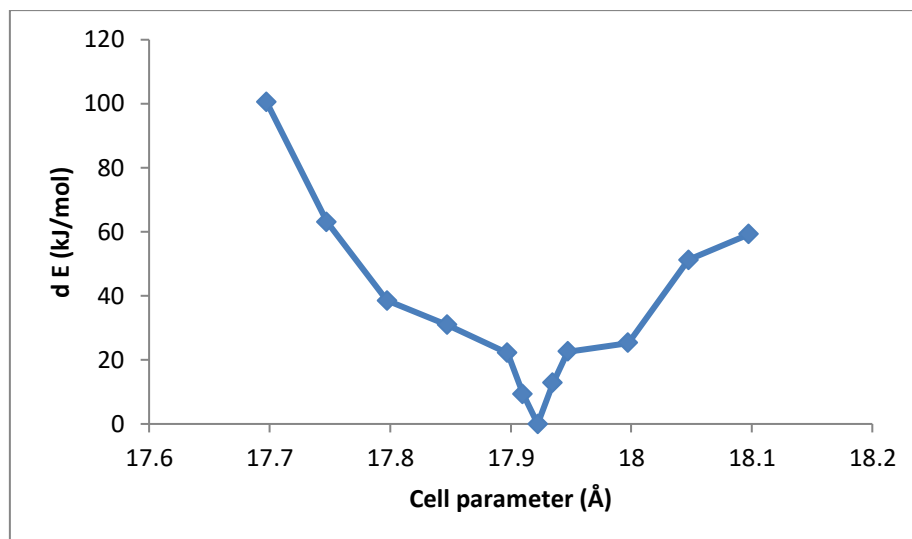


Figure VI- 2: Evolution of the electronic energy with the primitive cell parameter for CaLSX

The same procedure was applied for all zeolites with different Si/Al ratios and the most stable structures were selected for the adsorption study. *Figure VI- 3* shows the optimized cell parameters for all considered zeolites. The silicalite structure without cations presents the smallest parameter of 24.320 Å (conventional cell). NaFAU has a parameter of 24.391 Å, and all other cations afford a similar cell parameter of 24.674 Å. *Figure VI- 3* also compares the lattice parameters of zeolites LSX designed theoretically and zeolites X used in the previous chapter for the breakthrough experiments. We note that our calculations slightly overestimate the lattice cell parameter (difference of 0.362 Å for NaX and KX, 0.473 Å for CaX and 0.562 Å for SrX and BaX). This can be explained by the different Si/Al ratios (1.2 for the experimental zeolites X and exactly 1 for the computed zeolites LSX). Nevertheless, we notice a similar trend starting from Na experimentally and theoretically where the parameter increases exchanging Na to K, Sr and Ba, while Ca affords a similar cell parameter than Na.

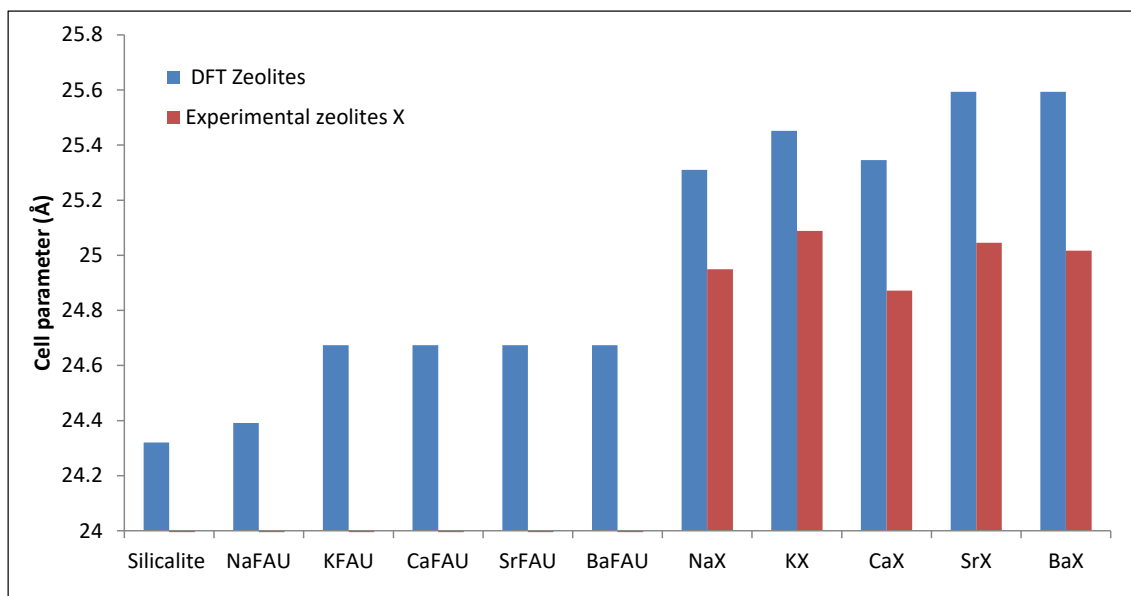


Figure VI- 3: Comparison between experimental and theoretical cell parameters

An interesting observation is illustrated in *Figure VI- 4* which shows the distance between the position of the bivalent ions in site II and the barycenter of the hexagonal plan of the supercell. The distance increases with the ionic radius of the cation ($0.248 \text{ \AA} < 0.410 \text{ \AA} < 0.814 \text{ \AA}$ for Ca, Sr and Ba respectively). As a result, the distance between two cations in the supercage is reduced to 10.930 \AA , 10.666 \AA and 9.866 \AA going from Ca to Sr and Ba, respectively. This increases the probability of interaction of the molecules with multiple counterions.

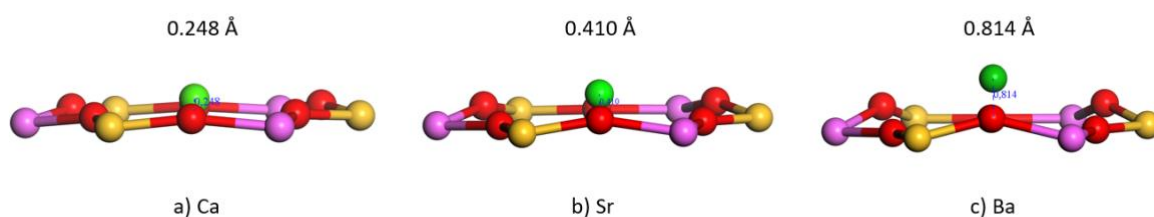


Figure VI- 4: Cation-hexagonal plan distance in a) *CaLSX*, b) *SrLSX* and c) *BaLSX* respectively. The center of the supercage is located to the top of the pictures.

After the optimization of sugar molecules and zeolite structures, each conformer of glucose and xylose will be placed in the supercage in numerous positions. The most stable structures, the adsorption energies and the dispersion contributions will be detailed in the next paragraph.

VI-3-3 Adsorption study

In this part, the adsorption study is done in (1) a siliceous structure to evaluate the effect of the framework without compensating cations, (2) in zeolites models containing 1 cation in the supercage to estimate the interactions of sugars with 1 cation in the confined space and (3) in LSX models completely exchanged to investigate the influence of multiple ions on the adsorption modes.

VI-3-3-1 Adsorption in a siliceous structure

This paragraph focuses on the adsorption energies of glucose and xylose in a siliceous faujasite structure. Only the β -pyranose form for each sugar was selected to simplify the study. The objective here is to estimate the (essentially non-covalent) interaction energies of the sugars with the lattice framework independently of the presence of a counterion and aluminum atoms.

Seven positions were considered during this study, sugars were placed close to each hexagonal plan of a supercage (4 plans in one supercage), at the center of the supercage and at the center of two 12-membered rings connecting two supercages and then optimized. Fourteen calculations in total were performed for both sugars and the most stable are reported. In siliceous faujasite, the computed adsorption free energies of β -glucopyranose (BGP) and β -xylopyranose (BXP) are -34 kJ mol^{-1} and -17 kJ mol^{-1} respectively at 300 K. Glucose and xylose $\Delta_r H_{ads}$ correspond to -96 kJ mol^{-1} and -79 kJ mol^{-1} respectively. A similar value of $\Delta_r S_{ads} = -208 \text{ J K}^{-1} \text{ mol}^{-1}$ ($T\Delta_r S_{ads}$ of -62 kJ mol^{-1} at 300 K) is obtained for both sugars. Thus, the enthalpic contribution is stronger than the entropic one. Adsorption energies are composed mainly from the dispersion energies where they constitute 88 % of the total energies ($E_{disp} = -93 \text{ kJ mol}^{-1}$ and -88 kJ mol^{-1} for BGP and BXP respectively), the remaining 12% is due to electronic contributions and hydrogen bonds if they exist. BGP is located at the center of the 12-membered ring with two hydrogen bonds between the hydrogen atoms of the second and the fourth hydroxyl groups of the sugar molecule and two oxygen atoms of the ring as shown in *Figure VI- 5*. We can also see from the Figure that BXP is placed almost in parallel with a hexagonal plan without any hydrogen bonds with the faujasite framework.

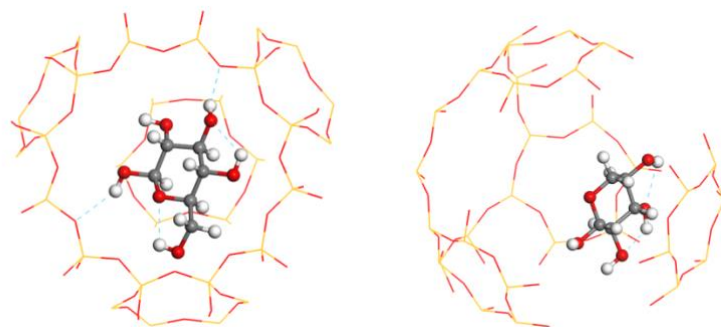


Figure VI- 5: Most stable adsorption modes of β -glucopyranose (left) and β -xylopyranose (right) in a siliceous faujasite

VI-3-3-2 Adsorption in single cation exchanged zeolites

The interactions between glucose or xylose tautomers and a single counterion were studied by placing each oxygen atom in front of the ion in the monodentate and bidentate modes and optimizing the resulting structure. Around twelve calculations were performed for each form which makes a total of around sixty calculations for all conformers of one sugar in one zeolite. Around six hundred calculations were performed for both sugars, nevertheless only the most stable structures will be presented and discussed in this section.

For all the structures, we notice that the adsorption energy becomes more negative by adding any cation in comparison to the siliceous zeolite discussed in the previous paragraph (*Table A 4*). In these zeolitic structures with one counterion, glucose linear form has the least stable adsorption mode in NaFAU and KFAU as illustrated in *Figure VI- 6*. NaFAU shows energies of the same order of magnitude for the furanose and pyranose rings with β -glucofuranose (BGF) exhibiting the lowest free energy ($\Delta_r G_{ads} = -91 \text{ kJ mol}^{-1}$). The pyranose forms are the most favored to be adsorbed in KFAU, the adsorption free energy is around -85 kJ mol^{-1} . For the bivalent ions, all the cyclic forms have close free energies in CaFAU ranging from -148 kJ mol^{-1} to -153 kJ mol^{-1} except for α -glucofuranose AGF (-129 kJ mol^{-1}). BGF has the lowest interaction energy in SrFAU (-149 kJ mol^{-1}) followed by the pyranose rings (-140 kJ mol^{-1}). BGP is favored to be adsorbed in BaFAU with an energy of -143 kJ mol^{-1} .

Calcium has the strongest interactions with glucose, however, the free energies of the β -pyranose tautomer (which is the most abundant in an aqueous solution) are quite close to the free energies of adsorption on strontium and barium with a difference of around -8 kJ mol^{-1} . Enthalpic contributions are stronger than entropic ones for all structures, all enthalpic and entropic values are presented in Tables A9-A28. In case of the adsorption of BGP in BaFAU

for example, $\Delta_r H_{ads}$ of -143 kJ mol^{-1} and $T\Delta_r S_{ads}$ of -61 kJ mol^{-1} are found respectively ($\Delta_r S_{ads} = -205 \text{ J K}^{-1} \text{ mol}^{-1}$). Close values of $T\Delta_r S_{ads}$ (around -61 kJ mol^{-1}) are obtained regardless the cation type or the tautomeric forms. Dispersion energies range between -55 kJ mol^{-1} and -92 kJ mol^{-1} and we notice that they became weaker compared to the siliceous zeolite (-96 kJ mol^{-1}).

Figure VI- 7 shows adsorption free energies of xylose tautomers in the models with 1 cation. Like glucose, the linear form has the weakest interaction energy in NaFAU and KFAU. In these systems, pyranose forms are more favored to be adsorbed than furanose forms with free energy differences between 17 kJ mol^{-1} and 32 kJ mol^{-1} . All xylose tautomers are relatively well stabilized in the presence of a bivalent cation. The strongest adsorption is found for β -xylofuranose (BXF), a free energy of -151 kJ mol^{-1} is calculated. Pyranose rings are more stable (-140 kJ mol^{-1}) than furanose cycles in CaFAU. In case of BaFAU, pyranose tautomers have close free energies of adsorption around -122 kJ mol^{-1} but the highest $\Delta_r G_{ads}$ is found with BXF (-129 kJ mol^{-1}).

Similar to glucose, enthalpic contributions are stronger than entropic ones. Values between $-181 \text{ J K}^{-1} \text{ mol}^{-1}$ and $-205 \text{ J K}^{-1} \text{ mol}^{-1}$ for $\Delta_r S_{ads}$ are obtained and $\Delta_r H_{ads}$ vary according to type of cation and the sugar form. Dispersion contributions are in the range of -67 and -77 kJ mol^{-1} for all tautomers in all zeolites, and we notice that they became weaker than the dispersion energy of the siliceous zeolite (-88 kJ mol^{-1}).

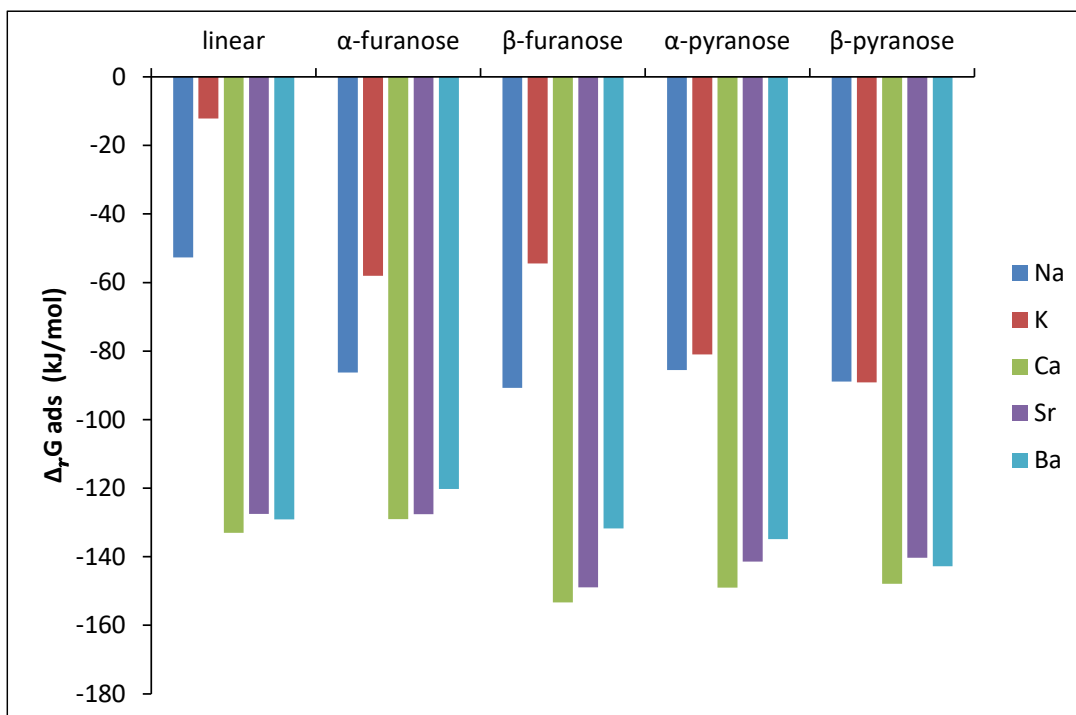


Figure VI- 6: Adsorption free energies of glucose tautomers in faujasite containing one Na, K (Si/Al = 47), Ca, Sr and Ba (Si/Al = 23) calculated at 300 K

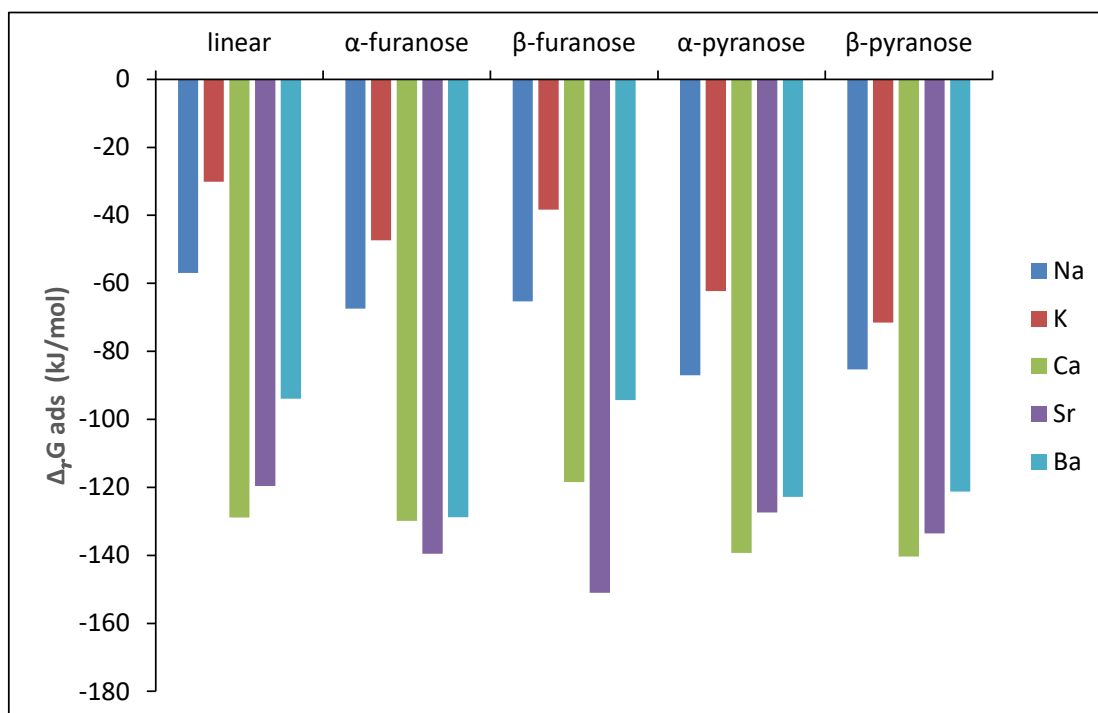


Figure VI- 7: Adsorption free energies of xylose tautomers in faujasite containing one Na, K (Si/Al = 47), Ca, Sr and Ba (Si/Al = 23) calculated at 300 K

Looking at the most stable structures (reported in *Table A 8*), the most noticeable and recurrent one is a bidentate complex between two oxygen atoms of two neighboring hydroxyl groups of the sugar conformer and the alkaline/alkaline earth metal atoms. Tridentate complexes are also identified for example for BGP in NaFAU, KFAU and BaFAU. These complexes are formed thanks to the free rotation of the sigma bond between C5 and C6 which allows a complex formation with O6, O1 (the oxygen atom in the cycle) and O2 (the oxygen atom in the hydroxyl group of the anomeric carbon) as illustrated in *Figure VI- 8*.

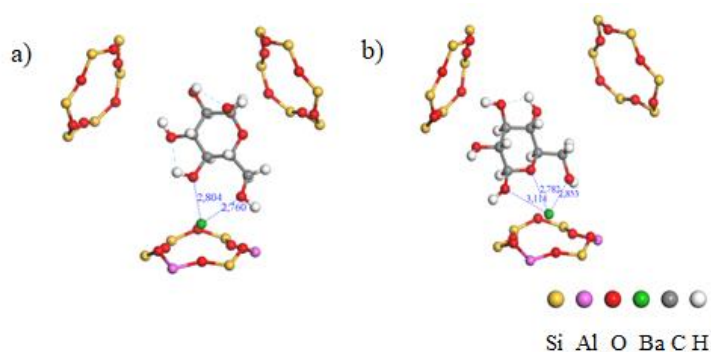


Figure VI- 8: Bidentate and tridentate coordination of a) AGP and b) BGP in BaFAU

The formation of the tridentate mode gives the strongest adsorption energy among the 5 tautomers (the case for NaFAU, KFAU and BaFAU). However, even stronger energies are obtained in CaFAU thanks to only bidentate complex (free energies between -129 kJ mol^{-1} and -153 kJ mol^{-1} compared to -120 kJ mol^{-1} and -143 kJ mol^{-1} for BaFAU). The distance O-cation is between 2.295 \AA (AGF in NaFAU) and 2.829 \AA (AGP in KFAU) in all cases except for tridentate ones where the distance O2-cation is superior to 3 \AA (3.459 \AA for NaFAU and KFAU, 3.114 \AA for BaFAU). The distance between the barium atom and the barycenter of the hexagonal plan was 1.229 \AA prior the structure optimization after placing BGP molecule. We notice that the barium is pulled toward the super cage and the distance increases to 1.498 \AA after adsorption. The same observations is found for calcium as well (0.602 \AA initially and 0.875 \AA after adsorption).

It is reported that the favored complex formation with alkaline and alkaline earth metals is according to the order axial-equatorial > equatorial-equatorial.⁶⁰ Therefore, it is expected to see axial-equatorial complexes with α -pyranose and α -furanose conformers where the hydroxyl

group on the anomeric carbon C1 is in the axial position. However, we found that the most stable complexes for all conformers are formed with an equatorial-equatorial sequence even in the presence of the axial OH in the α -pyranose forms.

In case of xylose, the most stable structures show the formation of only bidentate complexes (Table A 9). Interestingly for the pyranose tautomers (most abundant in an aqueous solution), two complexes stand out: the first one is between O3, O4 and Na, Ca (for both AXP and BXP), also with AXP in KFAU and BaFAU; the second one is between O4, O5 and Sr (for AXP and BXP) and with BXP in KFAU and BaFAU. For either complex, O4 is always involved in the formation. The distances O-cation are between 2.3 Å and 2.8 Å as shown in *Figure VI- 9*. Similar to glucose, cations are pulled inside the supercage after adsorption and the distance to the barycenter of the hexagonal plan increases (from 1.229 Å to 1.377 Å for BXP in BaFAU for instance).

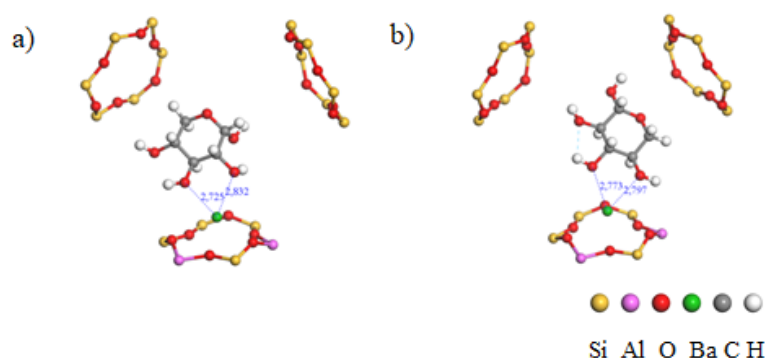
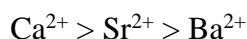
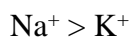


Figure VI- 9: Coordination with O3+O4 for AXP (a) and O4+O5 for BXP (b) in BaFAU

Furanose and pyranose rings for glucose and xylose give stable structures when one cation is placed in the faujasite framework.

In order to compare the zeolites with each other, we calculated the mean adsorption free energies as described in Paragraph II-3 and expose the results in *Figure VI- 10*. Overall, glucose adsorption energies are stronger than xylose energies except for NaFAU where close $\Delta_r G_{mean}$ of -87 kJ mol^{-1} is obtained. The free energies for bivalent ions are stronger than monovalent ions. The complexes are more stable according to the following order for both sugars with respect to the ion's valence:



Nevertheless, NaFAU and KFAU give close free energies of adsorption -86 kJ mol^{-1} for glucose as well as SrFAU and BaFAU (-140 kJ mol^{-1}). Interestingly, this order follows the Hard and Soft Acids and Basis (HSAB) theory, where the strongest interactions are found with the hardest metals sodium and calcium that have the smallest ionic radii and thus the highest hardness (the sugar being coordinated by the oxygen atoms from hydroxyl groups, considered rather hard ligands).¹²⁸

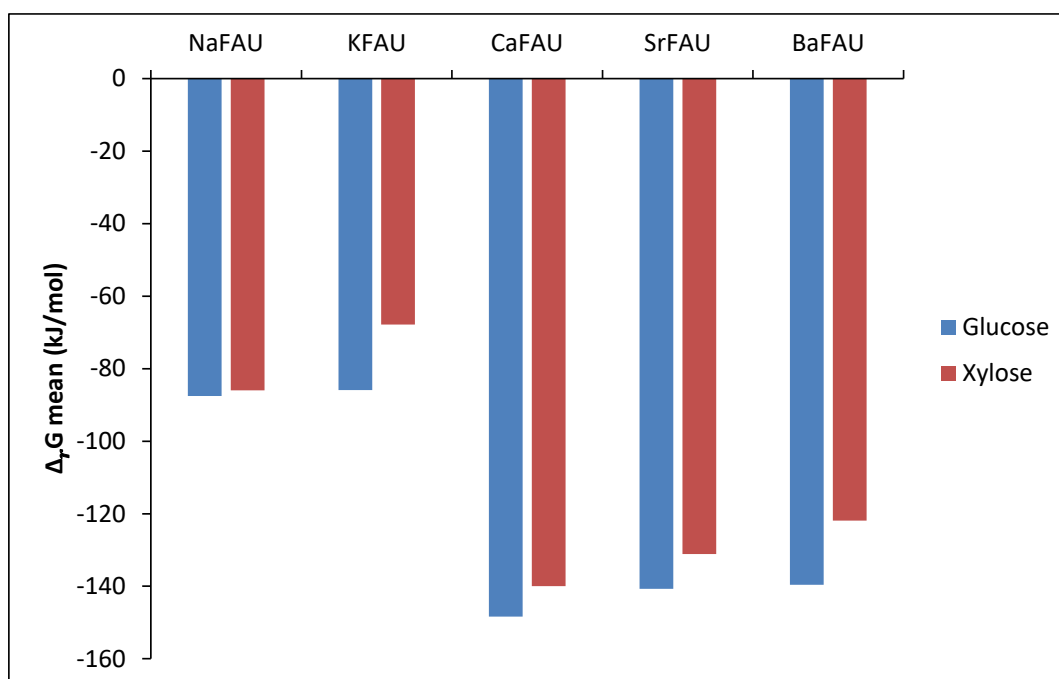


Figure VI- 10: Mean adsorption free energies of glucose and xylose relative to the pyranose rings at 300 K

VI-3-3-3 Adsorption on zeolites LSX

We then studied the adsorption of sugars on the exchanged LSX models, counting a significantly higher number of cations within the unit cell, in order to assess the effect of multiple cations in the lattice and examine a situation closer to the experimental one with the exchanged X zeolites. A similar initial location strategy was used as the previous paragraph before optimizations, and around 600 calculations in total were performed for glucose and xylose in all LSX zeolites. As before, only the most stable structures are presented in this part.

Energetic considerations

Overall, the adsorption free energies for all glucose tautomers are stronger than the ones obtained in the dealuminated zeolites in the previous paragraph by up to -140 kJ mol^{-1} as shown in *Figure VI- 11*. The linear form has in most cases the weakest energies among the five conformers and the pyranose forms have the strongest adsorption energies. The most negative energy is found for BGP in KLSX and BaLSX with the same energy of -268 kJ mol^{-1} . AGP is adsorbed stronger than BGP in NaLSX with a difference of -16 kJ mol^{-1} . Both pyranose tautomers have almost identical energies in KLSX and CaLSX (-265 kJ mol^{-1} and -209 kJ mol^{-1} respectively).

From *Table A 6*, we notice that the dispersion contribution is around -108 kJ mol^{-1} in KLSX, -85 kJ mol^{-1} in CaLSX and -87 kJ mol^{-1} in SrLSX for all conformers, it is in the range of -90 kJ mol^{-1} and -112 kJ mol^{-1} in NaX and between -97 kJ mol^{-1} and -129 kJ mol^{-1} in BaLSX. The adsorption of the pyranose rings in NaLSX shows the strongest dispersion compared to the furanose rings and the linear form. BGP presents the highest contribution in BaLSX with -129 kJ mol^{-1} . The dispersion effect didn't change drastically in CaLSX, SrLSX compared to the pure siliceous zeolite (-96 kJ mol^{-1}) but it is stronger in NaLSX, KLSX and BaLSX.

In case of xylose (*Figure VI- 12*), The strongest energy (-215 kJ mol^{-1}) is obtained by the adsorption of the BXP in NaLSX and BXF in KLSX. All cyclic forms are favored to be adsorbed in BaLSX with an average energy of -177 kJ mol^{-1} . The same goes for the cyclic tautomers in SrLSX, an average energy -142 kJ mol^{-1} is found. All tautomers have close energies of around -150 kJ mol^{-1} in CaLSX except for the α -pyranose form where its adsorption is weaker (-122 kJ mol^{-1}).

Here again, even by increasing the number of cations, Enthalpic contributions are stronger than entropic ones. An adsorption entropy $\Delta_r S_{ads}$ ranging from $-140 \text{ J K}^{-1} \text{ mol}^{-1}$ to $-273 \text{ J K}^{-1} \text{ mol}^{-1}$ is found for all structures. The dispersion contribution (*Table A 7*) in NaLSX, KLSX, CaLSX and SrLSX became weaker (from around -68 kJ mol^{-1} to -82 kJ mol^{-1}) compared to the adsorption in siliceous zeolite (-88 kJ mol^{-1}). However, these contributions became stronger in BaLSX and passed to around -109 kJ mol^{-1} for the furanose tautomers and -96 kJ mol^{-1} for the pyranose forms.

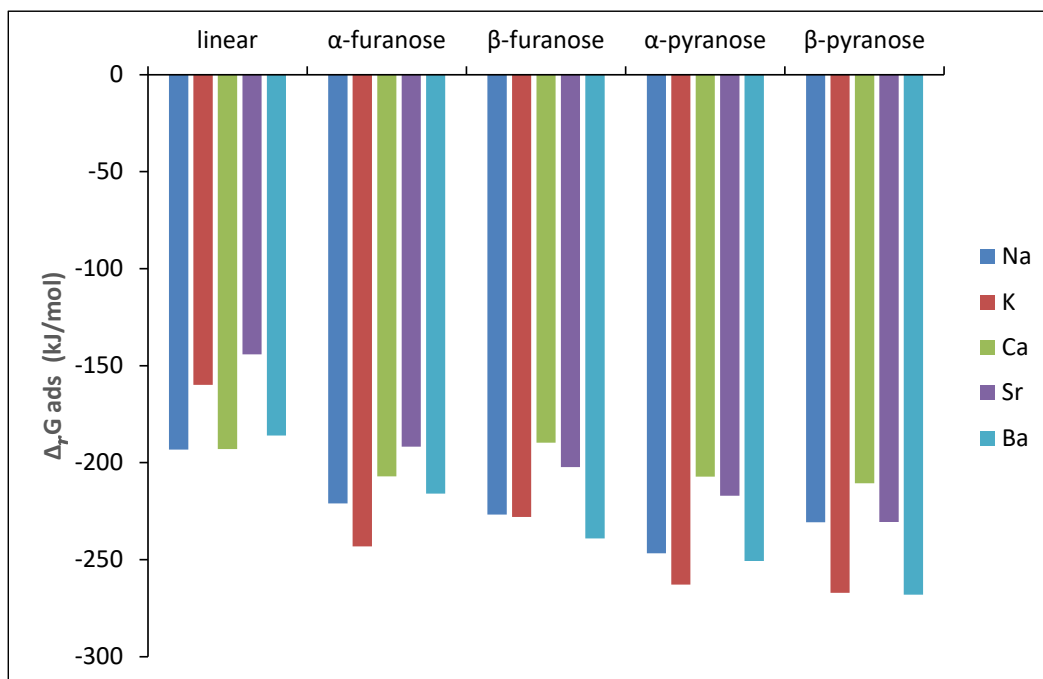


Figure VI- 11: Adsorption free energies of glucose tautomers in zeolites LSX at 300 K

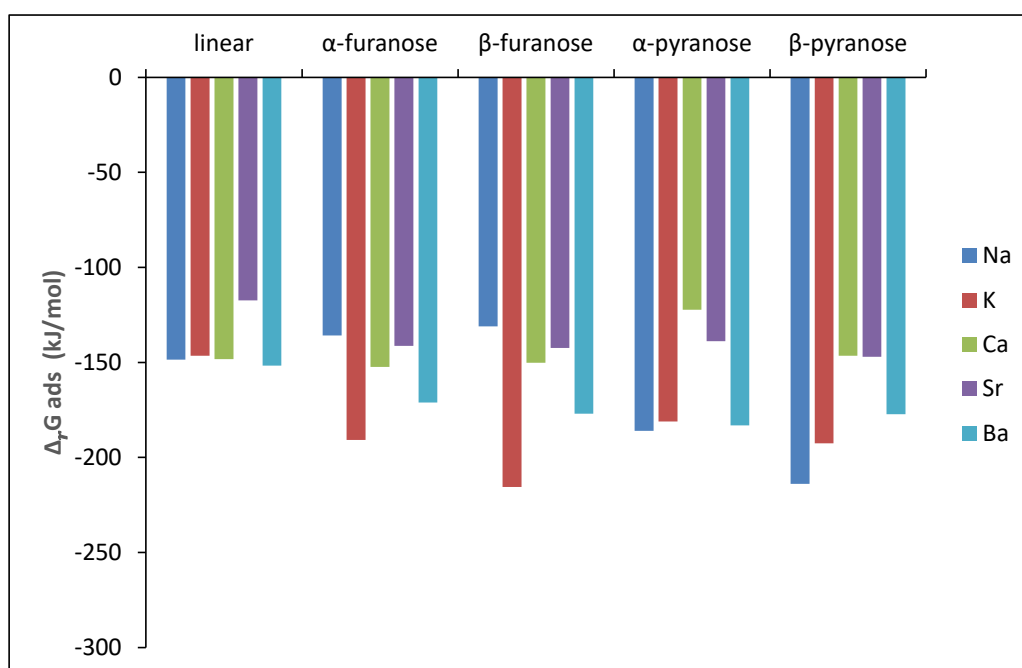


Figure VI- 12: Adsorption free energies of xylose tautomers in zeolites LSX at 300 K

Description of the structures

The most stable structure obtained is with BGP in KLSX, *Figure VI- 13(b)* shows that the molecule is positioned near the 12-membered ring and that there are four potassium atoms involved in the adsorption: three are placed in site III and one in site II. All oxygen atoms of the sugar molecule are bound to a counterion. We can identify a tridentate complex between O1, O2, O6 and a potassium in site III with an O-ion distances of 2.696 Å, 3.368 Å and 2.806 Å respectively, the rest of the complexes are bidentate and the distances range from 2.783 Å to 3.169 Å. It is important to note that ions in site III got displaced by around 0.2 Å from the initial structure before optimization, however they remain within 2.6 Å to 2.7 Å from an oxygen atom of the zeolitic framework. In case of the adsorption in NaLSX, two sodium atoms in site III and one in site II are responsible for the formation of a tridentate, bidentate and a monodentate structure (*Figure VI- 13 (a)*). BGP interacts with three Ba atoms located in sites II in BaLSX, one bidentate and two monodentate complexes can be seen in *Figure VI- 13 (d)*. These modes of interactions are possible thanks to the observation discussed previously in paragraph (III-2), where barium atoms are located more inside the supercage which increases the probability of a multi coordination. Coordination to two different cations can be seen for CaLSX and SrLSX, the first one is bidentate and the second is monodentate.

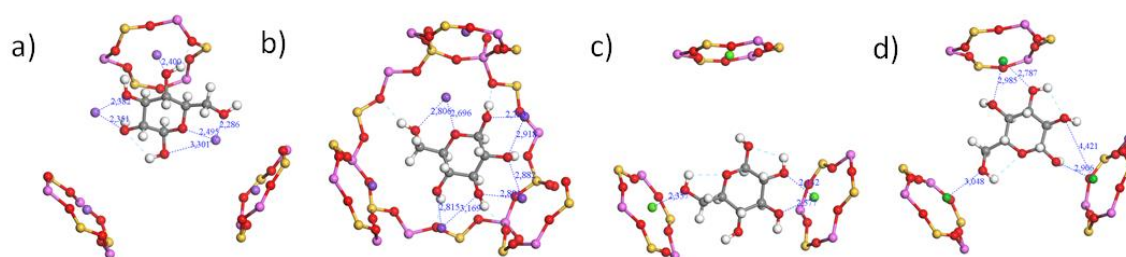


Figure VI- 13: Most stable structure of BGP in a) NaLSX, b) KLSX, c) CaLSX and d) BaLSX

Table A11 that shows the most stable structures with xylose tautomers, it can be seen that for bivalent exchanged zeolites, there is always a coordination with two different ions, mostly one bidentate and one monodentate structure. Noticeably, no coordination to three different cations can be observed in the case of xylose, even in BaLSX, which is due to the smallest size of xylose that cannot accommodate three ions through the supercell. These observations can be also seen in *Figure VI- 14 a)* and *b)* where BXP forms a bidentate complex with O2 and O3 and

a monodentate one with O5 in CaLSX and a bidentate complex with O4 and O5 plus a monodentate with O2 in BaLSX. In case of KLSX, we notice four coordinations in total with three ions in site III and one in site II. We can identify two bidentate complexes and two monodentate ones with distances ranging from 2.721 Å to 2.975 Å. As for NaLSX, *Figure VI- 14* d) shows two bidentate complexes with two ions located in site III and one monodentate bond with and ion in site II.

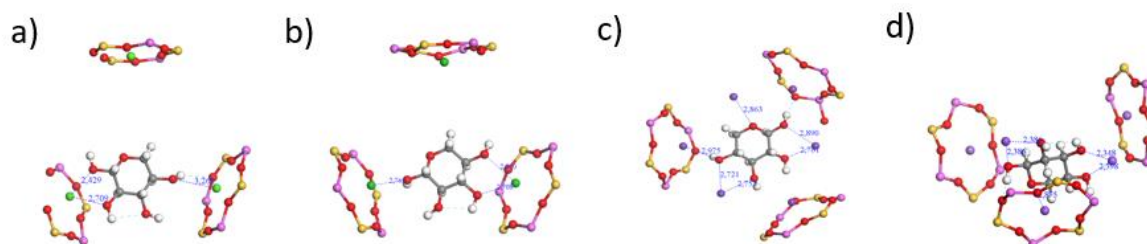
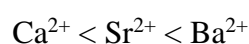
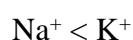


Figure VI- 14: Most stable structure of BXP in a) CaLSX, b) BaLSX, c) KLSX and d) NaLSX

Interpretations

The mean adsorption free energy for glucose and xylose is determined according to the same reasoning in (Paragraph II-3) and summarized in *Figure VI- 15*. Overall, adsorption free energies of glucose are stronger than $\Delta_r G_{mean}$ of xylose for all LSX models. The strongest glucose interactions around -263 kJ mol^{-1} are found with KLSX and BaLSX whereas for xylose, it is with NaLSX (-203 kJ mol^{-1}). KLSX and BaLSX show almost identical $\Delta_r G_{mean}$ around -184 kJ mol^{-1} for xylose. It is interesting to mention that KLSX and BaLSX give similar adsorption free energies for both sugars, although the composition of the two systems and the adsorption modes described above are different. Mean free energies are close for glucose in CaLSX and SrLSX, a difference of -16 kJ mol^{-1} is seen between the two zeolites. Similarly, a difference of -7 kJ mol^{-1} is obtained for xylose. Glucose adsorption free energies become stronger when the ionic radius increases for monovalent and bivalent cations according to the following order for both sugars:



An exception should be noted for xylose where $\text{K}^+ < \text{Na}^+$.

This is remarkable in comparison to the affinity order determined on the single-ion zeolites. In fact, we found earlier that the interaction with the isolated cations follows the general trend of the HSAB theory (within the series of either the monovalent or divalent ions), the interactions with Ca being for instance stronger than with Sr and Ba, and with Na stronger than with K. Here, the order is reversed. This is certainly due to the formation of multiple coordinations (double or even triple in some instances), for which the average distance between cations comes into play. In this regard, the average distances between larger cations like Ba²⁺ is found smaller in the zeolite than for smaller cations, better accommodated within the hexagonal windows (10.9 Å between two Ca²⁺ ions vs. 9.8 Å between two Ba²⁺).

We measured in our previous experimental study single component isotherms of glucose and xylose in exchanged zeolites X and Y (see chapter IV). Interestingly, the same affinity order (Na < K; Ca < Sr < Ba) is found with experimental single component isotherms for zeolites X (Si/Al=1.2) by comparing Henry's constants. The interaction modes identified in the above study for zeolites LSX could give satisfactory explanations to the adsorption behavior and interactions strength of sugars with different cations, regardless of the solvent-zeolite interactions and the hydration of the monosaccharides.

Nevertheless, according to this study, we find that the free energies of adsorption of glucose are stronger than that of xylose in all cases. However, the breakthrough experiments have found the BaX zeolite to be selective towards xylose. Thus, the complexation and therefore the enthalpic component does not explain by itself the experimental selectivities observed. This tends to indicate that collective behaviors, and a more accurate description of the entropic contribution, also certainly play a role in the phenomena leading to the selectivity, that can hardly be apprehended at the DFT level.

The affinity order found with models containing 1 cation does not match with the experimental results obtained on zeolites Y (same affinity order as zeolites X) due the large difference between the Si/Al ratios (Si/Al=2.6 for zeolites Y, NaFAU, KFAU Si/Al = 47 and CaFAU, SrFAU and BaFAU Si/Al = 23). However, the 1-cation zeolite was not intended to be a relevant model for the Y zeolites, only to assess the interaction of sugars with a single cation.

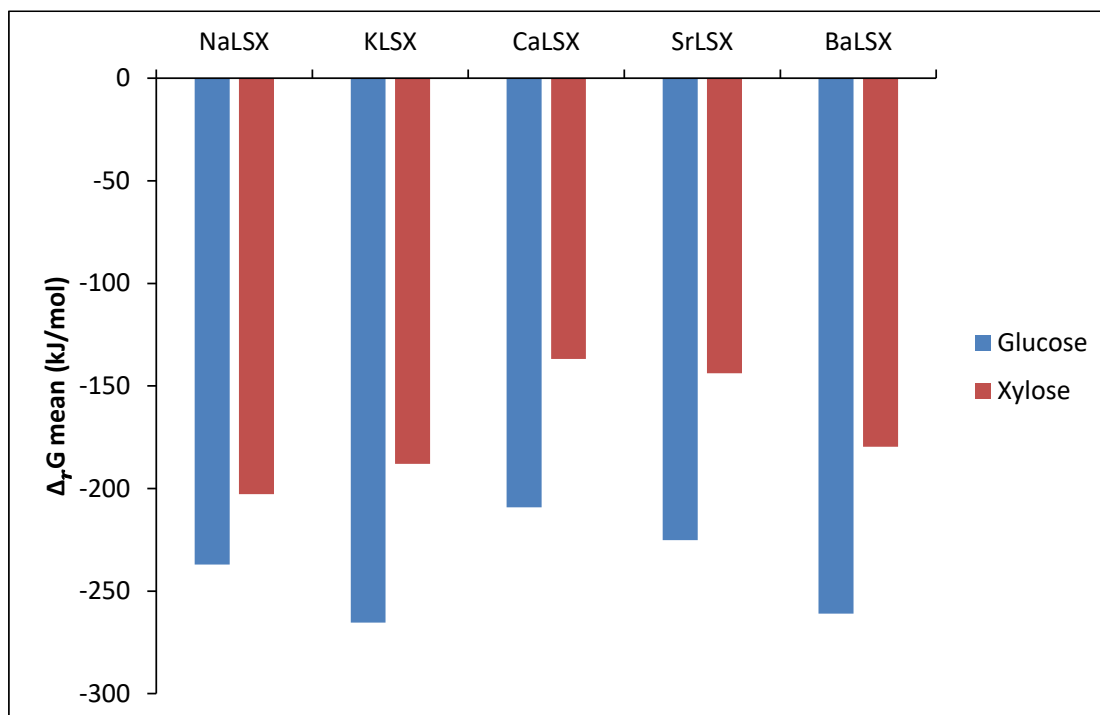


Figure VI- 15: Mean adsorption free energies of glucose and xylose relative to the pyranose rings at 300 K

Now we look at the dealumination effect and therefore the reduction of the number of cations in the zeolitic framework on the free energies of adsorption. *Figure VI- 16* and *Figure VI- 17* present the differences between the energies obtained for zeolites LSX and 1-cation models. Energy differences for sodium and potassium are stronger than bivalent ions (-150 and -180 kJ mol^{-1} for glucose with Na and K respectively and around -118 kJ mol^{-1} for xylose for the two monovalent cations). For both sugars, the difference increases with the ionic radius and the biggest energy changes reducing the cationic amount are with potassium for monovalent cations and barium for bivalent cations. In case of xylose, the reduction of the number of cations in the unit cell from 12 (in zeolites LSX) to 1 in the 1-cation zeolites for calcium and strontium does not impact the free energies of adsorption.

We showed experimentally that by increasing the Si/Al from 1.2 to 2.6 the Henry's constants decrease significantly for the monovalent ions sodium and potassium-exchanged zeolites. This result can be interpreted in light of our DFT results. Partially dealuminated NaY and KY zeolites Y do not have counterions in sites III.⁵⁷ Our calculation results tend to show that multiple coordinations and the proximity between the adsorption sites are key in the adsorption process, specifically on monovalent ions, hence a depletion of these sites III causes a reduction of the complexation sites which may results in a weakening of the global interactions.

Nevertheless, exchanged zeolites with divalent cations do not have ions placed in site III, the increase in Henry's constants experimentally observed from CaX, SrX to CaY, SrY, thus, another contribution is behind this increase of zeolite-sugars interaction aside from complex formation.

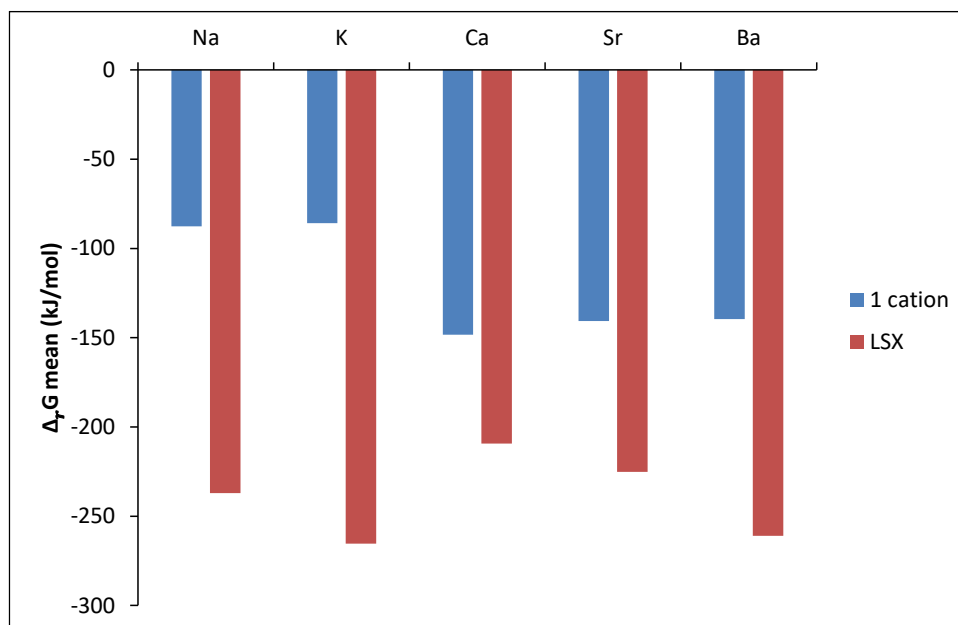


Figure VI- 16: Comparison between mean adsorption energies of glucose in 1-cation models and zeolites LSX

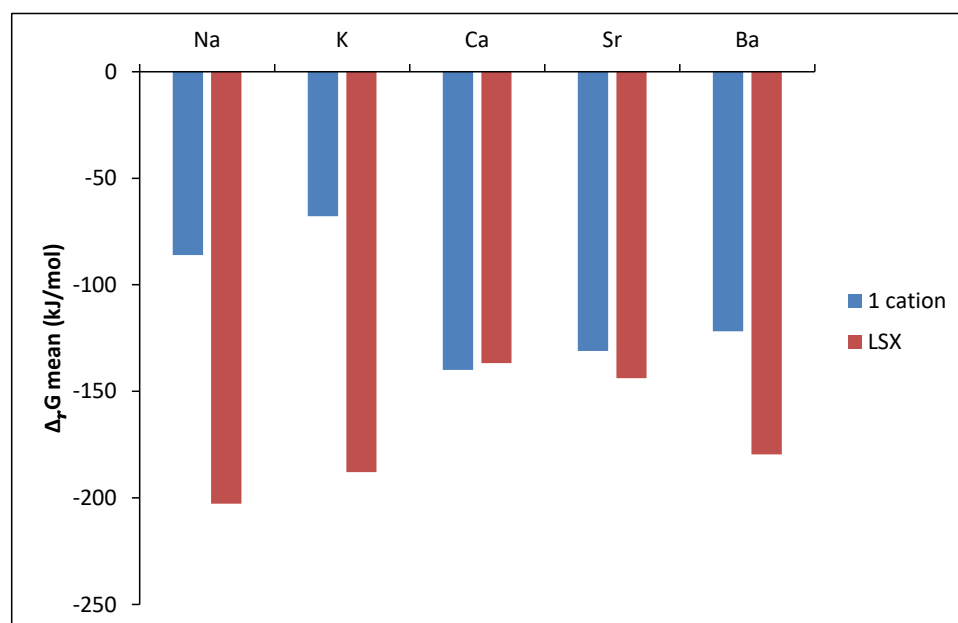


Figure VI- 17: Comparison between mean adsorption energies of xylose in 1-cation models and zeolites LSX

VI-3-3-4 Adsorption of water

In order to estimate the contribution of the solvent adsorption (water in this case) to the overall adsorption process as described on *Figure VI- 1*, we modelled possible adsorption modes of water on the cations of the zeolites.

In this paragraph, the adsorption of water in BaLSX is studied as an example. By analogy with the coordination modes obtained with the sugars (mainly bidentate modes with coordination of two hydroxyl groups), two water molecules were placed close to a barium atom. After optimization, oxygen atoms of water have distances of 2.863 Å and 2.881 Å to barium as presented in *Figure VI- 18*. Hydrogen atoms tend to be pointed toward the framework to form hydrogen bonds. Three hydrogen bonds are obtained for the two molecules.

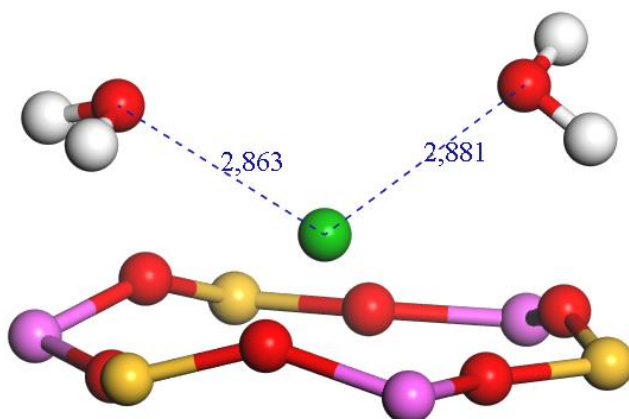


Figure VI- 18: Adsorption of two molecules of water in BaLSX

An adsorption Gibbs free energy of -40 kJ mol^{-1} is calculated per water molecule ($\Delta_r H_{ads} = -82 \text{ kJ mol}^{-1}$ and $\Delta_r S_{ads} = -0.142 \text{ kJ K}^{-1} \text{ mol}^{-1}$). We verified that little cooperative effect was to be expected from the adsorption of additional water molecules in the supercage by adsorbing eight water molecules (two per Ba^{2+} ion) in the supercage and found similar Gibbs free energies of adsorption (-39 kJ mol^{-1} per water molecule on average).

The same procedure was repeated for the other considered materials (CaLSX, SrLSX, KLSX and NaLSX) and the thermodynamic parameters are presented in *Table VI- 2*. Enthalpy and entropy of adsorption values did not vary much for all the LSX models, an average $\Delta_r H_{ads} = -$

79 kJ mol⁻¹ and $\Delta_r S_{ads} = -0.142$ kJ K⁻¹ mol⁻¹ are obtained. Therefore, Gibbs free energies of adsorption are close ranging from -34 kJ mol⁻¹ (NaLSX and SrLSX) to -39 kJ mol⁻¹ (BaLSX). These results show that regardless the composition and the cationic content of the zeolite, water adsorption have almost the same adsorption energies. This is unlike sugars adsorption where different adsorption free energies are found depending on the cationic distribution. Thus, specific interactions between sugars and cations are most likely responsible for the obtained affinities even in presence of water.

Table VI- 2: Adsorption enthalpies, entropies and free energies of water in zeolites LSX at 300 K

	$\Delta_r H_{ads}$ (kJ mol ⁻¹)	$\Delta_r S_{ads}$ (kJ K ⁻¹ mol ⁻¹)	$\Delta_r G_{ads}$ (kJ mol ⁻¹)
NaLSX	-78	-0.147	-34
KLSX	-80	-0.145	-36
CaLSX	-79	-0.138	-38
SrLSX	-76	-0.140	-34
BaLSX	-82	-0.142	-39

VI-3-3-5 Closing the thermodynamic cycle

For closing the Born-Haber cycle and to attempt to determine a free energy of exchange as described in the introduction of this chapter, we took into accounts our DFT-calculated values for the adsorption of water and sugars, as well as values from the literature for the other contributions. Free energy of solvation $\Delta_r G_{solv}^\circ(H_2O)$ was assimilated to the free energy of vaporization and was calculated from the thermodynamic data available in NIST website as follows¹²⁹:

$$\Delta_r H^\circ = \Delta_f H_{liquid}^\circ - \Delta_f H_{gas}^\circ$$

$$\Delta_r S^\circ = \Delta_f S_{liquid}^\circ - \Delta_f S_{gas}^\circ$$

Free energy of solvation can be deduced at the desired temperature (300 K in our case).

$\Delta_r G_{solv}^\circ(S)$ of glucose (5 kJ mol^{-1}) was taken from the literature thanks to Molecular Dynamics (MD) simulations from gas to liquid phase.¹³⁰ Solvation enthalpy (-135 kJ mol^{-1}) from Monte Carlo simulations was used and the entropy can be calculated ($-0.467 \text{ kJ K}^{-1} \text{ mol}^{-1}$).¹¹⁷

We consider the adsorption of BGP in BaLSX for this calculation. However, the number of water molecules n displaced by sugar molecule adsorbed is unknown. In order to estimate this number, we considered that, as shown in the experimental adsorption isotherms, the temperature does not have a large effect on the displacement of water by sugars and we measured that $\Delta_r H_{exc}^\circ = 0$. Thus, to obtain a similar value as computed in that way, we find that around 4.3 water molecules ($n = 4.3$, meaning between 4 and 5 water molecules by glucose) should be displaced as shown in *Table VI- 3*.

With this value for n , the computed $\Delta_r G_{exc}^\circ$ equals -130 kJ mol^{-1} which is very high and negative and should be interpreted as a very favorable adsorption on a thermodynamic point of view. However, the experimental results clearly tend to show that the adsorption is not that favorable (only the Henry regime can be attained in pure water) and this value is highly negative compared to the experimental value of 3 kJ mol^{-1} for glucose isotherm in BaX. We expect similar trends with other systems (sugars and zeolites). This inconsistency may be related to the description of the entropic components used in this study.

Table VI- 3: Thermodynamic parameters to calculate the free energy of exchange at 300 K. ^(a) Data provided by NIST website ; ^(b) Glucose solvation free energy from gas to liquid with Molecular Dynamics simulation ¹³⁰; ^(c) Value obtained from Monte Carlo simulations⁸¹

	$\Delta_r G^\circ \text{ (kJ mol}^{-1}\text{)}$	$\Delta_r H^\circ \text{ (kJ mol}^{-1}\text{)}$	$\Delta_r S^\circ \text{ (kJ K}^{-1} \text{ mol}^{-1}\text{)}$
$\Delta_r G_{ads}^\circ(H_2O)$	-40	-82	-0.142
$\Delta_r G_{solv}^\circ(H_2O)$ ^(a)	-8	-44	-0.119
$\Delta_r G_{solv}^\circ(S)$	5 ^(b)	-135 ^(c)	-0.467
$\Delta_r G_{ads}^\circ(S)$	-261	-299	-0.196
$\Delta_r G_{exc}^\circ$	-130	-1	0.370

VI-4 Conclusion

In order to gain further insight into the phenomena at stake at the molecular level and explore the interaction modes that may affect the selectivity of the adsorbants, adsorption of all glucose and xylose tautomers was studied thanks to DFT calculations in siliceous zeolite, one cation exchanged zeolites ($\text{Si/Al} = 23$ or $\text{Si/Al} = 47$) and zeolites LSX ($\text{Si/Al} = 1$).

The adsorption in the siliceous zeolite showed that the total interaction energy is mainly due to van der Waals interactions. In the one-cation exchanged zeolites, the order of affinity generally follows the Pearson Hard and Soft Acids and Bases (HSAB); the strongest adsorption free energies are found with bivalent ions for both sugars and the highest adsorption energies are obtained in CaFAU. Bidentate complexes are mostly responsible for the observed energies. In case of zeolites LSX (Si/Al close to the experimental system $\text{Si/Al}=1.2$), multiple coordination contributes to the obtained free adsorption energies and therefore the interactions strength. Remarkably, regarding the divalent cations, the order of affinity is inversed compared to the one when only one cation is present, which we assign to the closest proximity between larger cations and easier multiple coordination through the supercage. The results provided herein thus highlight the importance of the inter-cation distances in the adsorption process. The involvement of cations located at sites III in the case of NaLSX and KLSX yields the most stable structures which we assign partly to the even larger site proximity. The interaction strength order is in good agreement with the experimental order stating that glucose and xylose affinity towards zeolites X increases with the ionic radii of monovalent or bivalent cations. To the best of our knowledge, this work represents one of the first simulation works considering at the atomic level the adsorption of all glucose and xylose tautomers in exchanged faujasite-type zeolites.

Nevertheless, the adsorption free energies of glucose were higher than xylose energies in all cases which is not consistent with the experimental selectivities. Moreover, the displacement simulation attempt showed further the limitations of the employed DFT approach to explain the observed experimental results. Entropic and solvent effects have a large influence on the systems behavior, thus calculations at a different level of theory like Grand Canonical Monte Carlo (GCMC) simulations are recommended. Preliminary GCMC results will be discussed in the next paragraph.

Chapter VII: Adsorption study of sugars by Grand Canonical Monte Carlo (GCMC) simulations

VII-1 Introduction

In the previous sections, computational efforts were dedicated to rationalizing the experimental monosaccharides adsorption results by means of “*ab initio*” (DFT) calculations. Although the use of the mentioned techniques allowed for a significant understanding of different adsorption mechanisms at stake and their relations to the nature of the cationic distribution, some limitations appeared in the comparison with experimental data. In particular, when significant loadings are reached, quantum chemistry calculations become limited to efficiently capture the cooperative ensemble effects associated to the adsorption in the liquid phase. Besides, we showed thanks to breakthrough experiments (Chapter IV) the impact of the solvation on the adsorption. The presence of ethanol in the feed solution indeed significantly increased glucose and xylose uptakes in BaX and BaY compared to results obtained from aqueous solutions.

In a tentative to overcome such limitation, a second group of molecular simulation techniques (Molecular Mechanics) was implemented alongside to try to get more insights on the liquid adsorption of monosaccharides. Thus, Monte Carlo (MC) simulations are performed to study the sugar adsorption in zeolites. The choice of the mentioned technique is expected to round off the mainly enthalpic “*ab initio*” approach with the study of the cooperative interactions (entropic) of the system constituted by both monosaccharides and the solvent. The Monte Carlo technique presents a main advantage when compared to *ab initio* quantum chemistry calculations: it allows considering a much larger amount of system particles. In this way, the use of the MC technique can account for the cooperative ensemble effects associated to the adsorption in liquid phase.

In the next paragraphs, a short description of the methodology will be presented. First, a short introduction of the theoretical aspects of MC technique will be presented along with the parameterization of the system (as this thesis is not only oriented to the computational study, force fields available in the literature will be employed to avoid costly specific reparameterizations). Then, pure monosaccharides will be considered. Although experimental results are not available for comparison at such conditions (in the absence of solvent) two main

interests underlay in the study of the proposed systems. Firstly, by studying the adsorption behavior at low loading (Henry regime) the ability of the force field to reproduce the interaction between the sugars and the zeolite will be assessed. Thus, by calculating the isosteric heats of both pure monosaccharides (*glucose* and *xylose*) in a BaLSX system a comparison with the DFT picture will be available. Secondly, the system behavior at maximal loading will be considered before studying the competitive adsorption of both monosaccharides.

VII-2 Computational methods

GCMC simulations (μ VT ensemble) were performed to explore the adsorption of BGP and BXP in BaLSX at 333.15 K using the GIBBS code v 9.6. For each state point, 1.10^6 steps were considered for equilibration followed by 10.10^6 steps to sample the desired properties. A cutoff radius of 12.50 Å was applied to the Lenard-Jones (LJ) interactions, while the long-range electrostatic interactions were handled by the Ewald summation technique. Both the adsorbent and the adsorbates (water and sugars) are considered as rigid molecules, this allowed to simplify the general form of the force field that becomes reduced to only two contributions: the dispersion-repulsion and the electrostatic interaction forces.

$$U_{TOT} = U_{LJ} + U_{elec} \quad (\text{Eq VII-1})$$

In the case of the adsorption of monosaccharides, it is worth mentioning the importance of the electrostatic contribution when dealing with counter-cationic species hydroxyl groups. While the first contribution, corresponding to the dispersion-repulsion energy is described via a 12-6 Lennard-Jones potential, the second contribution (electrostatic) is treated by means of a coulombic term:

$$U_{LJ}^{ij}(r) = 4 \varepsilon_{ij} \left[\left(\frac{\sigma_{ij}}{r_{ij}} \right)^{12} - \left(\frac{\sigma_{ij}}{r_{ij}} \right)^6 \right] \quad (\text{Eq VII-2})$$

$$U_{elec}^{ij}(r) = \frac{q_i q_j}{4\pi \varepsilon_0 r_{ij}^2} \quad (\text{Eq VII-3})$$

where ε_{ij} is the depth potential energy, r_{ij} is the distance between two particles, σ_{ij} is the distance between two particles where the potential energy is equal to zero. The first term $\left(\frac{\sigma_{ij}}{r_{ij}} \right)^{12}$ describes repulsive interaction and the second one $\left(\frac{\sigma_{ij}}{r_{ij}} \right)^6$ attractive interaction. ε_0 is the

electrostatic vacuum permittivity, q_n is the electric charge and r is the distance between the charges.

The cross-interaction LJ parameters to describe the solute (sugars/water) /faujasite interactions were obtained using the Lorentz-Berthelot mixing rules.

VII-2-1 BaLSX force field

The faujasite structure was imported from the available database of Materials Studio software. The transferable potentials for phase equilibria (TraPPE) force field parameters were used to describe the dispersion-repulsion interactions of the framework.¹³¹ The parameters of barium atoms were determined according to the methodology proposed by Maurin et al.¹³² All the parameters are summarized in the following Table:

Table VII- 1: Lennard-Jones parameters and electrostatic charges of BaLSX

atom	σ (Å)	ϵ/k_B (K)	q (e) [†]
O _z	3.3	52.5	-1.2447
Si	2.3	21.85	2.1439
Al	2.3	21.85	1.9931
Ba	2.2	141.57	1.6834

[†]Average values

VII-2-2 Sugars force field

The optimized sugars' structures used in the previous DFT study were considered for the GCMC simulations. β -pyranose forms of glucose and xylose were taken since they are the major tautomers in an aqueous solution. The Lennard–Jones 12–6 (LJ) and Coulomb potentials, parameters were taken from OPLS-AA (Optimized Potentials for Liquid Simulations – All Atom) force field for β -glucopyranose (BGP) and adapted to β -xylopyranose (BXP).¹³³ Structures and all parameters are presented in the figures and tables below:

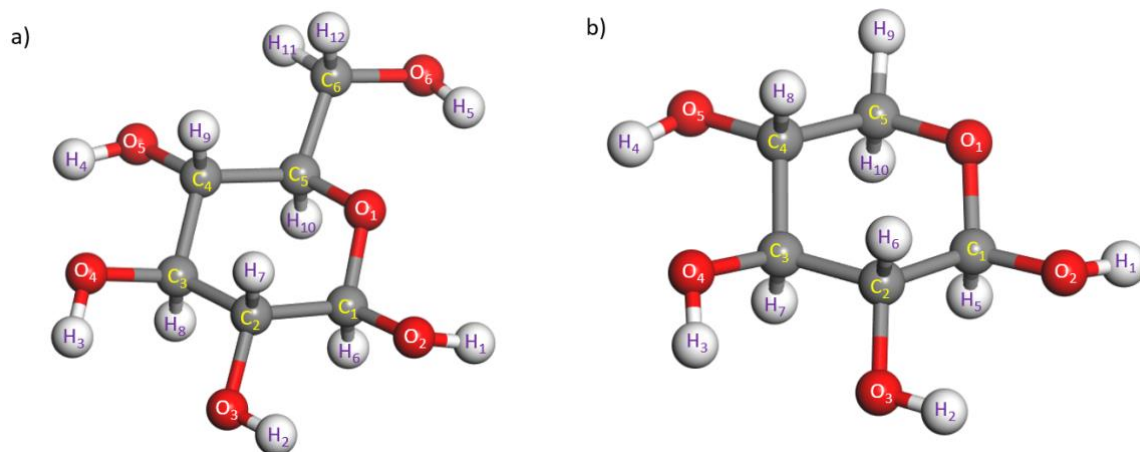


Figure VII- 1: Representation of the implementation of a) BGP and b) BXP

Table VII- 2: Lennard-Jones parameters and electrostatic charges of BGP

Atom	σ (Å)	ϵ/k_B (K)	q (e)
C ₁	3.5	33	0.365
C ₂ -C ₄	3.5	33	0.205
C ₅	3.5	33	0.170
C ₆	3.5	33	0.145
O ₁	2.9	70	-0.400
O ₂ -O ₅	3.07	85	-0.700
O ₆	3.12	85	-0.683
H ₁ -H ₄	0	0	0.435
H ₅	0	0	0.418
H ₆	2.5	15	0.100
H ₇ -H ₉	2.5	15	0.060
H ₁₀	2.5	15	0.030
H ₁₁ -H ₁₂	2.5	15	0.060

Table VII- 3: Lennard-Jones parameters and electrostatic charges of BXP

Atom	σ (Å)	ϵ/k_B (K)	q (e)
C ₁	3.5	33	0.365
C ₂ -C ₄	3.5	33	0.205
C ₅	3.5	33	0.080
O ₁	2.9	70	-0.400
O ₂ -O ₅	3.07	85	-0.700
H ₁ -H ₄	0	0	0.435
H ₅	0	0	0.100
H ₆ -H ₁₀	2.5	15	0.060

VII-2-3 Water force field

The TIP4P (Transferable Intermolecular Potential 4 Point) model was employed for water¹³⁴, the used parameters are listed in the following table:

Table VII- 4: Lennard-Jones parameters and electrostatic charges of the TIP4P model for water

Atom/(Site)	σ (Å)	ϵ/k_B (K)	q (e)
O _w	3.1536	78.03	---
H _w	0	0	0.52
(M)	---	---	-1.04

VII-2-4 Adsorption Equilibrium Theoretical Framework

For a multicomponent system, where the adsorbed and fluid phases consist of a mixture of n compounds (the sugars and the solvent), the equilibrium state is described by the following equations:

$$p^{ads} = p^f \quad (\text{Eq VII-4})$$

$$T^{ads} = T^f \quad (\text{Eq VII-5})$$

$$f_i^{ads} = f_i^f \quad (\text{Eq VII-6})$$

being f_i the fugacity of the i compound. The choice of the GCMC (μ VT) ensemble to perform the adsorption simulations intrinsically implies fulfilling the mentioned conditions. Thus, the

simulations are conducted at the selected temperature, volume (usually corresponding to a multiple of the zeolite unit cell volume) and fugacities. The coupling (thermal and particle exchange) between the simulation box and the external reservoir ensures the equality between the thermodynamic parameters of both the adsorbed and fluid phases. Nevertheless, it is crucial to determine the fugacity (or chemical potentials) of the different species in the fluid phase. The impact of the fugacity values is particularly important when comparing the simulation results to experimental data or when studying the competitive adsorption between different compounds (one of the main goals of this study). In other words, the adsorbed amounts are not uniquely conditioned by the interaction between both sugars and the zeolite in the simulation box but for the interactions between sugars in the fluid phase as well. The fugacity (in the mixture) of a given compound in the fluid (liquid) phase is given by:

$$f_i^f = f_i^l = x_i f_i^* \quad (\text{Eq VII-7})$$

f_i^* being the fugacity in the pure liquid phase. Besides, the fugacity of the i compound in the pure liquid can be expressed according to:

$$f_i^* = \varphi_i P_i^{sat} e^{\left(\frac{v(P - P_i^{sat})}{RT}\right)} \quad (\text{Eq VII-8})$$

where P^{sat} is the saturation pressure between liquid and gas phases in our case and φ the fugacity coefficient. Since the pressure value is low enough the latter can be approximated to one. For the same reason, the exponential term of the equation (also known as Poynting factor) can be as well approximated to one. By applying the mentioned assumptions, the fugacity (in the mixture) of a given compound in the fluid (liquid) phase can be finally approximated to:

$$f_i^f = f_i^l = x_i P_i^{sat} \quad (\text{Eq VII-9})$$

VII-3 Adsorption of pure sugars in BaLSX

As previously mentioned, pure sugars (both glucose and xylose) exist in the nature under the form of solid compounds. Then experimental results are not available for comparison in the case of the adsorption of pure compounds. Nevertheless, the study of the pure systems (in the

absence of a solvent) presents a strong interest. Thus, by considering the Henry regime, the ability of the implement force field to represent the interactions between the sugars and the zeolite can be assessed by comparison to the DFT results obtained in Chapter VI. In *Table VII- 5*, the isosteric heats of adsorption (determined by GCMC calculation in the Henry regime) are compared to the adsorption enthalpies (obtained by DFT in vacuum). As can be seen, the “standard” proposed force field reproduces well the order of adsorption strengths observed through the quantum calculations. Thus, the adsorption strengths of glucose (determined either by quantum or classical methods) are higher than those obtained for xylose. When comparing the absolute values, the GCMC calculations significantly underestimate the results obtained by DFT. This difference can be attributed to the lack of specificity of the force field for the case of the adsorption. In this direction, it is worth reminding that OPLS is a generic force field intended to reproduce general liquid properties like the specific volume or the vaporization heat. Nevertheless, the more valuable information lays on the gap between the estimation obtained by both methodologies for the respective compounds. Thus, in the case of xylose the gap between GCMC and DFT calculations is significantly lower than that observed for glucose (32.5 vs 60.8 kJ mol⁻¹). This fact agrees well with the results obtained in Chapter VI related to the average coordination number between both sugars and the cationic distribution. As a reminder, the DFT study of the preferential adsorption modes (in the vacuum) showed an important degree of association between the hydroxyl groups of the monosaccharides and the zeolite counterions. For the case of glucose (the system showing the higher gap between the computational methods) the average number of interactions stabilizing the adsorption mode was three. Instead, for the case of xylose where the gap is significantly lower only two interactions were observed. To summarize, although the selected force field presents some limitations linked to the high level of association observed in the case of the adsorption of monosaccharides, the competitive behavior between both sugars should be correctly captured. The previous assumption should be all the more correct that the loading of the zeolite is higher.

Table VII- 5: Comparison between the enthalpic behavior of monosaccharides adsorbed in *BaLSX*

Compound	Q_{st} (GCMC) (kJ mol⁻¹)	ΔH (DFT) (kJ mol⁻¹)	# of cationic coordinations (DFT)	Enthalpic gap between methods (kJ mol⁻¹)
Glucose	-242.2	-303	3	60.8
Xylose	-212.2	-245	2	32.5

At the opposite extreme of the isotherm, the GCMC adsorption simulations of pure compounds are well adapted to study the configurational behavior of both sugars at high loadings in the supercages. In *Table VII- 6*, the maximal adsorbed amounts of glucose and xylose are presented. As can be seen, in the case of xylose (slightly less bulky than glucose) loadings as high as 2.62 molecule per supercage are reached. In the case of glucose, the maximum value corresponds to 2.12. Such observation is qualitatively in good agreement with the experimental results obtained in Chapter IV where the saturation value of xylose inferred from Langmuir model (2 molecules per supercage) was higher than that obtained for glucose (1.5 molecules per supercage) in BaX. Nevertheless, it is worth reminding that the experimental values were obtained in conditions slightly different from those corresponding to the simulations. Firstly, the experimental isotherms were measured at 30 °C (60 °C in the case of the simulations). As showed in Chapter IV (section IV-2-5), the temperature effect was shown to have a very moderated effect in the adsorbed amounts. Secondly, the experimental data were obtained in the presence of a solvent (mixture of water and ethanol). As expected, the experimental values are lower than the computed ones due to the space occupied by the solvent.

Table VII- 6: Maximal loadings of monosaccharides in BaLSX

Compound	Source	Temperature (°C)	Ads. molecules (per unit cell)	Ads. molecules (Per supercage)	Qsat (molec/supercage)
Glucose	Exp.	30	---	---	1.5
Xylose	Exp.	30	---	---	2
Glucose	GCMC	60	17	2.12	---
Xylose	GCMC	60	21	2.62	---

VII-4 Adsorption of aqueous solutions of pure sugars in BaLSX

When dealing with the simulation of sugars adsorption, one of the main difficulties is constituted by the lack of thermodynamical information about their solutions necessary to establish the link between both the adsorbed and fluid phases (as previously treated in section VII-2-4). Thus, based on the available data, several approaches have been proposed to correlate/

predict the properties of the solid-liquid equilibria (under multiple forms like water activity, osmotic coefficients, vapor pressures, boiling temperatures, freezing points or solubility data). The data acquired in the experimental sections of this work intrinsically constitutes an additional source of experimental information. The adsorption study of pure solutions of monosaccharides presents the intrinsic interest of linking the properties of both adsorbed and fluid phases previously to studying the competitive adsorption of both sugars in the zeolite supercages.

Since the scope of this thesis is more related to shedding light on the sugar adsorption separation mechanisms than to the development of accurate force fields able to precisely fit the experimental data, a simplified approach is proposed. Thus, the proposed strategy consists in employing the experimental isotherms of pure solutions of sugars to infer the saturation pressures of both compounds. The latter parameter was determined from the Henry domain (more precisely at a filling of 20 g/kg). The mentioned region is denoted by dashed vertical lines in *Figure VII- 2* and *Figure VII- 3*. At this concentration, the same interpolated filling was fitted to the one obtained by simulation. Thus, the saturation pressure was determined thanks to Eq VII-9. Then, ideality will be assumed when studying the competition between the adsorption of monosaccharides. It is worth to recall here that notwithstanding the strength of the previous assumption when dealing with strong associative systems, the main objective here is to study general trends along with the development of computational simplified strategies allowing to optimize the conditions of sugar separation.

In *Figure VII- 2* and *Figure VII- 3*, the adsorbed amounts obtained for glucose and xylose (either experimentally or by molecular simulation) are presented. The molecular simulation amounts correspond to those calculated employing the fitted saturation pressures ($8 \cdot 10^{-8}$ Pa and $1 \cdot 10^{-6}$ Pa respectively for glucose and xylose).

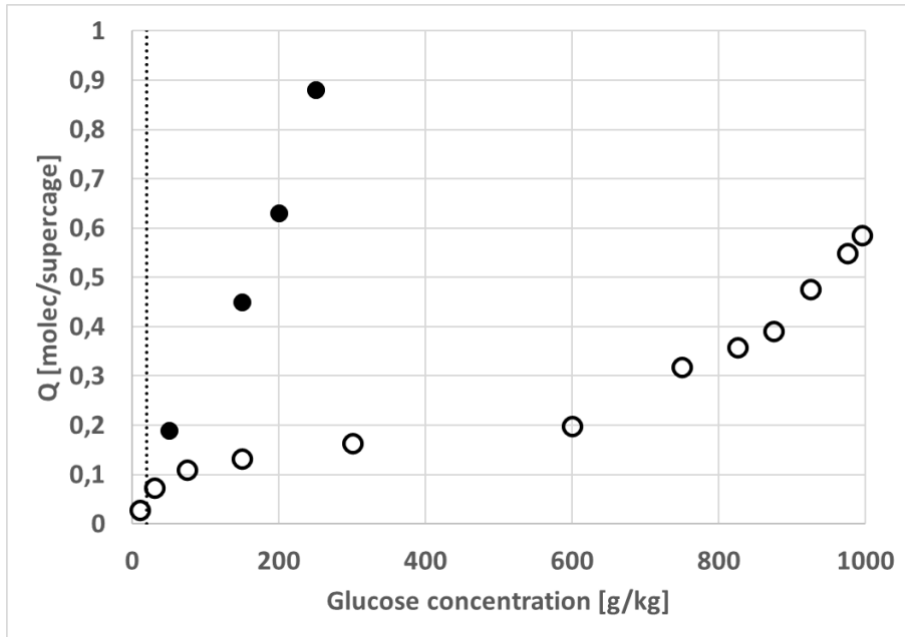


Figure VII- 2: Glucose adsorbed amounts. Filled symbols account for the experimental results while empty symbols are the simulation results obtained for $P_{sat} = 8 \cdot 10^{-8} \text{ Pa}$

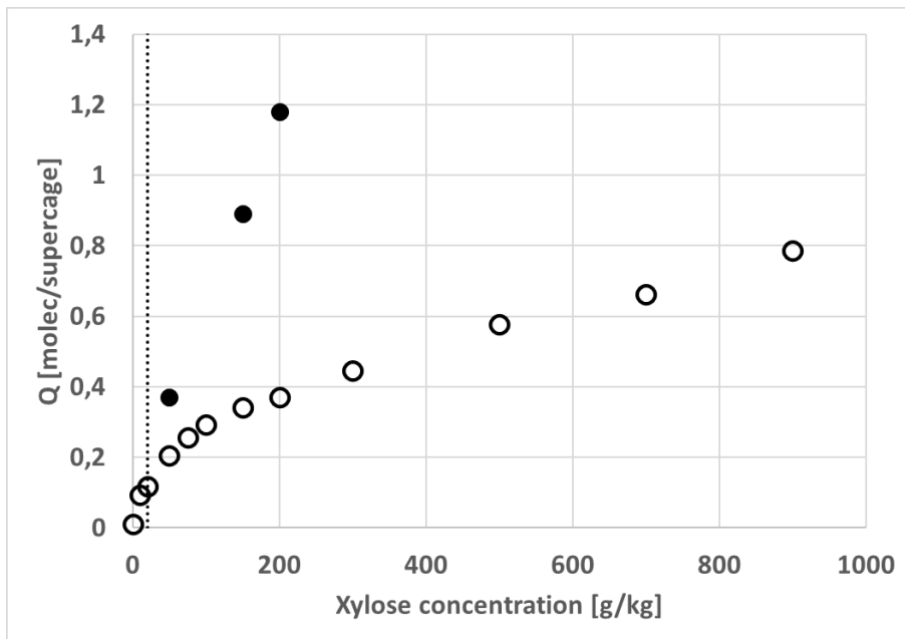


Figure VII- 3: Xylose adsorbed amounts. Filled symbols account for the experimental results while empty symbols are the simulation results obtained for $P_{sat} = 1 \cdot 10^{-6} \text{ Pa}$

As expected from the isosteric heats of adsorption, calculated in section VII-3, the simulated isotherms of both monosaccharides significantly underestimate the experimental measurements. This behavior is attributed to the lower adsorption strengths mimicked by the force field leading to an average description of the competitive adsorption between the solvent and the monosaccharides. This fact is expected to not be an obstacle to study in the following section the main trends of the adsorption competition between both monosaccharides. That

should be even more the case when significant loadings of monosaccharides are considered (as is the case of the experimental measurements).

Regarding the determined saturation pressures and although this kind of measurements are relatively scarce in the literature, (monosaccharides are typically considered nonvolatile and typically degrade prior to vaporizing) the obtained values are compared to experimental extrapolations in *Table VII- 7*. The values fitted through the proposed simplified strategy present a good level of agreement with the bibliographic data and this is particularly the case for glucose.

Table VII- 7: Saturation pressures of monosaccharides

Compound	Source	T (K)	T (Range of application)	Comment	Saturation Pressure (Pa)
Glucose	Oja <i>et al</i> ¹³⁵	333.15	370-395	Extrapolated	$4.0 \cdot 10^{-8}$
Xylose	Oja <i>et al</i>	333.15	395-406	Extrapolated	$2.1 \cdot 10^{-5}$
Glucose	Perozin <i>et al</i> ¹³⁶	333.15	296-318	Extrapolated (from Table 3 [†])	$1 \cdot 10^{-6}$
Xylose	Perozin <i>et al</i>	333.15	298-308	Extrapolated (from Table 4 [†])	$6.3 \cdot 10^{-5}$
Glucose	Perozin <i>et al</i>	333.15	296-318	Extrapolated (from Figure 3 [†])	$6 \cdot 10^{-8}$
Xylose	Perozin <i>et al</i>	333.15	298-308	Extrapolated (from Figure 4 [†])	$4 \cdot 10^{-5}$
Glucose	GCMC this work	333.15	333,15	Fitted	$8 \cdot 10^{-8}$
Xylose	GCMC this work	333.15	333,15	Fitted	$1 \cdot 10^{-6}$

[†]Referred to the cited reference

VII-5 Adsorption of solutions of monosaccharides mixtures in a BaLSX system

GCMC adsorption simulations of solutions containing identical masses of xylose and glucose were conducted in order to study the competitive adsorption of both monosaccharides at different loading levels. The calculated selectivities are presented in *Figure VII- 4* as a function of the loading.

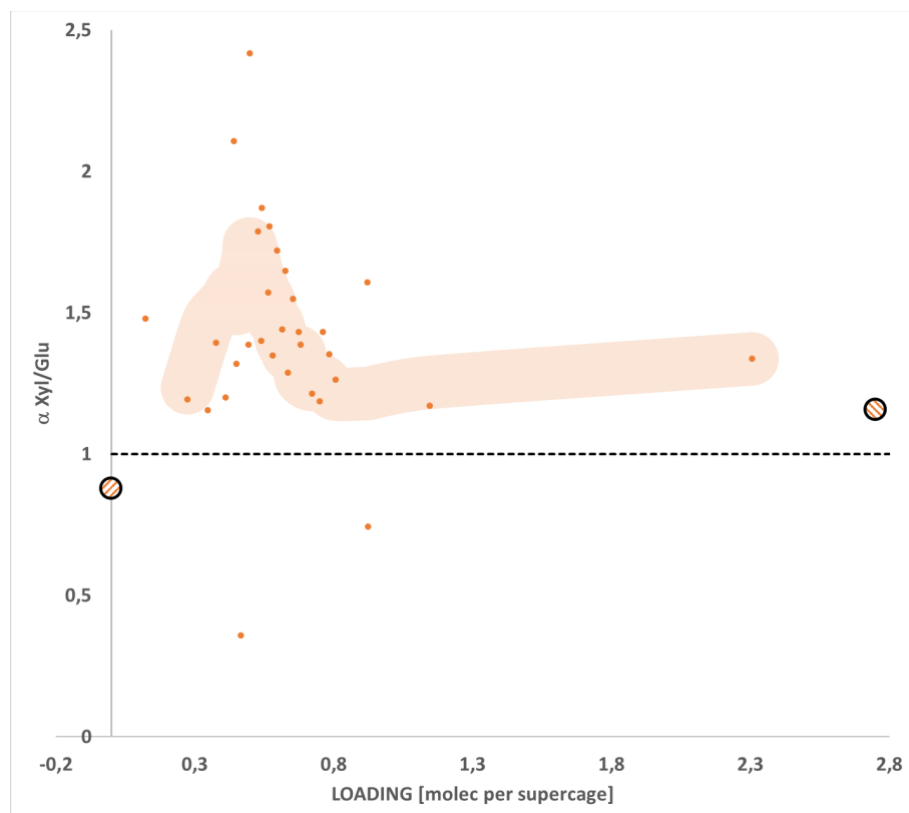


Figure VII- 4: Xylose/Glucose selectivity as a function of the supercage loading. Dashed symbols respectively correspond to the theoretical ratios of isosteric heats of adsorption and maximum loadings. Orange trace is a guide to the eye.

As can be seen, at low loadings the system is governed by the enthalpic interactions between the sugars and BaLSX zeolite. Thus, in agreement with the order of isosteric heats of adsorption, glucose is more adsorbed than xylose in the Henry regime. Progressively, as the loading is increased, xylose becomes preferentially adsorbed compared to glucose. Although the potential uncertainties associated either to the simplification in the description of the liquid phase or the sampling difficulties, the obtained values are in good agreement with the experimental values (selectivity of 1.52 for a total loading of 1.5 molecule/supercage using a feed mixture of 150 g kg^{-1} glucose and 150 g kg^{-1} xylose in BaX) It is worth underlining the fact that the xylose/glucose selectivity inversion takes place at loadings significantly lower than 0.5 molecule per supercage. This observation likely points the origin of the inversion to the availability of countercations stabilizing the sugars adsorption. As mentioned before, xylose preferably coordinates to two barium atoms and glucose to three. Although a more detailed analysis of the adsorption configurational modes would be necessary, this differentiated behavior between both sugars seems to not to be innocuous in the selectivity inversion. As a possible hypothesis, the next explanation could be given to the observed phenomenon : four

barium cations in site II are available in the supercage and when the loading increases, the system is potentially better stabilized by two xylose molecules coordinated to the ensemble of barium atoms rather than one glucose letting one free barium. This picture is significantly different from that observed in the case of the separation of xylenes with similar adsorbents (BaX or BaLSX). In the mentioned case, selectivity (through the para isomer) appears when loadings significantly higher than one (values close to three) are reached.¹³⁷ Thus, the separation of sugars in faujasite zeolites (and very likely in other topologies) seems to preferentially lay on a combination of electrostatic interactions (between the sugars and the cationic distribution) and configurational (entropic) behavior of the different compounds.

VII-6 Conclusion

To summarize, the GCMC methodology has been implemented to study the separation of monosaccharides in faujasite-type zeolites. Inherent difficulties are associated to the study of such systems. Thus, the presence of highly associative interactions between the hydroxy groups and the zeolite cationic distribution alongside with the low temperature operating conditions results in a challenging scenario for the configurational sampling. A derived consequence of this situation concerns the impracticability of studying at the mentioned conditions the fluid phase in equilibrium with the adsorbed phase. Such a possibility would have allowed to overcome the lack of reliable enough frameworks (either experimental or theoretical) dealing with monosaccharide solutions. Finally, the absence of dedicated intermolecular potentials for the adsorption of monosaccharides constitutes an additional complexity.

Despite the mentioned drawbacks, a simplified strategy was implemented by using a standard force field. The proposed approach constitutes, to the best of our knowledge, one of the first simulation works considering at the atomic scale the adsorption of binary solutions of monosaccharides in zeolites (or other adsorbents).¹³⁸ The approach consisted in establishing the link between the fluid and the adsorbed phases thanks to the experimental isotherms determined at 60 °C for aqueous solutions of glucose and xylose. Then, the adsorptive behavior of the mixture was considered to assess the impact of the cage filling on the selectivity. To lessen the configurational sampling limitations, the replica exchange methodology was adopted by parallelly simulating several loadings.¹³⁹ The obtained results confirm the importance of the entropic contribution in glucose/xylose separation. The weight of such contribution is reflected in the observed inversion of selectivity as a function of cage loading.

The promising results should be confirmed by the extension of the proposed methodology to other systems studied experimentally. In particular, (Na)BaY and KLSX seem excellent candidates to further benchmark the ability of the methodology to study the configurational effects on the selectivity between xylose and glucose.

Considering the impact of the solvation on the separative properties of zeolites is also one of the perspectives of the proposed methodology. Nevertheless, previous improvements to the potential to better account for the interactions between sugars and the adsorbent framework could be desirable. As shown in section VII-4, when dealing with pure sugar solutions, the underestimation of the energetic interactions between the hydroxy groups and the cationic distribution results in lower sugar adsorbed amounts when compared to the experimental results. Once this interaction reevaluated, the proposed methodology could be useful to optimize the solvation properties leading to enhanced separation properties.

General conclusion

The work presented in this report aims to understand the separation mechanisms of lignocellulosic biomass sugars (mainly glucose and xylose) involved in adsorption-based separation techniques when using zeolitic adsorbents. Both experimental and theoretical approaches were employed to rationalize the observed behaviors.

Although the separation of fructose and glucose is well treated in the literature thanks to its application in the food industry, fewer works can be found studying the separation of glucose and xylose. The majority of the studies employ exchanged resins as adsorbents and explain the separation mechanism by a complex formation between the cation and the sugar. The stability of such complex is associated to the orientation of the hydroxyl groups in each sugar ring. When comparing exchanged resins with zeolitic adsorbents presenting the same type of cations, better fructose/glucose selectivities are found for a CaY zeolite compared to a calcium-exchanged resin. Nevertheless, CaX was not selective in this case despite a higher number of potential complexation sites is available. This fact suggests that the introduction of a crystalline/ordered network can favor the separation ability of the selected adsorbent. Nonetheless, understanding and rationalizing the link between the nature of the ordered network and the adsorptive properties (both in terms of capacity and selectivity) becomes essential to develop and optimize the associated separation processes. Thus, the literature review performed in Chapter I confirmed that the confinement effect of the zeolite is rather unknown on the adsorption properties of sugars, particularly in the case of the selectivity. The literature review raised other important questions without clear answers: What is the influence of the cationic distribution on the interactions between the sugars and the different zeolitic adsorbents? Which is the relative weight between the electrostatic and Van der Waals contributions? DFT calculation could potentially give some clarification to these interrogations. However, most of studies in literature focus on the catalysis of glucose to fructose in Sn-BEA zeolite, and no study is found addressing the adsorption of sugars in faujasite-type zeolites.

In order to shed light on the previously mentioned questions, both experimental (mainly chromatographic) and theoretical approaches were combined. From the experimental point, a committed study was devoted to the analytical monitoring of the sugars involved in this work. Thus, to reduce the time associated to the measurement of the concentration profiles issued from dynamic experiments (breakthrough curves), online Raman spectroscopy was optimized to measure the column outlet concentrations. Simple univariate models and more sophisticated

chemometrics methods were compared to the offline reference technique which is HPLC to follow glucose, xylose and ethanol concentrations, detailed in Chapter II. Both univariate and multivariate models proved accurate compared to HPLC analysis. At the end the univariate models, which were simple to implement and provided robust results were chosen to continue the experimental adsorption study.

Prior to performing the “screening” strategy and besides the mentioned analytical improvements, different zeolitic adsorbents were prepared and characterized as described in Chapter III. Thus, two different sodium forms of the faujasite zeolite (X and Y) were selected to consider the impact of the electrostatic strength on the separation properties. The mentioned samples served as platforms to obtain by cationic exchange a wider variety of adsorbents allowing to study the impact of the cation nature. Therefore, zeolites NaX (Si/Al = 1.2) and NaY (Si/Al = 2.6) were exchanged into K, Ca, Sr and Ba forms and high exchange rates were targeted to evaluate the compensation ion effect on the separation. The textural and chemical properties of all exchanged adsorbents were determined thanks to several characterization techniques. The combination of the latter characterization results allowed to calculate the number of supercages per gram of each exchanged zeolite. This valuable information led to determine the sugar filling per supercage for every breakthrough test.

Additional series of experiments were carried out to get insights about the separation potential of the developed adsorbents and the results were also presented in Chapter III. Breakthrough experiments on the exchanged zeolites X and Y using a feed mixture of glucose and xylose were performed. Values of xylose/glucose selectivity increased with the ionic radii of monovalent and divalent cations for zeolites type X. KX and BaX were the most selective to xylose with selectivities of 1.18 and 1.52 respectively. The latter observation was found only with divalent ions for zeolites Y, but the adsorbents became selective to glucose. The highest glucose selectivities were obtained for SrY (0.89) and BaY (0.67). This screening strategy showed that the selectivity to glucose or xylose is controlled by the Si/Al ratio of the zeolite. Regardless of the Si/Al, the highest selectivities were obtained with barium, and thus, to enhance the selectivity, a smaller number of cations is preferred in the unit cell in comparison to monovalent ions. In addition, large ion size is privileged.

The separation tests showed that the cation type and Si/Al ratio have a large impact on selectivity. To have a deeper understanding of the interactions between cations and sugars, single adsorption isotherms were measured for glucose and xylose aqueous solutions in all

exchanged zeolites X and Y (Chapter IV). Linear isotherms in Henry's region were found in the studied concentration range and the saturation remained unknown. The order of affinities for both sugars was: Na<K for monovalent ions and Ca<Sr<Ba for bivalent ones. These results showed the specific confinement features of each zeolite on the sugar-adsorbent interactions. The electrostatic environment and Van der Waals components generated according to the chemical composition of the zeolite gave the obtained affinities order. The highest affinities were with potassium for zeolites X and with barium with zeolites Y. Henry's constants depend on the size and the number of cations, a higher number and increasing cation size resulted in a higher Henry's constant as it was the case for KX reflecting strong interactions.

Since it was not possible to clearly determine the saturation values from aqueous solutions, we employed a strategy consisting of partially replacing the solvent (water) with ethanol. The addition of ethanol in the feed enhanced glucose and xylose uptakes and allowed to determine the saturation value. The maximum loadings of glucose and xylose in BaX were 1.5 and 2 molecules per supercage, the same loading was found for glucose in BaY but an estimated 3 xylose molecules per supercage was calculated in BaY. Interestingly, when ethanol was introduced in a sugar mixture, the selectivity was impacted. CaX and SrX which were not selective when working with aqueous solutions, became selective to xylose. The same observation was found for NaY which became selective to glucose. Since ethanol increased the adsorbed amount in every zeolite, the latter results suggested that the selectivity starts from a specific sugars total uptake. Uptakes from aqueous solutions were below this specific amount which resulted into the observed non selectivity (the case of CaX, SrX and NaY). The addition of ethanol allowed to reach this amount and create a selectivity towards one of the sugars depending on the zeolites composition. In parallel, we showed that the temperature had no significant effect on adsorption isotherms on BaX and BaY, pointing to a rather athermic character of the adsorption process on these materials.

The experimental study showed in general that the cationic distribution had a large influence on the obtained affinities and selectivities. The number and size of the compensating ions directed the adsorption of glucose and xylose. In order to get deeper insights at the molecular level of the adsorption process, we first carried out a set of experiments aiming at observing the sugars in adsorbed phase as described in Chapter V. For the purpose of identifying and rationalizing glucose and xylose tautomers in solution and in adsorbed phases, ¹³C MAS NMR experiments were performed. BaX and BaY were chosen for this study since they were the most selective adsorbents. It was found that the adsorbed species are very similar to the tautomeric

forms in solution corresponding to pyranose forms. The β -pyranose: α -pyranose ratios in both phases (solution and adsorbed) were close around 60:40 at 25 °C. These results reflected that the pyranose forms were the most stable in solution and in the adsorbed phases. In addition, similar free energies of adsorption could be expected.

To investigate at the molecular level the effect of the chemical composition, adsorption of all glucose and xylose tautomers was studied thanks to DFT calculations in a siliceous faujasite-type zeolite, one cation exchanged zeolites (Si/Al = 23 or Si/Al = 47) and zeolites LSX (Si/Al = 1) in Chapter VI. The total interaction energy in the siliceous structure was mainly composed of Van der Waals interactions. By adding more ions in the cell, the electronic contribution became more apparent and dominant. Bidentate complexes are mostly responsible for the obtained adsorption energies in case of single exchanged zeolites. The order of affinity followed the Pearson Hard and Soft Acids and Bases theory (HSAB) order, the adsorption being the strongest with the hardest cation Ca^{2+} . For zeolites LSX, coordination to multiple cations contributed to the found free energies of adsorption. The distance between cations was the defining parameter in the latter system, which is close to the experimental structure (Si/Al = 1 close to Si/Al = 1.2 of zeolites X). NaLSX and KLSX presented ions in site III. The distance between a cation in site II and site III was about 5 Å, this proximity gave the most stable structures compared to zeolites LSX exchanged with divalent ions. The average distances between larger cations like Ba^{2+} was found smaller in the zeolite than for smaller divalent cations (10.9 Å between two Ca^{2+} ions vs. 9.8 Å between two Ba^{2+}). The adsorption of glucose and xylose tautomers in BaLSX gave surprisingly high free energies of adsorption, competing and very close to the stable structures found in NaLSX and KLSX, although the number of cations in the cell was significantly lower (12 barium in the primitive cell and 24 sodium or potassium). The identified adsorption modes gave satisfactory explanations to the adsorption behavior and interactions strength of sugars with different cations in zeolites X, regardless of the solvent-zeolite interactions and the hydration of the monosaccharides. A good agreement between experimental affinities with zeolites X and theoretical results with zeolites LSX was found, glucose and xylose affinity increased with the ionic radii of monovalent or bivalent cations.

Overall, the adsorption DFT study of glucose and xylose tautomers in several zeolites' models showed that adsorption free energies of glucose were stronger than the energies of xylose. This did not allow for explaining the experimental selectivities, BaX for instance was selective towards xylose. The attempt to incorporate water effect and reproduce a displacement did not

as well capture the experimental trends. *Ab initio* calculations did elucidate the specific interactions between sugars and the compensating ions of the zeolitic framework. This represented the electrostatic component of the adsorption system that reflects the enthalpic contribution. Nevertheless, the employed level of theory was not successful to describe well the cooperative effect between solvent and solute molecules on the adsorption, and thus the entropic contribution.

In order to get closer to the experimental system and complement the DFT study, GCMC simulations were performed to study the adsorption in presence of water in Chapter VII. This study was focused on the adsorption of glucose and xylose β -pyranose forms in BaLSX. At very low coverage and without water (conditions close to the DFT study), strong isosteric heats of adsorption were obtained in the same order of magnitude as the DFT values. Although the GCMC values were weaker than DFT values due to a lack of quality of force field parametrization, similar trends were captured where glucose heat of adsorption was higher than xylose. At high loadings, BaLSX showed the ability to accommodate more xylose molecules than glucose. This was consistent with the experimental observations from the single adsorption isotherms in presence of ethanol, higher saturation value of xylose was obtained compared to glucose. Saturation values found from simulations were higher than the experimental ones, the differences could most probably be related to the space occupied by the solvents. The competitive adsorption of the two sugars in presence of water showed that the computed selectivity values were in good agreement with the experimental ones. At very low loadings, glucose was preferably adsorbed which reminds the DFT results performed with one molecule. As the loading increased, the zeolite became selective to xylose.

The results provided in this work allowed to propose the following general considerations. For the separation of glucose and xylose at an industrial scale, the design of an adsorption process is founded on three parameters: the working capacity, the selectivity and the operating conditions of the process. This PhD project showed that the capacity can be controlled through the cationic distribution, the large size of cations and their proximity favors strong sugar-zeolite interactions and therefore high loadings. This was the case for KX, the presence of cations in site III gave the highest uptakes for both sugars. The capacity is controlled by the solvent as well, the addition of ethanol increased the adsorbed amount. Similarly, the selectivity could be tailored by changing the cationic distribution and the solvent, which are the two defining parameters to optimize this separation. When water is used as a solvent, a reduced number (bivalent cations) and big size cations are preferred to obtain high selectivities which is the case

for BaX and BaY. The solvent choice is important and drives the selectivity, the presence of ethanol in the feed rendered CaX and SrX selective to xylose despite they were non selective when sugars are dissolved in water.

Perspectives

Since the chemical composition is one of the key factors for the separation, it would be interesting to perform an exchange with different cations. Exchanging NaX with simultaneously potassium and barium could enhance the selectivity especially by adding cations in site III. Larger cations like cesium could be considered as well. In the same direction, we tested ethanol as a cosolvent in this study, other solvents could give useful results. Longer alcohols like propanol for example could be interesting (although it is known that the solvation of sugars is more difficult in higher alcohols). Besides, other zeolites with different structural properties than faujasites could be considered; mordenite for example which has a pore channel size of $6.5 \times 7.0 \text{ \AA}$ seems like a good candidate.

Additional work should be devoted to improve the simulations performed up to this point. The use of explicit and implicit solvation models in the DFT study could improve the description of the theoretical system. The electrostatic component has a large contribution in the zeolite-sugar interaction, force-field parameters; in particular the partial charges could be improved. These not only will allow to understand the mechanism of adsorption, but to better predict the experimental results. Partial charges could be extracted from the established DFT study. After reevaluation of the force field parameters, the method could be extended to other zeolites models like KLSX for example. The development of simulations with cosolvents like ethanol is highly recommended to understand the adsorption behavior in presence of different types of solvents. The calculation of the radial distribution functions (RDFs) between the sugars and zeolites will help to gain more insights into the adsorption mechanism.

Finally, let us remind that the work presented in this thesis was exclusively dedicated to the thermodynamic part of the adsorption process, since only data at equilibrium were used, both experimentally and computationally. Mass transfer is also an important component for the design of a separation application. Breakthrough experiments could be more exploited to determine diffusion coefficients in the fix bed.

Appendix

1. Processed Raman spectra

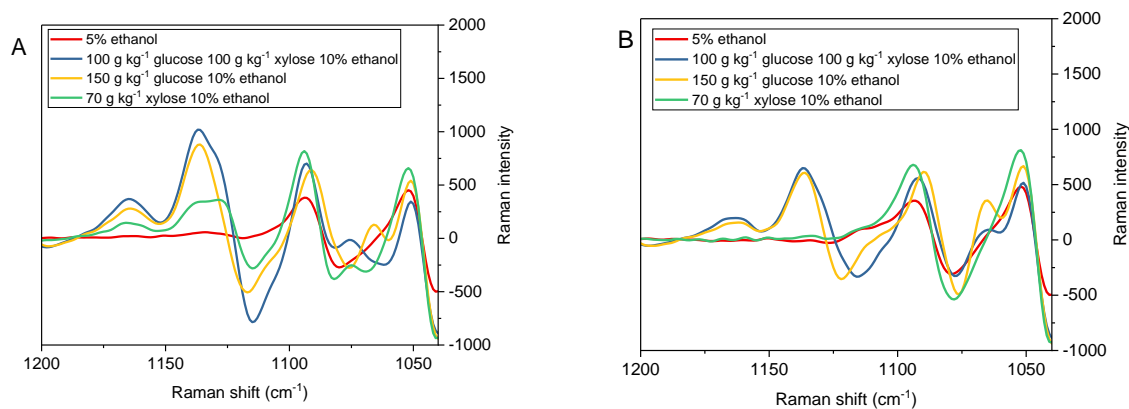


Figure A 1: Spectral subtraction effect on univariate modeling to isolate glucose peak ($1115\text{--}1215\text{ cm}^{-1}$) in presence of ethanol. (A) spectra with first derivative and without subtraction of the spectrum of 100 g kg^{-1} xylose aqueous solution, the model has a correlation coefficient (R^2) of 0.976 and a calibration error RMSEC of 47.1866 g kg^{-1} (B) spectra with first derivative and subtraction of the spectrum of 100 g kg^{-1} xylose aqueous solution, the model has a correlation coefficient (R^2) of 0.989 and a calibration error RMSEC of 2.4774 g kg^{-1}

2. X-ray diffraction analysis

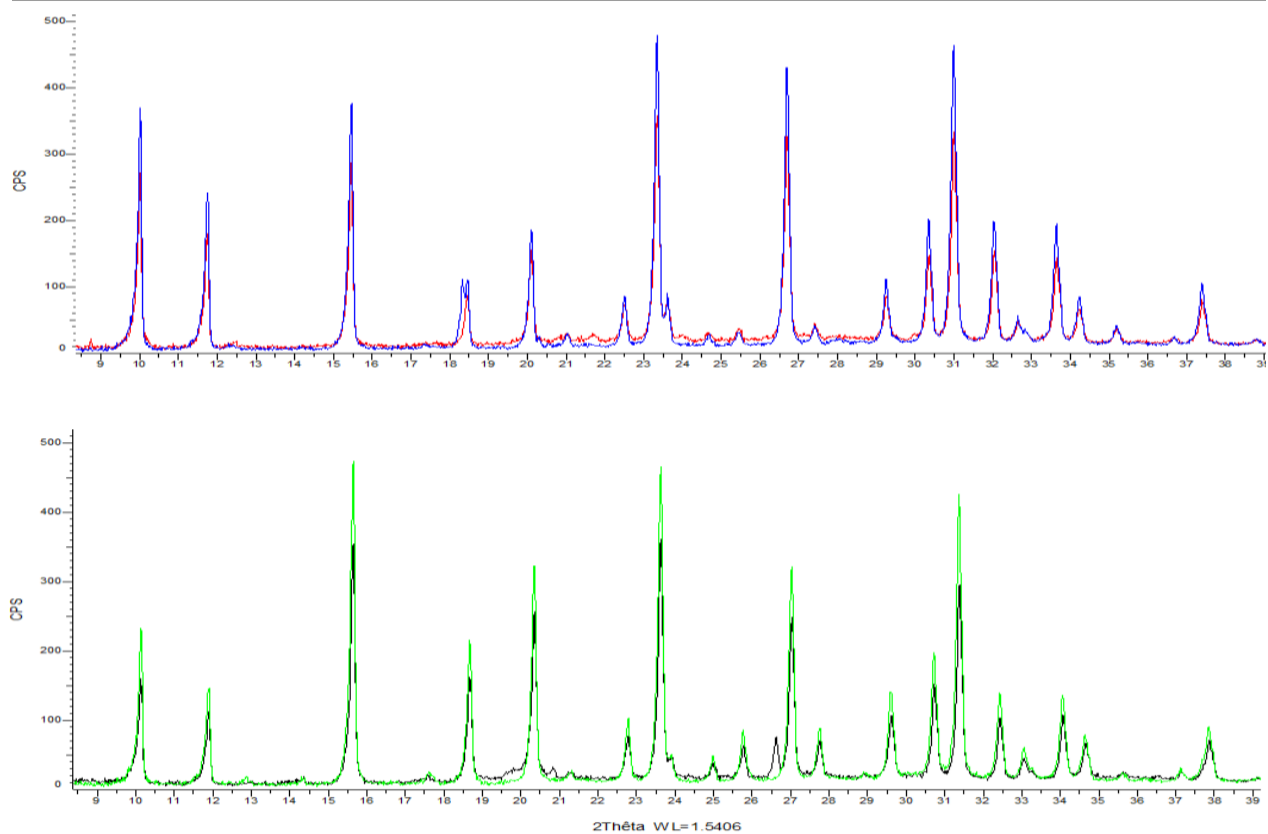


Figure A 2: diffractograms of shaped NaX (red), reference binderless NaX (blue), shaped NaY (black) and reference binderless NaY (green)

3. Textural properties

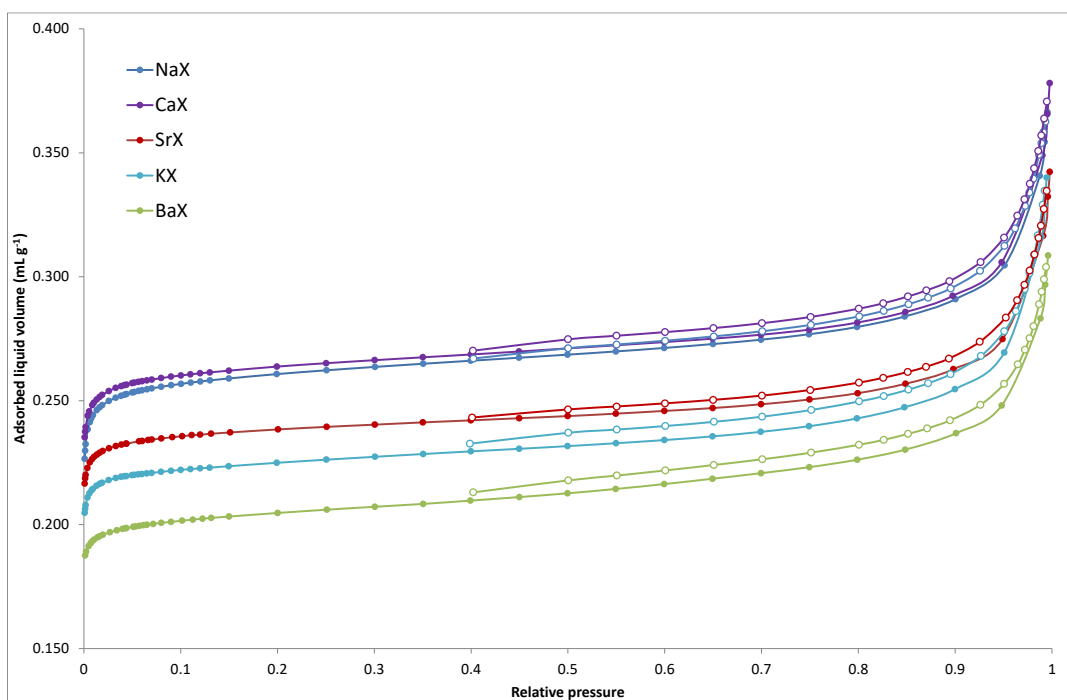


Figure A 3: N_2 adsorption isotherms of zeolites X (Full points: adsorption, empty points: desorption)

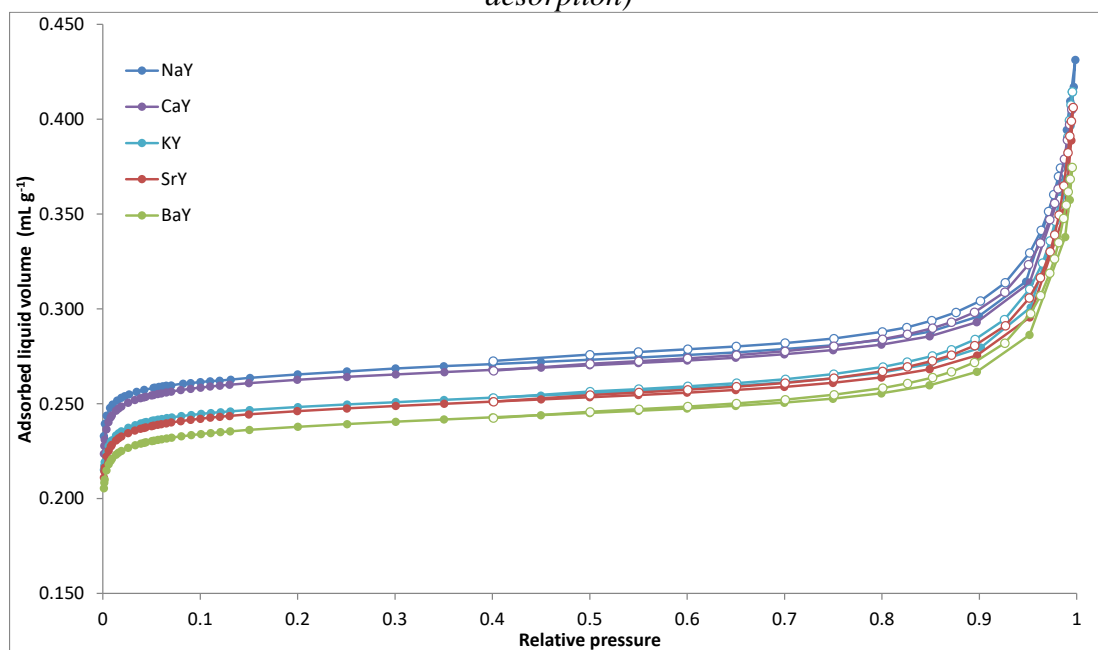


Figure A 4: N_2 adsorption isotherms of zeolites Y (Full points: adsorption, empty points: desorption)

Table A 1: Textural properties of exchanged zeolites X and Y

Zeolite	N ₂ physisorption		Mercury intrusion	
	S _{BET} (m ² g ⁻¹)	V _{micro} (cm ³ g ⁻¹)	V _{meso} (cm ³ g ⁻¹)	V _{macro} (cm ³ g ⁻¹)
NaX	688	0.260	0.05	0.29
KX	597	0.224	0.05	0.28
CaX	699	0.260	0.05	0.28
SrX	635	0.236	0.04	0.25
BaX	541	0.203	0.05	0.24
NaY	701	0.265	0.06	0.32
KY	654	0.248	0.06	0.32
CaY	690	0.262	0.06	0.33
SrY	646	0.245	0.05	0.31
BaY	625	0.237	0.05	0.29

4. Breakthrough curves

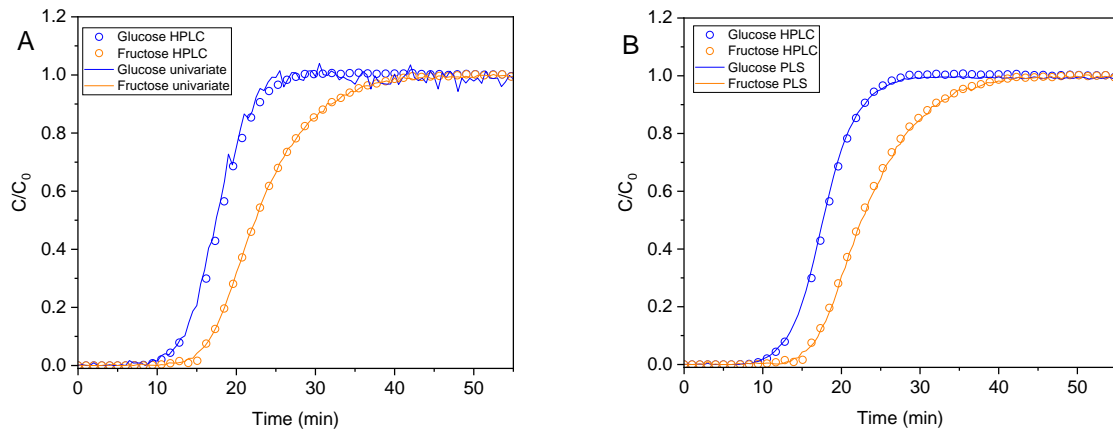


Figure A 5: Breakthrough curves predictions of an aqueous solution of 100 g kg^{-1} glucose and 100 g kg^{-1} fructose in a CaY zeolite with (A) univariate models and (B) PLS models

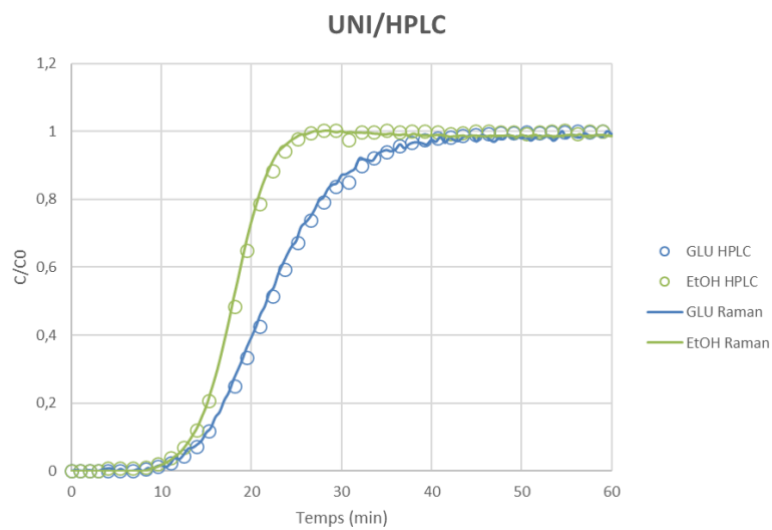


Figure A 6: Breakthrough curves recorded with Raman spectroscopy and HPLC of a feed mixture of 100 g kg^{-1} glucose and 5 % (%wt) ethanol in a BaY at $30 \text{ }^\circ\text{C}$ with a flow rate of 0.5 mL min^{-1}

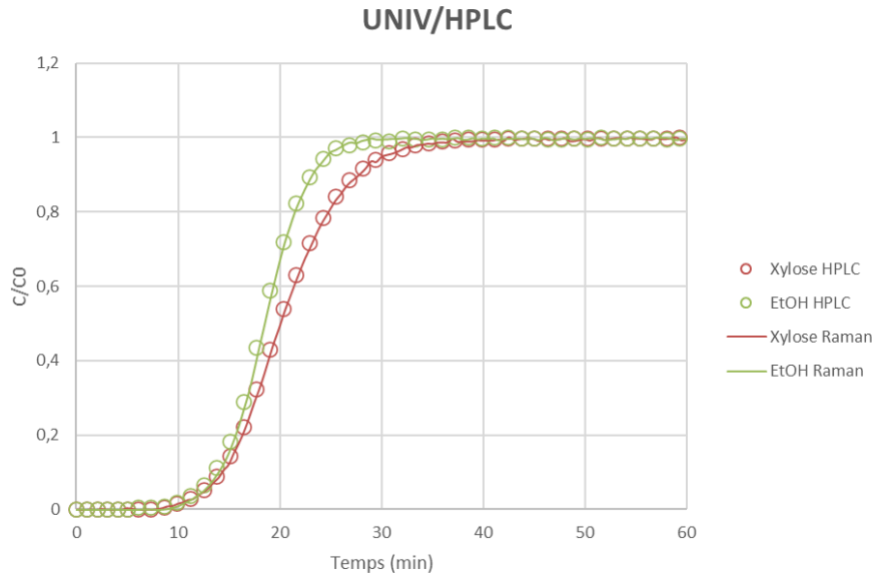


Figure A 7: Breakthrough curves recorded with Raman spectroscopy and HPLC of a feed mixture of 100 g kg^{-1} xylose and 5 % (%wt) ethanol in a BaY at $30 \text{ }^\circ\text{C}$ with a flow rate of 0.5 mL min^{-1}

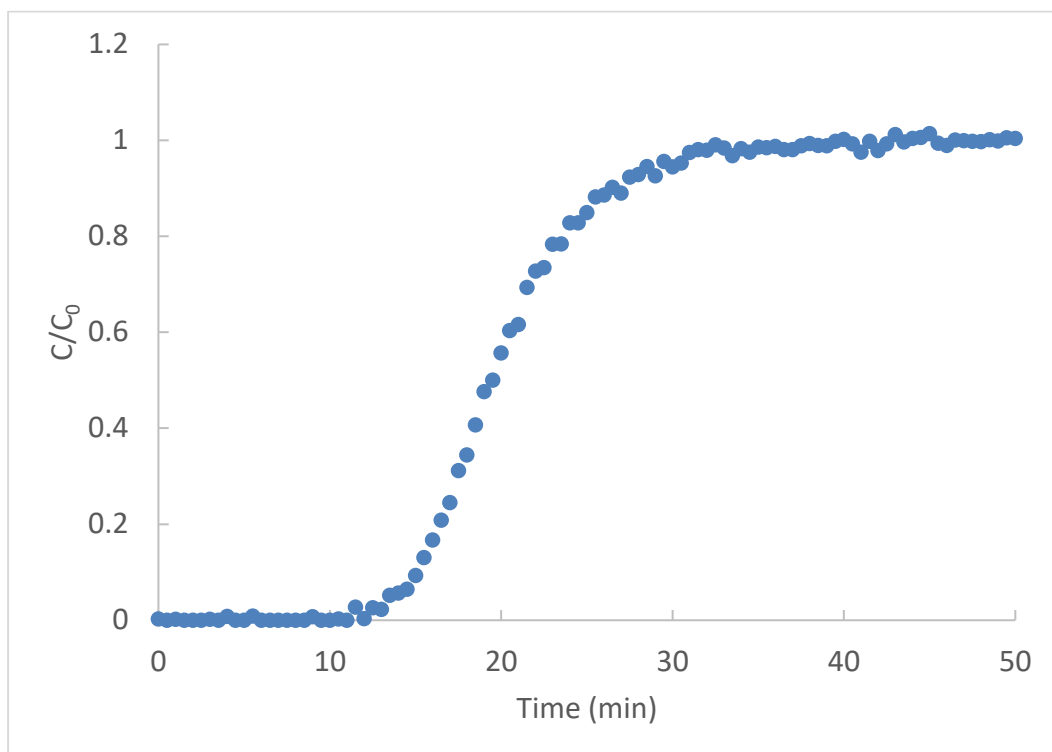


Figure A 8: Breakthrough curve of 100 g kg^{-1} glucose in a BaX at $30 \text{ }^\circ\text{C}$ with a flow rate of 0.5 mL min^{-1}

5. Determination of the Sanderson's intermediate electronegativity

The intermediate electronegativity of Sanderson is calculated thanks to the following equation:

$$S_{int} = \left(\prod_i S_i^{n_i} \right)^{1/\sum n_i}$$

where S_i is the Sanderson's electronegativity of the atom and n_i is the stoichiometry of the atom in a unit cell of zeolite.¹⁴⁰

Table A 2: Structural properties and intermediate electronegativities of the exchanged zeolites

Zeolite	Chemical formula	S_{int}
NaX	43.4 (Al ₂ O ₃) 105.1 (SiO ₂) 43.4 Na ₂ O	2.377
KX	43.4 (Al ₂ O ₃) 105.1 (SiO ₂) 40.8 K ₂ O 2.6 Na ₂ O	2.311
CaX	43.4 (Al ₂ O ₃) 105.1 (SiO ₂) 38.6 CaO 4.8 Na ₂ O	2.691
SrX	43.4 (Al ₂ O ₃) 105.1 (SiO ₂) 39.9 SrO 3.5 Na ₂ O	2.649
BaX	43.4 (Al ₂ O ₃) 105.1 (SiO ₂) 39.5 BaO 3.9 Na ₂ O	2.627
NaY	26.7(Al ₂ O ₃) 138.7 (SiO ₂) 26.7 Na ₂ O	2.597
KY	26.7(Al ₂ O ₃) 138.7 (SiO ₂) 25.6 K ₂ O 1.1 Na ₂ O	2.549
CaY	26.7(Al ₂ O ₃) 138.7 (SiO ₂) 19.2 CaO 7.5 Na ₂ O	2.771
SrY	26.7 (Al ₂ O ₃) 138.7 (SiO ₂) 19.8 SrO 6.9 Na ₂ O	2.753
BaY	26.7 (Al ₂ O ₃) 138.7 (SiO ₂) 15.5 BaO 11.2 Na ₂ O	2.710

6. Henry's constants

Table A 3: Henry's constants ($\text{molecule.L.SP}^{-1}.\text{mol}^{-1}$)

zeolite	K_{Xylose}		K_{Glucose}	
	X	Y	X	Y
Na	0.58	0.11	0.64	0.14
K	1.14	0.46	1.02	0.43
Ca	0.21	0.39	0.22	0.36
Sr	0.28	0.36	0.28	0.39
Ba	0.76	0.50	0.52	0.68

SP: supercage

7. Adsorption isotherms

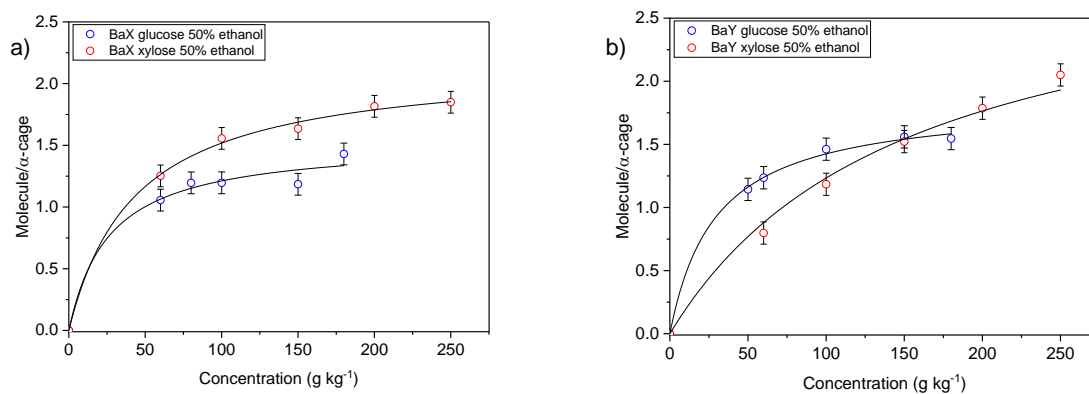


Figure A 9: glucose and xylose single adsorption isotherms with 50% wt ethanol in a) BaX and b) BaY

8. Liquid NMR spectra

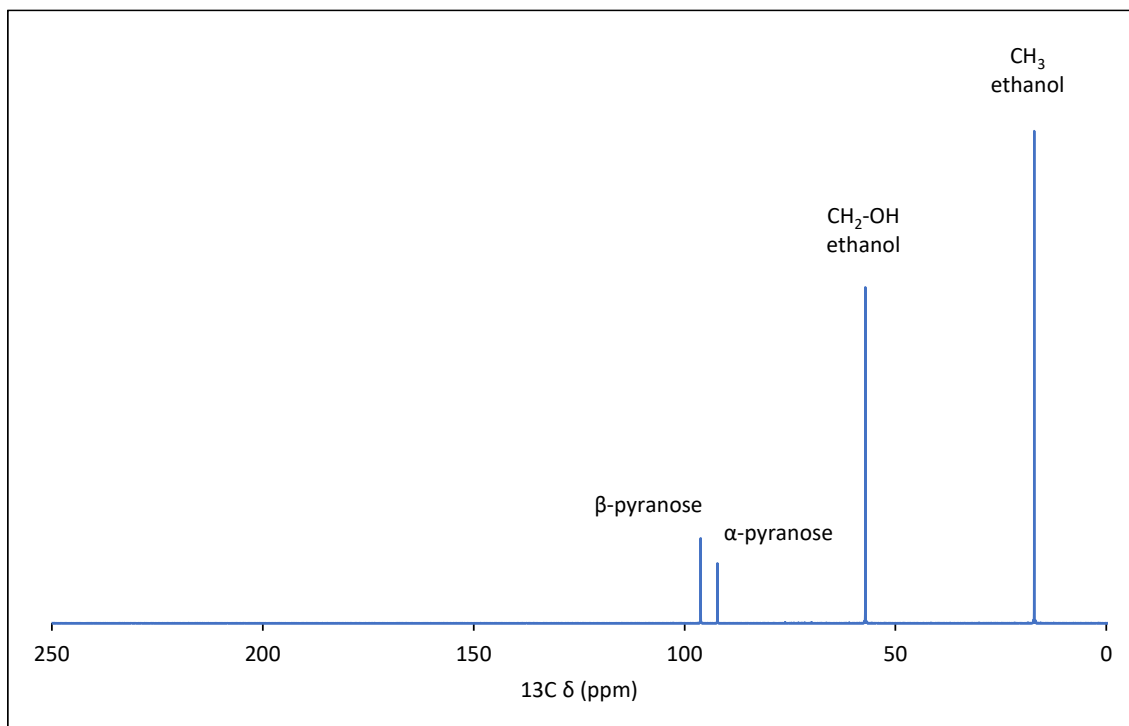


Figure A 10: Liquid Carbon NMR spectra of labelled C1-glucose dissolved in 50:50 %wt D_2O and ethanol at 25 °C

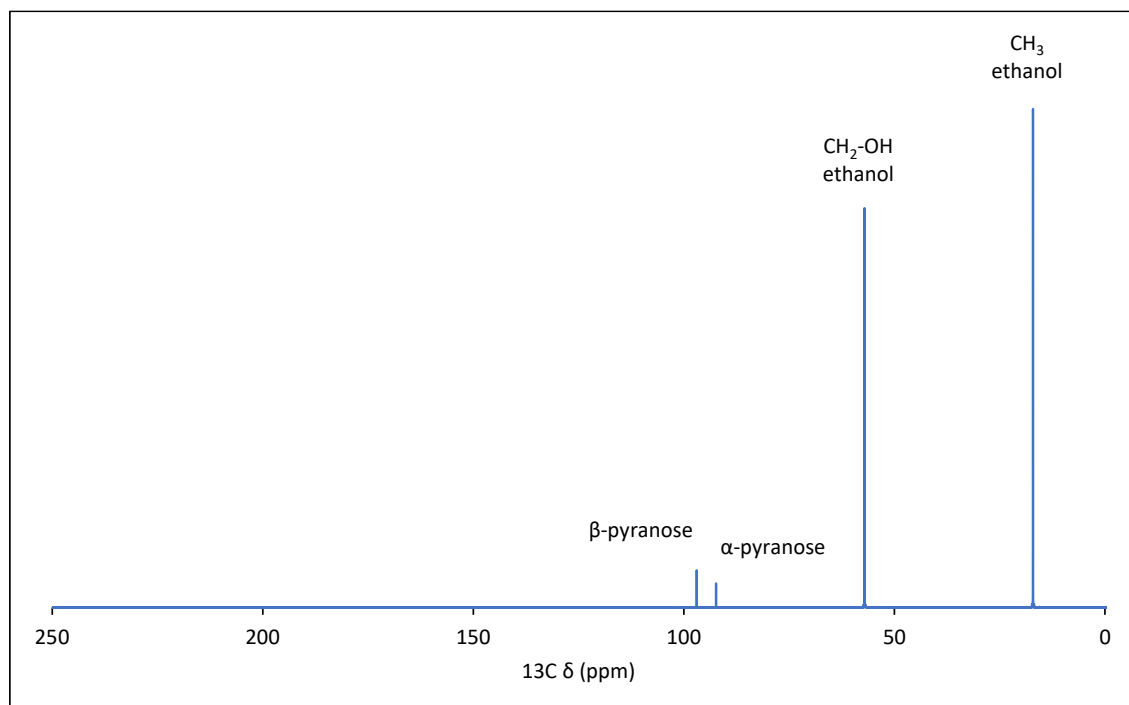


Figure A 11: Liquid Carbon NMR spectra of labelled C1-xylose dissolved in 50:50 %wt D_2O and ethanol at 25 °C

9. Adsorption and dispersion energies

Table A 4: Adsorption energies (E_{ads}) and dispersion contributions (E_{disp}) of glucose tautomers in NaFA, KFAU ($Si/Al = 47$) and CaFAU, SrFAU and BaFAU ($Si/Al = 23$)

Tautomer	Na		K	
	E_{ads} (kJ/mol)	E_{disp} (kJ/mol)	E_{ads} (kJ/mol)	E_{disp} (kJ/mol)
Linear	-113	-77	-65	-57
α -furanose	-155	-86	-123	-77
β -furanose	-158	-83	-113	-72
α -pyranose	-159	-84	-142	-73
β -pyranose	-164	-92	-150	-77

Tautomer	Ca		Sr		Ba	
	E_{ads} (kJ/mol)	E_{disp} (kJ/mol)	E_{ads} (kJ/mol)	E_{disp} (kJ/mol)	E_{ads} (kJ/mol)	E_{disp} (kJ/mol)
Linear	-192	-70	-182	-73	-185	-82
α -furanose	-215	-80	-190	-59	-199	-86
β -furanose	-219	-77	-217	-76	-199	-80
α -pyranose	-217	-68	-208	-78	-204	-76
β -pyranose	-214	-70	-208	-74	-211	-92

Table A 5: Adsorption energies (E_{ads}) and dispersion contributions (E_{VdW}) of xylose tautomers in NaFA, KFAU ($Si/Al = 47$) and CaFAU, SrFAU and BaFAU ($Si/Al = 23$)

tautomer	Na		K	
	E_{ads} (kJ/mol)	E_{disp} (kJ/mol)	E_{ads} (kJ/mol)	E_{disp} (kJ/mol)
Linear	-114	-72	-80	-55.0
α -furanose	-136	-66	-108	-61
β -furanose	-128	-59	-97	-58
α -pyranose	-160	-72	-132	-72
β -pyranose	-159	-77	-134	-69

tautomer	Ca		Sr		Ba	
	E_{ads} (kJ/mol)	E_{disp} (kJ/mol)	E_{ads} (kJ/mol)	E_{disp} (kJ/mol)	E_{ads} (kJ/mol)	E_{disp} (kJ/mol)
Linear	-184	-66	-172	-75	-151	-74
α -furanose	-194	-60	-206	-64	-194	-61
β -furanose	-183	-57	-205	-67	-158	-54
α -pyranose	-212	-68	-200	-66	-192	-75
β -pyranose	-207	-67	-205	-67	-191	-71

Table A 6: Adsorption energies (E_{ads}) and dispersion contributions (E_{VdW}) of glucose tautomers in zeolites LSX

tautomer	Na		K	
	E_{ads} (kJ/mol)	E_{disp} (kJ/mol)	E_{ads} (kJ/mol)	E_{disp} (kJ/mol)
Linear	-266	-102	-228	-110
α -furanose	-300	-90	-315	-108
β -furanose	-304	-92	-328	-109
α -pyranose	-331	-112	-336	-107
β -pyranose	-313	-111	-351	-105

tautomer	CaLSX		SrLSX		BaLSX	
	E_{ads} (kJ/mol)	E_{disp} (kJ/mol)	E_{ads} (kJ/mol)	E_{disp} (kJ/mol)	E_{ads} (kJ/mol)	E_{disp} (kJ/mol)
Linear	-257	-88	-240	-84	-221	-112
α -furanose	-274	-80	-263	-89	-269	-97
β -furanose	-258	-85	-259	-92	-281	-102
α -pyranose	-281	-84	-265	-92	-297	-105
β -pyranose	-283	-89	-268	-80	-309	-129

Table A 7: Adsorption energies (E_{ads}) and dispersion contributions (E_{VdW}) of xylose tautomers in zeolites LSX

tautomer	Na		K	
	E_{ads} (kJ/mol)	E_{disp} (kJ/mol)	E_{ads} (kJ/mol)	E_{disp} (kJ/mol)
Linear	-217	-76	-211	-91
α -furanose	-204	-67	-256	-75
β -furanose	-202	-73	-287	-85
α -pyranose	-268	-76	-251	-84
β -pyranose	-292	-94	-272	-77

tautomer	CaLSX		SrLSX		BaLSX	
	E_{ads} (kJ/mol)	E_{disp} (kJ/mol)	E_{ads} (kJ/mol)	E_{disp} (kJ/mol)	E_{ads} (kJ/mol)	E_{disp} (kJ/mol)
Linear	-205	-65	-183	-61	-194	-76
α -furanose	-207	-66	-214	-65	-239	-111
β -furanose	-212	-66	-216	-79	-241	-106
α -pyranose	-191	-68	-219	-88	-255	-97
β -pyranose	-213	-77	-219	-77	-252	-95

10. Most stable configurations

Table A 8: Adsorption modes of most stable configurations of glucose tautomers in NaFA, KFAU (Si/Al = 47) and CaFAU, SrFAU and BaFAU (Si/Al = 23)

	Linear	α -furanose	β -furanose	α -pyranose	β -pyranose
Na					
K					

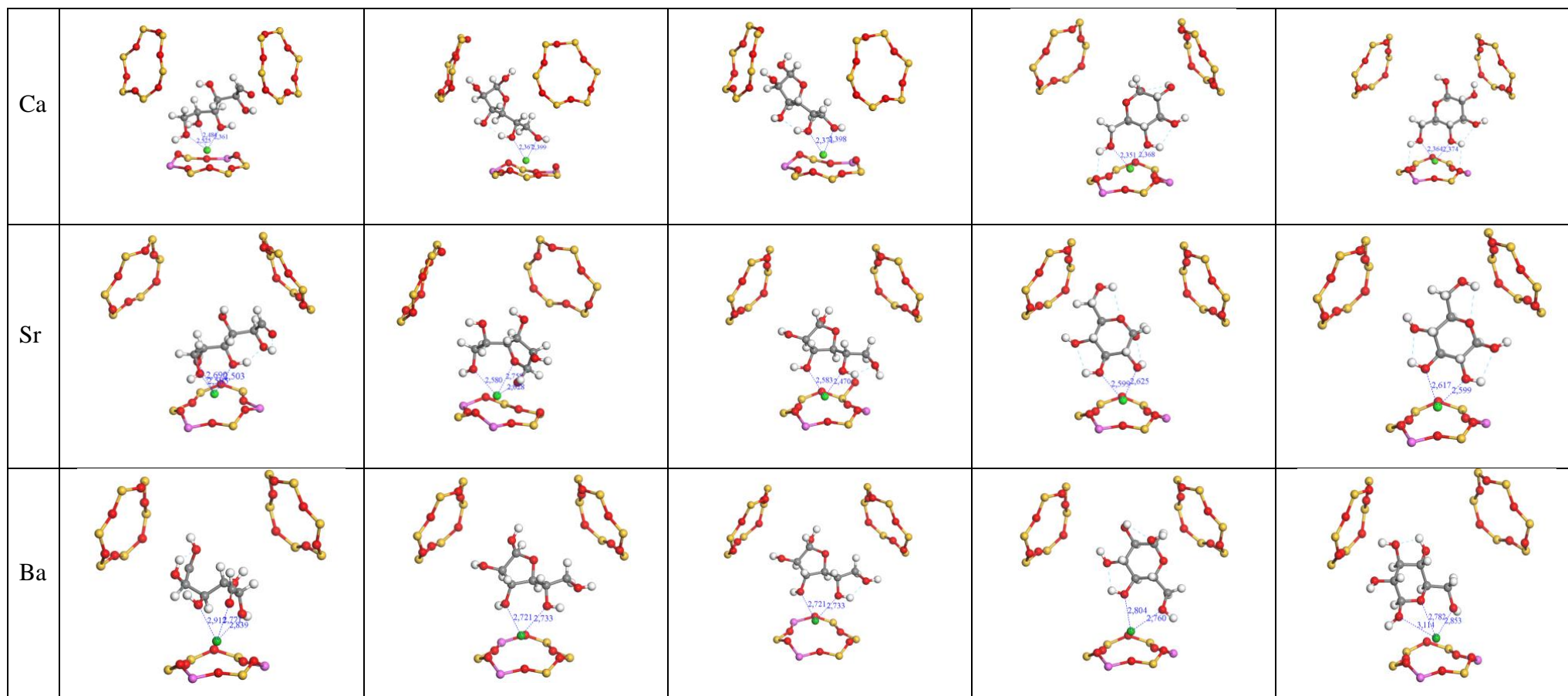
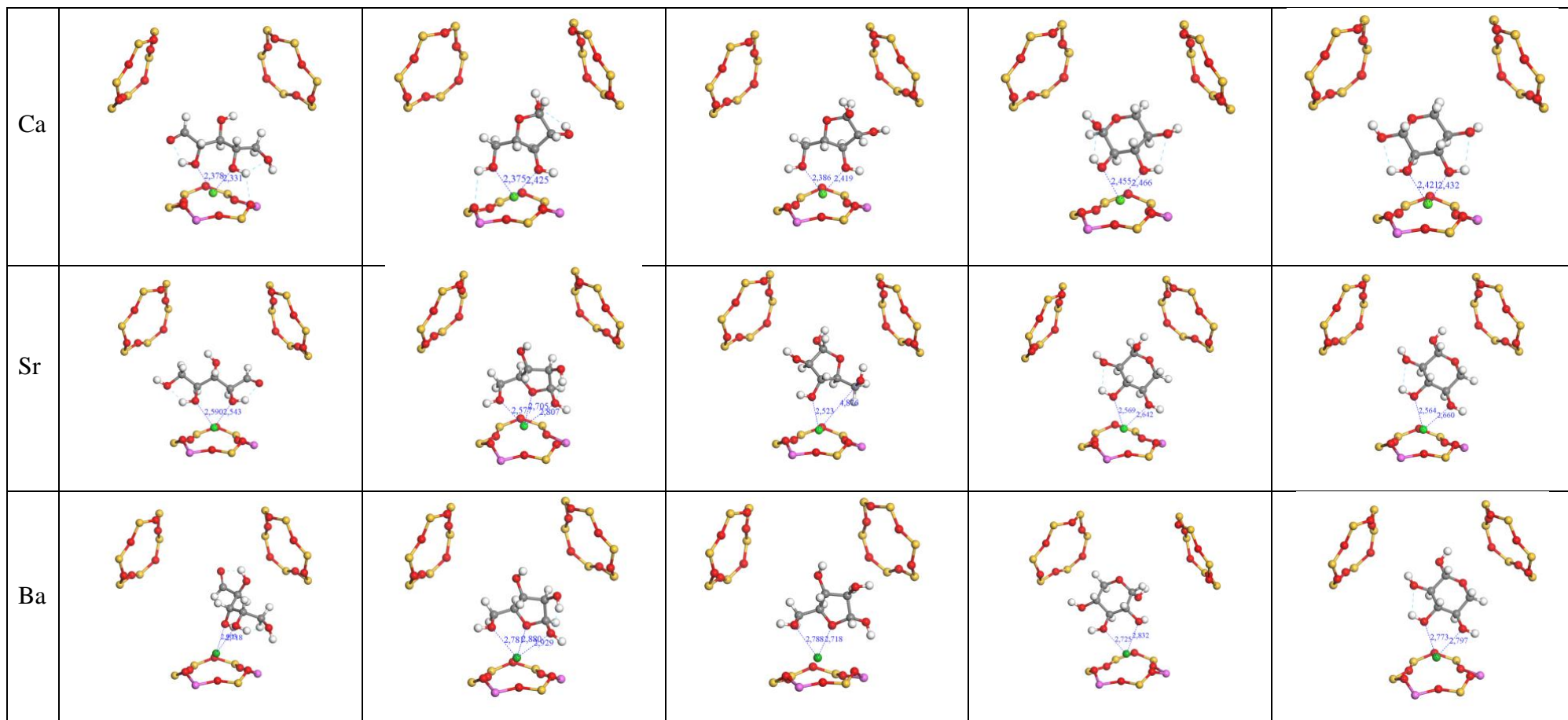


Table A9: Adsorption modes of most stable configurations of xylose tautomers in NaFA, KFAU (Si/Al = 47) and CaFAU, SrFAU and BaFAU (Si/Al = 23)

	Linear	α -furanose	β -furanose	α -pyranose	β -pyranose
Na					
K					



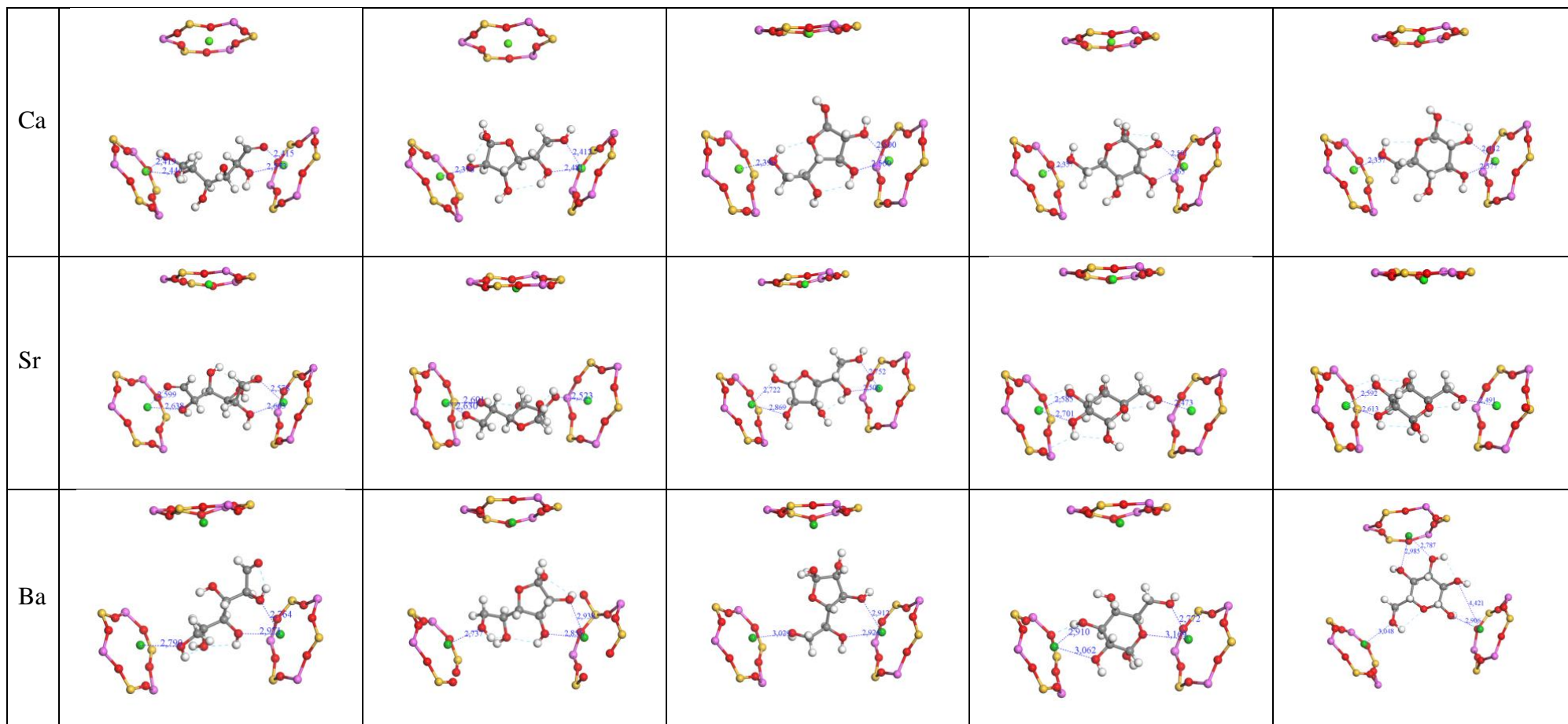
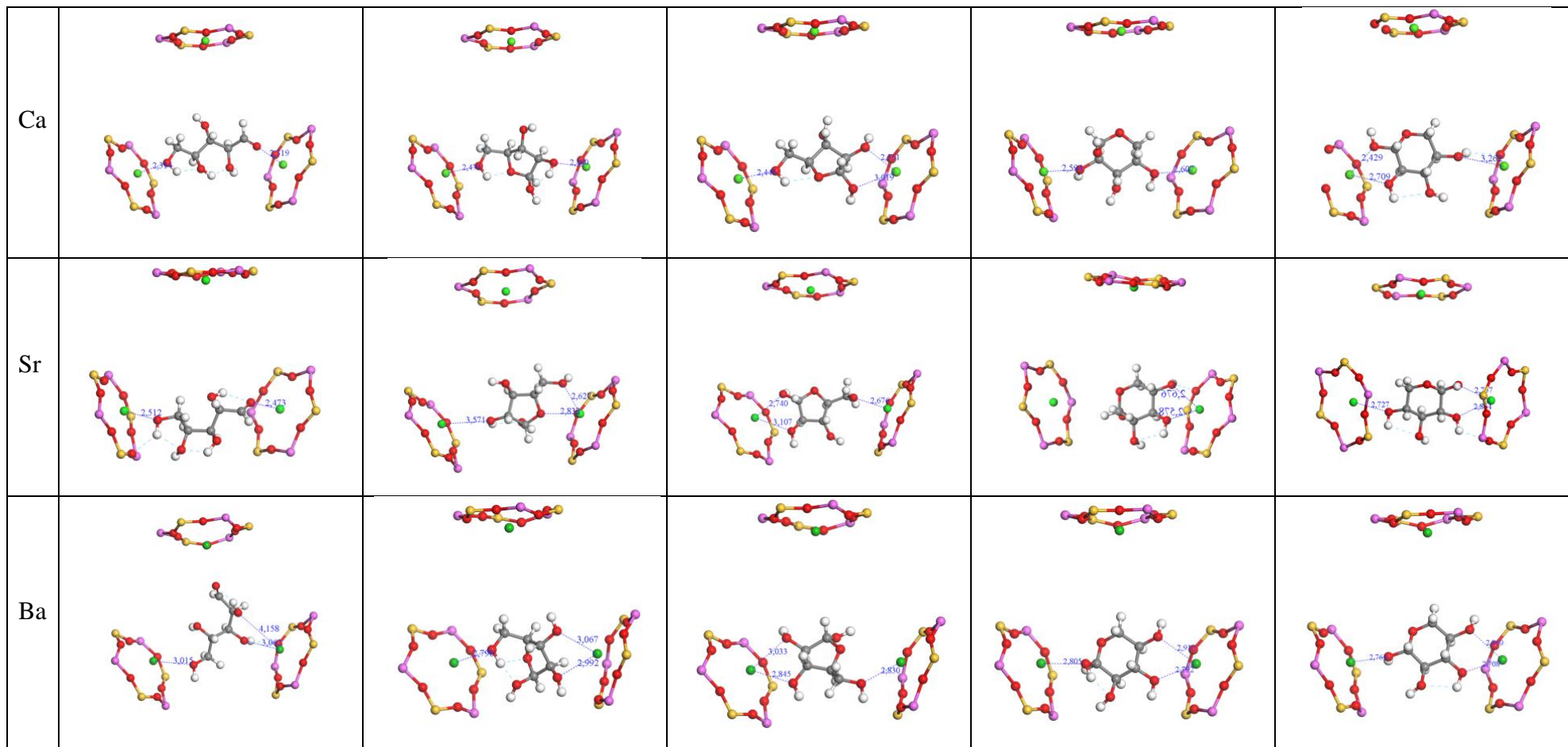


Table A11: Adsorption modes of most stable configurations of xylose tautomers in zeolites LSX

	Linear	α -furanose	β -furanose	α -pyranose	β -pyranose
Na					
K					



11. Adsorption enthalpies, entropies and free energies

Table A12: Adsorption thermodynamic parameters of glucose in NaLSX at 300 K

T(K)	β -pyranose			α -pyranose			β -furanose			α -furanose			Linear		
	$\Delta_r H_{ads}$ (kJ/mol)	$\Delta_r S_{ads}$ (kJ/K/mol)	$\Delta_r G_{ads}$ (kJ/mol)	$\Delta_r H_{ads}$ (kJ/mol)	$\Delta_r S_{ads}$ (kJ/K/mol)	$\Delta_r G_{ads}$ (kJ/mol)	$\Delta_r H_{ads}$ (kJ/mol)	$\Delta_r S_{ads}$ (kJ/K/mol)	$\Delta_r G_{ads}$ (kJ/mol)	$\Delta_r H_{ads}$ (kJ/mol)	$\Delta_r S_{ads}$ (kJ/K/mol)	$\Delta_r G_{ads}$ (kJ/mol)	$\Delta_r H_{ads}$ (kJ/mol)	$\Delta_r S_{ads}$ (kJ/K/mol)	$\Delta_r G_{ads}$ (kJ/mol)
275	-305	-0.247	-237	-323	-0.255	-253	-298	-0.237	-233	-292	-0.236	-227	-263	-0.233	-199
298.15	-305	-0.247	-231	-323	-0.255	-247	-298	-0.237	-227	-292	-0.236	-221	-263	-0.233	-194
300	-305	-0.247	-231	-323	-0.255	-247	-298	-0.237	-227	-292	-0.236	-221	-263	-0.233	-193
325	-305	-0.247	-224	-323	-0.256	-240	-298	-0.237	-221	-292	-0.237	-215	-263	-0.232	-187
350	-304	-0.247	-218	-323	-0.256	-233	-298	-0.237	-214	-292	-0.237	-209	-262	-0.232	-181
375	-304	-0.247	-211	-323	-0.256	-227	-297	-0.237	-208	-292	-0.237	-203	-262	-0.231	-175

Table A13: Adsorption thermodynamic parameters of xylose in NaLSX at 300 K

T(K)	β -pyranose			α -pyranose			β -furanose			α -furanose			Linear		
	$\Delta_r H_{ads}$ (kJ/mol)	$\Delta_r S_{ads}$ (kJ/K/mol)	$\Delta_r G_{ads}$ (kJ/mol)	$\Delta_r H_{ads}$ (kJ/mol)	$\Delta_r S_{ads}$ (kJ/K/mol)	$\Delta_r G_{ads}$ (kJ/mol)	$\Delta_r H_{ads}$ (kJ/mol)	$\Delta_r S_{ads}$ (kJ/K/mol)	$\Delta_r G_{ads}$ (kJ/mol)	$\Delta_r H_{ads}$ (kJ/mol)	$\Delta_r S_{ads}$ (kJ/K/mol)	$\Delta_r G_{ads}$ (kJ/mol)	$\Delta_r H_{ads}$ (kJ/mol)	$\Delta_r S_{ads}$ (kJ/K/mol)	$\Delta_r G_{ads}$ (kJ/mol)
275	-285	-0.237	-220	-258	-0.240	-192	-195	-0.214	-137	-196	-0.201	-141	-215	-0.222	-154
298.15	-285	-0.237	-214	-258	-0.240	-187	-195	-0.213	-131	-196	-0.201	-136	-215	-0.222	-149
300	-285	-0.237	-214	-258	-0.240	-186	-195	-0.213	-131	-196	-0.201	-136	-215	-0.222	-149
325	-285	-0.237	-208	-258	-0.240	-180	-195	-0.213	-126	-196	-0.200	-131	-215	-0.221	-143
350	-284	-0.237	-202	-258	-0.241	-174	-194	-0.212	-120	-195	-0.200	-125	-214	-0.220	-137
375	-284	-0.237	-195	-258	-0.241	-167	-194	-0.212	-114	-195	-0.200	-120	-214	-0.220	-131

Table A14: Adsorption thermodynamic parameters of glucose in KaLSX at 300 K

T(K)	β -pyranose			α -pyranose			β -furanose			α -furanose			Linear		
	$\Delta_r H_{ads}$ (kJ/mol)	$\Delta_r S_{ads}$ (kJ/K/mol)	$\Delta_r G_{ads}$ (kJ/mol)	$\Delta_r H_{ads}$ (kJ/mol)	$\Delta_r S_{ads}$ (kJ/K/mol)	$\Delta_r G_{ads}$ (kJ/mol)	$\Delta_r H_{ads}$ (kJ/mol)	$\Delta_r S_{ads}$ (kJ/K/mol)	$\Delta_r G_{ads}$ (kJ/mol)	$\Delta_r H_{ads}$ (kJ/mol)	$\Delta_r S_{ads}$ (kJ/K/mol)	$\Delta_r G_{ads}$ (kJ/mol)	$\Delta_r H_{ads}$ (kJ/mol)	$\Delta_r S_{ads}$ (kJ/K/mol)	$\Delta_r G_{ads}$ (kJ/mol)
275	-349	-0.273	-274	-333	-0.235	-269	-297	-0.228	-234	-310	-0.221	-249	-227	-0.222	-166
298.15	-349	-0.273	-268	-333	-0.235	-263	-296	-0.228	-228	-310	-0.221	-244	-226	-0.222	-160
300	-349	-0.273	-267	-333	-0.235	-263	-296	-0.228	-228	-310	-0.221	-243	-226	-0.221	-160
325	-349	-0.273	-260	-333	-0.235	-257	-296	-0.229	-222	-309	-0.221	-237	-226	-0.221	-154
350	-349	-0.273	-253	-333	-0.235	-251	-296	-0.229	-216	-309	-0.222	-232	-225	-0.220	-148
375	-348	-0.273	-246	-333	-0.235	-245	-296	-0.229	-210	-309	-0.222	-226	-225	-0.219	-143

Table A15: Adsorption thermodynamic parameters of xylose in KaLSX at 300 K

T(K)	β -pyranose			α -pyranose			β -furanose			α -furanose			Linear		
	$\Delta_r H_{ads}$ (kJ/mol)	$\Delta_r S_{ads}$ (kJ/K/mol)	$\Delta_r G_{ads}$ (kJ/mol)	$\Delta_r H_{ads}$ (kJ/mol)	$\Delta_r S_{ads}$ (kJ/K/mol)	$\Delta_r G_{ads}$ (kJ/mol)	$\Delta_r H_{ads}$ (kJ/mol)	$\Delta_r S_{ads}$ (kJ/K/mol)	$\Delta_r G_{ads}$ (kJ/mol)	$\Delta_r H_{ads}$ (kJ/mol)	$\Delta_r S_{ads}$ (kJ/K/mol)	$\Delta_r G_{ads}$ (kJ/mol)	$\Delta_r H_{ads}$ (kJ/mol)	$\Delta_r S_{ads}$ (kJ/K/mol)	$\Delta_r G_{ads}$ (kJ/mol)
275	-255	-0.207	-198	-246	-0.217	-187	-284	-0.226	-221	-256	-0.215	-196	-213	-0.222	-152
298.15	-255	-0.207	-193	-246	-0.217	-181	-283	-0.226	-216	-255	-0.215	-191	-213	-0.221	-147
300	-255	-0.207	-193	-246	-0.217	-181	-283	-0.226	-216	-255	-0.215	-191	-213	-0.221	-147
325	-254	-0.207	-187	-246	-0.217	-175	-283	-0.226	-210	-255	-0.215	-185	-212	-0.220	-141
350	-254	-0.206	-182	-246	-0.217	-170	-283	-0.226	-204	-255	-0.215	-180	-212	-0.220	-135
375	-254	-0.206	-176	-245	-0.217	-164	-283	-0.225	-198	-254	-0.215	-174	-211	-0.219	-129

Table A16: Adsorption thermodynamic parameters of glucose in CaLSX at 300 K

T(K)	β -pyranose			α -pyranose			β -furanose			α -furanose			Linear		
	$\Delta_r H_{ads}$ (kJ/mol)	$\Delta_r S_{ads}$ (kJ/K/mol)	$\Delta_r G_{ads}$ (kJ/mol)	$\Delta_r H_{ads}$ (kJ/mol)	$\Delta_r S_{ads}$ (kJ/K/mol)	$\Delta_r G_{ads}$ (kJ/mol)	$\Delta_r H_{ads}$ (kJ/mol)	$\Delta_r S_{ads}$ (kJ/K/mol)	$\Delta_r G_{ads}$ (kJ/mol)	$\Delta_r H_{ads}$ (kJ/mol)	$\Delta_r S_{ads}$ (kJ/K/mol)	$\Delta_r G_{ads}$ (kJ/mol)	$\Delta_r H_{ads}$ (kJ/mol)	$\Delta_r S_{ads}$ (kJ/K/mol)	$\Delta_r G_{ads}$ (kJ/mol)
275	-279	-0.226	-216	-276	-0.228	-213	-256	-0.220	-195	-270	-0.211	-212	-259	-0.220	-199
298.15	-278	-0.225	-211	-275	-0.227	-208	-255	-0.219	-190	-270	-0.210	-207	-259	-0.219	-193
300	-278	-0.225	-211	-275	-0.227	-207	-255	-0.219	-190	-270	-0.210	-207	-259	-0.219	-193
325	-278	-0.224	-205	-275	-0.226	-201	-255	-0.218	-184	-269	-0.209	-202	-258	-0.217	-187
350	-277	-0.223	-199	-274	-0.225	-195	-254	-0.216	-178	-269	-0.207	-196	-257	-0.216	-182
375	-276	-0.222	-193	-274	-0.224	-190	-253	-0.215	-173	-268	-0.206	-191	-256	-0.214	-176

Table A17: Adsorption thermodynamic parameters of xylose in CaLSX at 300 K

T(K)	β -pyranose			α -pyranose			β -furanose			α -furanose			Linear		
	$\Delta_r H_{ads}$ (kJ/mol)	$\Delta_r S_{ads}$ (kJ/K/mol)	$\Delta_r G_{ads}$ (kJ/mol)	$\Delta_r H_{ads}$ (kJ/mol)	$\Delta_r S_{ads}$ (kJ/K/mol)	$\Delta_r G_{ads}$ (kJ/mol)	$\Delta_r H_{ads}$ (kJ/mol)	$\Delta_r S_{ads}$ (kJ/K/mol)	$\Delta_r G_{ads}$ (kJ/mol)	$\Delta_r H_{ads}$ (kJ/mol)	$\Delta_r S_{ads}$ (kJ/K/mol)	$\Delta_r G_{ads}$ (kJ/mol)	$\Delta_r H_{ads}$ (kJ/mol)	$\Delta_r S_{ads}$ (kJ/K/mol)	$\Delta_r G_{ads}$ (kJ/mol)
275	-209	-0.208	-152	-187	-0.214	-128	-208	-0.194	-155	-212	-0.198	-158	-204	-0.185	-153
298.15	-209	-0.207	-147	-186	-0.212	-123	-208	-0.192	-151	-212	-0.197	-153	-203	-0.184	-149
300	-208	-0.207	-146	-186	-0.212	-122	-208	-0.192	-150	-211	-0.197	-152	-203	-0.184	-148
325	-208	-0.205	-141	-185	-0.211	-117	-207	-0.191	-145	-211	-0.196	-147	-203	-0.182	-143
350	-207	-0.204	-136	-185	-0.210	-111	-207	-0.190	-140	-210	-0.195	-142	-202	-0.181	-139
375	-207	-0.203	-130	-184	-0.209	-106	-206	-0.189	-135	-210	-0.194	-137	-201	-0.180	-134

Table A18: Adsorption thermodynamic parameters of glucose in SrLSX at 300 K

T(K)	β -pyranose			α -pyranose			β -furanose			α -furanose			Linear		
	$\Delta_r H_{ads}$ (kJ/mol)	$\Delta_r S_{ads}$ (kJ/K/mol)	$\Delta_r G_{ads}$ (kJ/mol)	$\Delta_r H_{ads}$ (kJ/mol)	$\Delta_r S_{ads}$ (kJ/K/mol)	$\Delta_r G_{ads}$ (kJ/mol)	$\Delta_r H_{ads}$ (kJ/mol)	$\Delta_r S_{ads}$ (kJ/K/mol)	$\Delta_r G_{ads}$ (kJ/mol)	$\Delta_r H_{ads}$ (kJ/mol)	$\Delta_r S_{ads}$ (kJ/K/mol)	$\Delta_r G_{ads}$ (kJ/mol)	$\Delta_r H_{ads}$ (kJ/mol)	$\Delta_r S_{ads}$ (kJ/K/mol)	$\Delta_r G_{ads}$ (kJ/mol)
275	-301	-0.235	-237	-289	-0.238	-223	-275	-0.241	-208	-262	-0.233	-198	-219	-0.248	-151
298.15	-301	-0.234	-231	-288	-0.238	-218	-274	-0.240	-203	-261	-0.232	-192	-218	-0.247	-145
300	-301	-0.234	-231	-288	-0.238	-217	-274	-0.240	-202	-261	-0.232	-192	-218	-0.247	-144
325	-300	-0.233	-225	-288	-0.237	-211	-274	-0.240	-196	-261	-0.231	-186	-218	-0.247	-138
350	-300	-0.233	-218	-288	-0.236	-205	-274	-0.239	-190	-261	-0.231	-180	-217	-0.246	-131
375	-299	-0.232	-212	-287	-0.236	-199	-273	-0.239	-184	-260	-0.230	-174	-217	-0.245	-125

Table A19: Adsorption thermodynamic parameters of xylose in SrLSX at 300 K

T(K)	β -pyranose			α -pyranose			β -furanose			α -furanose			Linear		
	$\Delta_r H_{ads}$ (kJ/mol)	$\Delta_r S_{ads}$ (kJ/K/mol)	$\Delta_r G_{ads}$ (kJ/mol)	$\Delta_r H_{ads}$ (kJ/mol)	$\Delta_r S_{ads}$ (kJ/K/mol)	$\Delta_r G_{ads}$ (kJ/mol)	$\Delta_r H_{ads}$ (kJ/mol)	$\Delta_r S_{ads}$ (kJ/K/mol)	$\Delta_r G_{ads}$ (kJ/mol)	$\Delta_r H_{ads}$ (kJ/mol)	$\Delta_r S_{ads}$ (kJ/K/mol)	$\Delta_r G_{ads}$ (kJ/mol)	$\Delta_r H_{ads}$ (kJ/mol)	$\Delta_r S_{ads}$ (kJ/K/mol)	$\Delta_r G_{ads}$ (kJ/mol)
275	-212	-0.216	-153	-210	-0.236	-145	-209	-0.221	-148	-207	-0.219	-147	-179	-0.205	-123
298.15	-212	-0.215	-148	-210	-0.235	-139	-209	-0.221	-143	-207	-0.218	-142	-179	-0.204	-118
300	-212	-0.215	-147	-209	-0.235	-139	-209	-0.221	-142	-207	-0.218	-141	-179	-0.204	-117
325	-211	-0.214	-142	-209	-0.235	-133	-208	-0.220	-137	-206	-0.218	-136	-178	-0.203	-112
350	-211	-0.214	-136	-209	-0.235	-127	-208	-0.219	-131	-206	-0.217	-130	-177	-0.201	-107
375	-210	-0.213	-130	-208	-0.234	-121	-207	-0.218	-125	-206	-0.216	-124	-177	-0.200	-102

Table A20: Adsorption thermodynamic parameters of glucose in BaLSX at 300 K

	β -pyranose			α -pyranose			β -furanose			α -furanose			Linear		
T(K)	$\Delta_r H_{ads}$ (kJ/mol)	$\Delta_r S_{ads}$ (kJ/K/mol)	$\Delta_r G_{ads}$ (kJ/mol)	$\Delta_r H_{ads}$ (kJ/mol)	$\Delta_r S_{ads}$ (kJ/K/mol)	$\Delta_r G_{ads}$ (kJ/mol)	$\Delta_r H_{ads}$ (kJ/mol)	$\Delta_r S_{ads}$ (kJ/K/mol)	$\Delta_r G_{ads}$ (kJ/mol)	$\Delta_r H_{ads}$ (kJ/mol)	$\Delta_r S_{ads}$ (kJ/K/mol)	$\Delta_r G_{ads}$ (kJ/mol)	$\Delta_r H_{ads}$ (kJ/mol)	$\Delta_r S_{ads}$ (kJ/K/mol)	$\Delta_r G_{ads}$ (kJ/mol)
275	-306	-0.193	-252	-291	-0.202	-235	-279	-0.200	-224	-264	-0.227	-201	-221	-0.183	-170
298.15	-305	-0.192	-248	-290	-0.201	-230	-278	-0.199	-219	-263	-0.227	-196	-220	-0.182	-166
300	-305	-0.192	-247	-290	-0.201	-230	-278	-0.199	-218	-263	-0.227	-195	-220	-0.182	-165
325	-304	-0.191	-242	-290	-0.200	-225	-278	-0.198	-213	-263	-0.227	-190	-219	-0.180	-161
350	-304	-0.190	-237	-289	-0.200	-220	-277	-0.197	-208	-263	-0.226	-184	-219	-0.179	-156
375	-303	-0.189	-232	-289	-0.199	-214	-277	-0.196	-203	-263	-0.226	-178	-218	-0.178	-151

Table A21: Adsorption thermodynamic parameters of xylose in BaLSX at 300 K

	β -pyranose			α -pyranose			β -furanose			α -furanose			Linear		
T(K)	$\Delta_r H_{ads}$ (kJ/mol)	$\Delta_r S_{ads}$ (kJ/K/mol)	$\Delta_r G_{ads}$ (kJ/mol)	$\Delta_r H_{ads}$ (kJ/mol)	$\Delta_r S_{ads}$ (kJ/K/mol)	$\Delta_r G_{ads}$ (kJ/mol)	$\Delta_r H_{ads}$ (kJ/mol)	$\Delta_r S_{ads}$ (kJ/K/mol)	$\Delta_r G_{ads}$ (kJ/mol)	$\Delta_r H_{ads}$ (kJ/mol)	$\Delta_r S_{ads}$ (kJ/K/mol)	$\Delta_r G_{ads}$ (kJ/mol)	$\Delta_r H_{ads}$ (kJ/mol)	$\Delta_r S_{ads}$ (kJ/K/mol)	$\Delta_r G_{ads}$ (kJ/mol)
275	-246	-0.228	-183	-248	-0.217	-189	-236	-0.195	-182	-233	-0.204	-176	-196	-0.147	-156
298.15	-246	-0.228	-178	-248	-0.217	-184	-235	-0.194	-177	-232	-0.204	-171	-195	-0.144	-152
300	-246	-0.228	-177	-248	-0.217	-183	-235	-0.194	-177	-232	-0.204	-171	-195	-0.144	-152
325	-245	-0.227	-171	-248	-0.217	-177	-235	-0.193	-172	-232	-0.204	-166	-194	-0.142	-148
350	-245	-0.227	-166	-247	-0.216	-172	-234	-0.192	-167	-232	-0.203	-161	-193	-0.140	-144
375	-245	-0.226	-160	-247	-0.216	-166	-234	-0.191	-162	-231	-0.203	-155	-192	-0.138	-141

Table A22: Adsorption thermodynamic parameters of glucose in NaFAU at 300 K

	β -pyranose			α -pyranose			β -furanose			α -furanose			Linear		
T(K)	$\Delta_r H_{ads}$ (kJ/mol)	$\Delta_r S_{ads}$ (kJ/K/mol)	$\Delta_r G_{ads}$ (kJ/mol)	$\Delta_r H_{ads}$ (kJ/mol)	$\Delta_r S_{ads}$ (kJ/K/mol)	$\Delta_r G_{ads}$ (kJ/mol)	$\Delta_r H_{ads}$ (kJ/mol)	$\Delta_r S_{ads}$ (kJ/K/mol)	$\Delta_r G_{ads}$ (kJ/mol)	$\Delta_r H_{ads}$ (kJ/mol)	$\Delta_r S_{ads}$ (kJ/K/mol)	$\Delta_r G_{ads}$ (kJ/mol)	$\Delta_r H_{ads}$ (kJ/mol)	$\Delta_r S_{ads}$ (kJ/K/mol)	$\Delta_r G_{ads}$ (kJ/mol)
275	-158	-0.229	-95	-152	-0.222	-91	-152	-0.204	-96	-149	-0.207	-92	-112	-0.196	-58
298.15	-157	-0.228	-89	-152	-0.221	-86	-152	-0.203	-91	-148	-0.206	-87	-111	-0.194	-53
300	-157	-0.227	-89	-152	-0.221	-86	-151	-0.203	-91	-148	-0.206	-86	-111	-0.194	-53
325	-157	-0.226	-83	-151	-0.220	-80	-151	-0.202	-85	-147	-0.205	-81	-110	-0.192	-48
350	-156	-0.225	-77	-151	-0.219	-74	-150	-0.201	-80	-147	-0.204	-76	-109	-0.191	-43
375	-156	-0.224	-71	-150	-0.218	-68	-150	-0.200	-75	-146	-0.203	-70	-109	-0.190	-38

Table A23: Adsorption thermodynamic parameters of xylose in NaFAU at 300 K

	β -pyranose			α -pyranose			β -furanose			α -furanose			Linear		
T(K)	$\Delta_r H_{ads}$ (kJ/mol)	$\Delta_r S_{ads}$ (kJ/K/mol)	$\Delta_r G_{ads}$ (kJ/mol)	$\Delta_r H_{ads}$ (kJ/mol)	$\Delta_r S_{ads}$ (kJ/K/mol)	$\Delta_r G_{ads}$ (kJ/mol)	$\Delta_r H_{ads}$ (kJ/mol)	$\Delta_r S_{ads}$ (kJ/K/mol)	$\Delta_r G_{ads}$ (kJ/mol)	$\Delta_r H_{ads}$ (kJ/mol)	$\Delta_r S_{ads}$ (kJ/K/mol)	$\Delta_r G_{ads}$ (kJ/mol)	$\Delta_r H_{ads}$ (kJ/mol)	$\Delta_r S_{ads}$ (kJ/K/mol)	$\Delta_r G_{ads}$ (kJ/mol)
275	-151	-0.220	-91	-151	-0.213	-93	-121	-0.185	-70	-130	-0.207	-73	-112	-0.184	-62
298.15	-151	-0.219	-86	-151	-0.212	-87	-121	-0.184	-66	-129	-0.206	-68	-112	-0.183	-57
300	-151	-0.219	-85	-151	-0.212	-87	-121	-0.184	-65	-129	-0.206	-67	-112	-0.183	-57
325	-150	-0.218	-80	-150	-0.211	-82	-120	-0.183	-61	-129	-0.204	-62	-111	-0.181	-52
350	-150	-0.217	-74	-150	-0.211	-76	-119	-0.182	-56	-128	-0.203	-57	-110	-0.179	-47
375	-149	-0.216	-68	-149	-0.210	-71	-119	-0.180	-51	-127	-0.202	-52	-110	-0.178	-43

Table A24: Adsorption thermodynamic parameters of glucose in KFAU at 300 K

	β -pyranose			α -pyranose			β -furanose			α -furanose			Linear		
T(K)	$\Delta_r H_{ads}$ (kJ/mol)	$\Delta_r S_{ads}$ (kJ/K/mol)	$\Delta_r G_{ads}$ (kJ/mol)	$\Delta_r H_{ads}$ (kJ/mol)	$\Delta_r S_{ads}$ (kJ/K/mol)	$\Delta_r G_{ads}$ (kJ/mol)	$\Delta_r H_{ads}$ (kJ/mol)	$\Delta_r S_{ads}$ (kJ/K/mol)	$\Delta_r G_{ads}$ (kJ/mol)	$\Delta_r H_{ads}$ (kJ/mol)	$\Delta_r S_{ads}$ (kJ/K/mol)	$\Delta_r G_{ads}$ (kJ/mol)	$\Delta_r H_{ads}$ (kJ/mol)	$\Delta_r S_{ads}$ (kJ/K/mol)	$\Delta_r G_{ads}$ (kJ/mol)
275	-144	-0.184	-94	-136	-0.183	-86	-107	-0.176	-59	-118	-0.199	-63	-64	-0.171	-17
298.15	-144	-0.182	-89	-135	-0.181	-81	-107	-0.174	-55	-117	-0.198	-58	-63	-0.169	-12
300	-144	-0.182	-89	-135	-0.181	-81	-107	-0.174	-54	-117	-0.198	-58	-63	-0.169	-12
325	-143	-0.181	-84	-135	-0.180	-76	-106	-0.173	-50	-117	-0.197	-53	-62	-0.167	-8
350	-143	-0.180	-80	-134	-0.179	-72	-105	-0.171	-45	-116	-0.196	-48	-61	-0.166	-3
375	-142	-0.178	-75	-133	-0.177	-67	-105	-0.170	-41	-116	-0.195	-43	-61	-0.164	1

Table A25: Adsorption thermodynamic parameters of xylose in KFAU at 300 K

	β -pyranose			α -pyranose			β -furanose			α -furanose			Linear		
T(K)	$\Delta_r H_{ads}$ (kJ/mol)	$\Delta_r S_{ads}$ (kJ/K/mol)	$\Delta_r G_{ads}$ (kJ/mol)	$\Delta_r H_{ads}$ (kJ/mol)	$\Delta_r S_{ads}$ (kJ/K/mol)	$\Delta_r G_{ads}$ (kJ/mol)	$\Delta_r H_{ads}$ (kJ/mol)	$\Delta_r S_{ads}$ (kJ/K/mol)	$\Delta_r G_{ads}$ (kJ/mol)	$\Delta_r H_{ads}$ (kJ/mol)	$\Delta_r S_{ads}$ (kJ/K/mol)	$\Delta_r G_{ads}$ (kJ/mol)	$\Delta_r H_{ads}$ (kJ/mol)	$\Delta_r S_{ads}$ (kJ/K/mol)	$\Delta_r G_{ads}$ (kJ/mol)
275	-128	-0.186	-76	-122	-0.198	-67	-91	-0.173	-43	-101	-0.177	-52	-78	-0.158	-34
298.15	-127	-0.185	-72	-121	-0.197	-63	-90	-0.172	-39	-100	-0.176	-48	-77	-0.156	-30
300	-127	-0.185	-72	-121	-0.197	-62	-90	-0.172	-38	-100	-0.176	-47	-77	-0.156	-30
325	-126	-0.184	-67	-121	-0.196	-57	-89	-0.171	-34	-99	-0.174	-43	-76	-0.154	-26
350	-126	-0.183	-62	-120	-0.195	-52	-89	-0.170	-29	-99	-0.173	-38	-75	-0.153	-22
375	-125	-0.182	-57	-120	-0.194	-47	-88	-0.168	-25	-98	-0.172	-34	-75	-0.151	-18

Table A26: Adsorption thermodynamic parameters of glucose in CaFAU at 300 K

T(K)	β -pyranose			α -pyranose			β -furanose			α -furanose			Linear		
	$\Delta_r H_{ads}$ (kJ/mol)	$\Delta_r S_{ads}$ (kJ/K/mol)	$\Delta_r G_{ads}$ (kJ/mol)	$\Delta_r H_{ads}$ (kJ/mol)	$\Delta_r S_{ads}$ (kJ/K/mol)	$\Delta_r G_{ads}$ (kJ/mol)	$\Delta_r H_{ads}$ (kJ/mol)	$\Delta_r S_{ads}$ (kJ/K/mol)	$\Delta_r G_{ads}$ (kJ/mol)	$\Delta_r H_{ads}$ (kJ/mol)	$\Delta_r S_{ads}$ (kJ/K/mol)	$\Delta_r G_{ads}$ (kJ/mol)	$\Delta_r H_{ads}$ (kJ/mol)	$\Delta_r S_{ads}$ (kJ/K/mol)	$\Delta_r G_{ads}$ (kJ/mol)
275	-209	-0.204	-153	-211	-0.205	-154	-215	-0.204	-159	-192	-0.209	-134	-192	-0.2	-138
298.15	-209	-0.202	-148	-210	-0.204	-149	-214	-0.203	-154	-191	-0.207	-129	-191	-0.2	-133
300	-209	-0.202	-148	-210	-0.203	-149	-214	-0.203	-153	-191	-0.207	-129	-191	-0.2	-133
325	-208	-0.201	-143	-210	-0.202	-144	-214	-0.201	-148	-191	-0.206	-124	-191	-0.2	-128
350	-207	-0.200	-137	-209	-0.201	-138	-213	-0.200	-143	-190	-0.205	-118	-190	-0.2	-123
375	-207	-0.199	-132	-208	-0.200	-133	-212	-0.199	-138	-190	-0.204	-113	-189	-0.2	-118

Table A27: Adsorption thermodynamic parameters of xylose in CaFAU at 300 K

T(K)	β -pyranose			α -pyranose			β -furanose			α -furanose			Linear		
	$\Delta_r H_{ads}$ (kJ/mol)	$\Delta_r S_{ads}$ (kJ/K/mol)	$\Delta_r G_{ads}$ (kJ/mol)	$\Delta_r H_{ads}$ (kJ/mol)	$\Delta_r S_{ads}$ (kJ/K/mol)	$\Delta_r G_{ads}$ (kJ/mol)	$\Delta_r H_{ads}$ (kJ/mol)	$\Delta_r S_{ads}$ (kJ/K/mol)	$\Delta_r G_{ads}$ (kJ/mol)	$\Delta_r H_{ads}$ (kJ/mol)	$\Delta_r S_{ads}$ (kJ/K/mol)	$\Delta_r G_{ads}$ (kJ/mol)	$\Delta_r H_{ads}$ (kJ/mol)	$\Delta_r S_{ads}$ (kJ/K/mol)	$\Delta_r G_{ads}$ (kJ/mol)
275	-201	-0.200	-146	-204	-0.215	-145	-177	-0.195	-124	-188	-0.194	-135	-183	-0.181	-134
298.15	-200	-0.199	-141	-204	-0.214	-140	-177	-0.194	-119	-188	-0.193	-130	-183	-0.179	-129
300	-200	-0.199	-140	-204	-0.214	-139	-177	-0.194	-118	-188	-0.193	-130	-183	-0.179	-129
325	-199	-0.198	-135	-203	-0.213	-134	-176	-0.192	-113	-187	-0.192	-125	-182	-0.178	-124
350	-199	-0.197	-130	-203	-0.212	-128	-175	-0.191	-108	-187	-0.191	-120	-181	-0.177	-120
375	-198	-0.196	-125	-202	-0.211	-123	-175	-0.190	-103	-186	-0.190	-115	-181	-0.176	-115

Table A28: Adsorption thermodynamic parameters of glucose in SrFAU at 300 K

T(K)	β -pyranose			α -pyranose			β -furanose			α -furanose			Linear		
	$\Delta_r H_{ads}$ (kJ/mol)	$\Delta_r S_{ads}$ (kJ/K/mol)	$\Delta_r G_{ads}$ (kJ/mol)	$\Delta_r H_{ads}$ (kJ/mol)	$\Delta_r S_{ads}$ (kJ/K/mol)	$\Delta_r G_{ads}$ (kJ/mol)	$\Delta_r H_{ads}$ (kJ/mol)	$\Delta_r S_{ads}$ (kJ/K/mol)	$\Delta_r G_{ads}$ (kJ/mol)	$\Delta_r H_{ads}$ (kJ/mol)	$\Delta_r S_{ads}$ (kJ/K/mol)	$\Delta_r G_{ads}$ (kJ/mol)	$\Delta_r H_{ads}$ (kJ/mol)	$\Delta_r S_{ads}$ (kJ/K/mol)	$\Delta_r G_{ads}$ (kJ/mol)
275	-203	-0.210	-146	-201	-0.198	-147	-211	-0.208	-154	-186	-0.195	-133	-181	-0.179	-132
298.15	-203	-0.209	-141	-201	-0.197	-142	-211	-0.207	-149	-186	-0.194	-128	-181	-0.177	-128
300	-203	-0.209	-140	-201	-0.197	-141	-211	-0.207	-149	-186	-0.194	-128	-180	-0.177	-128
325	-202	-0.208	-135	-200	-0.196	-136	-211	-0.207	-144	-185	-0.193	-123	-180	-0.175	-123
350	-202	-0.207	-129	-199	-0.195	-131	-210	-0.206	-138	-185	-0.192	-118	-179	-0.173	-118
375	-201	-0.206	-124	-199	-0.194	-126	-210	-0.205	-133	-184	-0.191	-113	-178	-0.172	-114

Table A29: Adsorption thermodynamic parameters of xylose in SrFAU at 300 K

T(K)	β -pyranose			α -pyranose			β -furanose			α -furanose			Linear		
	$\Delta_r H_{ads}$ (kJ/mol)	$\Delta_r S_{ads}$ (kJ/K/mol)	$\Delta_r G_{ads}$ (kJ/mol)	$\Delta_r H_{ads}$ (kJ/mol)	$\Delta_r S_{ads}$ (kJ/K/mol)	$\Delta_r G_{ads}$ (kJ/mol)	$\Delta_r H_{ads}$ (kJ/mol)	$\Delta_r S_{ads}$ (kJ/K/mol)	$\Delta_r G_{ads}$ (kJ/mol)	$\Delta_r H_{ads}$ (kJ/mol)	$\Delta_r S_{ads}$ (kJ/K/mol)	$\Delta_r G_{ads}$ (kJ/mol)	$\Delta_r H_{ads}$ (kJ/mol)	$\Delta_r S_{ads}$ (kJ/K/mol)	$\Delta_r G_{ads}$ (kJ/mol)
275	-198	-0.215	-139	-192	-0.215	-133	-200	-0.161	-155	-200	-0.201	-145	-170	-0.167	-124
298.15	-198	-0.214	-134	-192	-0.214	-128	-199	-0.160	-151	-200	-0.200	-140	-169	-0.166	-120
300	-198	-0.214	-134	-192	-0.214	-127	-199	-0.160	-151	-199	-0.200	-140	-169	-0.165	-120
325	-197	-0.213	-128	-191	-0.213	-122	-198	-0.158	-147	-199	-0.199	-134	-168	-0.164	-115
350	-197	-0.212	-122	-191	-0.212	-116	-198	-0.157	-143	-198	-0.198	-129	-168	-0.162	-111
375	-196	-0.212	-117	-190	-0.211	-111	-197	-0.156	-139	-198	-0.197	-124	-167	-0.161	-107

Table A30: Adsorption thermodynamic parameters of glucose in BaFAU at 300 K

	β -pyranose			α -pyranose			β -furanose			α -furanose			Linear		
T(K)	$\Delta_r H_{ads}$ (kJ/mol)	$\Delta_r S_{ads}$ (kJ/K/mol)	$\Delta_r G_{ads}$ (kJ/mol)	$\Delta_r H_{ads}$ (kJ/mol)	$\Delta_r S_{ads}$ (kJ/K/mol)	$\Delta_r G_{ads}$ (kJ/mol)	$\Delta_r H_{ads}$ (kJ/mol)	$\Delta_r S_{ads}$ (kJ/K/mol)	$\Delta_r G_{ads}$ (kJ/mol)	$\Delta_r H_{ads}$ (kJ/mol)	$\Delta_r S_{ads}$ (kJ/K/mol)	$\Delta_r G_{ads}$ (kJ/mol)	$\Delta_r H_{ads}$ (kJ/mol)	$\Delta_r S_{ads}$ (kJ/K/mol)	$\Delta_r G_{ads}$ (kJ/mol)
275	-205	-0.206	-148	-197	-0.206	-140	-193	-0.204	-137	-190	-0.231	-126	-184	-0.181	-134
298.15	-204	-0.205	-143	-196	-0.205	-135	-193	-0.203	-132	-190	-0.231	-121	-183	-0.180	-129
300	-204	-0.205	-143	-196	-0.205	-135	-193	-0.203	-132	-190	-0.231	-120	-183	-0.180	-129
325	-204	-0.204	-137	-196	-0.204	-130	-192	-0.202	-126	-189	-0.231	-114	-182	-0.178	-124
350	-203	-0.203	-132	-195	-0.203	-124	-192	-0.201	-121	-189	-0.230	-108	-182	-0.176	-120
375	-203	-0.202	-127	-195	-0.202	-119	-191	-0.200	-116	-189	-0.230	-102	-181	-0.175	-115

Table A31: Adsorption thermodynamic parameters of xylose in BaFAU at 300 K

	β -pyranose			α -pyranose			β -furanose			α -furanose			Linear		
T(K)	$\Delta_r H_{ads}$ (kJ/mol)	$\Delta_r S_{ads}$ (kJ/K/mol)	$\Delta_r G_{ads}$ (kJ/mol)	$\Delta_r H_{ads}$ (kJ/mol)	$\Delta_r S_{ads}$ (kJ/K/mol)	$\Delta_r G_{ads}$ (kJ/mol)	$\Delta_r H_{ads}$ (kJ/mol)	$\Delta_r S_{ads}$ (kJ/K/mol)	$\Delta_r G_{ads}$ (kJ/mol)	$\Delta_r H_{ads}$ (kJ/mol)	$\Delta_r S_{ads}$ (kJ/K/mol)	$\Delta_r G_{ads}$ (kJ/mol)	$\Delta_r H_{ads}$ (kJ/mol)	$\Delta_r S_{ads}$ (kJ/K/mol)	$\Delta_r G_{ads}$ (kJ/mol)
275	-183	-0.206	-127	-183	-0.201	-128	-151	-0.189	-99	-187	-0.194	-134	-149	-0.182	-99
298.15	-183	-0.205	-122	-183	-0.200	-123	-151	-0.188	-95	-187	-0.193	-129	-148	-0.181	-94
300	-183	-0.205	-121	-183	-0.200	-123	-151	-0.188	-94	-187	-0.193	-129	-148	-0.181	-94
325	-182	-0.204	-116	-182	-0.199	-118	-150	-0.187	-89	-186	-0.192	-124	-148	-0.179	-89
350	-182	-0.203	-111	-182	-0.198	-112	-150	-0.185	-85	-186	-0.191	-119	-147	-0.178	-85
375	-181	-0.202	-105	-181	-0.197	-107	-149	-0.184	-80	-185	-0.190	-114	-146	-0.177	-80

References

- (1) Chen, G.-Q.; Patel, M. K. *Chemical reviews* **2012**, *112*, 2082–2099.
- (2) Bozell, J. J.; Petersen, G. R. *Green Chem.* **2010**, *12*, 539.
- (3) Azadi, P.; Inderwildi, O. R.; Farnood, R.; King, D. A. *Renewable and Sustainable Energy Reviews* **2013**, *21*, 506–523.
- (4) Armaroli, N.; Balzani, V. *Angewandte Chemie (International ed. in English)* **2007**, *46*, 52–66.
- (5) Kamm, B. *Angewandte Chemie (International ed. in English)* **2007**, *46*, 5056–5058.
- (6) Li, Y.; Khanal, S. K. *Bioenergy: Principles and Applications*; Wiley, 2016.
- (7) Isikgor, F. H.; Becer, C. R. *Polym. Chem.* **2015**, *6*, 4497–4559.
- (8) Ho, C.; Ching, C. B.; Ruthven, M. D. *Ind. Eng. Chem. Res.* **1987**, *26*, 1407–1412.
- (9) Ching, C. B.; Ruthven, M. D. *ZEOLITES* **1988**, *8*, 68–73.
- (10) Ching, C. B.; Ho, C.; Hidajat, K.; Ruthven, M. D. *Chemical Engineering Science*, **1987**, *42*, 2547–2555.
- (11) Lei, H.; Bao, Z.; Xing, H.; Yang, Y.; Ren, Q.; Zhao, M.; Huang, H. *J. Chem. Eng. Data* **2010**, *55*, 735–738.
- (12) Saari, P.; Heikkilä, H.; Hurme, M. *J. Chem. Eng. Data* **2010**, *55*, 3462–3467.
- (13) Wooley, R.; Ma, Z.; Wang, N.-H. L. *Ind. Eng. Chem. Res.* **1998**, *37*, 3699–3709.
- (14) Chen, K.; Luo, G.; Lei, Z.; Zhang, Z.; Zhang, S.; Chen, J. *Separation and Purification Technology* **2018**, *195*, 288–294.
- (15) Ayhan Demirbas. *Energy Conversion and Management* **2001**, *42*, 1357–1378.
- (16) Haghghi Mood, S.; Hossein Golfeshan, A.; Tabatabaei, M.; Salehi Jouzani, G.; Najafi, G. H.; Gholami, M.; Ardjmand, M. *Renewable and Sustainable Energy Reviews* **2013**, *27*, 77–93.
- (17) Kim, J. S.; Lee, Y. Y.; Kim, T. H. *Bioresource technology* **2016**, *199*, 42–48.
- (18) Dai, J.; Grace, J. R. *Powder Technology* **2008**, *186*, 56–64.
- (19) Carvalheiro, F.; Duarte, L. C.; Gírio, F. M. *Journal of Scientific & Industrial Research* **2008**, *67*, 849–864.
- (20) Ye Sun, J. C. *Bioresource technology* **2002**, *83*, 1–11.
- (21) Zimbardi, F.; Viola, E.; Nanna, F.; Larocca, E.; Cardinale, M.; Barisano, D. *Industrial Crops and Products* **2007**, *26*, 195–206.
- (22) Lynd, L. R.; Weimer, P. J.; van Zyl, W. H.; Pretorius, I. S. *Microbiology and molecular biology reviews* **2002**, *66*, 506–77.

- (23) Abdel-Hamid, A. M.; Solbiati, J. O.; Cann, I. K. O. *Advances in applied microbiology* **2013**, *82*, 1–28.
- (24) Renders, T.; van den Bossche, G.; Vangeel, T.; van Aelst, K.; Sels, B. *Current opinion in biotechnology* **2019**, *56*, 193–201.
- (25) Kim, D. *Molecules* **2018**, *23*, 1–21.
- (26) Alriksson, B.; Cavka, A.; Jönsson, L. J. *Bioresource technology* **2011**, *102*, 1254–1263.
- (27) Rosales-Calderon, O.; Arantes, V. *Biotechnology for biofuels* **2019**, *12*, 240.
- (28) Esteban, J.; Yustos, P.; Ladero, M. *Catalysts* **2018**, *8*, 637.
- (29) Tong, X.; Ma, Y.; Li, Y. *Applied Catalysis A: General* **2010**, *385*, 1–13.
- (30) Zheng, M.; Pang, J.; Sun, R.; Wang, A.; Zhang, T. *ACS Catal.* **2017**, *7*, 1939–1954.
- (31) Song, J.; Fan, H.; Ma, J.; Han, B. *Green Chem.* **2013**, *15*, 2619.
- (32) Sun, J.; Liu, H. *Green Chem* **2011**, *13*, 135–142.
- (33) Sun, J.; Liu, H. *Catalysis Today* **2014**, *234*, 75–82.
- (34) Janice Gorzynski Smith. *McGraw-Hill* **2011**.
- (35) Bajpai, P. Carbohydrate Chemistry. In *Biermann's Handbook of Pulp*; pp 363–371.
- (36) Cui, S. W. *Food carbohydrates: Chemistry, physical properties, and applications*; Taylor & Francis, 2005.
- (37) Hyvonenh, L.; Varo, P.; Koivistoinen, P. *Journal of food science* **1977**, *42*, 652–653.
- (38) Yaylayan, V. A.; Ismail, A. A.; Mandeville, S. *Carbohydrate research* **1993**, *248*, 355–360.
- (39) Steven, R. M.; Adam, A. *J. Am. Chem. Soc* **1987**, *109*, 3168–3169.
- (40) Hyvonenh, L.; Varo, P.; Koivistoinen, P. *Journal of food science* **1977**, *42*, 657–659.
- (41) Horton, D.; Wałaszek, Z. *Carbohydrate research* **1982**, *105*, 145–153.
- (42) Que, L.; Gray, G. R. *Biochemistry* **1974**, *13*, 146–153.
- (43) Vitor H. Pomin. Unravelling Glycobiology by NMR Spectroscopy. In *Open access peer-reviewed chapter*; pp 63–89. DOI: 10.5772/48136.
- (44) Barclay, T.; Ginic-Markovic, M.; Johnston, M. R.; Cooper, P.; Petrovsky, N. *Carbohydrate research* **2012**, *347*, 136–141.
- (45) Le Barc'H, N.; Grossel, J. M.; Looten, P.; Mathlouthi, M. *Food Chemistry* **2001**, *74*, 119–124.
- (46) Franks, F. *Royal Society of Chemistry* **2000**, *2*, 86–107.
- (47) Rao, V. *Conformation of Carbohydrates*; CRC Press, 2019.
- (48) Sing, K. S. W. *Pure and Applied Chemistry* **1982**, *54*, 2201–2218.
- (49) Douglas M. Ruthven. *Wiley* **1984**.

- (50) Françoise Rouquerol, Jean Rouquerol, Isabelle Beurroies, Philip Llewellyn, Renaud Denoyel. *Techniques de l'ingénieur* **2017**, 4, 1–22.
- (51) Abdehagh, N.; Tezel, F. H.; Thibault, J. *Adsorption* **2016**, 22, 357–370.
- (52) Lowenstein, W. *Am. Mineral* **1954**, 39, 92–96.
- (53) Heper, M.; Türker, L.; Kincal, N. S. *Journal of colloid and interface science* **2007**, 306, 11–15.
- (54) *Database of Zeolite Structures*, www.iza-structure.org. <http://www.iza-structure.org/databases/> (accessed 2022-08-24).
- (55) John M. Thomas. *Angew. Chem Int.* **1988**, 27, 1673–1691.
- (56) Izabel Cristina Medeiros Costa IFPEN Thesis **2018**.
- (57) Frising, T.; Leflaive, P. *Microporous and Mesoporous Materials* **2008**, 114, 27–63.
- (58) Khosravanipour Mostafazadeh, A.; Sarshar, M.; Javadian, S.; Zarefard, M. R.; Amirifard Haghighi, Z. *Separation and Purification Technology* **2011**, 79, 72–78.
- (59) Vente, J. A.; Bosch, H.; Haan, A. B. de; Bussmann, P. J. T. *Journal of chromatography. A* **2005**, 1066, 71–79.
- (60) Ronald W. Goulding. *Journal of chromatography* **1975**, 103, 229–239.
- (61) Vente, J. A.; Bosch, H.; Haan, A. B. de; Bussmann, P. J. T. *Chemical Engineering Communications* **2005**, 192, 23–33.
- (62) Angyal, S. J. *Advances in carbohydrate chemistry and biochemistry*, 1989, 1–43.
- (63) Caruel, H.; Rigal, L.; Gaset, A. *Journal of chromatography* **1991**, 558, 89–104.
- (64) Saari, P.; Hurme, M. *Chem. Eng. Technol.* **2011**, 34, 282–288.
- (65) Tiihonen, J.; Markkanen, I.; Paatero, E. *Chemical Engineering Communications* **2002**, 189, 995–1008.
- (66) US patent 4340724 **1982**.
- (67) Wach, W.; Fornefett, I.; Buttersack, C.; Buchholz, K. *Anal. Methods* **2018**, 10, 1817–1832.
- (68) Rolf Schollner, Wolf-Dietrich Einicke and Barbel Glaser. *J. CHEM. SOC.* **1993**, 89, 1871–1879.
- (69) US patent number 4340724 **1982**.
- (70) US Patent Number 4,471,114 **1984**.
- (71) Th. M. Wortel and H. van Bekkum. *Journal of the royal Netherlands Chemical Society* **1978**, 97, 156–158.
- (72) Fornefett, I.; Rabet, D.; Buttersack, C.; Buchholz, K. *Green Chem.* **2016**, 18, 3378–3388.

- (73) Chethana, B. K.; Mushrif, S. H. *Journal of Catalysis* **2015**, *323*, 158–164.
- (74) Li, G.; Pidko, E. A.; Hensen, E. J. M. *Catal. Sci. Technol.* **2014**, *4*, 2241–2250.
- (75) Rai, N.; Caratzoulas, S.; Vlachos, D. G. *ACS Catal.* **2013**, *3*, 2294–2298.
- (76) Li, S.; Josephson, T.; Vlachos, D. G.; Caratzoulas, S. *Journal of Catalysis* **2017**, *355*, 11–16.
- (77) Yang, G.; Li, X.; Zhou, L. *RSC Adv.* **2016**, *6*, 8838–8847.
- (78) Cheng, L.; Curtiss, L. A.; Assary, R. S.; Greeley, J.; Kerber, T.; Sauer, J. *J. Phys. Chem. C* **2011**, *115*, 21785–21790.
- (79) Yang, G.; Zhu, C.; Zhou, L. *ChemistrySelect* **2016**, *1*, 6834–6840.
- (80) van der Graaff, W. N. P.; Tempelman, C. H. L.; Li, G.; Mezari, B.; Kosinov, N.; Pidko, E. A.; Hensen, E. J. M. *ChemSusChem* **2016**, *9*, 3145–3149.
- (81) Bai, P.; Siepmann, J. I.; Deem, M. W. *AIChE J.* **2013**, *59*, 3523–3529.
- (82) Koli, A. R.; Yeole, S. D. *J Chem Sci* **2020**, *132*, 1–7.
- (83) Song, R.; Chen, D.; Suo, C.; Guo, Z. *Carbohydrate research* **2020**, *496*, 108114.
- (84) Sjomanan, E.; MANTTARI, M.; Nystroma, M.; Koivikkob, H.; HEIKKILA, H. *Journal of Membrane Science* **2007**, *292*, 106–115.
- (85) Bilal, M.; Asgher, M.; Iqbal, H. M. N.; Hu, H.; Zhang, X. *International journal of biological macromolecules* **2017**, *98*, 447–458.
- (86) Pontalier, P. Y.; Ismail, A.; Ghoul, M. *Separation and Purification Technology* **1997**, *12*, 175–181.
- (87) Sjomanan, E.; MANTTARI, M.; Nystroma, M.; Koivikkob, H.; HEIKKILA, H. *Journal of Membrane Science* **2007**, *292*, 106–115.
- (88) Vanneste, J.; Ron, S. de; Vandecruys, S.; Soare, S. A.; Darvishmanesh, S.; van der Bruggen, B. *Separation and Purification Technology* **2011**, *80*, 600–609.
- (89) Kuhn, R. C.; Maugeri Filho, F. *Journal of chromatography. B, Analytical technologies in the biomedical and life sciences* **2010**, *878*, 2023–2028.
- (90) Stanford, J. P.; Hall, P. H.; Rover, M. R.; Smith, R. G.; Brown, R. C. *Separation and Purification Technology* **2018**, *194*, 170–180.
- (91) Nitzsche, R.; Gröngröft, A.; Kraume, M. *Separation and Purification Technology* **2019**, *209*, 491–502.
- (92) Ramos, J.; Duarte, T. C.; Rodrigues, A.; Silva, I. J.; Cavalcante, C. L.; Azevedo, D. *Journal of Food Engineering* **2011**, *102*, 355–360.
- (93) Feller, C.; Fink, M. *HortScience* **2007**, *57*–60.

- (94) Lines, A. M.; Tse, P.; Felmy, H. M.; Wilson, J. M.; Shafer, J.; Denslow, K. M.; Still, A. N.; King, C.; Bryan, S. A. *Ind. Eng. Chem. Res.* **2019**, *58*, 21194–21200.
- (95) Lupoi, J. S.; Singh, S.; Simmons, B. A.; Henry, R. J. *Bioenerg. Res.* **2014**, *7*, 1–23.
- (96) Lupoi, J. S.; Gjersing, E.; Davis, M. F. *Frontiers in bioengineering and biotechnology* **2015**, *3*, 50.
- (97) Lackey, H. E.; Colburn, H. A.; Olarte, M. V.; Lemmon, T.; Felmy, H. M.; Bryan, S. A.; Lines, A. M. *ACS omega* **2021**, *6*, 35457–35466.
- (98) Shih, C.-J.; Lupoi, J. S.; Smith, E. A. *Bioresource technology* **2011**, *102*, 5169–5176.
- (99) Schalk, R.; Heintz, A.; Braun, F.; Iacono, G.; Rädle, M.; Gretz, N.; Methner, F.-J.; Beuermann, T. *Applied Sciences* **2019**, *9*, 2472.
- (100) Schalk, R.; Braun, F.; Frank, R.; Rädle, M.; Gretz, N.; Methner, F.-J.; Beuermann, T. *Bioprocess and biosystems engineering* **2017**, *40*, 1519–1527.
- (101) Shih, C.-J.; Smith, E. A. *Analytica chimica acta* **2009**, *653*, 200–206.
- (102) Gray, S. R.; Peretti, S. W.; Lamb, H. H. *Biotechnology and bioengineering* **2013**, *110*, 1654–1662.
- (103) Wold, S.; Sjostrom, M.; Eriksson, L. *Chemometrics and Intelligent Laboratory Systems* **2001**, *58*, 109–130.
- (104) Dudek, M.; Zajac, G.; Szafraniec, E.; Wiercigroch, E.; Tott, S.; Malek, K.; Kaczor, A.; Baranska, M. *Spectrochimica acta. Part A, Molecular and biomolecular spectroscopy* **2019**, *206*, 597–612.
- (105) Ewanick, S.; Schmitt, E.; Gustafson, R.; Bura, R. *Pure and Applied Chemistry* **2014**, *86*, 867–879.
- (106) Sivakesava, S.; Irudayaraj, J.; Demirci, A. *Journal of Industrial Microbiology & Biotechnology* **2001**, *26*, 185–190.
- (107) US patent 4293346 **1981**.
- (108) US patent 4157267 **1977**.
- (109) Cherif, L.; El-Berrichi, F.-Z.; Bengueddach, A.; Tougne, P.; Fraissard, J. *Colloids and Surfaces A: Physicochemical and Engineering Aspects* **2003**, *220*, 83–89.
- (110) Sherry, H. S. *The Journal of Physical Chemistry* **1966**, *70*, 1158.
- (111) Khabzina, Y.; Laroche, C.; Pagis, C.; Farrusseng, D. *Physical chemistry chemical physics : PCCP* **2017**, *19*, 17242–17249.
- (112) Sherry, H. S. *The Journal of Physical Chemistry* **1968**, *72*, 4086.
- (113) Kulprathipanja, S., Ed. *Zeolites in industrial separation and catalysis*; Wiley-VCH, 2010.

- (114) Alves, L. A.; Almeida e Silva, J. B.; Giuliatti, M. *J. Chem. Eng. Data* **2007**, *52*, 2166–2170.
- (115) Gong, X.; Wang, C.; Zhang, L.; Qu, H. *J. Chem. Eng. Data* **2012**, *57*, 3264–3269.
- (116) Liu, Y. *J. Chem. Eng. Data* **2009**, *54*, 1981–1985.
- (117) Bai, P.; Siepmann, J. I.; Deem, M. W. *AIChE J.* **2013**, *59*, 3523–3529.
- (118) Alexandersson, E.; Nestor, G. *Carbohydrate research* **2022**, *511*, 108477.
- (119) J.F. Verchere and S. Chapelle. *Polyhedron* **1989**, *8*, 333–340.
- (120) Qi, L.; Alamillo, R.; Elliott, W. A.; Andersen, A.; Hoyt, D. W.; Walter, E. D.; Han, K. S.; Washton, N. M.; Rioux, R. M.; Dumesic, J. A.; Scott, S. L. *ACS Catal.* **2017**, *7*, 3489–3500.
- (121) Kresse, G.; Hafner, J. *Phys. Rev. B* **1994**, *49*, 14251–14269.
- (122) Kresse, G.; Furthmüller, J. *Phys. Rev. B* **1996**, *54*, 11169–11186.
- (123) Perdew, J. P.; Burke, K.; Ernzerhof, M. *Phys. Rev. Lett.* **1996**, *77*, 3865–3868.
- (124) Kresse, G.; Joubert, D. *Phys. Rev. B* **1999**, *59*, 1758–1775.
- (125) Blöchl, P. E. *Phys. Rev. B* **1994**, *50*, 17953–17979.
- (126) Grimme, S. *Journal of computational chemistry* **2006**, *27*, 1787–1799.
- (127) Cui, S. W. *Food carbohydrates: Chemistry, physical properties, and applications*; Taylor & Francis, 2005.
- (128) Peter Atkins . Julio De Paula. *Atkins' physical chemistry*, 2006.
- (129) National Institute of Standards and Technology | NIST, <https://www.nist.gov/>.
- (130) Graf, M. M. H.; Zhixiong, L.; Bren, U.; Haltrich, D.; van Gunsteren, W. F.; Oostenbrink, C. *PLoS computational biology* **2014**, *10*, e1003995.
- (131) Bai, P.; Tsapatsis, M.; Siepmann, J. I. *J. Phys. Chem. C* **2013**, *117*, 24375–24387.
- (132) Maurin, G.; Llewellyn, P.; Poyet, T.; Kuchta, B. *The journal of physical chemistry. B* **2005**, *109*, 125–129.
- (133) Damm, W.; Frontera, A.; Tirado-Rives, J.; Jorgensen, W.; L. *Journal of computational chemistry* **1997**, *18*, 1955–1970.
- (134) Jorgensen, W. L.; Chandrasekhar, J.; Madura, J. D.; Impey, R. W.; Klein, M. L. *The Journal of Chemical Physics* **1983**, *79*, 926–935.
- (135) Oja, V.; Suuberg, E. M. *J. Chem. Eng. Data* **1999**, *44*, 26–29.
- (136) Perozin, D.; Oliveira, A. L.; Cabral, F. A. *Journal of Food Process Engineering* **2007**, *30*, 593–606.
- (137) Medeiros-Costa, I. C.; Laroche, C.; Coasne, B.; Pérez-Pellitero, J. *Ind. Eng. Chem. Res.* **2022**, *61*, 10184–10194.

- (138) Losada, I. B.; Grobas-Illobre, P.; Misturini, A.; Polaina, J.; Seminovski, Y.; Sastre, G. *Microporous and Mesoporous Materials* **2021**, *319*, 111031.
- (139) Robert H. Swendsen and Jian-Sheng Wang. *PHYSICAL REVIEW LETTERS* **1986**, *57*.
- (140) Sanderson, R. T. *J. Am. Chem. Soc* **1983**, *105*, 2259–2261.